



NASA CR-54939  
APS-5223-R

FINAL REPORT  
INVESTIGATIONS OF GAS BEARING  
COMPRESSIBILITY NUMBER AND  
PIVOT FLEXURE IN TILTING PAD BEARINGS

FACILITY FORM 602

(ACCESSION NUMBER)	(THRU)
158	1
(PAGES)	(CODE)
175.7 CR-54939	75
(NASA CR OR TMX OR AD NUMBER)	(CATEGORY)

prepared for  
National Aeronautics and Space Administration

Contract NAS3-7633

**BLANK PAGE**

# NOTICE

This report was prepared as an account of Government sponsored work. Neither the United States, nor the National Aeronautics and Space Administration (NASA), nor any person acting on behalf of NASA:

- A.) Makes any warranty or representation, expressed or implied, with respect to the accuracy, completeness, or usefulness of the information contained in this report, or that the use of any information, apparatus, method, or process disclosed in this report may not infringe privately owned rights; or
- B.) Assumes any liabilities with respect to the use of, or for damages resulting from the use of any information, apparatus, method or process disclosed in this report.

As used above, "person acting on behalf of NASA" includes any employee or contractor of NASA, or employee of such contractor, to the extent that such employee or contractor of NASA, or employee of such contractor prepares, disseminates, or provides access to, any information pursuant to his employment or contract with NASA, or his employment with such contractor.

Requests for copies of this report should be referred to

National Aeronautics and Space Administration  
Office of Scientific and Technical Information  
Attention: ATSS  
Washington, D.C. 20546

NASA CR 54030  
APS 5223 R

FINAL REPORT  
INVESTIGATIONS OF GAS BEARING  
COMPRESSIBILITY NUMBER AND  
PIVOT FLEXURE IN TILTING PAD BEARINGS

prepared for  
National Aeronautics and Space Administration  
by  
AiResearch Manufacturing Company of Arizona

March 31, 1967

Contract NAS3-7633

Technical Management  
NASA Lewis Research Center  
Cleveland, Ohio  
Space Power Systems Division  
Jack A. Heller  
Fluid Systems Components Division  
George K. Fischer

**BLANK PAGE**

## FOREWORD

The research described herein, which was conducted by the AiResearch Manufacturing Company of Arizona, a division of The Garrett Corporation, was performed under NASA Contract NAS3-7633. The work was accomplished under the technical management of Mr. Jack A. Heller, Space Power Systems Division, Lewis Research Center, with Mr. George K. Fischer of the Fluid System Components Division, Lewis Research Center, as technical consultant.

# ABSTRACT

N6-7-28680

Analytical and experimental investigations were conducted on a vertically oriented rotor, supported on resiliently mounted tilting pad gas bearings to determine which bearing pad parameters govern the threshold of resonant whirl. Results show that for the particular configuration tested, there exists a critical value of pad eccentricity ratio for a given pad compressibility number.

The above criteria are then theoretically applied to the analysis of an existing gas bearing turbocompressor in an effort to determine whether or not the turbocompressor rotor-bearing system will be stable at off-design conditions.

Elastically pivoted partial-arc gas bearings were also tested. Under almost ideal isothermal conditions the tests demonstrated that this concept is a workable system affording rotor dynamic stability over a wide range of bearing pad loads.

*Author*

## CONTRIBUTING PERSONNEL

The following personnel of the AiResearch Manufacturing Company of Arizona were responsible for the conduct of the work performed under Contract NAS3-7633.

R. J. Bazaz  
D. J. Brandes  
R. W. Elliott  
R. B. Gildersleeve  
W. G. Heinrich  
F. E. Johnson  
L. A. Matsch  
H. H. Milligan  
R. Shriver  
P. J. Spencer  
E. L. Wheeler



## TABLE OF CONTENTS

	<u>Page</u>
FOREWORD	
ABSTRACT	
SUMMARY	1
1.0 INTRODUCTION	2
2.0 TASK I, TURBOCOMPRESSOR GAS BEARING ANALYSIS	6
2.1 General	6
2.2 Journal Bearings	7
2.3 Thrust Bearing	9
2.4 Turbocompressor Thermal Analysis at 6 psia Ambient	23
2.5 Discussion of Results	31
3.0 TASK II, GAS BEARING - ROTOR WHIRL INVESTIGATIONS	35
3.1 General	35
3.2 Test Rig	37
3.3 Instrumentation	40
3.4 Test Hardware	41
3.5 Test Procedure	48
3.6 Test Results	49
3.7 Data Reduction and Analysis	55
3.7.1 Sample Data Reduction Calculation	71
3.7.2 Test Data Correlation and Discussion	73
3.8 Application of Stability Criteria to Delivered Turbocompressor	85

## TABLE OF CONTENTS (Contd.)

	<u>Page</u>
4.0 TASK III, EXPERIMENTAL INVESTIGATION OF NONPIVOTED TYPE, PARTIAL ARC GAS BEARINGS	89
4.1 General	89
4.2 Test Rig	90
4.3 Instrumentation	91
4.4 Test Hardware	91
4.5 Test Procedure and Results	96
4.5.1 Test Series 1	96
4.5.2 Test Series 2	104
4.6 Discussion	104
5.0 TASK IV, GAS BEARING PARTS AND SPECIAL HARDWARE	114
5.1 General	114
5.2 Essential Spares	114
5.3 Surface Coatings of Bearings	115
5.4 Proximity Probe Installation	134
5.5 Hardware Identification	124
5.6 Hardware Calibration	126
6.0 CONCLUSIONS	132
7.0 RECOMMENDATIONS	133
APPENDIX I	134

## LIST OF FIGURES

<u>Figure</u>		<u>Page</u>
1	Turbocompressor Gas Bearing Shoe	8
2	Predicted Turbocompressor Journal Bearing Pad Load vs Minimum Film Thickness	10
3	Predicted Turbocompressor Journal Bearing Pad Load vs Minimum Film Thickness	11
4	Predicted Turbocompressor Journal Bearing Pad Load vs Minimum Film Thickness	12
5	Predicted Turbocompressor Journal Bearing Pad Load vs Minimum Film Thickness	13
6	Predicted Turbocompressor Journal Bearing Pad Load vs Friction	14
7	Predicted Turbocompressor Journal Bearing Pad Load vs Friction	15
8	Predicted Turbocompressor Journal Bearing Pad Load vs Friction at Various Ambient Pressures and 80°F	16
9	Predicted Turbocompressor Journal Bearing Pad Load vs Friction at Various Ambient Pressures and 500°F	17
10	Hydrodynamic Thrust Bearing Geometry for NASA Gas Generator	18
11	Predicted Hydrodynamic Performance of Thrust Bearing for NASA Turbocompressor	19
12	Predicted Hydrodynamic Performance of Thrust Bearing for NASA Turbocompressor	20
13	Predicted Hydrodynamic Performance of Thrust Bearing for NASA Turbocompressor	21
14	Predicted Hydrodynamic Performance of Thrust Bearing for NASA Turbocompressor	22

# LIST OF FIGURES (Contd.)

<u>Figure</u>		<u>Page</u>
15	Preliminary Steady-State Temperature Distribution, NASA Brayton-Cycle Gas Generator	24
16	Final Steady-State Temperature Distribution Brayton-Cycle Gas Generator	25
17	Thermal Analysis, NASA Brayton-Cycle Gas Generator, 6 PSIA	28
18	Thermal Analysis, NASA Brayton-Cycle Gas Generator, 6 PSIA	29
19	Thermal Analysis, NASA Brayton-Cycle Gas Generator, 6 PSIA	30
20	Dynamic Two-Bearing Test Rig	38
21	Test Rotor - Gas Bearing Rotor Whirl Investigations	42
22	Test Rotor - Gas Bearing Rotor Whirl Investigations	43
23	Gas Bearing Pads and Resilient Mount, Rotor Whirl Investigation	45
24	Gas Bearing Pad, Rotor Whirl Investigations	46
25	Task II, Rotor Whirl Investigations, Resilient Mount Configuration	47
26	Average Bearing Pad Load, Temperature and Hydrodynamic Pressure at Whirl Threshold vs Rotor Speed, $\lambda = 1.5$	50
27	Average Bearing Pad Load, Temperature and Hydrodynamic Pressure at Whirl Threshold vs Rotor Speed	50
28	Average Bearing Pad Load, Temperature and Hydrodynamic Pressure at Whirl Threshold vs Rotor Speed	52

# LIST OF FIGURES (Contd.)

<u>Figure</u>		<u>Page</u>
29	Average Bearing Pad Load, Temperature and Hydrodynamic Pressure at Whirl Threshold vs Rotor Speed	53
30	Typical Lissajous Patterns of Rotor with and without Whirl	56
31	NASA Gas Bearing Stability Study, Typical Critical Sped Oscilloscope Patterns (Rotor a)	57
32	NASA Gas Bearing Stability Study, Shaft Motions at 38,500 rpm, 35,000 rpm, 30,000 rpm, 25,000 rpm, and 20,000 rpm (Rotor a)	58
33	NASA Gas Bearing Stability Study, Shaft Motions at 38,500 rpm, 35,000 rpm, 30,000 rpm, 25,000,rpm, and 20,000 rpm (Rotor b)	59
34	NASA Gas Bearing Stability Study, Shaft Motionsat at 38,500 rpm, 35,000 rpm, 30,000 rpm, 25,000 rpm, and 20,000 rpm (Rotor c)	60
35	NASA Gas Bearing Stability Study, Shaft Motionsat 38,500 rpm, 35,000 rpm, 30,000 rpm, 25,000 rpm, and 20,000 rpm (Rotor d)	61
36	Absolute Viscosity of Air at Atmospheric Pressure	62
37	Predicted Performance, Pad Eccentricity vs Pivot Film-Thickness Ratio	64
38	Changes in Pad Orientation with Change in Pivot Film Thickness ( $\Lambda = 1.5$ )	65
39	Predicted Performance, Pad Load vs. Pivot Film Thickness	66
40	Predicted Performance, Pad Load vs Pivot Film Thickness	67

# LIST OF FIGURES (Contd.)

<u>Figure</u>		<u>Page</u>
41	Predicted Performance, Pad Load vs Pivot Film Thickness	68
42	Centrifugal Growth at Journals of Test Rotor	69
43	Predicted Performance, Pad Film Spring Rate vs Pivot Film Thickness	70
44	Reduced Test Data, Gas Bearing Stability Study	75
45	Reduced Test Data, Gas Bearing Stability Study	76
46	Reduced Test Data, Gas Bearing Stability Study	77
47	Reduced Test Data, Gas Bearing Stability Study	79
48	Theoretical Support Spring Rate versus Speed, Rigid Unsymmetric Rotor Equations Using Experimental Whirl CPS	82
49	Reduced Test Data, Pad Film Spring Rate vs Speed	84
50	Predicted Gas Generator Operating Points Compared with Threshold of Whirl Curves	87
51	Predicted Gas Generator Operating Points Compared with Threshold of Whirl Curves	88
52	"Elastically" Pivoted Partial-Arc Bearing Pads	92
53	Task III, Nonpivoted Type, Partial-Arc Bearing Resilient Mount Configuration - Test 1	94
54	Task III, Nonpivoted Type, Partial-Arc Bearing Resilient Mount Configuration - Test 2	95

# LIST OF FIGURES (Contd.)

<u>Figures</u>		<u>Page</u>
55	Test Series 1, Nonpivoted Partial-Arc Gas Bearing Tests, 5-Pound Initial Preload	98
56	Test Series 1, Nonpivoted Partial-Arc Gas Bearing Test, 3-Pound Initial Preload	99
57	Test Series 1, Nonpivoted Partial-Arc Gas Bearing Test, 1-Pound Initial Preload	100
58	Test Series 1, Nonpivoted Partial-Arc Gas Bearing Test, 1-Pound Initial Preload	101
59	Test Series 1, Nonpivoted Partial-Arc Gas Bearing Test, Negative 3 Pounds Initial Preload	103
60	Test Series 2, Nonpivoted Partial-Arc Gas Bearing Tests, 5-Pound Initial Preload	106
61	Test Series 2, Nonpivoted Partial-Arc Gas Bearing Tests, 3-Pound Initial Preload	107
62	Test Series 2, Nonpivoted Partial-Arc Gas Bearing Tests, 1-Pound Initial Preload	108
63	Test Series 2, Nonpivoted Partial-Arc Gas Bearing Tests, Bearing Diametral Clearance 0.0013 Inch	109
64	Test Series 2, Nonpivoted Partial-Arc Gas Bearing Tests, Bearing Diametral Clearance 0.0033 Inch	110
65	Conceptual Design, Elastically Pivoted Pads with Initial Alignment Capability	112
66	Delivered Gas Bearing Pads and Shaft Mounts and	116
67	Cross-Section of Chrome-Oxide Platings	118

LIST OF FIGURES (Contd.)

<u>Figure</u>		<u>Page</u>
68	Plating Requirement Certification of Compliance Affidavit	120
69	Plating Requirement Certification of Compliance Affidavit	121
70	Location of Chrome-Oxide Plating on Shaft Assembly	122
71	Installation of Proximity Probe in Instrumented Shoes Part 699453-1 and Part 699454-1	123



**BLANK PAGE**

## SUMMARY

Completion of the effort required under this program has resulted in the generation of significant data applicable to the turbocompressor, already delivered to the NASA under Contract NAS3-2778. Gas-operated journal pad and thrust bearing performance characteristics at the off-design point of 6 psia bearing ambient pressure were analytically determined. An updated thermal analysis computer program was used to define the effects of varying the cycle cooling bleed flows in the journal bearings.

A satisfactory dimensionless stability criterion was defined for a journal rotor-bearing system as used in the turbocompressor. The threshold of whirl can thus be defined as a function of the bearing compressibility number ( $\Lambda$ ) and bearing eccentricity ratio ( $\epsilon$ ). Experimental test results, for the particular system under evaluation, verified that rotor whirl frequency is controlled by the journal lubricant film spring rate, and can be used as an additional stability criterion.

For the same dynamic bearing system, test results indicate that the concept of elastically pivoted journal bearings, with reduced resilient-mount spring rates, affords rotor dynamic stability over a wide range of bearing loads.

Certain essential spare parts, for the reference turbocompressor, were fabricated and delivered.

FINAL REPORT  
INVESTIGATIONS OF GAS BEARING  
COMPRESSIBILITY NUMBER AND  
PIVOT FLEXURE IN TILTING PAD BEARINGS

## 1.0 INTRODUCTION

The NASA-Lewis Research Center is presently conducting an evaluation of closed recuperated Brayton-cycle space power systems that use solar energy as the heat source and an inert gas as the working fluid. Under NASA Contract NAS3-2778, the Contractor designed, fabricated, and delivered to the NASA a radial turbo-compressor utilizing self-acting gas journal and thrust bearings. The Turbocompressor Part 699339 was designed to be compatible with a reference system employing a 30-foot-diameter mirror, and the rotor gas bearing suspension system was designed to operate at the reference system design power level (delivering 8 kw<sub>e</sub> minimum), using the system gas, argon, as the lubricant. The gas bearing cavity ambient pressure corresponding to the design power level is approximately 12.0 psia.

As a part of the above program, the Contractor investigated the performance of several configurations of resiliently mounted partial-arc self-acting journal bearings, with hydrostatic lift-off provisions for starting and stopping. A decision was required regarding the preferred rotor orientation (vertical or horizontal) to be used for stability investigations. Since rotors with lightly loaded bearings tend to be more unstable than with bearings under moderate or heavy loads, it was believed that the limiting case, zero bearing loads, should be studied. Therefore, in agreement with the NASA, all testing was accomplished with vertically oriented rotors simulating, as closely as possible, a zero-"g" space

environment. Neglecting small rotor unbalanced forces the journal bearings were operated without loading. The journal bearing configuration chosen for the turbocompressor, as a result of the investigations, used three tilting pads per journal with lapped ball and socket pivots.

At the conclusion of NASA Contract NAS3-2778, the NASA desired additional information relative to the developed gas bearing concept. Answers were sought to the following questions:

- (a) Can the gas bearing system of the turbocompressor be operated at lower power levels without changing or adjusting the "as-delivered" turbocompressor?
- (b) Can the ball and socket pivots of the partial-arc journal bearings be eliminated?

The first question was brought about by an additional operational requirement generated by the NASA. The reason for the second question is one of reliability. Due to normal rotor orbiting during operation, the ball and socket pivots are subjected to relative sliding motions which might produce some deleterious wear during extended operation. Since the integrity of the ball and socket pivots cannot be assured for the required 10,000 hours of turbocompressor operational life, a potential solution to the problem would be to eliminate the sliding joint and replace it with an elastic coupling. As background for this, the Contractor had previously demonstrated (under Contract NAS3-2778) the feasibility of using elastically pivoted partial-arc bearings.

The aforementioned questions serve as the basis for Contract NAS3-7633. The objectives of the program undertaken in accordance with the contract were three fold, as follows:

- (1) To study the performance of the gas bearings of the reference turbocompressor at a lower bearing cavity ambient pressure level to determine if the applicability of the machine could be extended to lower power solar and nuclear systems.
- (2) To further investigate the potential application of resiliently mounted, nonpivoted, partial-arc gas bearings.
- (3) To fabricate and deliver to the NASA certain special critical replaceable gas bearing components for the turbomachinery developed under NASA Contract NAS3-2778.

The work described in this report was broken into four general tasks as follows:

- Task I - (a) Analytical studies to predict turbo-compressor gas bearing performance when operating in argon at an ambient pressure of 6 psia (one-half power ambient pressure level) and at the anticipated temperature levels.
- (b) Steady-state thermal analysis of the reference turbocompressor at one-half power level conditions.

- Task II - Analytical and experimental investigations to determine which journal bearing parameters govern the threshold of whirl for a vertically oriented rotor with inertial and mass properties similar to those of the delivered turbocompressor.
- Task III - Experimental investigations of elastically pivoted partial-arc gas bearings to determine the effect of resilient mounting spring rates with respect to rotor stability, and improved alignment techniques.
- Task IV - Fabrication and delivery of special turbocompressor spare gas bearing hardware items (special bearings, mounts, and shaft) as specified by the NASA.

## 2.0 TASK I, TURBOCOMPRESSOR GAS BEARING ANALYSIS

### 2.1 General

The gas-lubricated journal and thrust bearing suspension system of the reference turbocompressor, delivered to the NASA under Contract NAS3-2778, was designed to operate at a bearing cavity ambient pressure of 12.0 psia with use of the system process gas, argon. These conditions are for the design output power level of 10.0 kw. If the reference turbocompressor is required to operate at half power output, the overall system pressure level would be halved (with the turbine inlet temperature assumed to remain the same), and the gas bearing system would thus be required to operate at 6.0 psia ambient conditions. Lowering the ambient pressure in the bearing cavity will reduce the load-carrying capacity of the reference bearings. With the bearing load requirements assumed to remain the same at the lower system pressures, and with a reduction in bearing load-carrying capacity, the bearings will operate with a smaller film thickness. Reduction of the film thickness will, in turn, increase the frictional power loss in the bearings, which will to some extent change the thermal balance in the turbocompressor. It should be noted that the above-mentioned effects play an important role in the operation of machinery supported on gas bearings due to the small lubricant film thicknesses involved. This is especially true of space-power turbomachinery. Without a unidirectional gravity loading, the bearing shoes may become sufficiently lightly loaded due to differential thermal expansion effects (carrier support structure-to-shoes-to-rotor) that whirl instability may be excited. Alternately, bearing failure may result as a consequence of inadequate lubricant film thickness if thermal expansion effects force bearing loads to become excessive.

The objective of this task was to gain insight into the feasibility of operating the reference turbocompressor at half-power conditions by using analytical methods. To support the study, the following steps were taken:

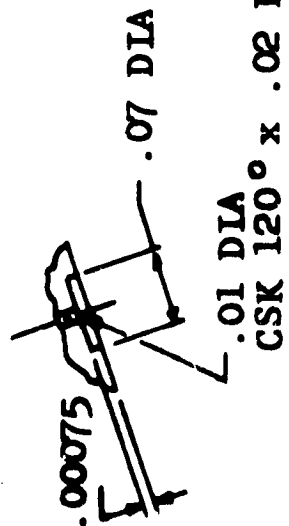
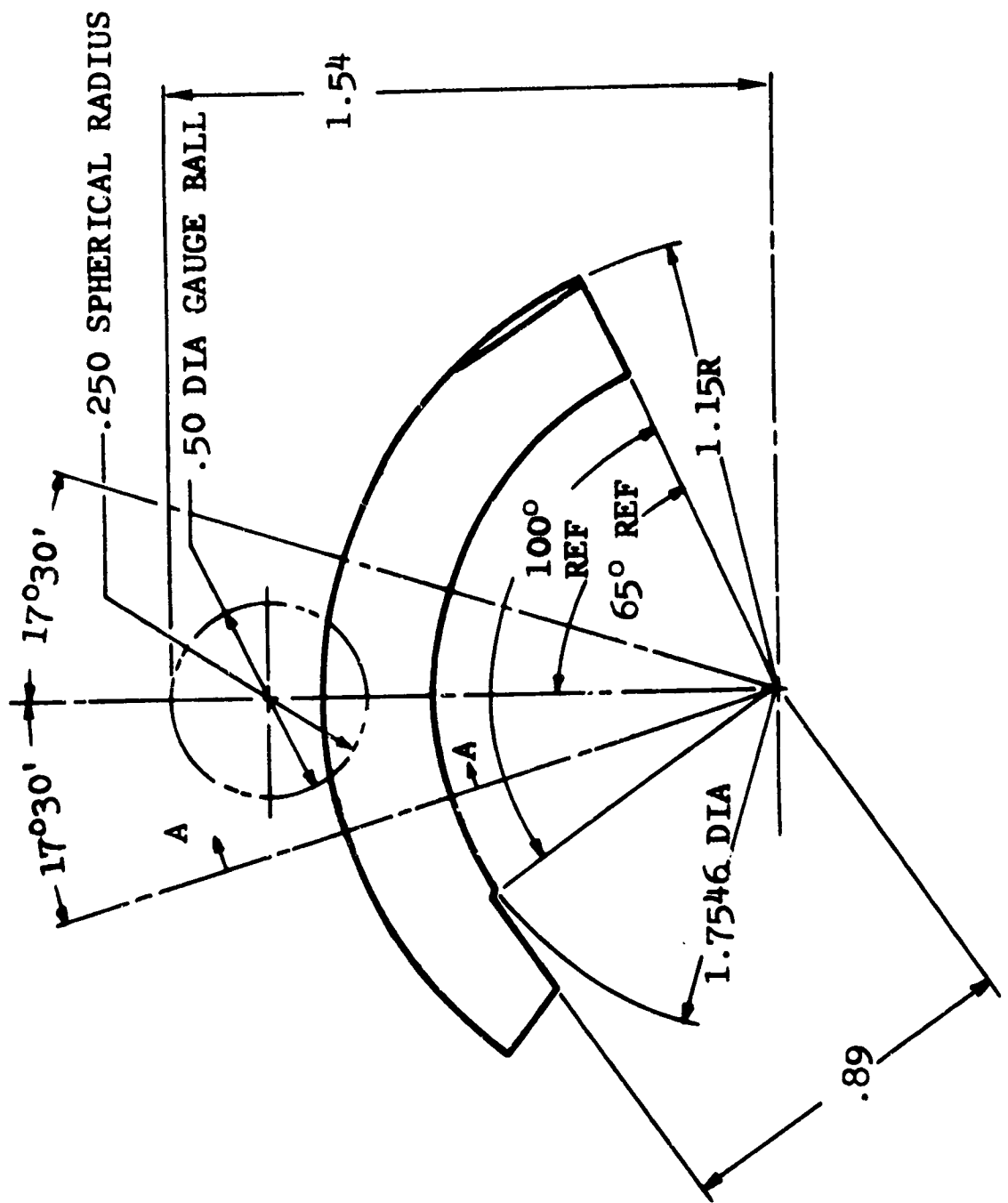
- (a) The performance of the reference turbocompressor journal and thrust bearings under a low (6-psia) ambient-pressure condition was predicted.
- (b) A steady-state temperature analysis of the reference turbocompressor at the half-power-level conditions was conducted by assuming appropriate bearing power losses from the predicted bearing performance at 6 psia (half-power-bearing ambient).

## 2.2 Journal Bearings

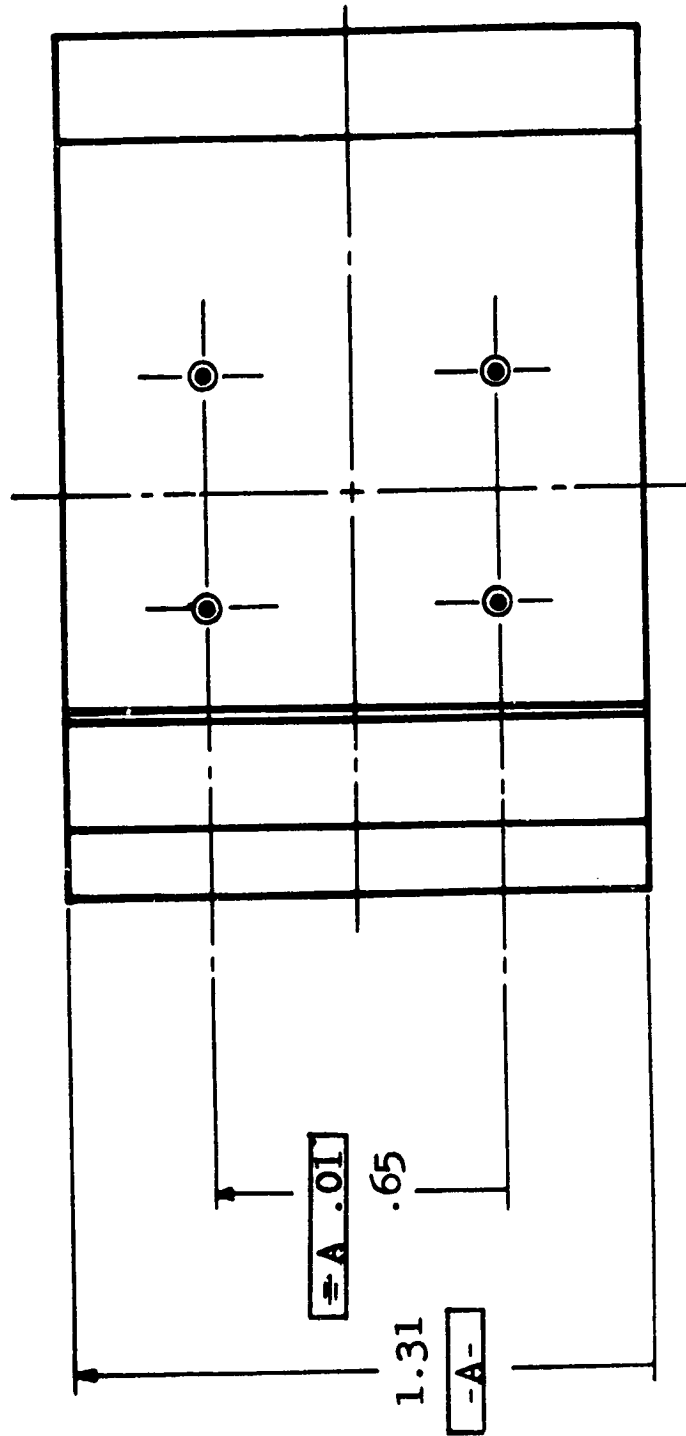
The journal bearings of the reference turbocompressor are of the partial-arc pivoted-pad type (refer to Figure 1). There are three pads per journal bearing; one pad of each bearing is resiliently mounted. The pads have the following geometry:

- (a) Journal radius 0.875 inch
- (b) Journal-to-shoe geometric clearance ratio  $(\frac{C}{R}) = 0.0026$
- (c) Shoe arc length  $100^\circ$
- (d) Pivot location (from shoe leading edge)  $65^\circ$
- (e) Shoe length-to-diameter ratio  $(\frac{L}{D}) = 0.75$





SECTION A - A  
(TYP & ORIFICES)



TURBOCOMPRESSOR  
GAS BEARING SHOE

FIGURE 1

The aforementioned geometry was chosen for turbocompressor design operating conditions of 38,500 rpm, 12 psia bearing ambient pressure, argon gas lubricant, and a journal ambient temperature level of 500°F.

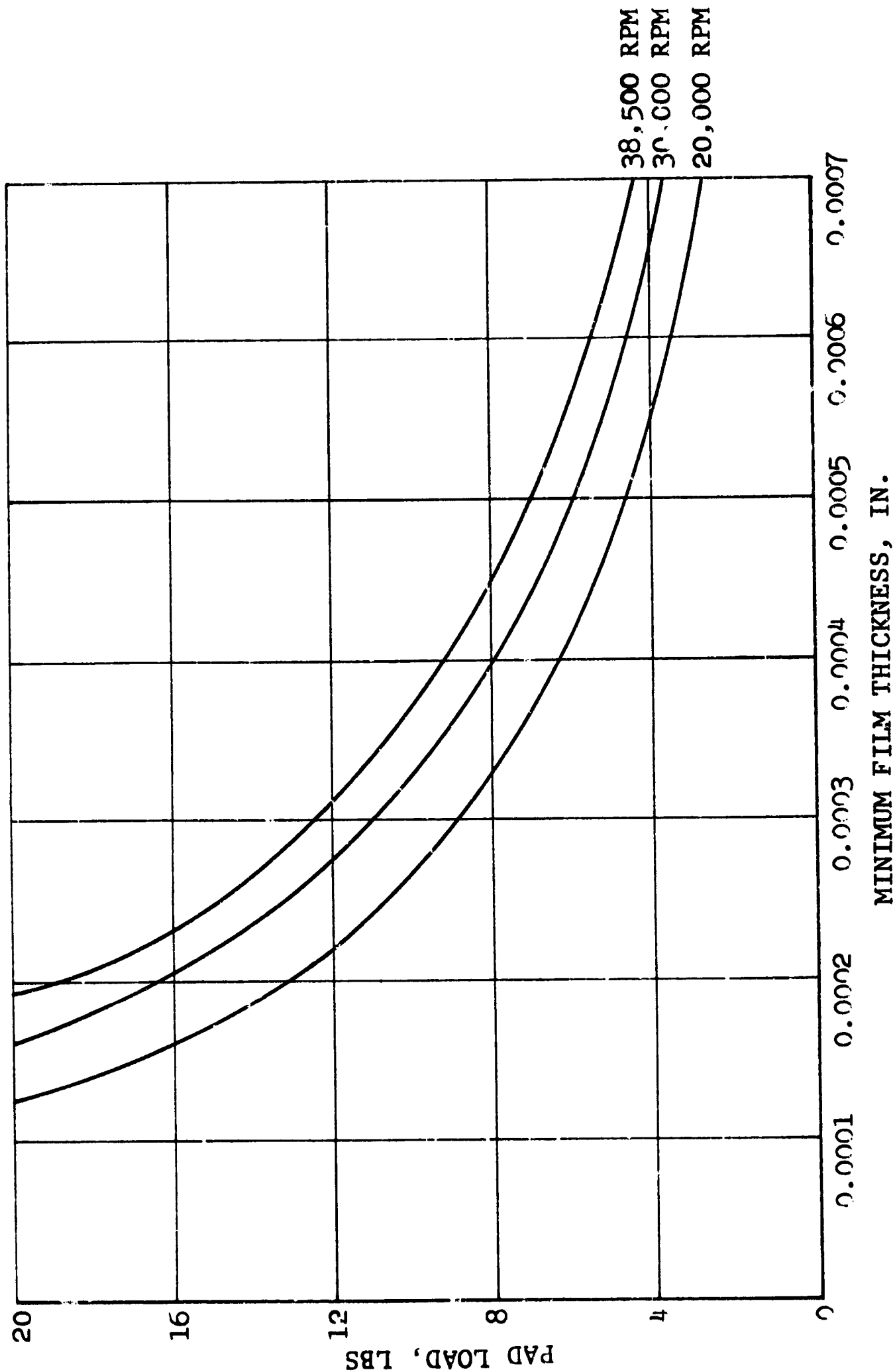
The hydrodynamic performance analysis of the reference journal bearing pad was made by use of a digital computer program at the 6-psia (half power) ambient conditions. Input data consisted of the above pad geometry, an ambient pressure of 6 psia, argon lubricant, and bearing nominal temperatures of 80°F and 500°F (assumed turbocompressor bearing temperatures at start and steady-state conditions, respectively). The predicted 6-psia bearing pad performance at speeds of 20,000, 30,000, and 38,500 rpm is presented in Figures 2 through 7 for the two temperatures, 80°F and 500°F. Figures 8 and 9 present the single-pad power loss as a function of load and ambient pressure at a rotor speed of 38,500 rpm for various ambient pressures. For a vertically oriented rotor (zero bearing load), the power loss of a journal bearing assembly would be (neglecting unbalance loads) three times the single-pad value.

### 2.3 Thrust Bearing

The geometry of the hydrodynamic thrust bearing delivered in the referenced turbocompressor is shown in Figure 10. This bearing was optimized for the 12-psia (full power) ambient conditions and is a conventional stepped-sector design with four orifices for hydrostatic lift-off. The predicted hydrodynamic performance of this bearing at 6 psia with argon lubricant at 80°F and 500°F is shown in Figures 11, 12, 13, and 14. For comparison by the reader, the predicted performance of this bearing at full power design load conditions (12 psia) is shown as a dotted line on Figures 13 and 14.

NOTES:

1.  $L/D = 0.75$
2. JOURNAL RADIUS = 0.875 IN.
3. ARC LENGTH = 100°
4. PIVOT POINT: 65°
5. CLEARANCE RATIO = 0.0026
6. AMBIENT PRESSURE = 6.0 PSIA
7. LUBRICANT: ARGON AT 80°F
8. VISCOSITY =  $3.3 \times 10^{-9}$  REYNS

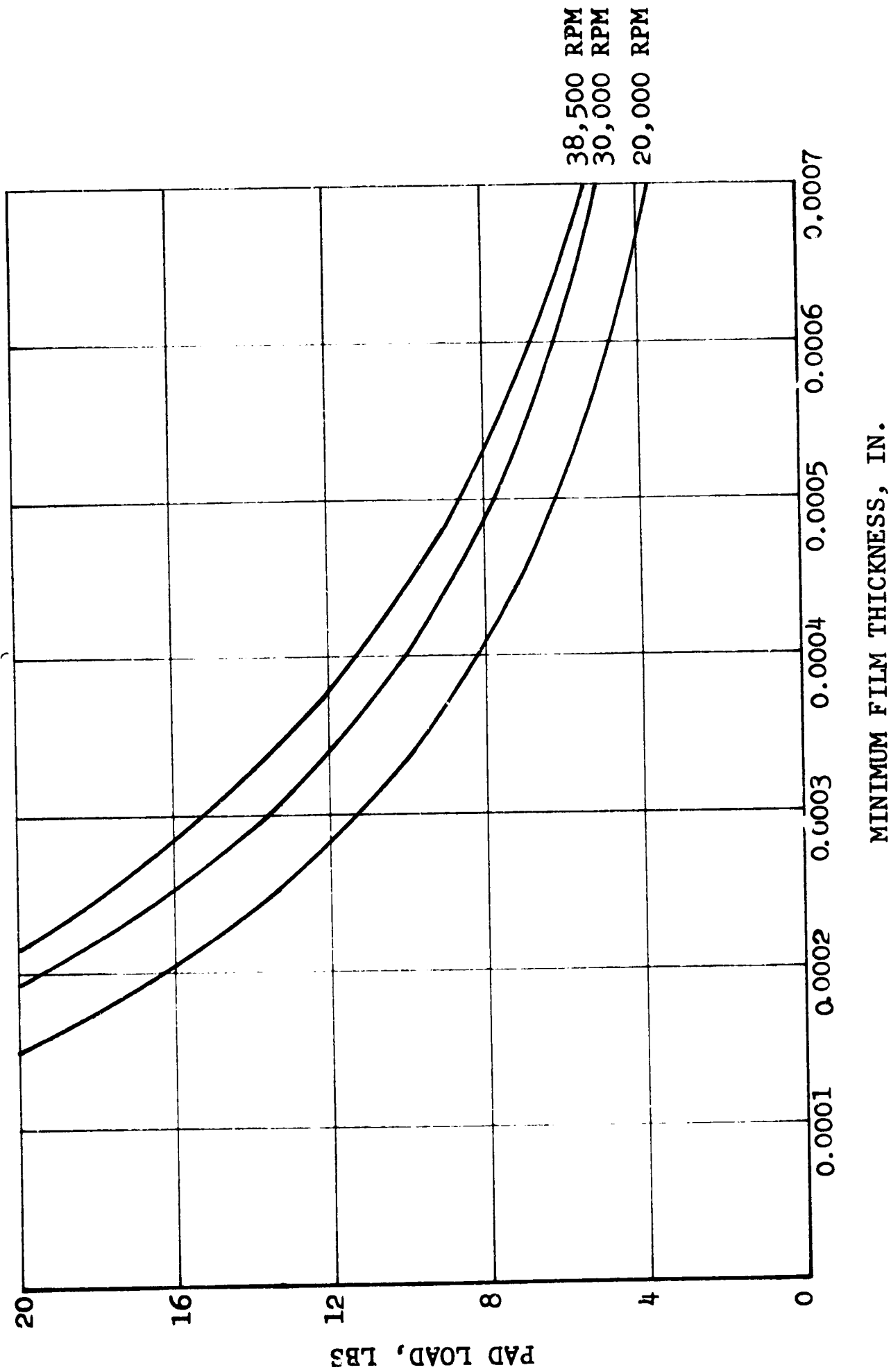


PREDICTED TURBOCOMPRESSOR JOURNAL  
BEARING PAD LOAD VS  
MINIMUM FILM THICKNESS

FIGURE 2

NOTES:

1.  $L/D = 0.75$
2. JOURNAL RADIUS = 0.875 IN.
3. ARC LENGTH =  $100^\circ$
4. PIVOT POINT:  $65^\circ$
5. CLEARANCE RATIO = 0.0026
6. AMBIENT PRESSURE = 6.0 PSIA
7. LUBRICANT: ARGON AT  $500^\circ\text{F}$
8. VISCOSITY =  $5 \times 10^{-8}$  REYNS

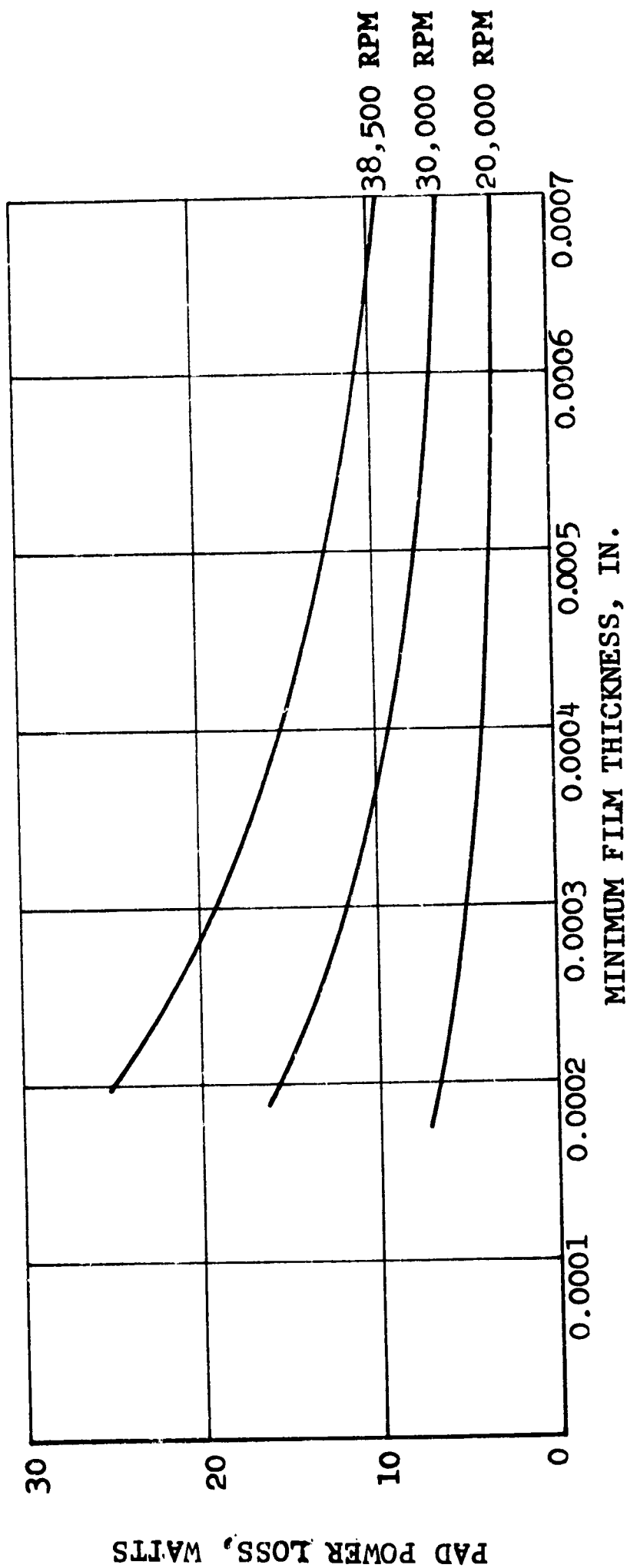


PREDICTED TURBOCOMPRESSOR  
JOURNAL BEARING PAD LOAD  
VS MINIMUM FILM THICKNESS

FIGURE 3

NOTES:

1.  $L/D = 0.75$
2. JOURNAL RADIUS = 0.875 IN.
3. ARC LENGTH =  $100^\circ$
4. PIVOT POINT:  $65^\circ$
5. CLEARANCE RATIO = 0.0026
6. AMBIENT PRESSURE = 6.0 PSIA
7. LUBRICANT: ARGON AT  $80^\circ\text{F}$
8. VISCOSITY =  $3.3 \times 10^{-8}$  REYNS

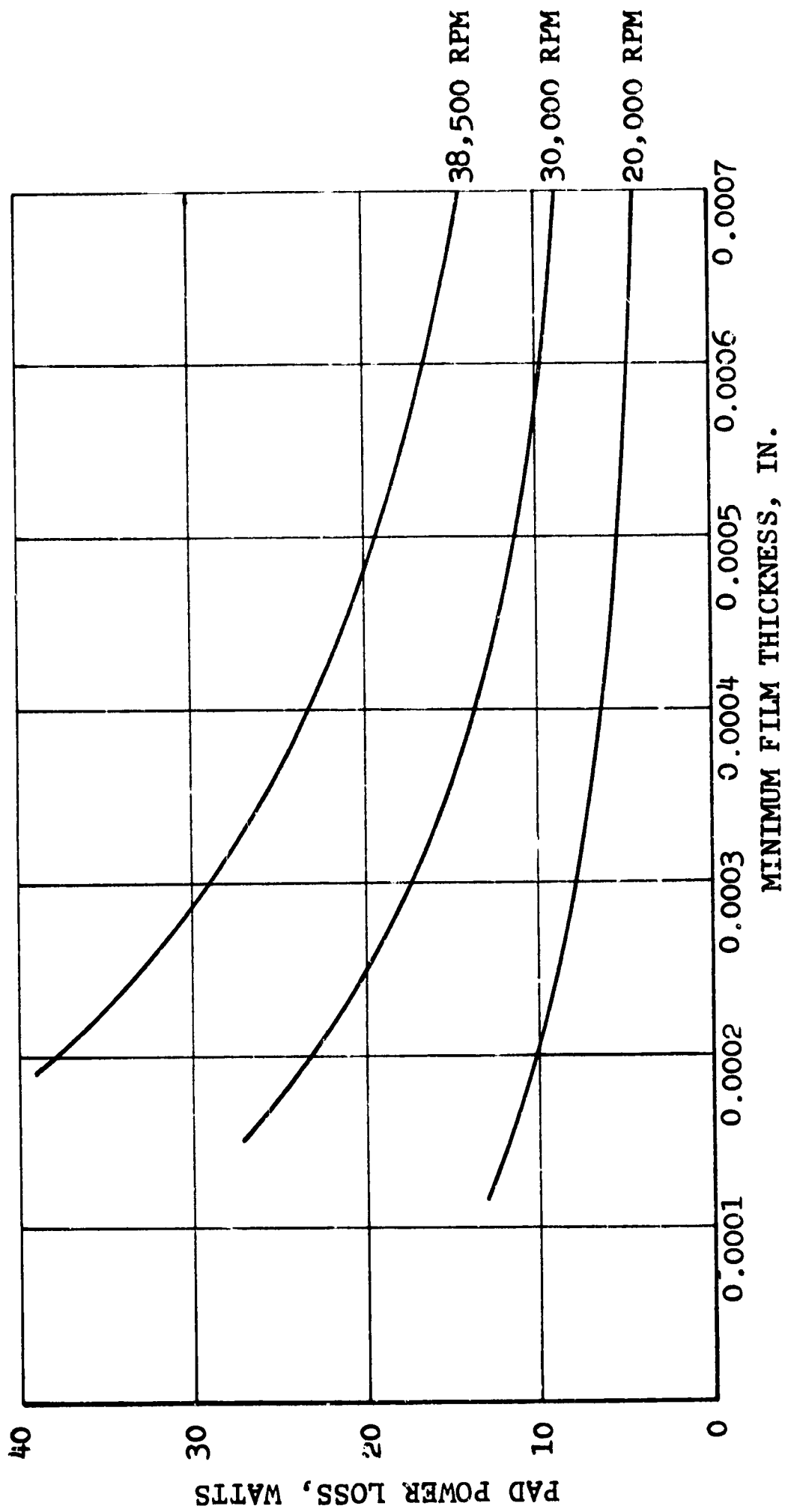


PREDICTED TURBOCOMPRESSOR JOURNAL BEARING PAD  
FRICTION VS MINIMUM FILM THICKNESS

FIGURE 4

NOTES:

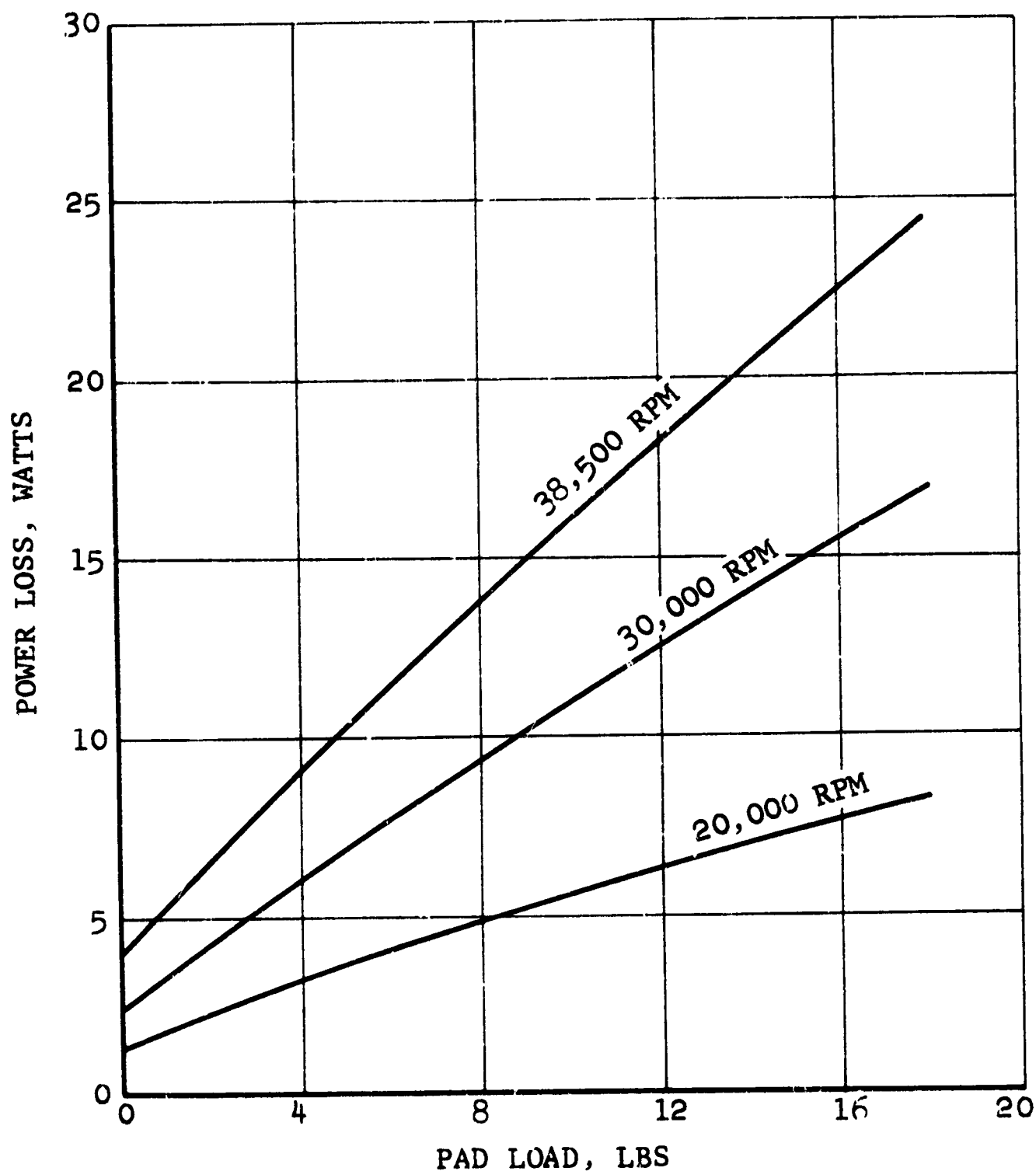
1.  $L/D = 0.75$
2. JOURNAL RADIUS = 0.875 IN.
3. ARC LENGTH =  $100^\circ$
4. PIVOT POINT:  $65^\circ$
5. CLEARANCE RATIO = 0.0026
6. AMBIENT PRESSURE = 6.0 PSIA
7. LUBRICANT: ARGON AT  $500^\circ\text{F}$
8. VISCOSITY =  $5.0 \times 10^{-8}$  REYNS



PREDICTED TURBOCOMPRESSOR JOURNAL BEARING PAD  
FRICTION VS MINIMUM FILM THICKNESS

FIGURE 5

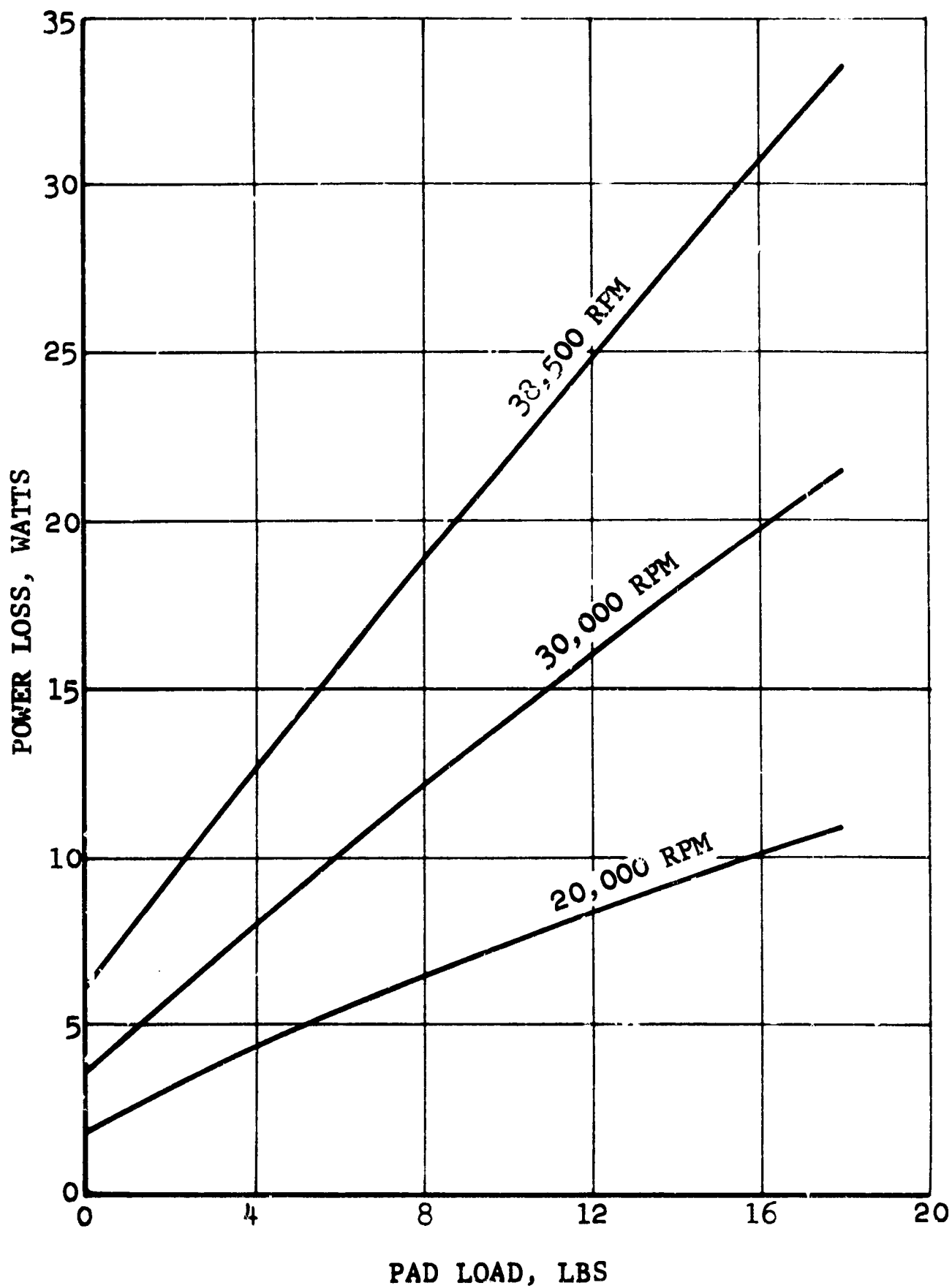
- NOTES: 1.  $L/D = 0.75$   
2. JOURNAL RADIUS = 0.875 IN.  
3. ARC LENGTH =  $100^\circ$   
4. PIVOT POINT:  $65^\circ$   
5. CLEARANCE RATIO = 0.0026  
6. AMBIENT PRESSURE = 6.0 PSIA  
7. LUBRICANT: ARGON AT  $80^\circ\text{F}$   
8. VISCOSITY =  $3.3 \times 10^{-9}$  REYNS



PREDICTED TURBOCOMPRESSOR  
JOURNAL BEARING PAD LOAD VS FRICTION

FIGURE 6

- NOTES:
1.  $L/D = 0.75$
  2. JOURNAL RADIUS = 0.875 IN.
  3. ARC LENGTH =  $100^\circ$
  4. PIVOT POINT:  $65^\circ$
  5. CLEARANCE RATIO = 0.0026
  6. AMBIENT PRESSURE = 6.0 PSIA
  7. LUBRICANT: ARGON AT  $500^\circ\text{F}$
  8. VISCOSITY =  $5.0 \times 10^{-8}$  REYNS

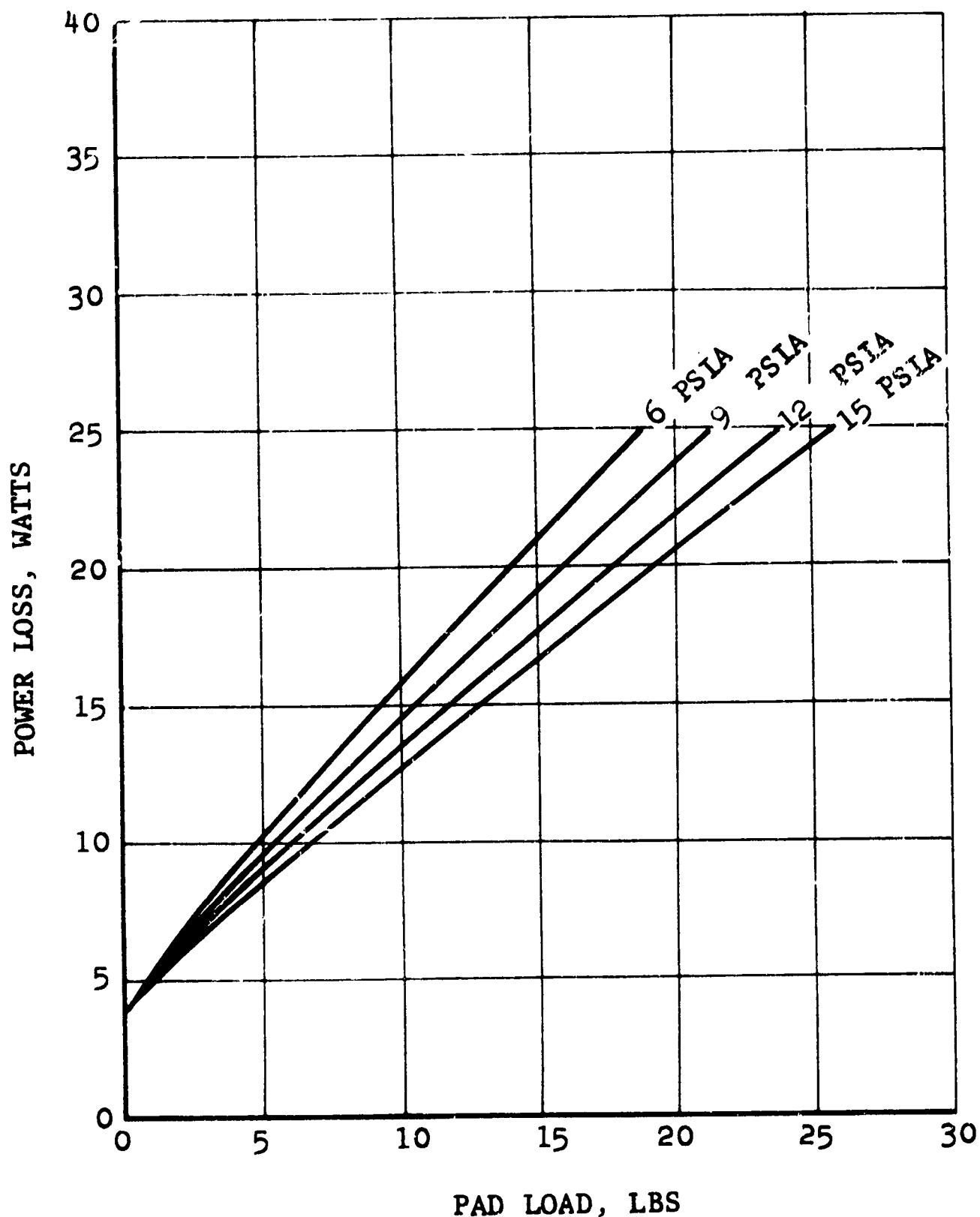


PREDICTED TURBOCOMPRESSOR  
JOURNAL BEARING PAD LOAD VS FRICTION

FIGURE 7



- NOTES:
1.  $L/D = 0.75$
  2. JOURNAL RADIUS = 0.875 IN.
  3. ARC LENGTH =  $100^\circ$
  4. PIVOT POINT:  $65^\circ$
  5. CLEARANCE = 0.0021 IN. (ADJUSTED FOR GROWTH)
  6. LUBRICANT: ARGON AT  $80^\circ\text{F}$
  7. VISCOSITY =  $3.3 \times 10^{-8}$  REYNS
  8. SPEED = 38,500 RPM



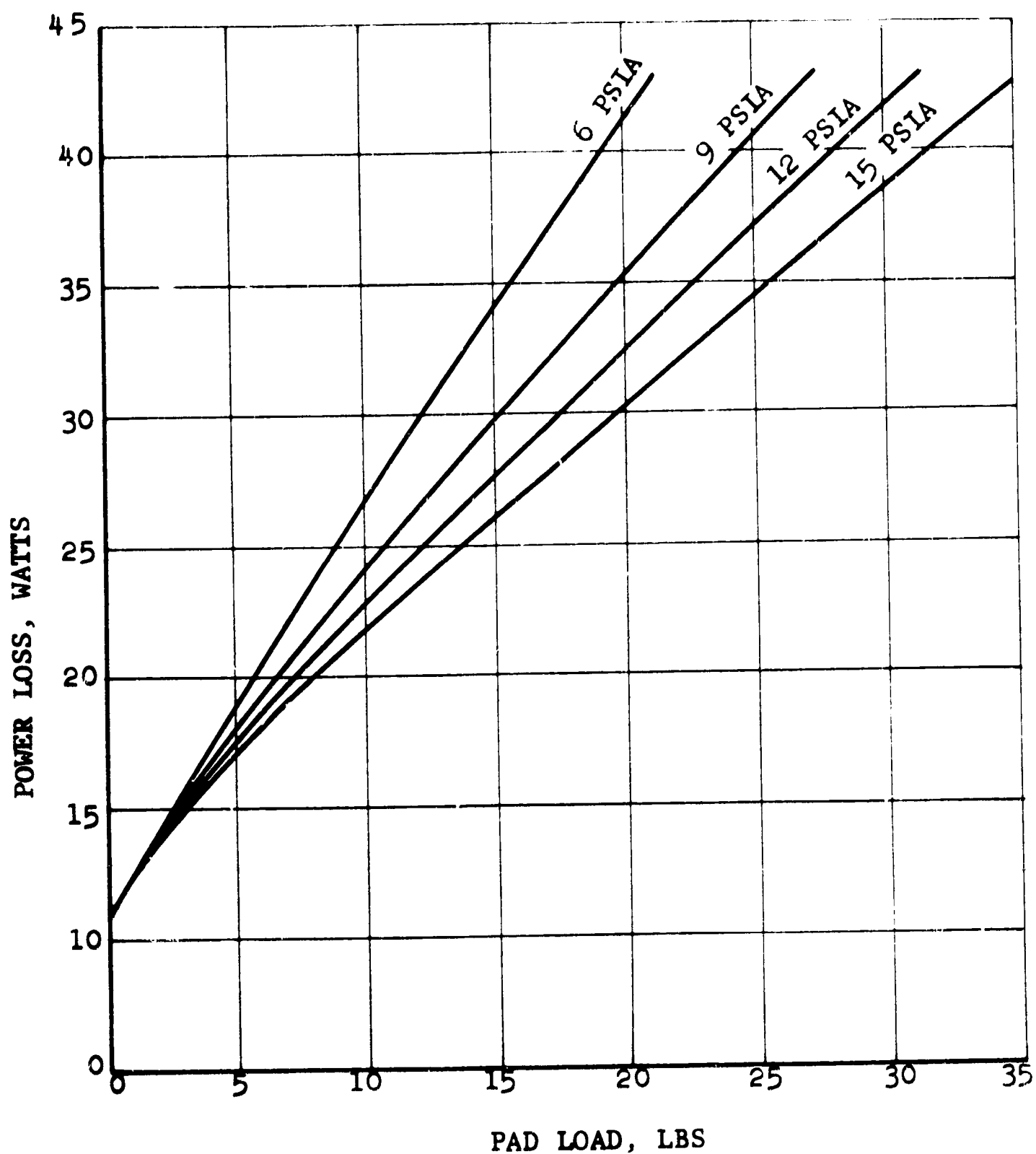
PREDICTED TURBOCOMPRESSOR JOURNAL BEARING PAD  
LOAD VS FRICTION AT VARIOUS AMBIENT PRESSURES AND  $80^\circ\text{F}$

FIGURE 8

NOTES:

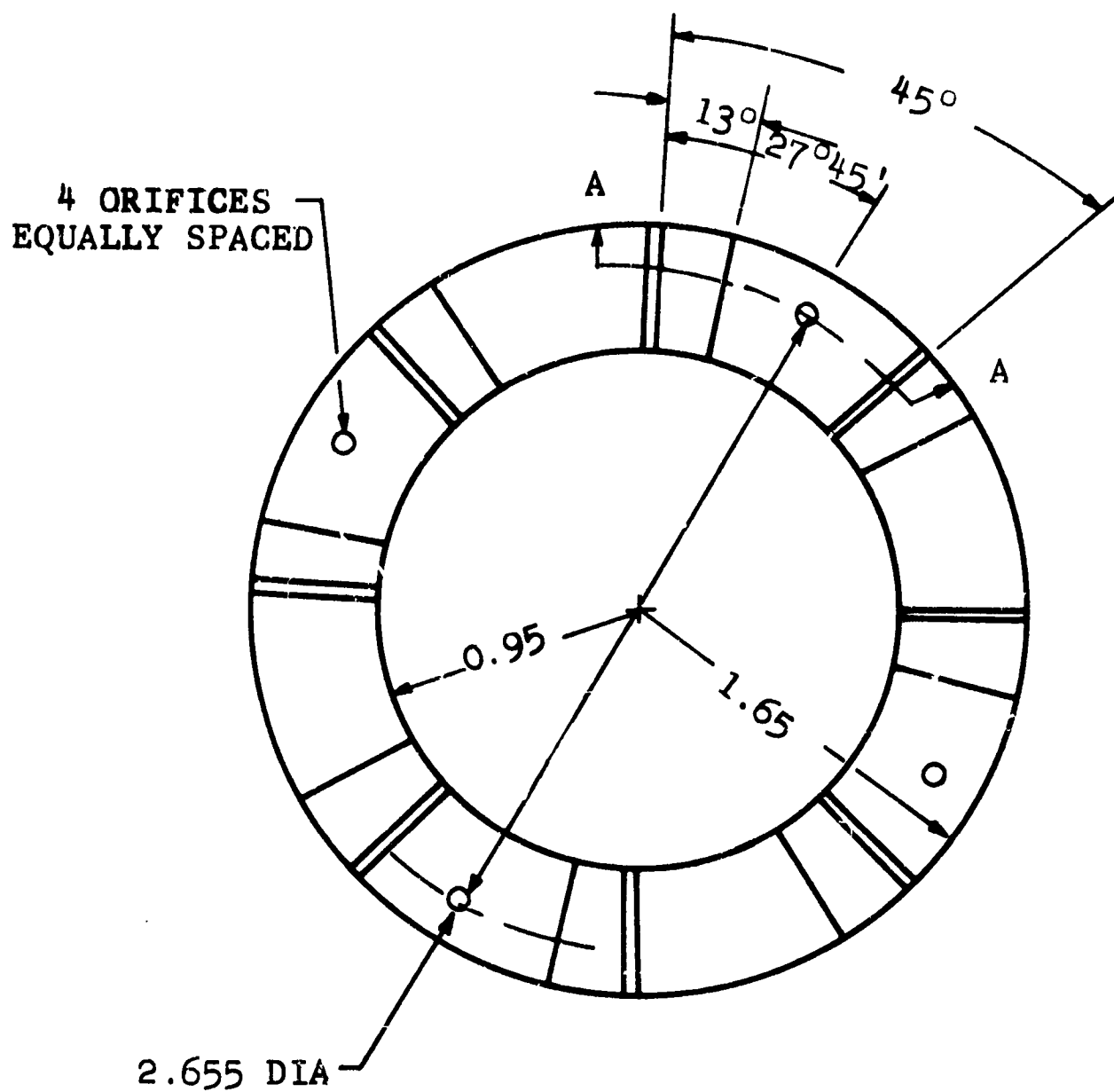
1. L/R = 0.75
2. JOURNAL RADIUS = 0.875 IN.
3. ARC LENGTH =  $100^\circ$
4. PIVOT POINT:  $65^\circ$

5. CLEARANCE 0.0021  
(ADJUSTED FOR GROWTH)
6. LUBRICANT: ARGON AT  $500^\circ\text{F}$
7. VISCOSITY  $5.0 \times 10^{-9}$  REYNS
8. SPEED 38,500 RPM

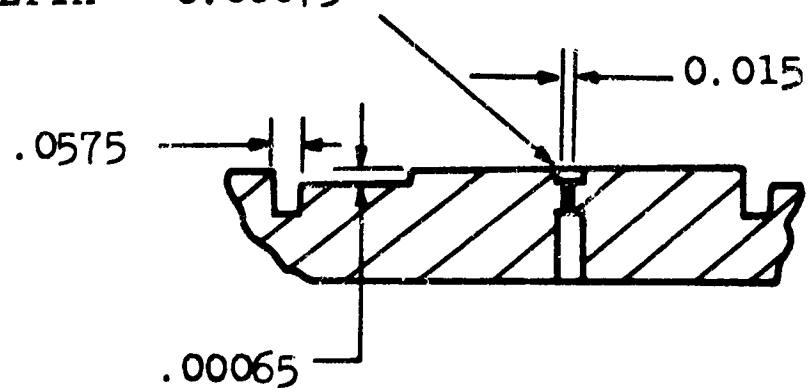


PREDICTED TURBOCOMPRESSOR JOURNAL BEARING PAD  
LOAD VS. FRICTION AT VARIOUS AMBIENT PRESSURES AND  $500^\circ\text{F}$

FIGURE 9



PAD DIA. = 0.08 IN.  
PAD DEPTH = 0.00075



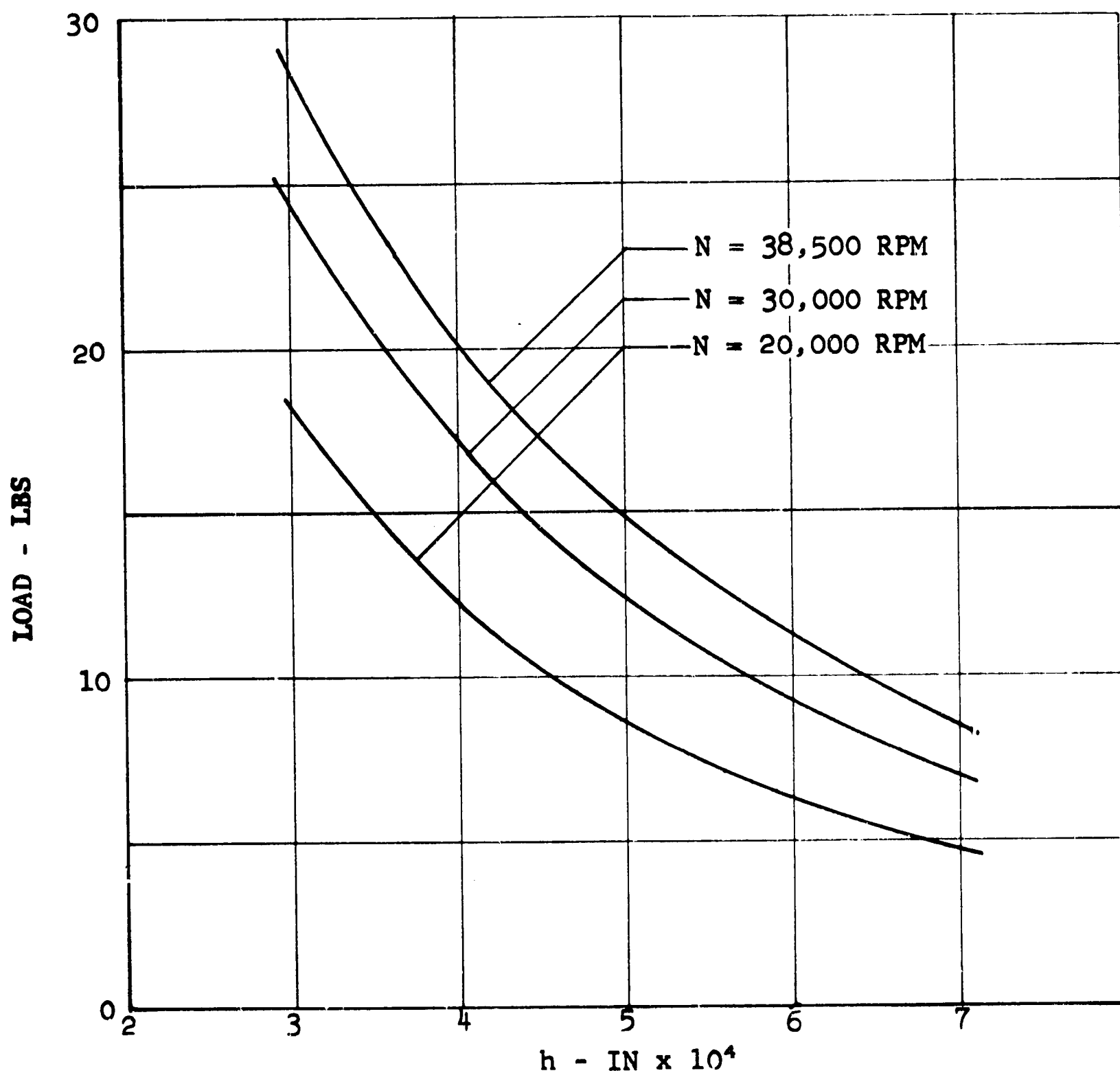
SECTION A - A

HYDRODYNAMIC THRUST BEARING GEOMETRY  
FOR NASA GAS GENERATOR

FIGURE 10

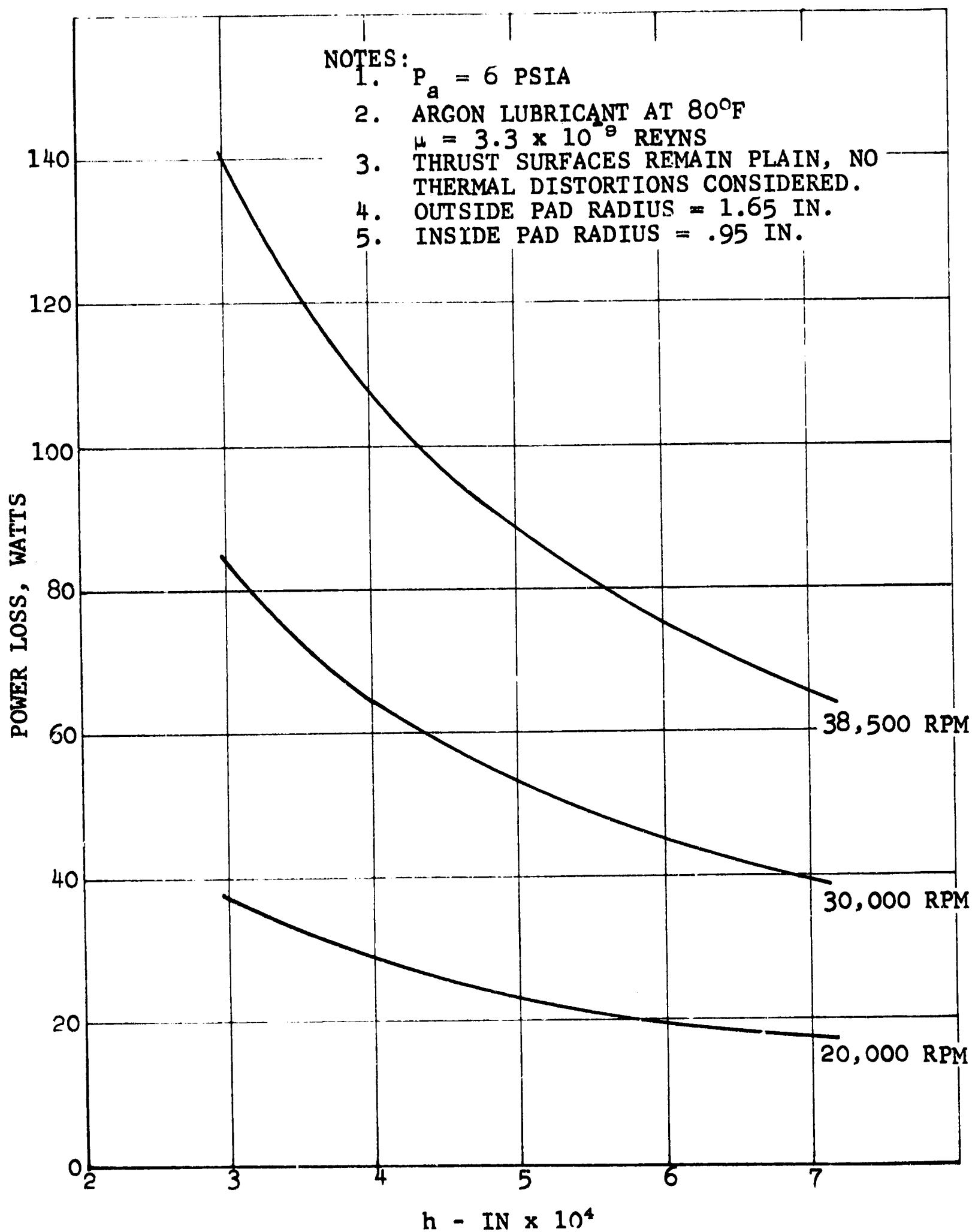
NOTES:

1.  $P_a = 6$  PSIA
2. ARGON LUBRICANT AT 80°F  
 $\mu = 3.3 \times 10^{-9}$  REYNS.
3. THRUST SURFACES REMAIN PLAIN,  
NO THERMAL DISTORTIONS CONSIDERED.
4. OUTSIDE PAD RADIUS = 1.65 IN.
5. INSIDE PAD RADIUS = .95 IN.



PREDICTED  
HYDRODYNAMIC PERFORMANCE  
OF THRUST BEARING FOR NASA  
TURBOCOMPRESSOR

FIGURE 11



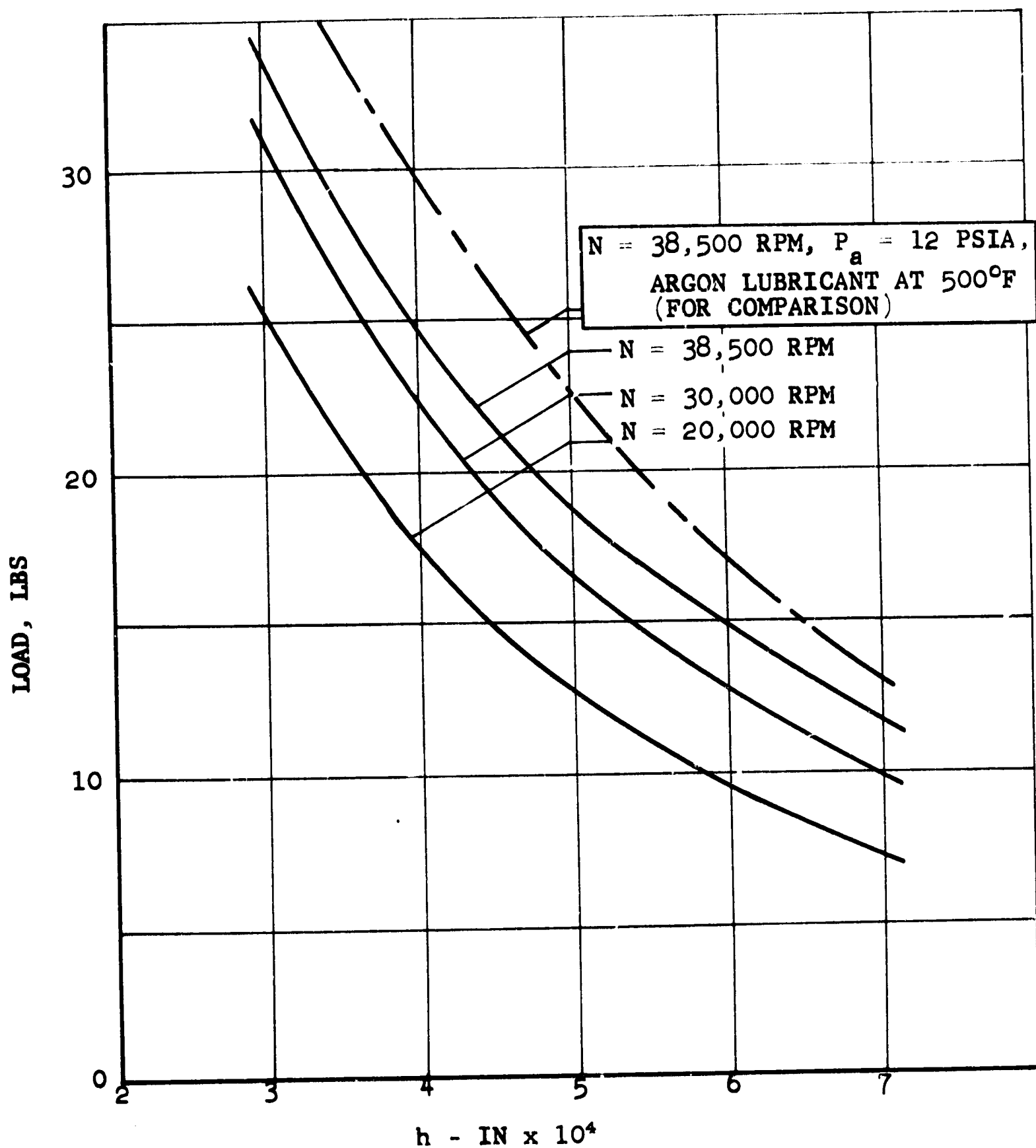
PREDICTED  
HYDRODYNAMIC PERFORMANCE  
OF THRUST BEARING FOR NASA  
TURBOCOMPRESSOR

FIGURE 12

NOTES:

1.  $P_a = 6$  PSIA
2. ARGON LUBRICANT AT  $500^\circ\text{F}$   
 $\mu = 5 \times 10^{-9}$  REYNS.
3. THRUST SURFACES REMAIN PLAIN,  
NO THERMAL DISTORTIONS CONSIDERED.

4. OUTSIDE PAD RADIUS 1.65 IN.
5. INSIDE PAD RADIUS .95 IN.

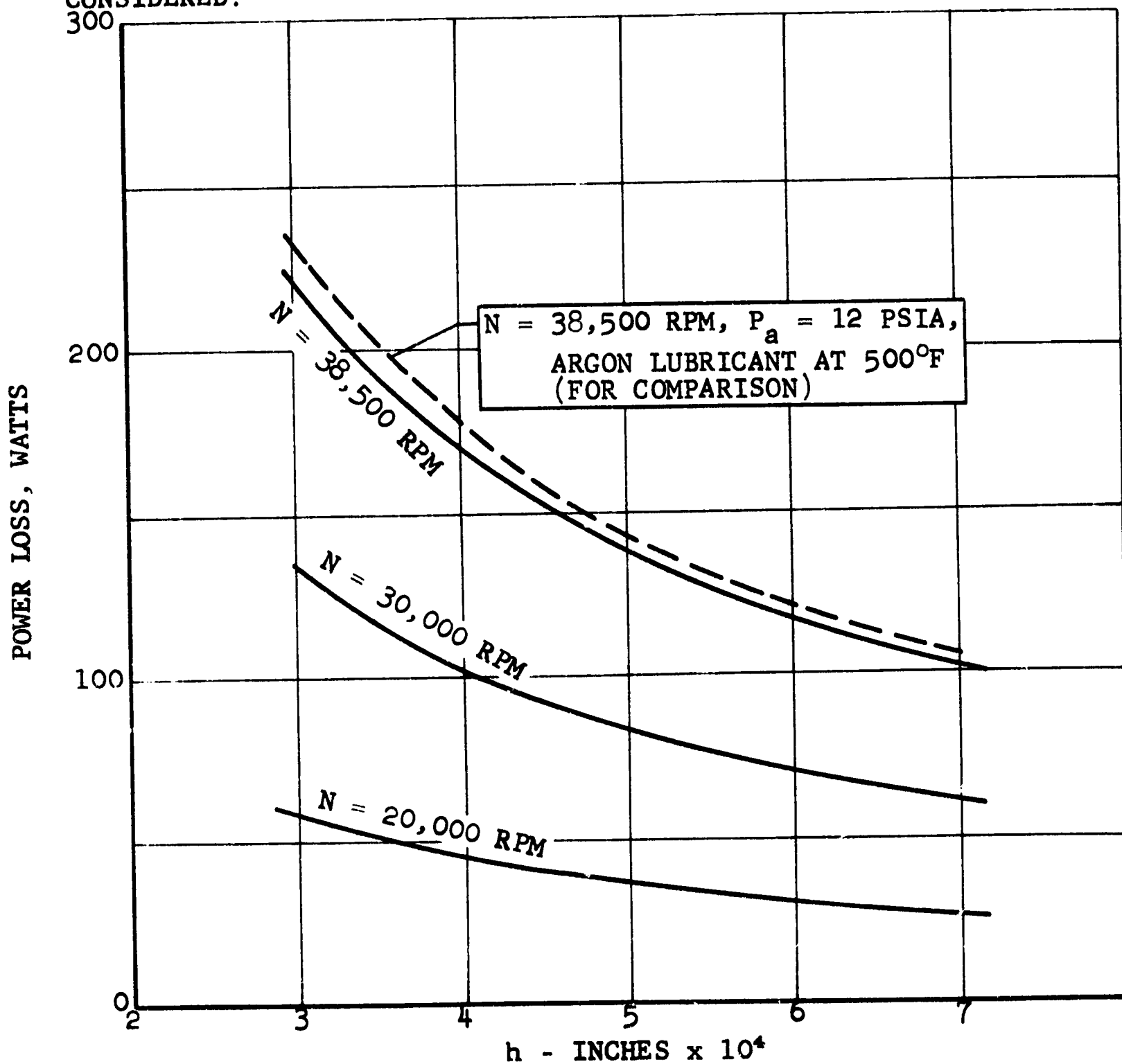


PREDICTED  
HYDRODYNAMIC PERFORMANCE  
OF THRUST BEARING FOR NASA  
TURBOCOMPRESSOR

FIGURE 13

NOTES:

1.  $P_a$  6 PSIA
2. ARGON LUBRICANT AT 500°F  
 $\mu$   $5 \times 10^{-9}$  REYNS
3. THRUST SURFACES REMAIN  
PLAIN, NO THERMAL DISTORTIONS  
CONSIDERED.
4. OUTSIDE PAD RADIUS 1.65 IN.
5. INSIDE PAD RADIUS .95 IN.



PREDICTED  
HYDRODYNAMIC PERFORMANCE  
OF THRUST BEARING FOR NASA  
TURBOCOMPRESSOR

FIGURE 14

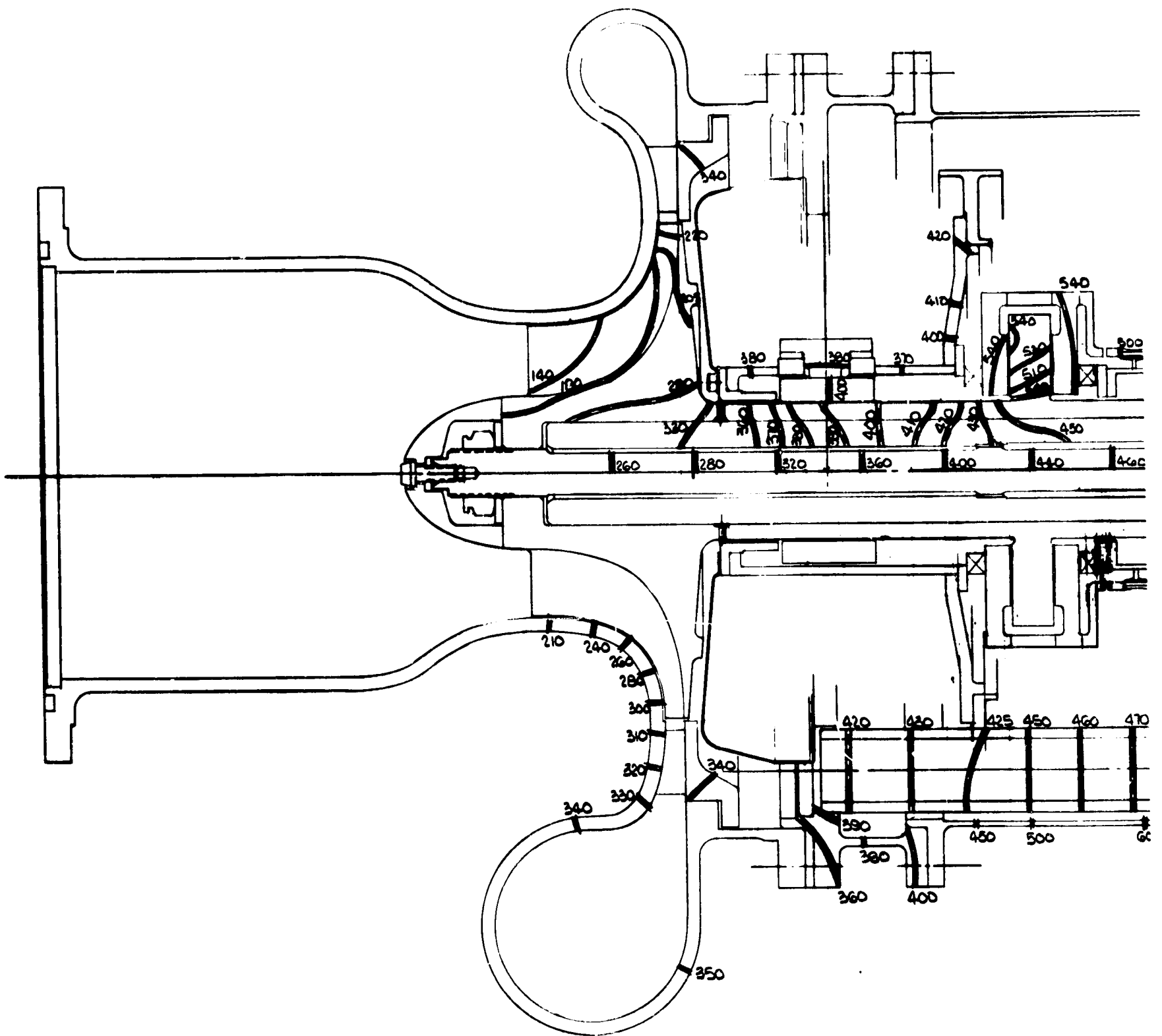
## 2.4 Turbocompressor Thermal Analysis at 6 psia Ambient \*

A complete thermal analysis of a piece of turbomachinery, such as the reference turbocompressor, is a laborious iterative process. In addition to the known thermal inputs to a computer program, some assumption must be made as to the bearing loads and resultant power losses. Once a preliminary thermal analysis is completed, the bearing loads may be computed from the differential thermal growths of the bearing carrier system and the rotor journals. These loads are then compared to the assumed loads. If there are inconsistencies, new bearing loads are assumed and the process is repeated until there is good agreement between the assumed and calculated bearing loads.

A thermal analysis was performed on the reference turbocompressor for design conditions (12 psia) under NASA Contract NAS3-2778. That analysis was conducted to support a design review contractual requirement. Figure 15 presents the thermal map resulting from that analysis. It should be noted that radiation effects could not be handled by the computer program at the time of that analysis. Subsequent final design of the turbocompressor, and bearing integration tests, dictated some modifications in the turbocompressor hardware geometry from that assumed for the design review thermal analysis. Much later, the computer program was revised to handle radiation effects as well as the changes made to the actual turbocompressor hardware, and a revised thermal analysis was performed. The result of this late analysis (completed after the final Contract NAS3-2778) is presented in Figure 16. This thermal map is for the full-power (12-psia) condition and is presented to enable the reader to compare the relative operation of the turbocompressor at this condition to the anticipated operation at 6 psia. It should be noted that all thermal analyses performed under this contract, and reported herein, were accomplished with the revised computer program.

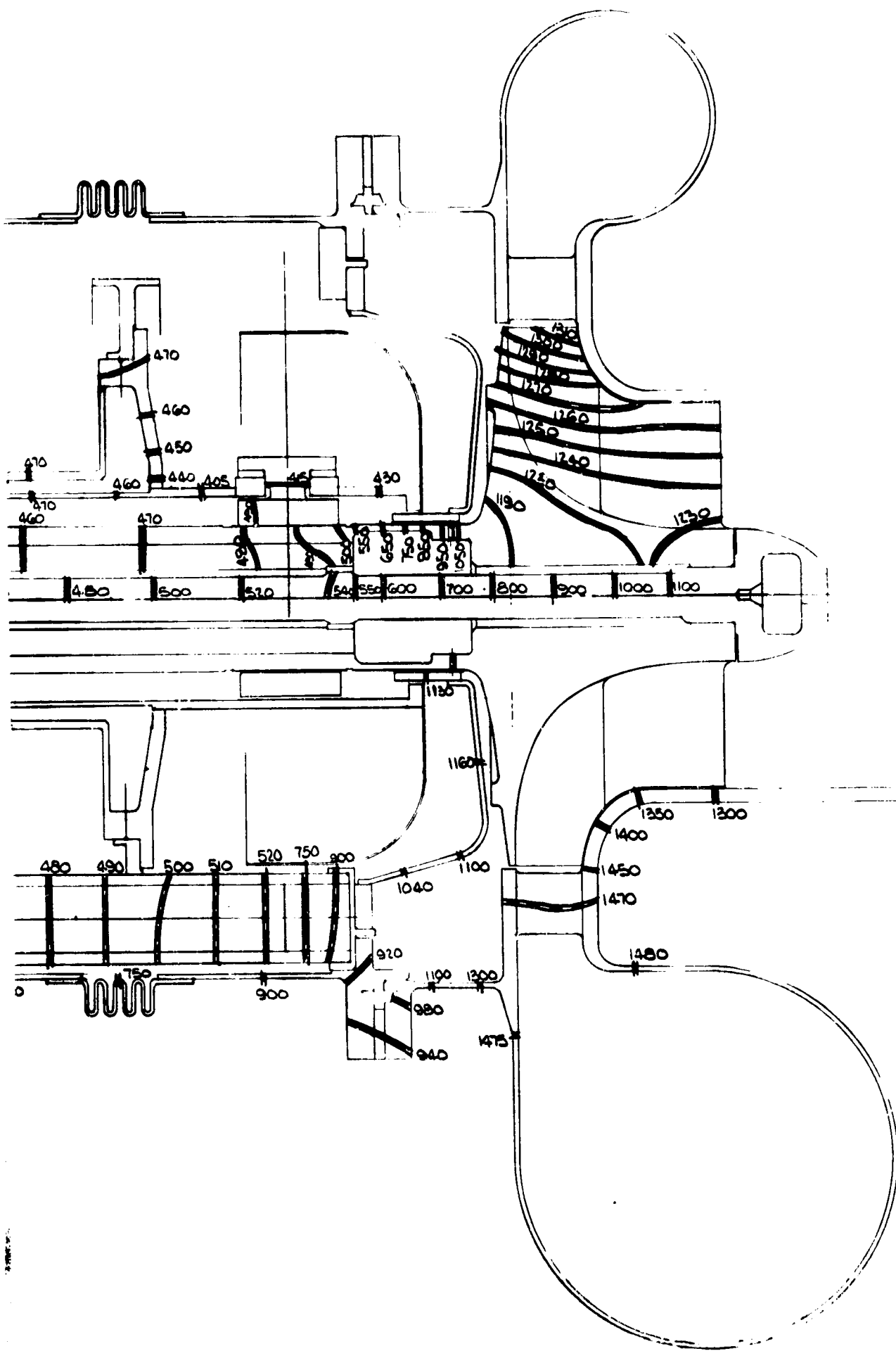
\*Applies only to a vertically oriented turbocompressor rotor with negligible bearing loads.





**ASSUMED CONDITIONS:**

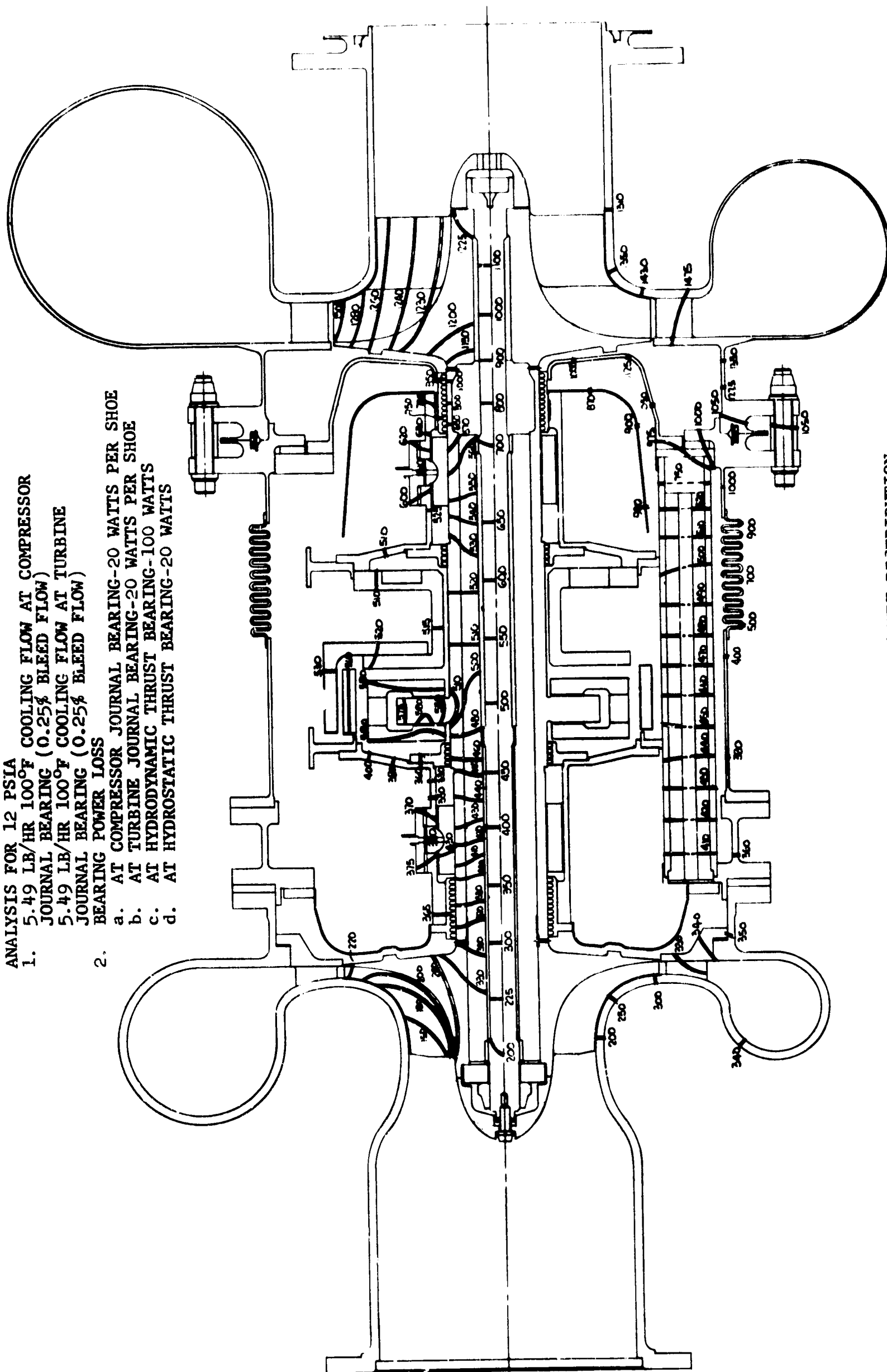
1. 25%-100°F COOLING FLOW AT COMPRESSOR JOURNAL BEARING  
25%-100°F COOLING FLOW AT TURBINE JOURNAL BEARING
2. BEARING POWER LOSS
  - a. AT JOURNALS-20 WATTS PER SHOE
  - b. AT HYDRODYNAMIC THRUST BEARING-100 WATTS
  - c. AT HYDROSTATIC THRUST BEARING-20 WATTS



PRELIMINARY STEADY STATE TEMPERATURE DISTRIBUTION,  
N.A.S.A. BRAYTON CYCLE GAS GENERATOR

FIGURE 10  
TEMPERATURE DISTRIBUTION

- ALL TEMPERATURES, °F  
 ASSUMED CONDITIONS FOR STEADY STATE  
 ANALYSIS FOR 12 PSIA
1. 5.49 LB/HR 100°F COOLING FLOW AT COMPRESSOR JOURNAL BEARING (0.25% BLEED FLOW)
  - 5.49 LB/HR 100°F COOLING FLOW AT TURBINE JOURNAL BEARING (0.25% BLEED FLOW)
  2. BEARING POWER LOSS
    - a. AT COMPRESSOR JOURNAL BEARING-20 WATTS PER SHOE
    - b. AT TURBINE JOURNAL BEARING-20 WATTS PER SHOE
    - c. AT HYDRODYNAMIC THRUST BEARING-100 WATTS
    - d. AT HYDROSTATIC THRUST BEARING-20 WATTS



FINAL STEADY-STATE TEMPERATURE DISTRIBUTION  
 BRAYTON-CYCLE GAS GENERATOR

FIGURE 16

**BLANK PAGE**

Due to the rather limited scope of this program and the laborious task involved in conducting a complete thermal analysis, the Contractor, with the concurrence of the NASA, accomplished the required thermal analyses by making the following assumptions:

(a) Assumed Journal Bearing Power Losses

The differential thermal growths of the bearing carriers and rotor journals were calculated from the temperature distributions shown in the original thermal map, Figure 15 (historically this was the thermal map available at the start of this program). The journal bearing pad preloads (6.0 pounds at turbine journal and 5.4 pounds at the compressor journal as set in the delivered turbocompressor) were adjusted due to the above differential thermal growths and the rotor centrifugal growth at design operating speed (38,500 rpm). The adjusted preloads, coupled with the resilient mounts spring rate (4,000 lb-in.) when plotted on the journal bearing pad predicted performance curves (6 psia at 500°F), produce equilibrium pad loads of 17.0 pounds and 12.5 pounds at the turbine and compressor journals, respectively. These loads produce power losses of 32 and 25 watts per bearing pad, respectively.

(b) Assumed Hydrodynamic Thrust Bearing Power Loss

The net thrust load\* supported on the hydrodynamic thrust bearing of the reference turbogenerator has been calculated to be approximately 16 pounds at the full-power design condition. However, this value has not as yet been substantiated by testing. For purposes of this analysis, the same net thrust load was assumed for the half-power turbogenerator analysis. This assumption is conservative and should cover unforeseen contingencies in calculated

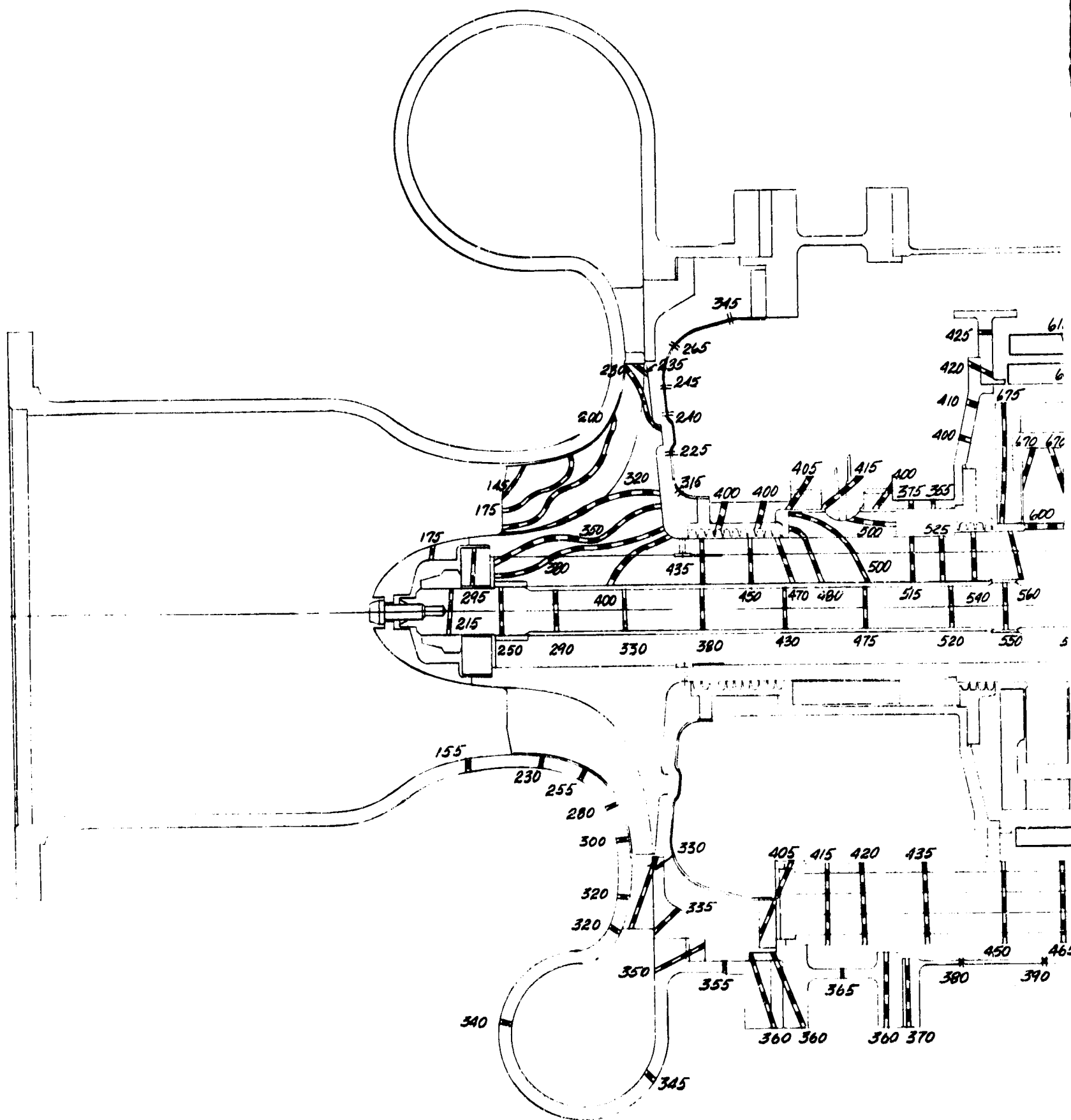
\*Net thrust load here refers to the aerodynamic thrust load minus the 1-g weight of the vertically oriented turbocompressor rotor.

thrust load determinations. The power loss corresponding to this load (16 pounds) is 120 watts at the 6-psia ambient condition at 500°F. The parasitic power loss of the reverse hydrostatic thrust bearing which is unloaded (approximate 0.004-inch film thickness) was calculated to be 24 watts.

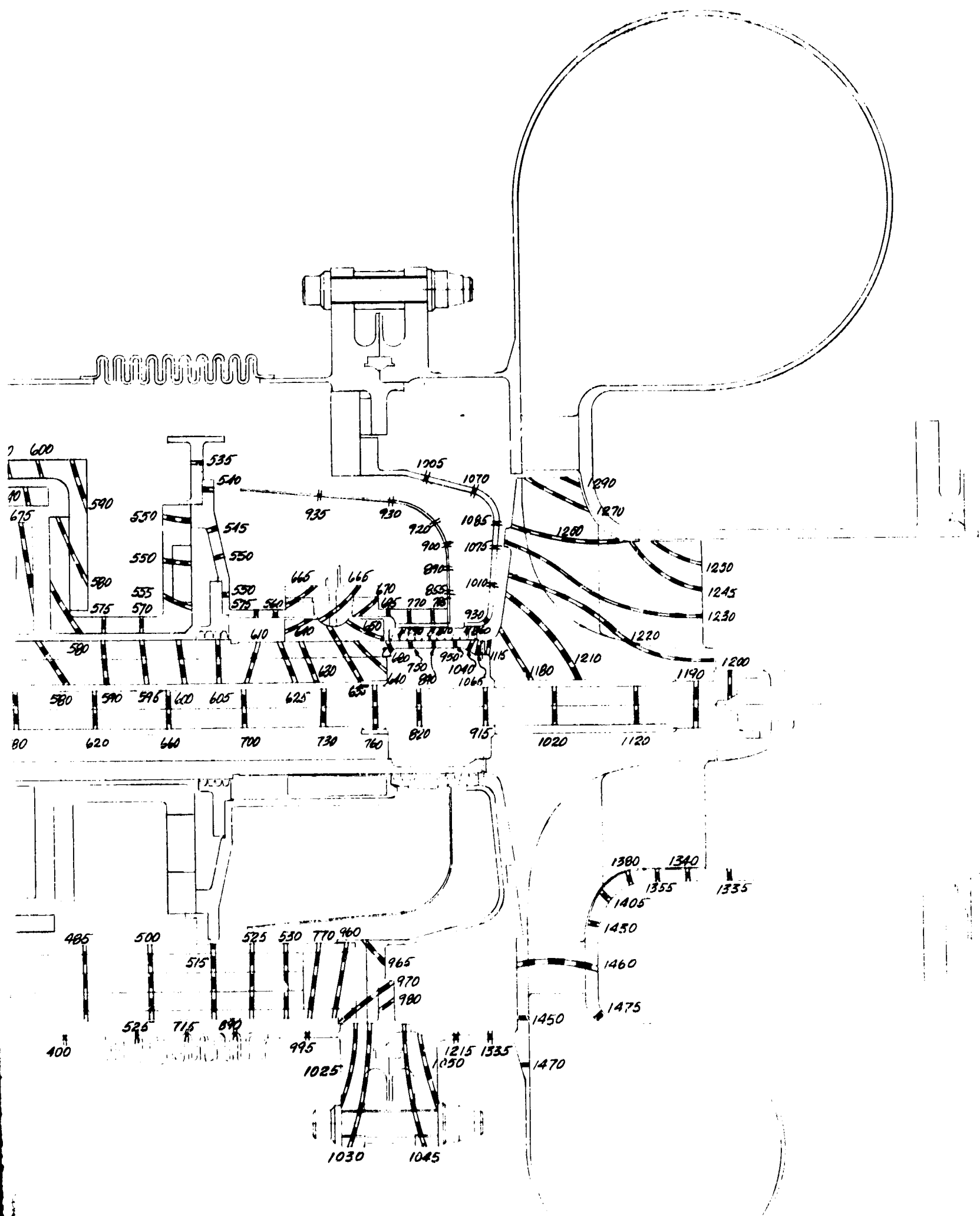
(c) Assumed Cycle Bleed Cooling Flow Rates

Gaseous cooling of the turbocompressor journal bearings is accomplished by extracting bleed flow from the compressor discharge. The cycle bleed flow recommended for the reference turbocompressor at full-power design conditions is a total of 0.5 percent (0.25 percent across each journal bearing). This percentage of bleed flow represents 5.49 pounds per hour of argon subcooled to 100°F per bearing. It was believed that the temperature levels throughout the turbocompressor at the 6 psia condition would be the same as for the full-power condition (12 psia) condition. Therefore, the same absolute value of bleed flow rate would be required. The same 5.49 pounds per hour argon bleed flow per bearing at the half-power condition represents a 1-percent cycle bleed flow. Two other bleed flows of 2 percent (10.98 pounds per hour to each bearing) and 4 percent (21.96 pounds per hour to each bearing) were also analyzed.

The results of the thermal analyses for cycle bleed cooling flows of 1, 2, and 4 percent are shown in Figures 17, 18, and 19.



ALL TEMPERATURE, °F  
 ASSUMED CONDITIONS FOR STEADY-STATE  
 ANALYSIS FOR 6 PSIA  
 1-5.49 LB/HR, 100°F COOLING FLOW AT COMPRESSOR  
 JOURNAL BEARING (0.5% BLEED FLOW)  
 5.49 LB/HR, 100°F COOLING FLOW AT TURBINE  
 JOURNAL BEARING (0.5% BLEED FLOW)  
 2-BEARING POWER LOSS  
 a. AT COMPRESSOR JOURNAL BEARING-25 WATTS  
 b. AT TURBINE JOURNAL BEARING-32 WATTS PER  
 c. AT HYDRODYNAMIC THRUST BEARING-120 WATTS  
 d. AT HYDROSTATIC THRUST BEARING-24 WATTS



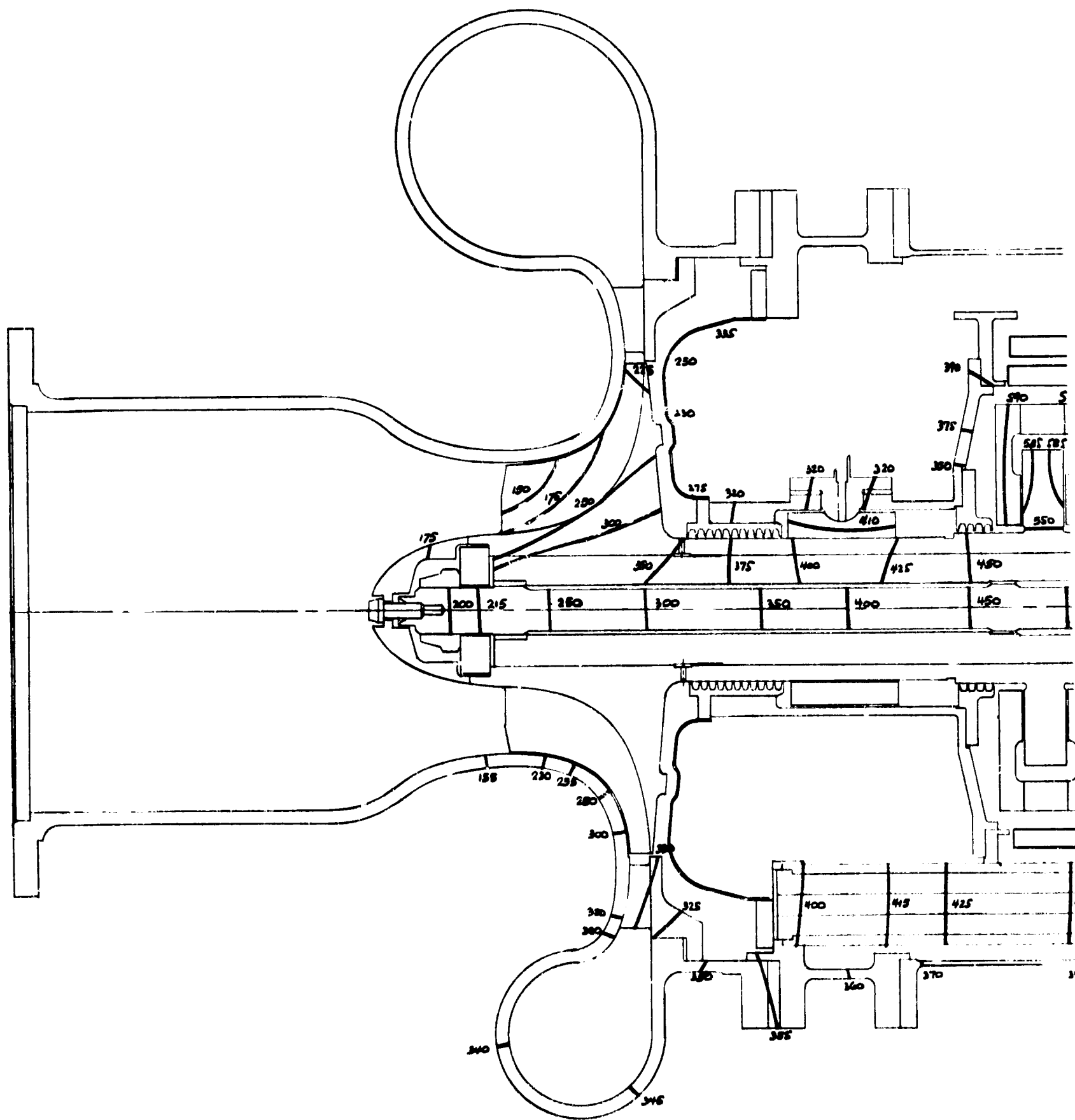
THERMAL ANALYSIS, N.A.S.A. BRAYTON CYCLE  
GAS GENERATOR, 6 PSIA

FIGURE 17  
APS-5223-R  
Page 2

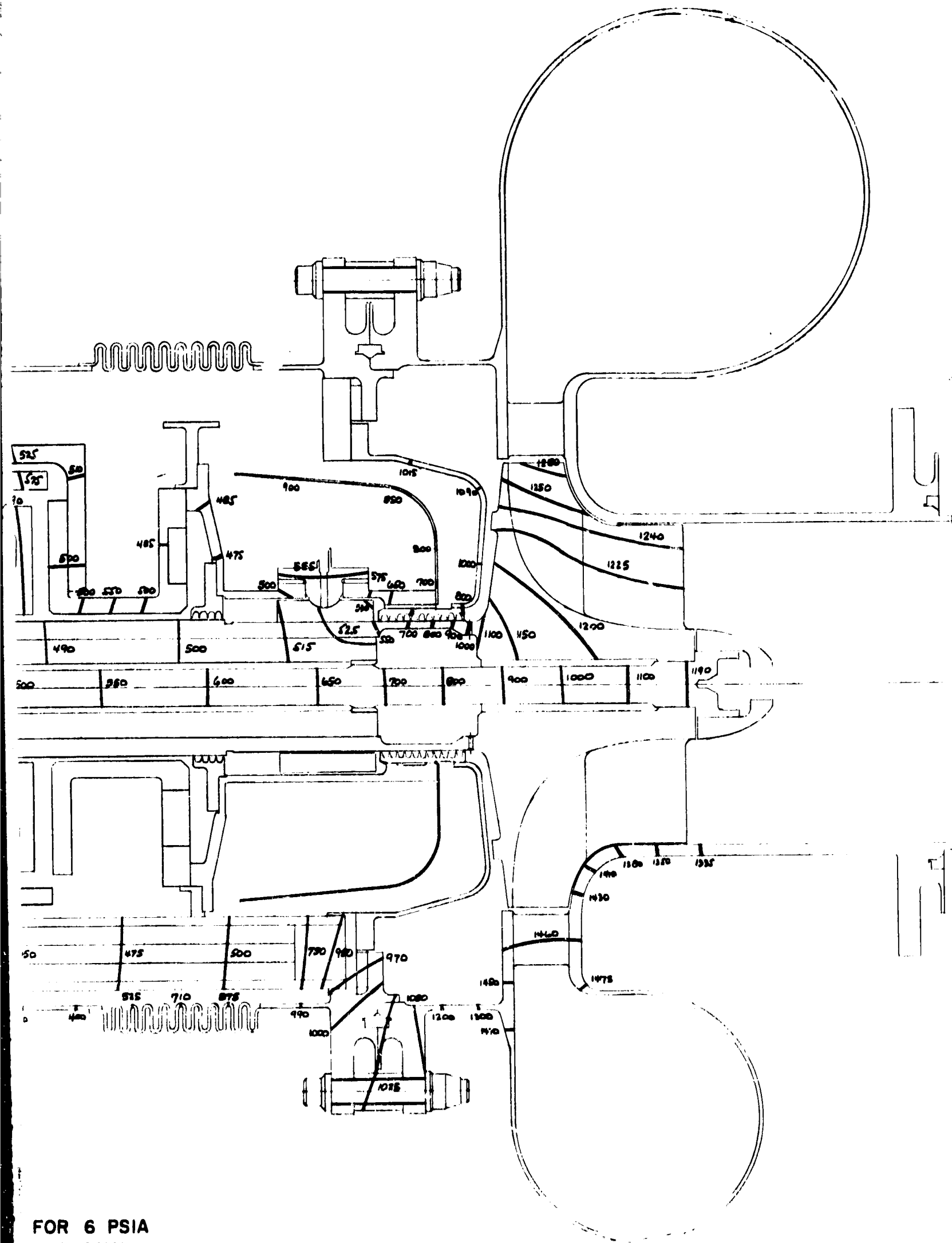
OR

PER SHOE  
SHOE





ALL TEMPERATURES, °F  
 ASSUMED CONDITIONS FOR STEADY STATE ANALYSIS  
 1 10.98 LB/HR 100 °F COOLING FLOW AT COMPRESSOR BEARING (1.0% BLEED FLOW)  
 10.98 LB/HR 100 °F COOLING FLOW AT TURBINE JO (1.0% BLEED FLOW)  
 2 BEARING POWER LOSS  
 a. AT COMPRESSOR JOURNAL BEARING-25 WATTS PE  
 b. AT TURBINE JOURNAL BEARING-32 WATTS PER S  
 c. AT HYDRODYNAMIC THRUST BEARING-120 WATTS  
 d. AT HYDROSTATIC THRUST BEARING-24 WATTS



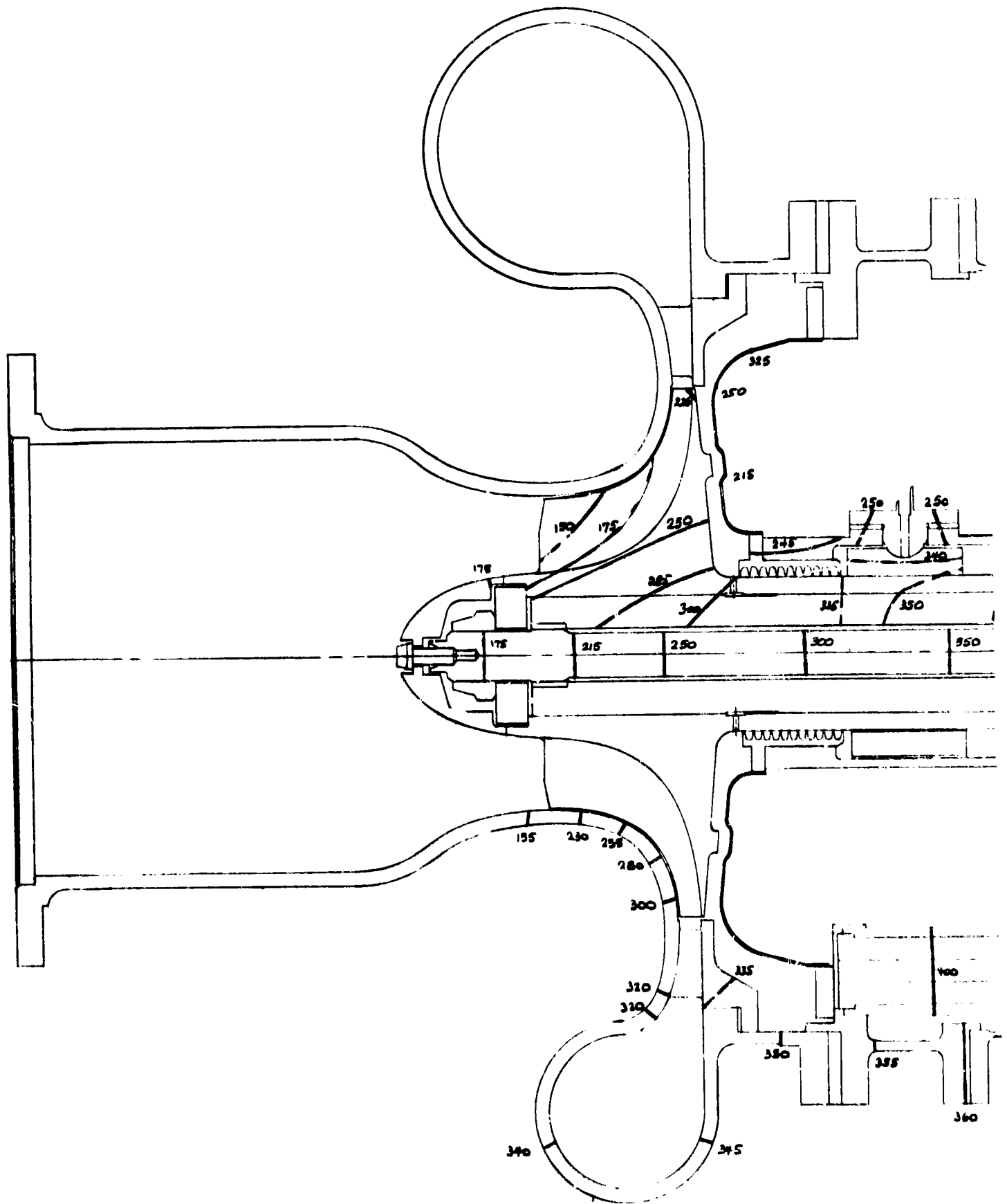
FOR 6 PSIA  
JOURNAL

JOURNAL BEARING

R SHOE  
SHOE

# THERMAL ANALYSIS, NASA BRAYTON-CYCLE GAS GENERATOR, 6 PSIA

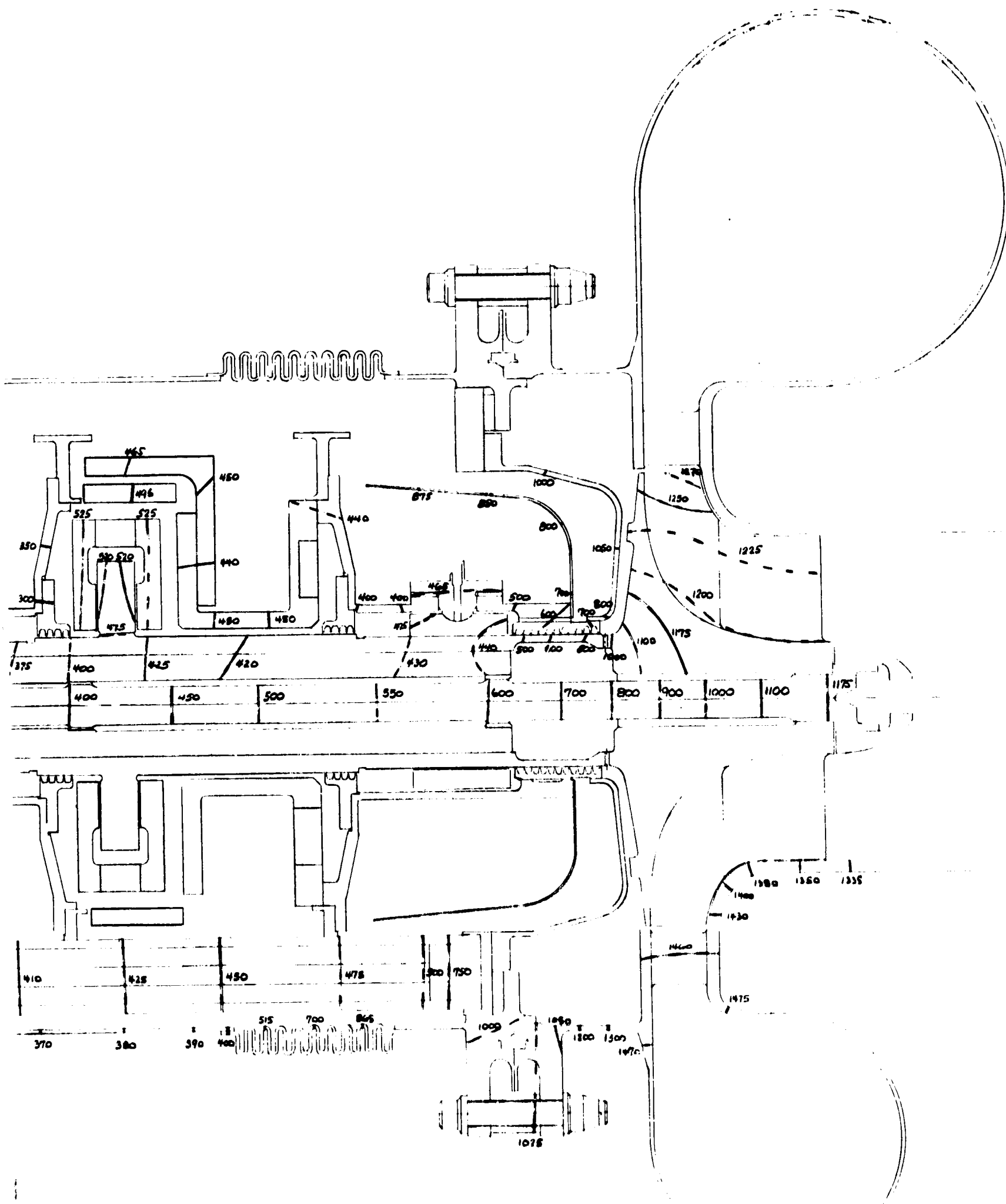
FIGURE 18  
APS-5223-R  
Page 29



ALL TEMPERATURES, °F

ASSUMED CONDITIONS FOR STEADY STATE ANALYSIS FOR 6

1. 21.96 LB/HR 100°F COOLING FLOW AT COMPRESSOR JOURNAL  
21.96 LB/HR 100°F COOLING FLOW AT TURBINE JOURNAL
2. BEARING POWER LOSS
  - a. AT COMPRESSOR JOURNAL BEARING - 25 WATTS PER
  - b. AT TURBINE JOURNAL BEARING - 32 WATTS PER SHOE
  - c. AT HYDRODYNAMIC THRUST BEARING - 120 WATTS
  - d. AT HYDROSTATIC THRUST BEARING - 24 WATTS



6 PSIA  
 MAIN BRG (2.0% BLEED FLOW)  
 BRG (2.0% BLEED FLOW)

SHOE

THERMAL ANALYSIS,  
 NASA BRAYTON-CYCLE  
 GAS GENERATOR, 6 PSIA

FIGURE 19

APS-5223-R

Page 30-2

**BLANK PAGE**

## 2.5 Discussion of Results

Based on purely analytical methods\* the operation of the "as delivered" referenced turbocompressor at half-design-power conditions appears quite feasible. Two important criteria can be met, namely:

- (a) Adequate journal and thrust bearing load capacities are available at half-power ambient conditions. Operation to date with the reference turbocompressor with pad preloads of approximately 6.0 pounds has shown the bearing pad loads to range from approximately 7 to 20 pounds. These pad loads, at the 6-psia ambient condition at 500°F bearing temperature, will produce bearing pad pivotal clearances of 0.00059 and 0.00022 inch. These values are acceptable for successful turbocompressor operation. The 16-pound assumed load on the hydrodynamic thrust bearing will produce a lubricant film thickness of 0.00057 inch. Again, this is a reasonable value.
- (b) The turbine journal bearing can be maintained at approximately 525°F by utilizing a 2-percent cycle bleed cooling flow rate, subcooled to 100°F at the half-power condition. This bearing temperature can be reduced to approximately 435°F by utilizing a 4-percent cycle bleed cooling flow. The NASA desires a maximum journal bearing temperature of 500°F. This condition can be met by choosing the appropriate cycle bleed cooling flow rate.

\*The reader should note that the thermal analyses conducted during the course of this program are incomplete in that iteration was not continued to obtain total agreement between bearing power losses and steady-state temperatures.

Table 1 lists the predicted turbine end bearing temperature distribution of the reference turbocompressor at both full power level (12.0 psia ambient) and half power level (6.0 psia) with various bleed cooling flow rates. Also shown in this table is the predicted bearing temperature distribution based on the preliminary, and incomplete, thermal analysis shown in Figure 15. It should be remembered that the design of the turbocompressor was based on the preliminary thermal analysis. That analysis predicted an average bearing carrier temperature of  $415^{\circ}\text{F}$  and a rotor-bearing pad temperature of  $490^{\circ}\text{F}$  with a differential temperature (carrier temperature minus rotor-bearing pad temperature) of minus  $75^{\circ}\text{F}$ . Based on the steady-state minus  $75^{\circ}\text{F}$  temperature differential, materials in the bearing carrier region were chosen for thermal expansion properties such that at the steady-state temperatures (shown in Figure 15) the bearing pad loads would be very nearly the same as at start-up conditions. However, the results of the revised thermal analysis (Figure 16) are much more representative of the steady-state temperature distribution that will exist in the "as delivered" turbocompressor. In this case the predicted average turbine bearing carrier temperature is shown to be  $610^{\circ}\text{F}$  and the rotor-bearing pad temperature is  $560^{\circ}\text{F}$ . The differential temperature (as defined above) is a plus  $50^{\circ}\text{F}$ . Therefore, it can be predicted that the bearing carrier will grow away from the rotor, due to the adverse differential temperature gradients, which will produce lighter bearing pad loads. Although the "as delivered" turbocompressor has not been tested at full-power steady-state conditions, there are indications that these adverse thermal expansions will cause a nonsynchronous whirl of the rotor system. A duplicate of the reference turbocompressor was tested at the Contractor's facility several months after delivery of the NASA turbocompressor. The turbine inlet temperature was raised to approximately  $1550^{\circ}\text{F}$  during

"open-cycle" testing. Although steady-state temperatures were not attained during this test, the turbine bearing pad loads had reduced to such low values after 45 minutes of testing as to cause rotor whirl. The testing was terminated without incident. At the time of shutdown, the turbine bearing pad temperatures were approximately 600°F and the bearing carrier temperature 660°F (a differential temperature of plus 60°F). The NASA was apprised of these findings and informed that this condition could be rectified by reworking components in the turbine bearing carrier area to provide better control over the thermal gradients that produce these adverse differential growths.

As can be seen in Table 1, adverse thermal gradients are predicted in the turbine journal area at the 6-psia ambient half-power conditions. Therefore, it can be assumed that the bearing pad loads may be low enough to produce rotor instabilities. This area of turbocompressor operation at half-power conditions will be discussed further under Task II (Discussion).



TABLE 1  
PREDICTED TURBINE END BEARING TEMPERATURE  
DISTRIBUTION IN REFERENCE TURBOCOMPRESSOR

<u>Ambient Pressure psia</u>	<u>Bleed Cooling Flow Rate p Cycle Flow</u>	<u>Thermal Map Fig. No.</u>	<u>Turbine Bearing Carrier Avg Temp °F</u>	<u>Turbine Journal Avg Temp °F</u>	<u>Differential Temperature (Carrier Temp, Journal Temp) °F</u>
12*	0.5	15	415	490	-75
12**	0.5	16	610	560	+50
6	1.0	17	665	635	+30
6	2.0	18	555	525	+30
6	4.0	19	465	435	+30

\*Original thermal analysis for NASA Contract NAS3-2778.

\*\*Revised thermal analysis completed after termination of NASA Contract NAS3-2778

### 3.0 TASK II, GAS BEARING - ROTOR WHIRL INVESTIGATIONS

#### 3.1 General

The predicted bearing pad performance and thermal analyses covered under Task I partly define the off-performance operation of the turbocompressor. The important aspect of rotor dynamic stability for the reference "as delivered" turbocompressor gas journal bearing suspension system remains unanswered. In lieu of actually running the turbocompressor at off-performance conditions (to verify dynamic stability), there are two avenues of attacking this problem. One method would consist of the use of an orbital computer program, which is very time-consuming and costly. At the conclusion of such a program, experimentation would be necessary to verify the analytical results. Another method, and the one chosen for this program, is experimental in nature and supported by analyses to determine, if possible, which bearing pad parameters govern the lower threshold of whirl for a vertically oriented rotor.

Under the previous NASA contract, NAS3-2778, the Contractor designed and fabricated a two-bearing dynamic test rig, which was used to develop the journal bearings of the turbocompressor. This rig was used in this program to investigate the subsynchronous whirl threshold of a vertically oriented rotor as a function of the relative compressibility of the lubricant film. Specifically, the intention of the program was to determine if the bearing pad eccentricity ratio at whirl threshold could be plotted as a function of the bearing pad film compressibility number.

The bearing film compressibility number is usually represented by the dimensionless group:

$$\Lambda = \frac{6\mu\Omega}{P_a} \left(\frac{R}{C}\right)^2$$

where  $\mu$  = lubricant viscosity, lb sec. per sq in.

$\Omega$  = rotor angular speed, radians per second

$C$  = bearing clearance (dimension by which the bearing pad radius exceeds that of the rotor journal radius), inches

$P_a$  = ambient pressure, psia

$R$  = rotor journal radius, inches

At full-power design conditions ( $P_a = 12.0$  psia)  $\Lambda$  for the reference turbocompressor journal bearing pads is approximately 1.5. At half-power conditions (ambient pressure of 6 psia), the  $\Lambda$  value for the journal bearing pads would be approximately 3.0. This change of  $\Lambda$  is, in this case, a direct function of the ambient pressure,  $P_a$ . It can be seen that the value of  $\Lambda$  is also a function of other variables such as speed ( $\Omega$ ) and the ratio  $\left(\frac{R}{C}\right)$ . Therefore for experimental purposes on the two-bearing rig, with existing bearings, the two variables available for a change of the  $\Lambda$  value were the rotor angular speed ( $\Omega$ ) and journal radius ( $R$ ).

During the experimental program the compressibility number,  $\Lambda$ , was varied by establishing suitable bearing clearances and running over a specified speed range. At each speed point, the lowest

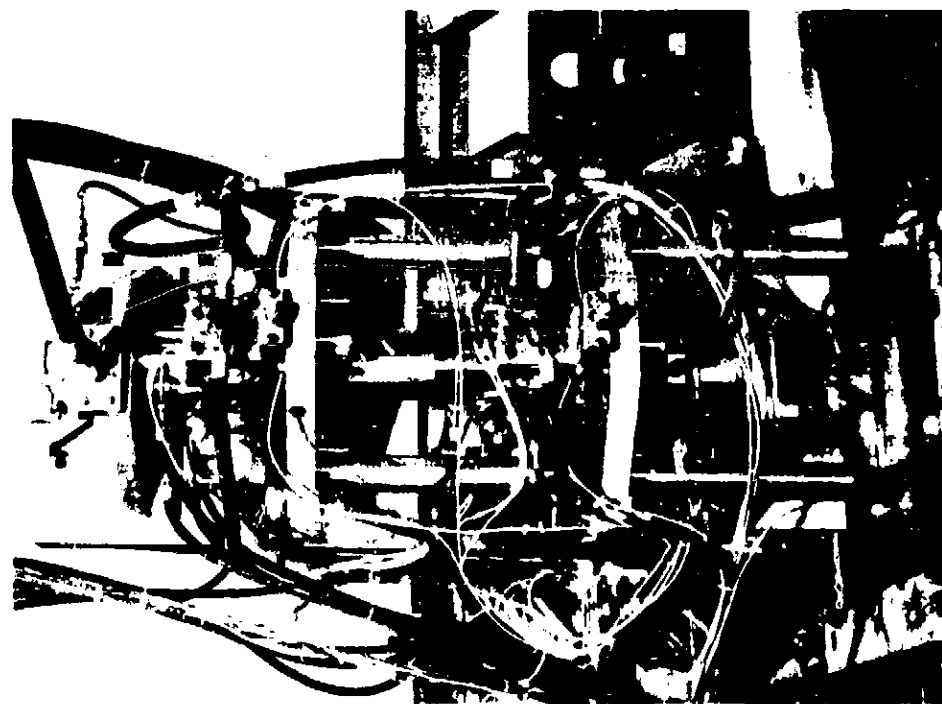
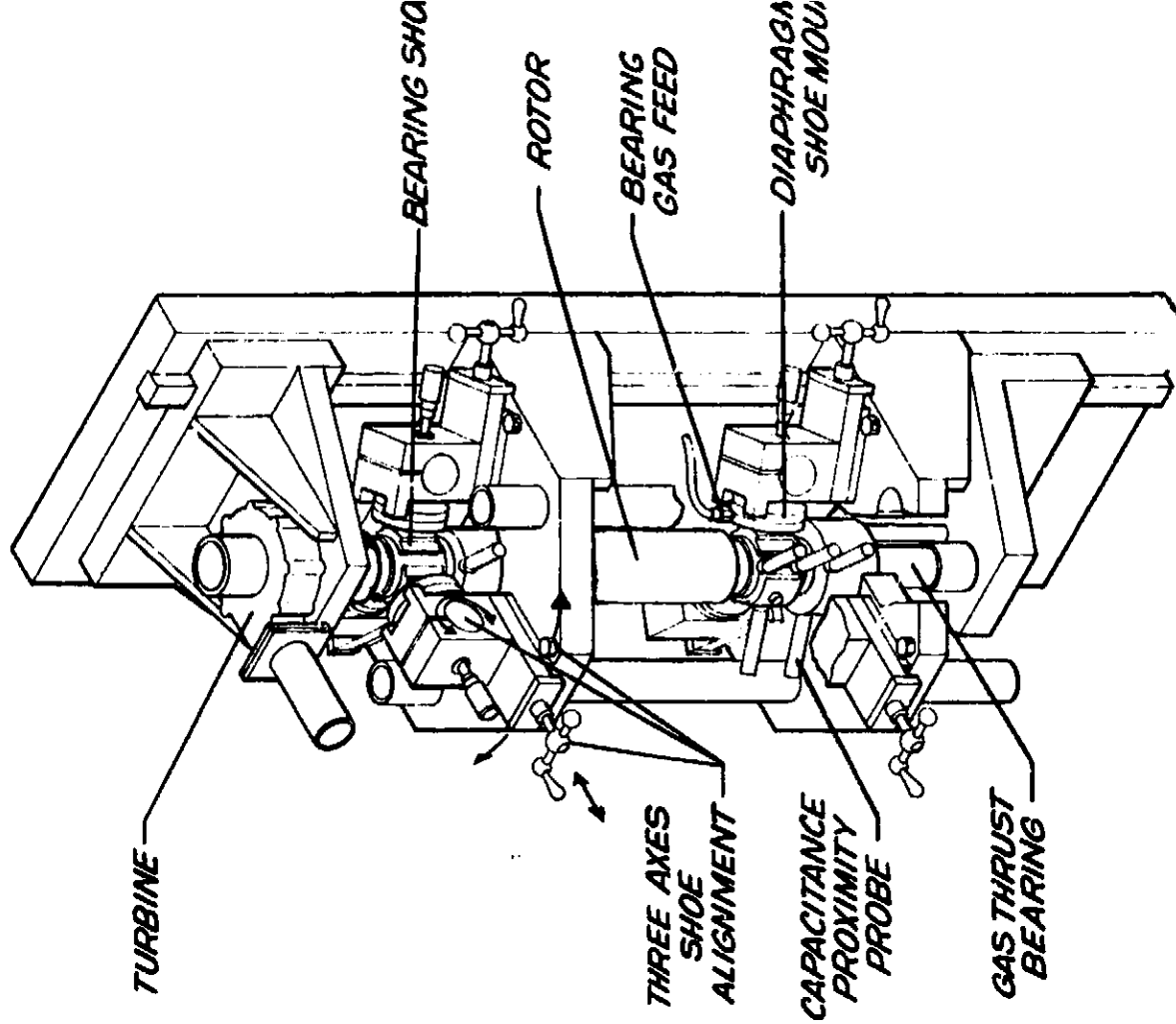
bearing pad load below which a resonant instability was observed was determined. The clearance values were chosen to provide nominal test values within a lambda range ( $\Lambda$ ) of 0.5 to 3.0. Thus, the same  $\Lambda$  value could be established in some cases at three different bearing clearances by suitably choosing the rotational speed for each configuration.

Since, for a vertically oriented rotor, the bearing pad eccentricity ratio ( $e$ ) is a function of bearing pad load and can be determined by use of a journal bearing pad computer program, it was believed that the final result of the data points might form a smooth plot of pad eccentricity ratio versus  $\Lambda$ . If such a relation exists, the information may be used to determine initial turbocompressor journal bearing pad preload necessary to provide the desired steady-state bearing eccentricity ratio for any desired  $\Lambda$  value (or ambient pressure level).

### 3.2 Test Rig

The two-bearing rotor dynamic test rig shown in Figure 20 was utilized throughout this development program to investigate the dynamic behavior as well as other aspects of the system comprising the gas bearings and test rotor.

The test rotor is vertically supported in the test rig and is driven by a turbine wheel mounted at the rotor upper end. A hydrostatic thrust bearing supports the rotor at the lower end. Each bearing pad assembly is secured to a support assembly. This support assembly is mounted to a track directed radially with respect to the rotor, and radial positioning of the assembly is



DYNAMIC TWO-BEARING TEST RIG  
FIGURE 20

provided by a calibrated screw thread. In addition, the support assembly has provision for pivoting of the bearing pad assembly about a horizontal axis directed perpendicularly to the track. Thus, the angular attitude of each bearing pad assembly (in the case of elastically pivoted pads tested under Task III) may be adjusted mechanically about three orthogonal axes, and any initial clearance or interference between the pads and shaft may be established.

The test-rig bearing support brackets are made so that the bearing span may be varied to accommodate rotors of various lengths.

Capacitance probes (Photocons), mounted in quadrature with respect to the rotor axes on each bearing bracket, monitor shaft dynamic motions in the radial direction near each bearing. A Photocon at the bottom of the rotor (at the thrust bearing surface) senses the axial motions of the rotor.

For each test, initial alignment of each bearing pad was obtained with the test rotor supported on alignment center pins at each end. After alignment was achieved, the center pins were removed, and the hydrostatic thrust bearing was replaced at the bottom of the shaft. The resilient supports consist of circular plates (diaphragms) with a known spring rate. Strain gauges cemented to these diaphragms were calibrated as functions of linear displacement of the bearing pad.

One each of these diaphragms at each of the bearing locations acted, in addition, as a variable loading device. This was accomplished by pneumatically pressurizing the back side of the diaphragm, which caused the diaphragm to bow toward the rotor center. The bearing pad preload was established by loading the pad against the rotor (which was on the alignment centers) with a specified diaphragm pressurization (10 psig for all testing accomplished under this program). Thus, any reduction in the diaphragm pressure lessened the pad load (this was accomplished during the operating test.) The strain-gauged diaphragms (circular plates) were previously calibrated with known deadweights at various diaphragm pressures (0, 2.5, 5.0, 7.5, and 10.0 psi). The two signals, diaphragm pressure, and strain-gauge output were then mapped as a function of bearing pad load. In practice, both diaphragms (one at each bearing location) were pressurized from a single source. The diaphragm pressure and the two strain-gauge signals (one from each bearing location) were displayed on two X-Y plotters which gave an instantaneous readout of bearing pad load at each journal position. Thus, the pad load at each bearing could be reduced, or increased, by reducing or increasing the diaphragm pressurization.

### 3.3 Instrumentation

The signals from the shaft capacitance probes, as well as the speed and voice channels, were connected to a 14-channel magnetic-tape recorder providing a means of recording the continuous history of the test runs. Visual observation of the capacitance probe outputs (Lissajous figures) was made on two oscilloscopes. The hydrostatic supply pressure, or pad hydrodynamic back pressure (during hydrodynamic operation), along with individual shoe temperatures, diaphragm strain-gauge output signals, and diaphragm pressure, were continuously monitored on a seven-channel Sanborn recorder.

### 3.4 Test Hardware

The test components for the test series were as follows:

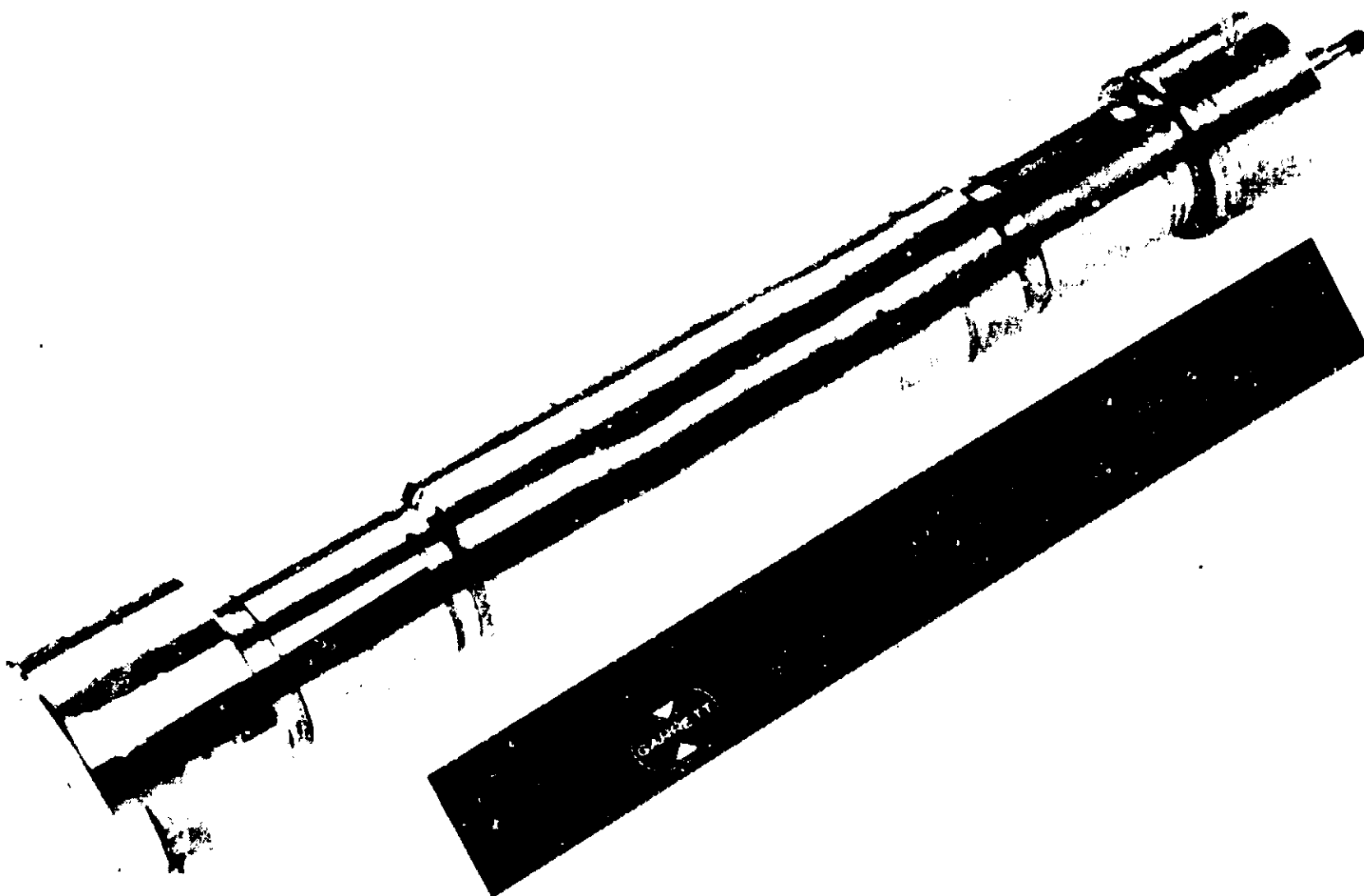
- (a) The 11-inch bearing span rotors are shown in Figures 21 and 22. The properties of the rotors are tabulated in Table 2.

These rotors have mass and inertial properties nominally similar to those of the reference turbocompressor.

- (b) Pivoted-pad bearing shoes (three per journal) with a diametral curvature of 2.0221 inches (see Figures 23 and 24). These shoes have an L/D ratio of 0.75, a pivot location of 65 percent back from the shoe leading edge, 100 degrees arc span, a spherical ball-socket pivot of 0.25-inch radius, and a hydrostatic lift-off system comprising four 0.010-inch-diameter orifices and 0.001/0.0005-inch-deep by 0.080/0.070-inch-diameter orifice pads.
- (c) A resilient mounting configuration comprising two fixed-ball ends and one spring ( a diaphragm or circular plate with approximately 2,075\*-pounds-per-inch- rate) per journal (Figure 25).

\*This spring rate varied during testing from 1,900 to 2,250 pounds per inch as a function of diaphragm bowing from internal pressurization (variable loading device).





TEST ROTOR, GAS BEARING--  
ROTOR-WHIRL INVESTIGATIONS

FIGURE 21



TABLE 2

## DYNAMIC TWO-BEARING TEST RIG ROTOR PARAMETERS

<u>Rotor</u>	<u>Part No.</u>	<u>Journal Diam. Inches</u>	<u><math>I_p</math> In. Lb. Sec. <sup>2</sup></u>	<u>M Lb-Sec. <sup>2</sup> per In.</u>	<u><math>I_D</math> In. -Lb. Sec. <sup>2</sup></u>	<u>Approx. <math>\Lambda</math> at 38,500 rpm *</u>
a**	699380-40	2.0187	0.035	0.0417	1.343	1.50
b	699455	2.0192	0.035	0.0417	1.343	2.25
c	699456-40	2.0196	0.035	0.0417	1.343	3.00
d	699540	2.0160	0.035	0.0417	1.343	0.49

\*Neglecting rotor centrifugal growth effects.

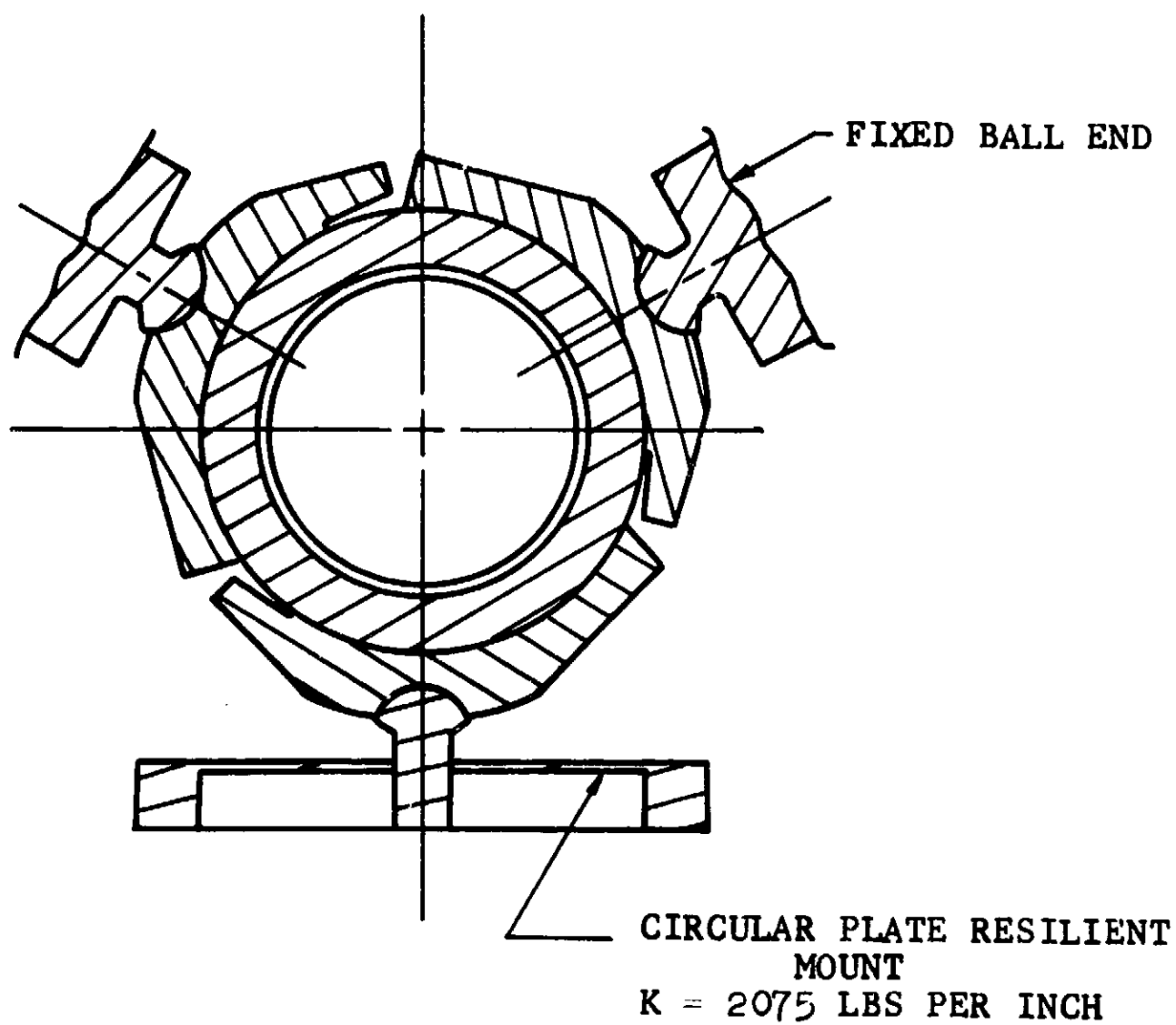
\*\*Standard rotor used in the development tests under NASA Contract NAS3-2778.



GAS BEARING PADS AND  
RESILIENT MOUNT,  
ROTOR WHIRL INVESTIGATIONS

FIGURE 23





TASK II  
ROTOR WHIRL INVESTIGATIONS  
RESILIENT MOUNT CONFIGURATION

FIGURE 25

### 3.5 Test Procedure

The tests described hereinafter were all conducted with vertically oriented rotors. Each series of tests with the various rotors was performed with the same set of six pivoted-pad bearing shoes, and attendant resilient mounts. The instrumentation in each test series was exactly the same. There were no failures during the course of the testing. This point is made to assure the reader that no undesirable variables (such as a change of shoe parts, etc.) were introduced into the test procedure. The only test variable was the change of rotor journal diameter.

The rotor was set up on the test rig alignment centers and the pivoted-pad shoes were adjusted to present a nominal preload of 2.0 pounds (shoes spring-loaded against rotor journals). A diaphragm pressure of 10 psi was used. The fixture centers were removed and the bottom center was replaced with the thrust bearing. A journal bearing hydrostatic supply pressure of 15 psig was used to float the rotor. The bearing pad loads (at zero speed) with this supply pressure were in the order of 5.5 pounds (2.0 pounds preload plus 3.5 pounds due to hydrostatic lift-off). The rotor was accelerated to 38,500 rpm (reference turbocompressor design speed), the hydrostatic lift-off air shut off, and the bearings became self-acting (hydrodynamic). Under these conditions (rotor/pad temperature stabilized) the average bearing pad loads were in the order of 10.5 pounds. The bearing pad loads were then slowly reduced in increments of about 1 pound by reducing the diaphragm pressurization. At each increment of load change, the bearing pad temperatures were allowed to stabilize before proceeding to the next load change. Shaft orbital motions (displayed on two CRO's\*) were scrutinized during each load change to detect any indication of resonant whirl. The procedure was repeated until the threshold

\*Cathode ray oscilloscope

of whirl was clearly evident in the Lissajous figures. This load was then recorded, along with bearing pad temperature, rotor speed, and the bearing pad hydrodynamic back pressure as sensed from the hydrostatic supply system.

The diaphragm pressure was then increased a small amount (about 2 psi) to obtain stable operation, and the speed was reduced to 35,000 rpm and the above procedure repeated and data logged as before. The procedure was repeated for rotor speeds of 30,000, 25,000, and 20,000 rpm. At the conclusion of each test series, the journal bearing hydrostatic supply pressure was readmitted before the rotor was allowed to coast to a standstill.

### 3.6 Test Results

The results of the four series of tests are shown in Figures 26, 27, 28, and 29 and are summarized in Table 3.

The whirl component frequency (last column in Table 3) was obtained from tape playback of the tests. The manner in which this was accomplished is as follows:

- (a) The recorded signal from one of the rotor orthogonal capacitance probes was fed into a panoramic scanner to determine the approximate frequency of the low-frequency whirl component. The frequency was always found to be less than 100 cps.



TWO-BEARING RIG EXPERIMENTAL DATA  
11-INCH BEARING SPAN  
(ROTOR a)

ROTOR DIAMETER - 2.0187 INCHES

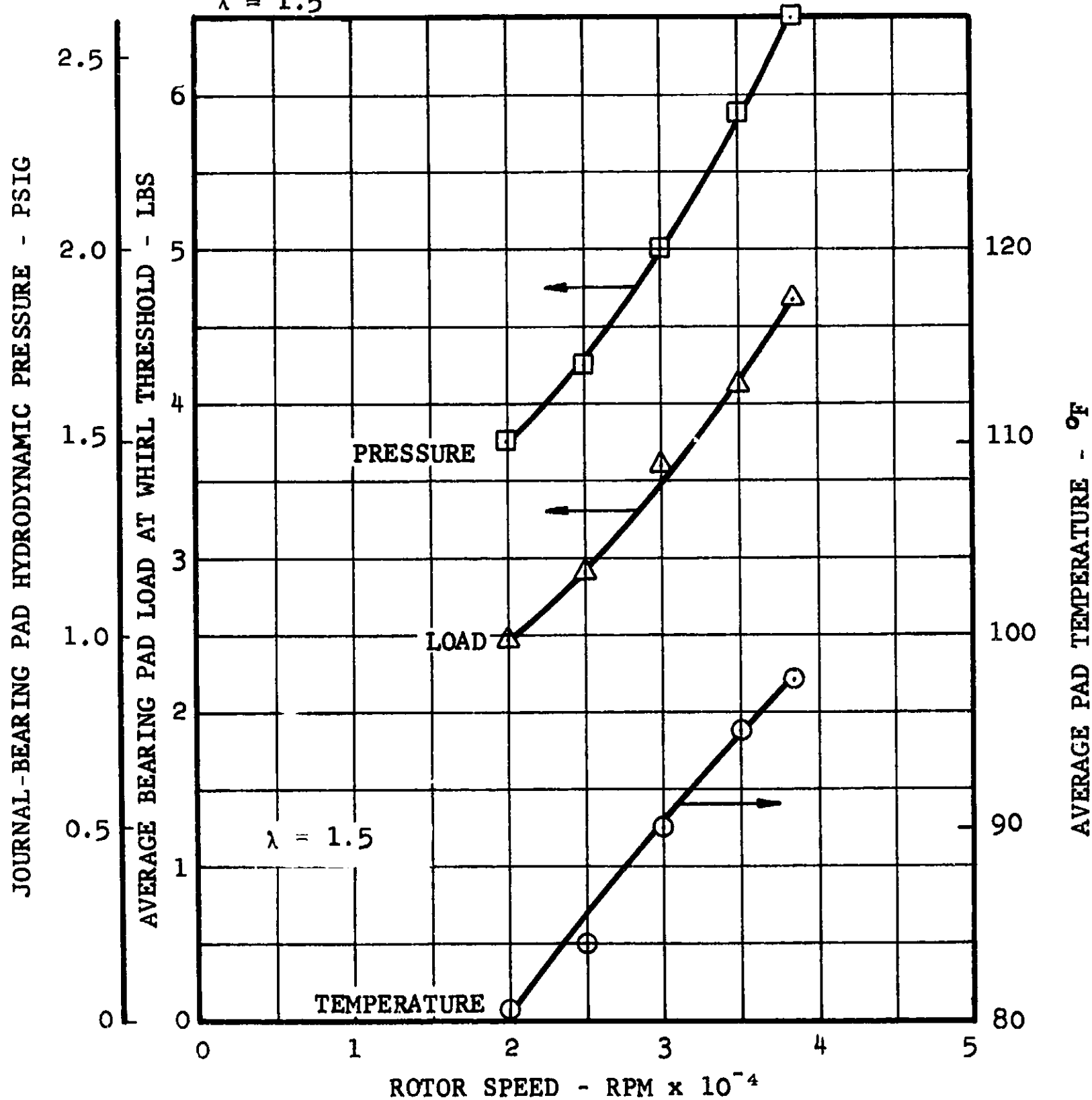
SHOE CURVATURE - 2.0221 INCHES

LUBRICANT - AIR

BAROMETRIC PRESSURE - 28.77 IN. Hg ABS

AMBIENT TEMPERATURE - 72°F

$\lambda = 1.5$



AVERAGE BEARING PAD LOAD, TEMPERATURE  
AND HYDRODYNAMIC PRESSURE AT WHIRL  
THRESHOLD VS ROTOR SPEED,  $\lambda = 1.5$

TWO BEARING RIG EXPERIMENTAL  
DATA

11-INCH BEARING SPAN (ROTOR b)

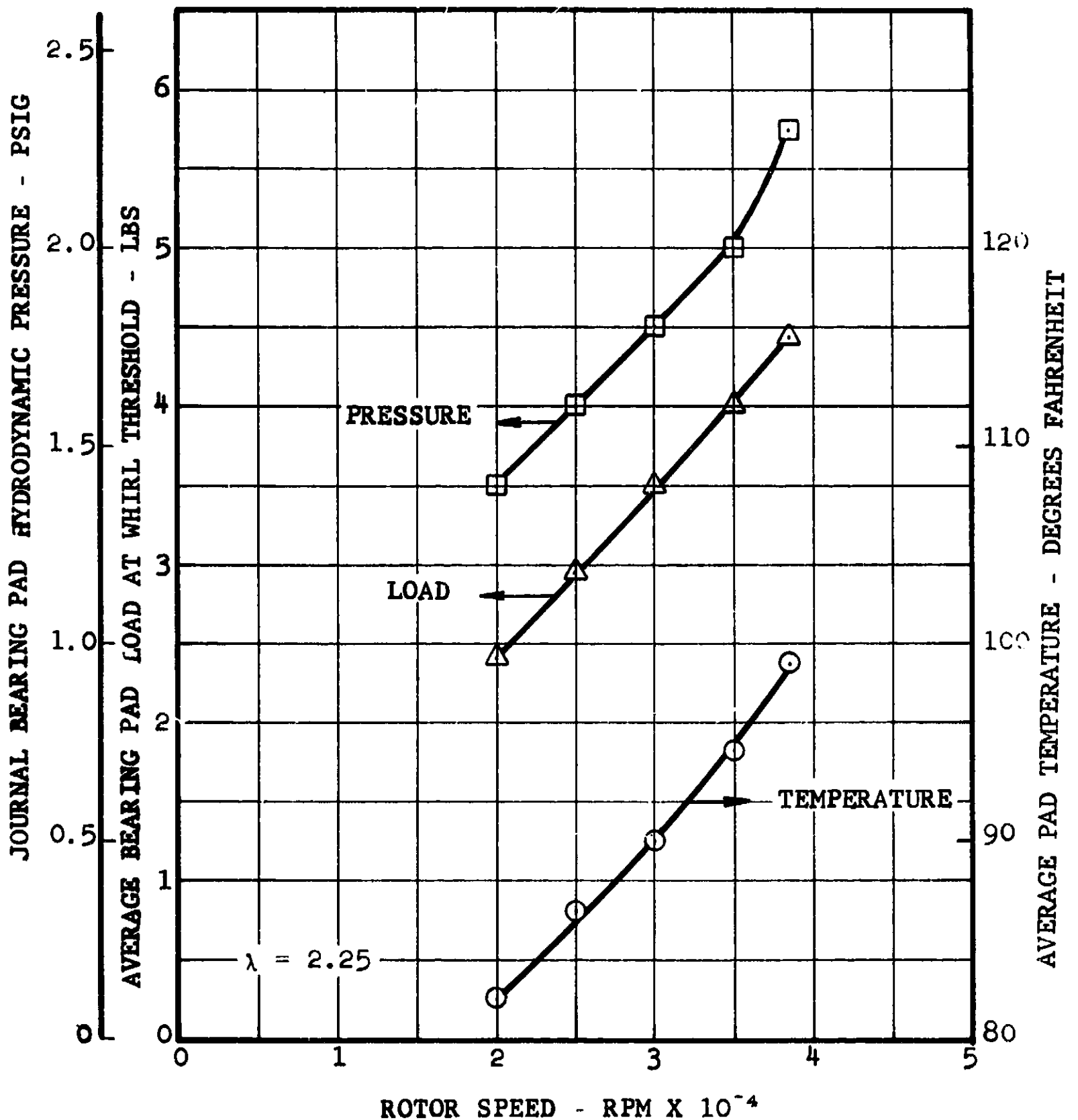
ROTOR DIAMETER - 2.0192 INCHES

SHOE CURVATURE DIAMETER - 2.0221 INCHES

LUBRICANT-AIR

BAROMETRIC PRESSURE - 29.10 INCH HG.

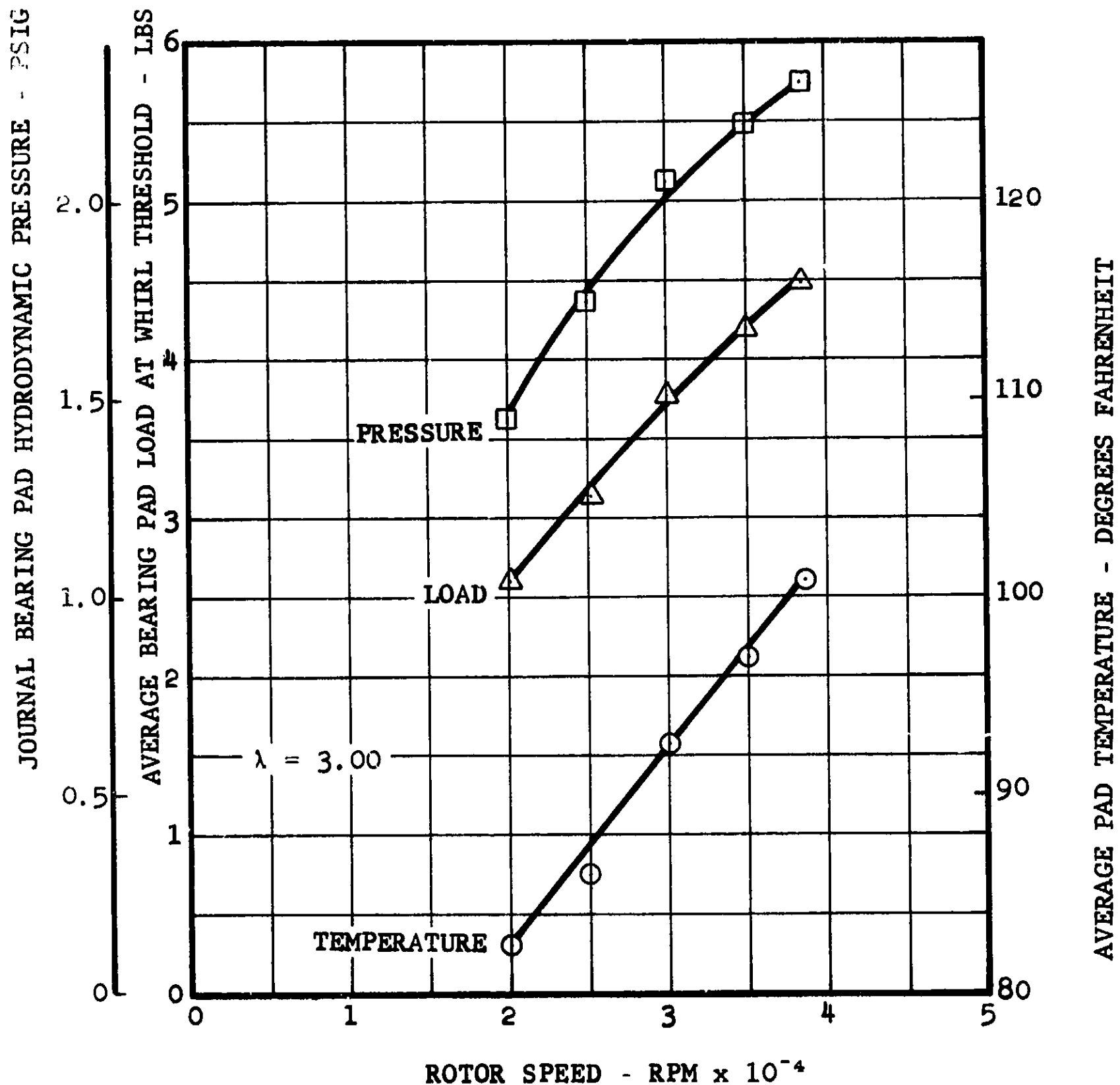
AIR TEMPERATURE - 75°F



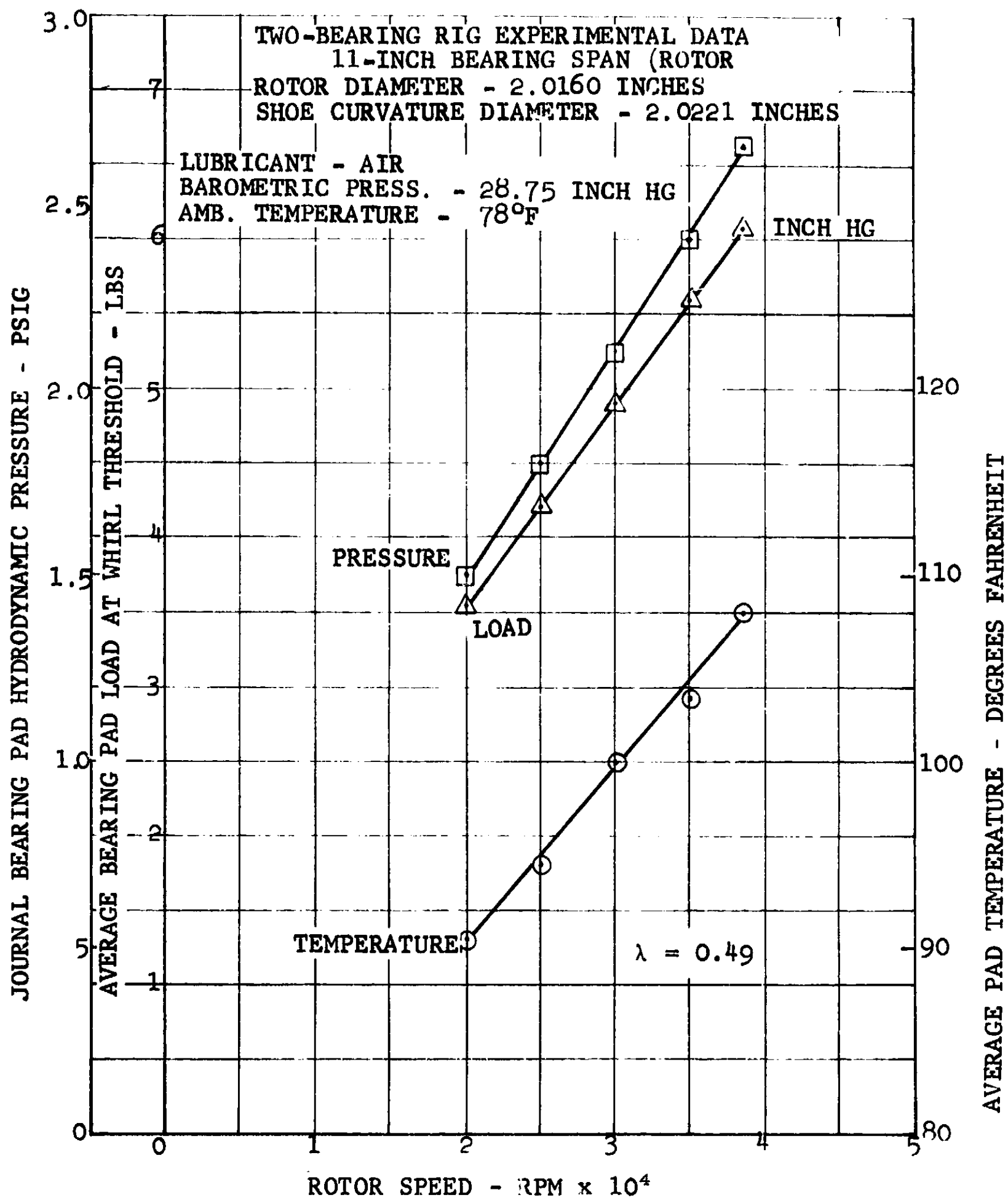
AVERAGE BEARING PAD LOAD, TEMPERATURE  
AND HYDRODYNAMIC PRESSURE AT WHIRL  
THRESHOLD VS ROTOR SPEED

TWO BEARING RIG EXPERIMENTAL  
DATA  
11-INCH BEARING SPAN (ROTOR c)  
ROTOR DIAMETER - 2.0196 INCHES

LUBRICANT - AIR  
BAROMETRIC PRESSURE - 28.75 INCH HG ABS  
AMBIENT TEMPERATURE - 75°F



AVERAGE BEARING PAD LOAD, TEMPERATURE  
AND HYDRODYNAMIC PRESSURE AT  
WHIRL THRESHOLD VS ROTOR SPEED



**AVERAGE BEARING PAD LOAD, TEMPERATURE  
 AND HYDRODYNAMIC PRESSURE AT  
 WHIRL THRESHOLD VS. ROTOR SPEED**

TABLE 3

SUMMARIZATION OF TWO-BEARING RIG EXPERIMENTAL  
DATA (FIGURES 26, 27, 28, AND 29)

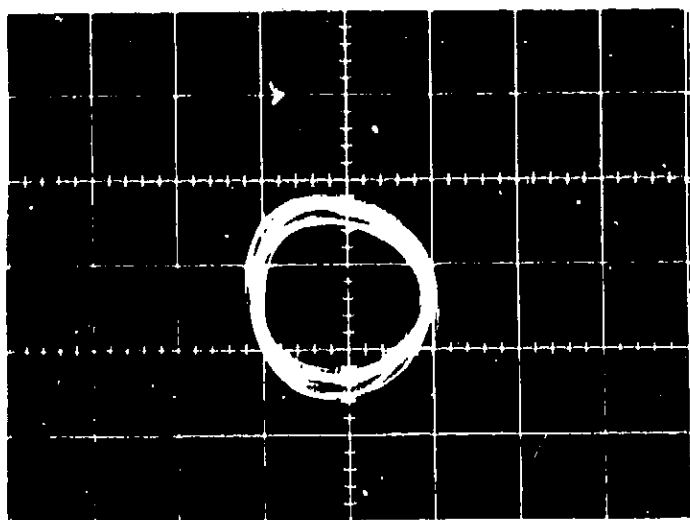
Test Rotor	Rotor Speed (rpm)	Pad Hydrodynamic Pressure (psig)	Average Bearing Pad Load at Whirl (lbs)	Average Pad Temperature (°F)	Whirl Component Frequency (cps)
(a)	38,500	2.6	4.70	97	91
	35,000	2.3	4.12	95	87
	30,000	2.0	3.57	90	82
	25,000	1.8	2.92	84	76
	20,000	1.5	2.55	80	72
(b)	38,500	2.3	4.45	99	90
	35,000	2.0	4.00	94	85
	30,000	1.8	3.50	90	80
	25,000	1.6	2.95	86	76
	20,000	1.4	2.40	82	71
(c)	38,500	1.6	4.50	104	95
	35,000	1.3	4.20	100	92
	30,000	1.2	3.80	95	88
	25,000	0.9	3.05	90	82
	20,000	0.8	2.60	87	79
(d)	38,500	2.65	6.08	108	96
	35,000	2.4	5.60	103.5	93
	30,000	2.1	4.90	100	86
	25,000	1.8	4.20	94.5	80
	20,000	1.5	3.55	90.5	76

- (b) The recorded signal was then filtered to remove all rotational synchronous frequencies (above 200 cps) and fed to one input of a dual-beam oscilloscope. A variable-frequency oscillator was connected to the other oscilloscope input such that the two signals produced a Lissajous figure.
- (c) The oscillator was then tuned to produce a synchronous Lissajous figure with the filtered recorded signal and the oscillator frequency was recorded, and thus defined the whirl component frequency.

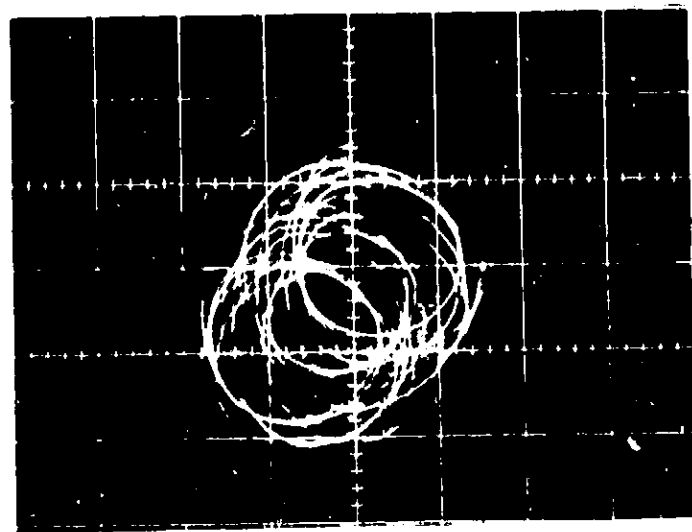
Oscilloscope photographs of the test-data points are presented in Figures 30 to 35. The typical Lissajous patterns displayed in Figure 30 are included to acquaint the reader with visual oscillograph readout of stable rotor operation and indication of whirl threshold. The oscilloscope patterns shown in Figure 31 are typical of those observed in all tests when passing through the first system critical speed using hydrostatic supply to the journal bearings.

### 3.7 Data Reduction and Analysis

To facilitate data reduction, parametric performance curves for  $100^\circ$  partial-arc bearings with an L/D ratio of 0.75 and a 65-percent pivot location were constructed. The analysis leading to these curves was performed on a finite-length partial-arc compressible hydrodynamic bearing pad computer program. From these curves the pivot film thickness, eccentricity ratio, and attitude angle were obtained for each of the experimentally determined load data points. The air viscosity curve shown in Figure 36 was used in the calculation of the bearing pad compressibility number,  $\Lambda$ , for each of the data points.



LISSAJOUS OF SHAFT  
MOTIONS WITHOUT WHIRL



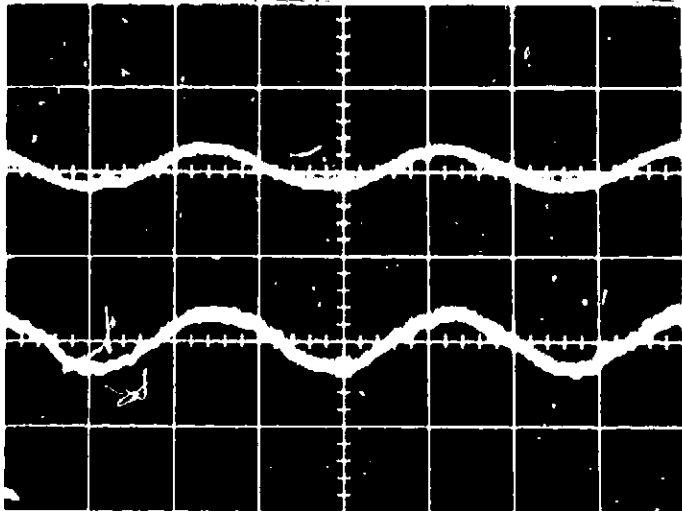
LISSAJOUS OF SHAFT MOTIONS  
WITH A WHIRL AT 90 CPS

TYPICAL LISSAJOUS PATTERNS OF  
ROTOR WITH AND WITHOUT WHIRL

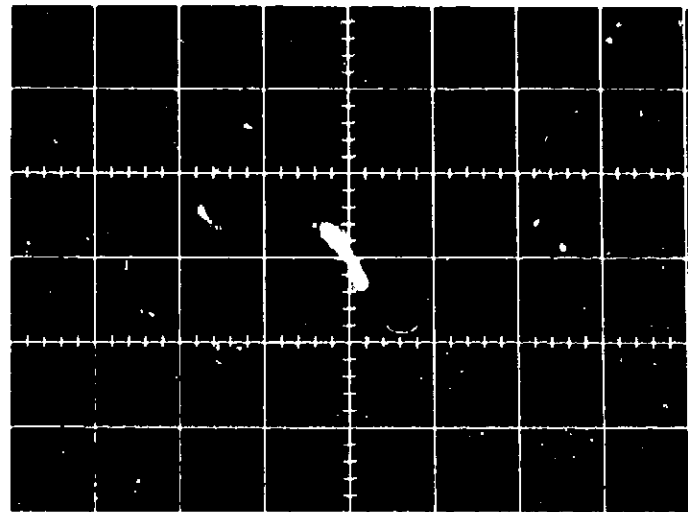
FIGURE 30

APS 5223 R

Page 56



CRITICAL SPEED AT 70 CPS



LISSAJOUS OF CRITICAL  
SPEED AT 70 CPS

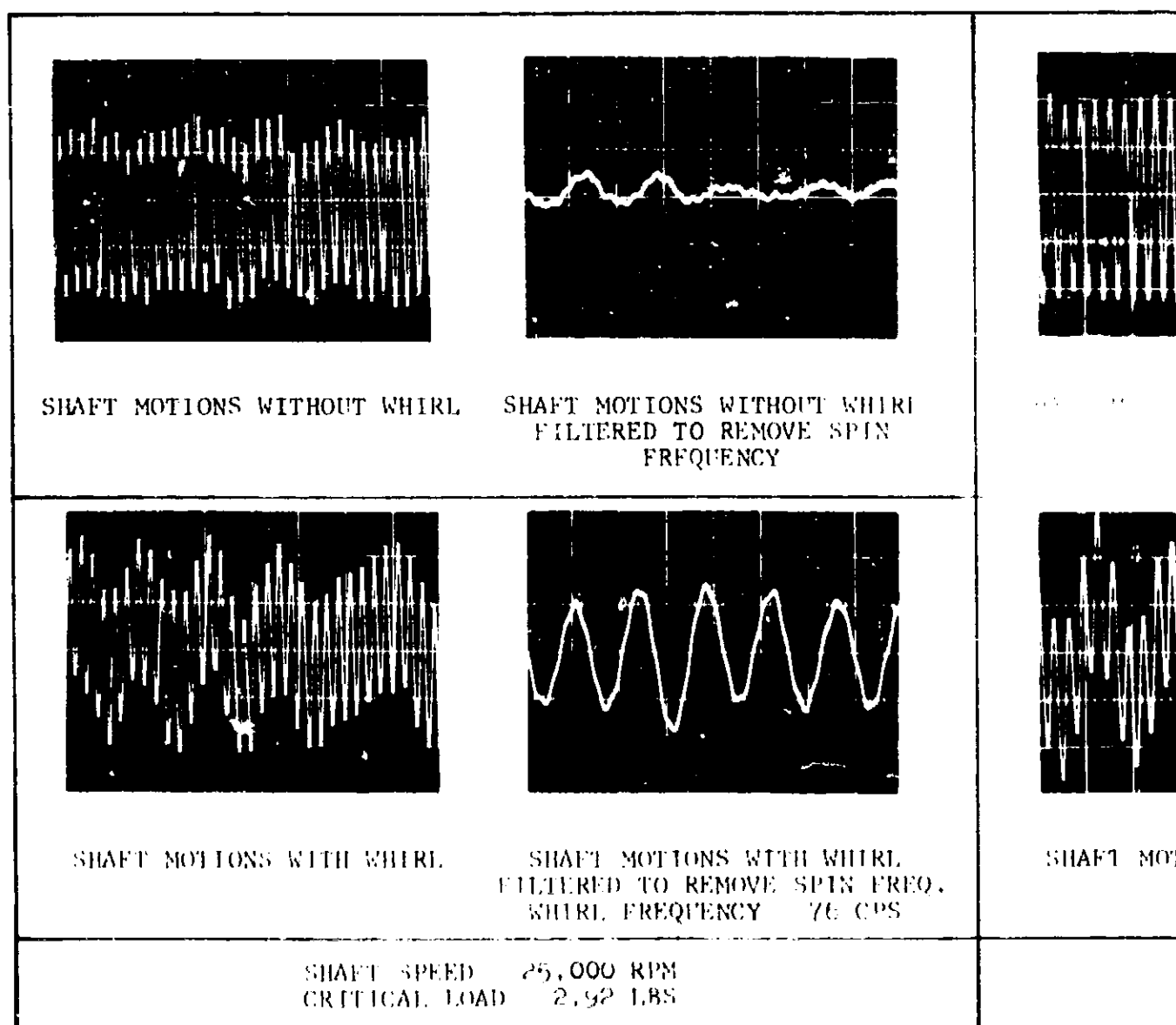
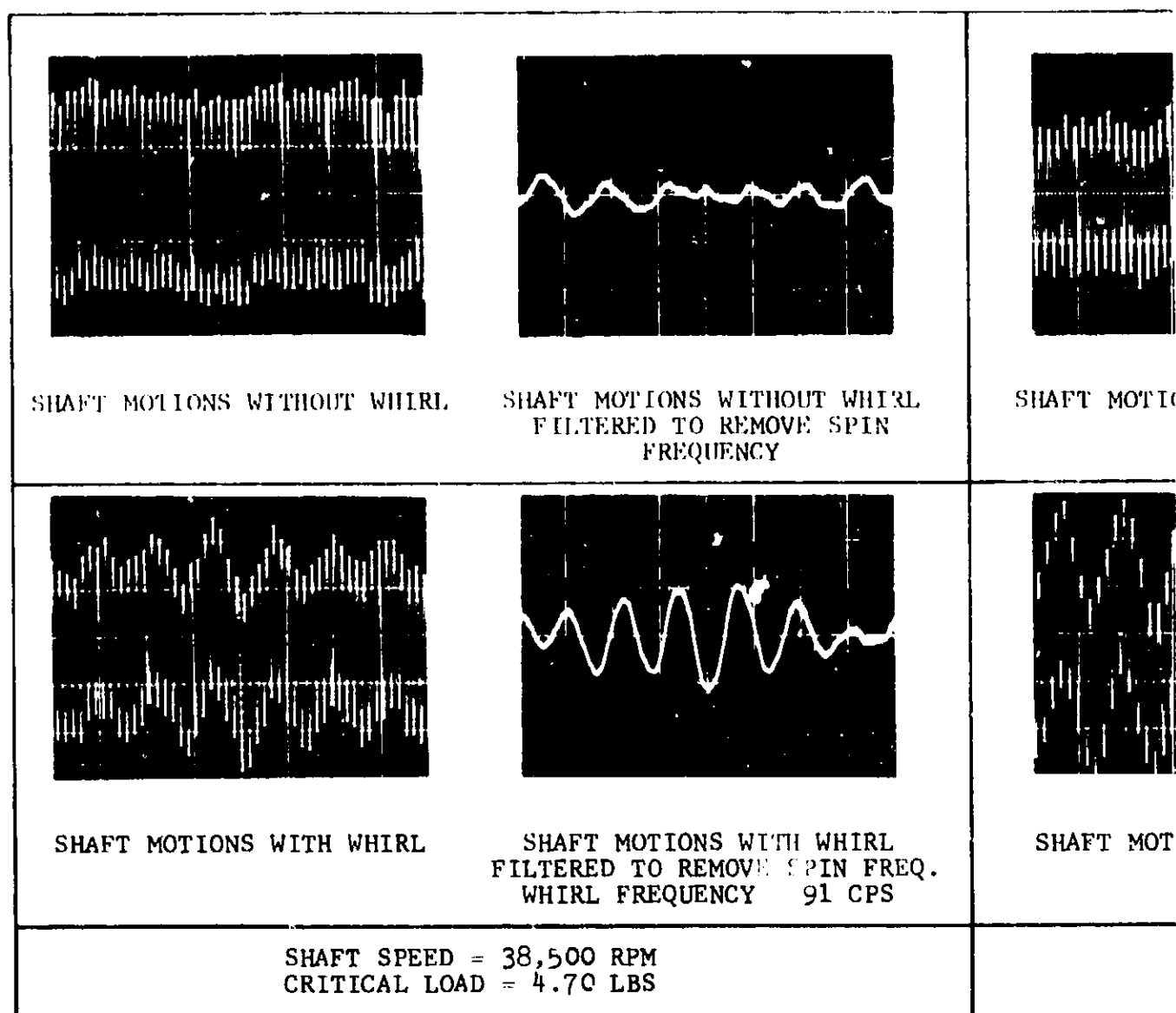
NOTES:

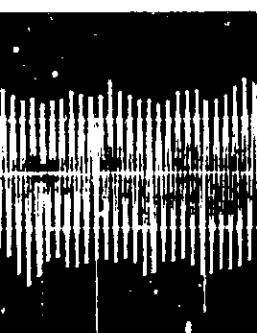
1. PAD RADIUS 1.01105 IN.
2. JOURNAL RADIUS 1.00935 IN.
3. PAD L D 0.75
4. SWEEP FREQUENCY 5 MS/SEC.

NASA GAS BEARING STABILITY STUDY  
TYPICAL CRITICAL SPEED  
OSCILLOSCOPE PATTERNS  
ROTOR a

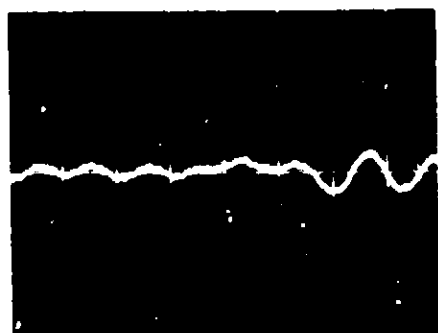
FIGURE 31  
APS 5223 R  
Page 37



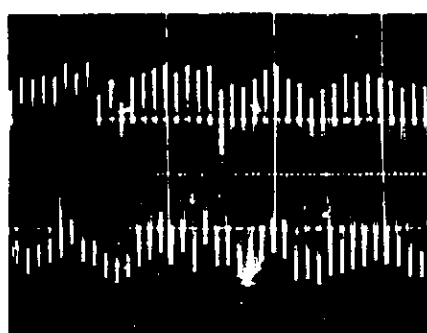




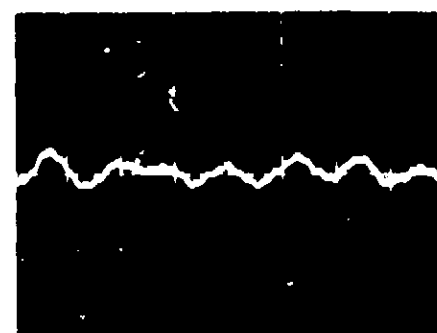
SHAFT MOTIONS WITHOUT WHIRL



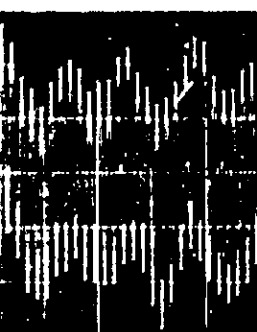
SHAFT MOTIONS WITHOUT WHIRL  
FILTERED TO REMOVE SPIN  
FREQUENCY



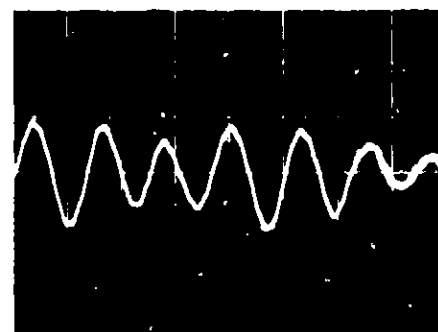
SHAFT MOTIONS WITHOUT WHIRL



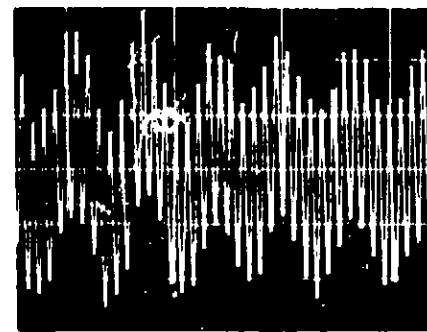
SHAFT MOTIONS WITHOUT WHIRL  
FILTERED TO REMOVE SPIN  
FREQUENCY



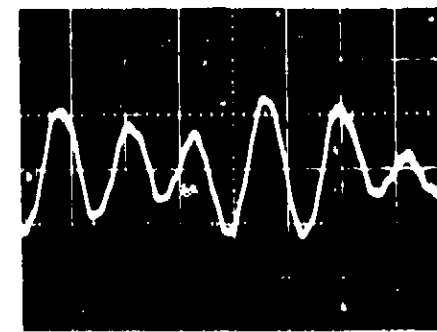
SHAFT MOTIONS WITH WHIRL



SHAFT MOTIONS WITH WHIRL  
FILTERED TO REMOVE SPIN FREQ.  
WHIRL FREQUENCY = 87 CPS



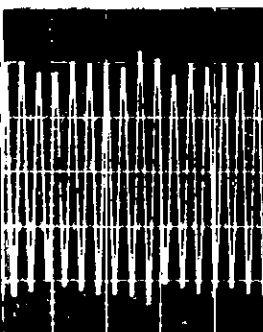
SHAFT MOTIONS WITH WHIRL



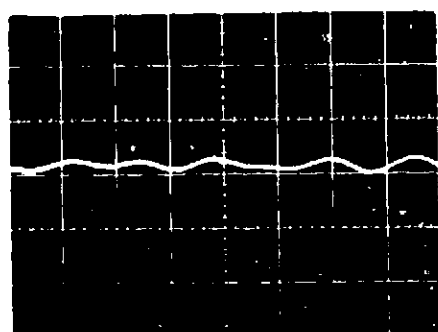
SHAFT MOTIONS WITH WHIRL  
FILTERED TO REMOVE SPIN FREQ.  
WHIRL FREQUENCY = 82 CPS

SHAFT SPEED = 35,000 RPM  
CRITICAL LOAD = 4.12 LBS

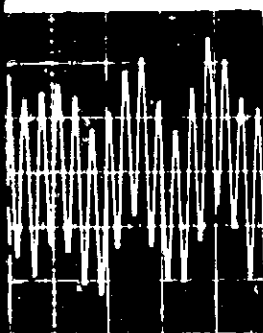
SHAFT SPEED 30,000 RPM  
CRITICAL LOAD = 3.57 LBS



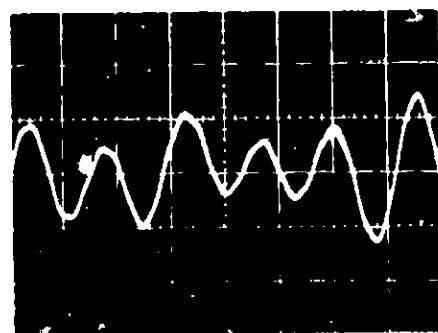
SHAFT MOTIONS WITHOUT WHIRL



SHAFT MOTIONS WITHOUT WHIRL  
FILTERED TO REMOVE SPIN  
FREQUENCY



SHAFT MOTIONS WITH WHIRL



SHAFT MOTIONS WITH WHIRL  
FILTERED TO REMOVE SPIN FREQ.  
WHIRL FREQUENCY = 72 CPS

SHAFT SPEED 20,000 RPM  
CRITICAL LOAD 2.55 LBS

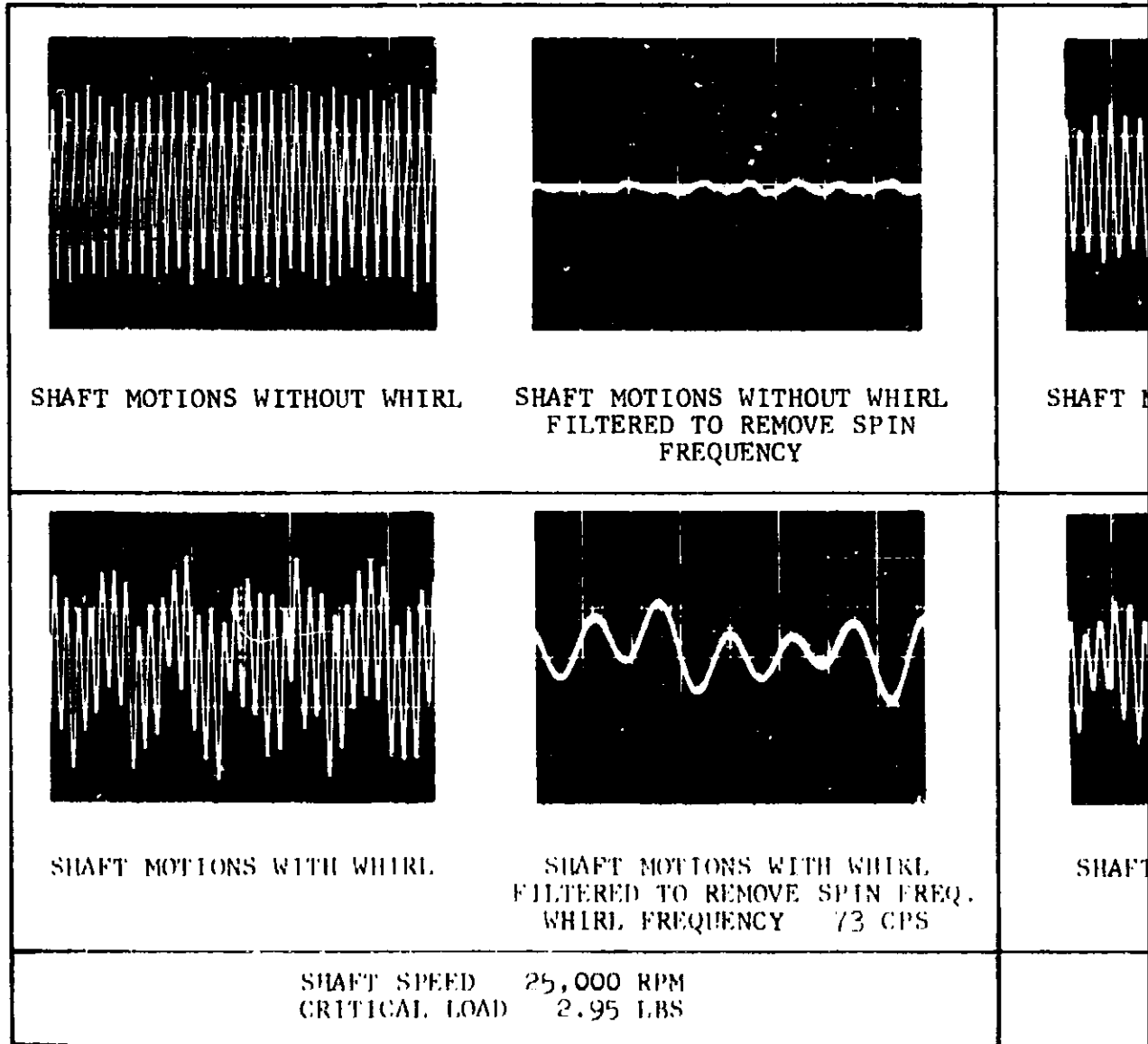
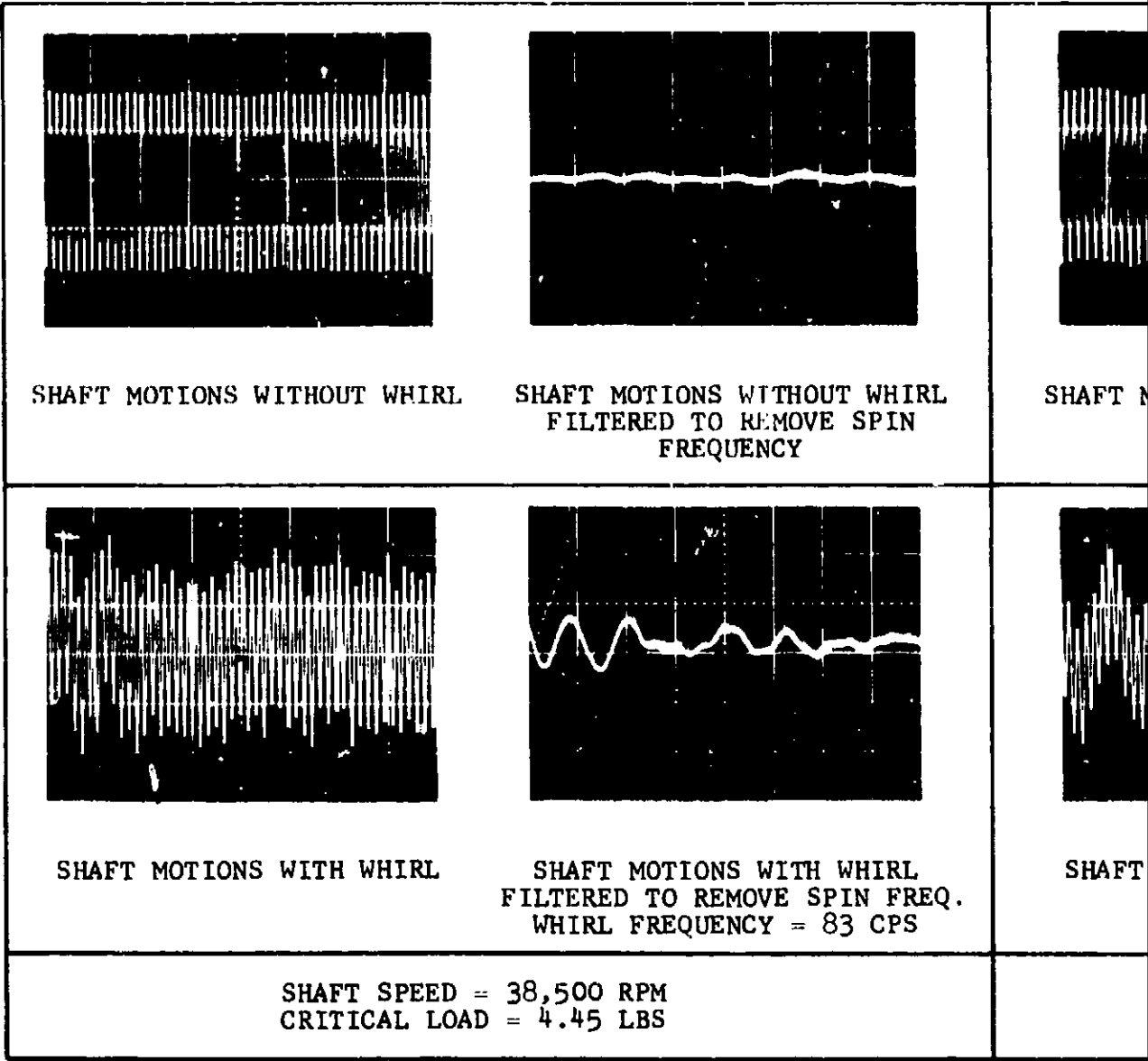
#### NOTES:

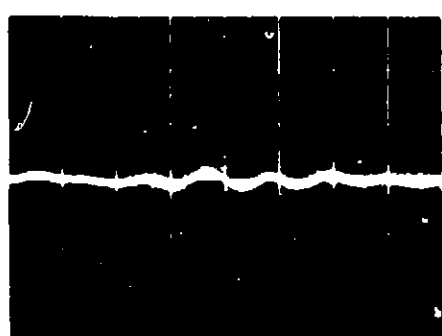
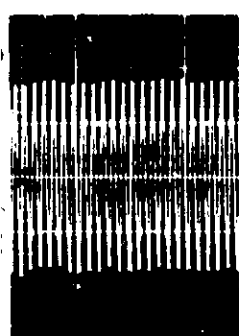
1. PAD RADIUS 1.0110 IN.
2. JOURNAL RADIUS 1.0095 IN.
3. PAD L/D 0.75
4. SWEEP SCALE 10 MS PER CM

NASA GAN BEARING STABILITY TEST  
SHAFT MOTIONS AT 35,000 RPM, 30,000 RPM,  
20,000 RPM, 15,000 RPM, AND 10,000 RPM  
ROTOR A

FIGURE 32

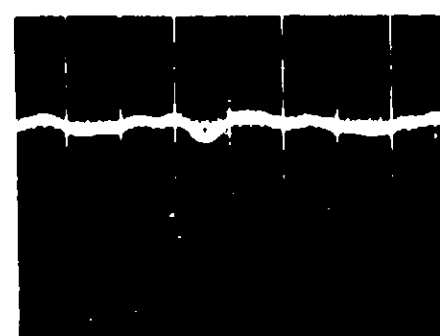
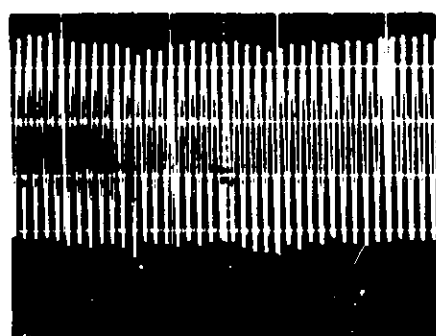
APR 5, 1978  
Page 32-2





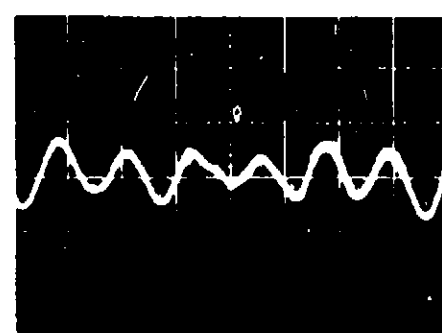
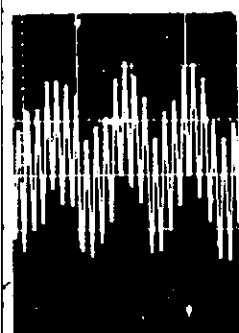
WITHOUT WHIRL

SHAFT MOTIONS WITHOUT WHIRL  
FILTERED TO REMOVE SPIN  
FREQUENCY



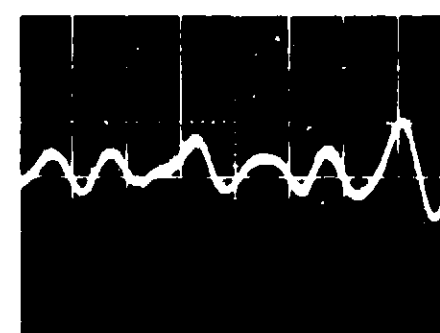
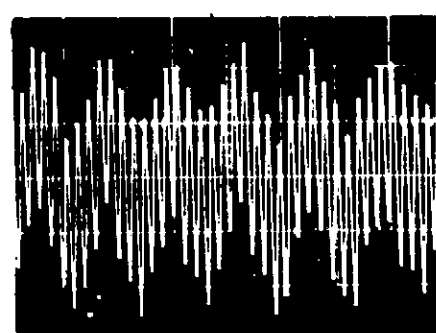
SHAFT MOTIONS WITHOUT WHIRL

SHAFT MOTIONS WITHOUT WHIRL  
FILTERED TO REMOVE SPIN  
FREQUENCY



NS WITH WHIRL

SHAFT MOTIONS WITH WHIRL  
FILTERED TO REMOVE SPIN FREQ.  
WHIRL FREQUENCY = 81 CPS

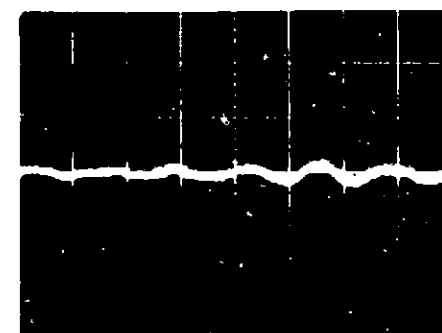
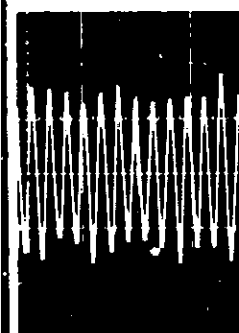


SHAFT MOTIONS WITH WHIRL

SHAFT MOTIONS WITH WHIRL  
FILTERED TO REMOVE SPIN FREQ.  
WHIRL FREQUENCY 76 CPS

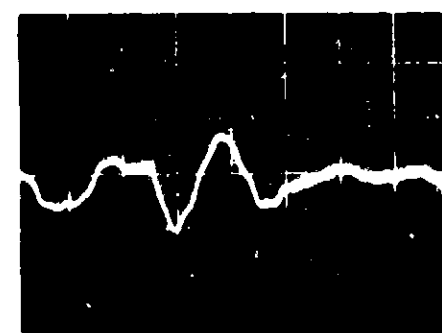
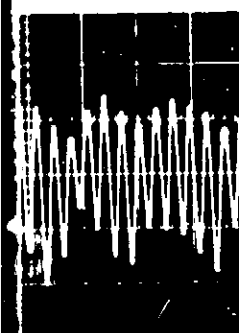
SHAFT SPEED = 35,000 RPM  
CRITICAL LOAD = 4.0 LBS

SHAFT SPEED = 30,000 RPM  
CRITICAL LOAD = 3.50 LBS



WITHOUT WHIRL

SHAFT MOTIONS WITHOUT WHIRL  
FILTERED TO REMOVE SPIN  
FREQUENCY



NS WITH WHIRL

SHAFT MOTIONS WITH WHIRL  
FILTERED TO REMOVE SPIN FREQ.  
WHIRL FREQUENCY 69 CPS

SHAFT SPEED 20,000 RPM  
CRITICAL LOAD 2.40 LBS

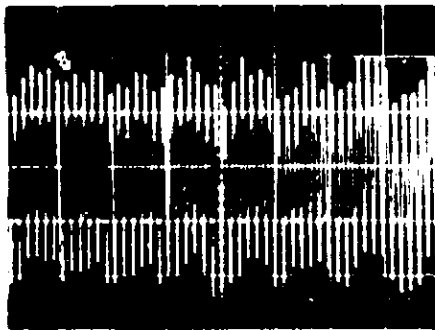
#### NOTES:

1. PAD RADIUS 1.01105 IN.
2. JOURNAL RADIUS 1.00960 IN.
3. PAD L D 0.75
4. SWEEP SCALE 10 MS PER CM

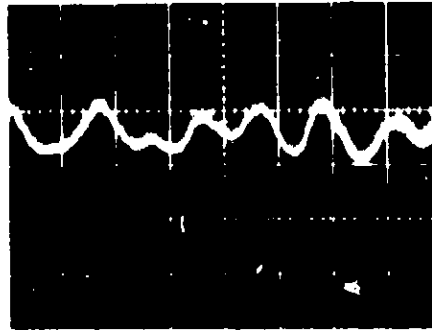
NASA GAS BEARING STABILITY STUDY  
SHAFT MOTIONS AT 32,500 RPM, 35,000 RPM,  
30,000 RPM, 25,000 RPM, AND 20,000 RPM  
(ROTOR B)

FIGURE 53

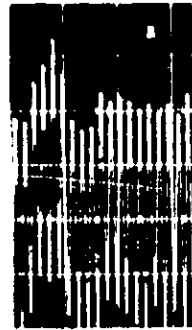
APS 5222 R  
Page 55 -2



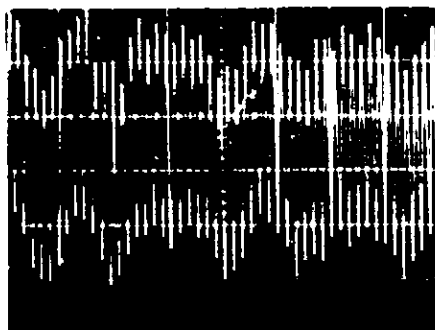
SHAFT MOTIONS WITHOUT WHIRL



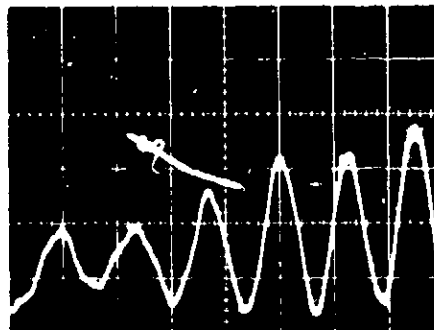
SHAFT MOTIONS WITHOUT WHIRL  
FILTERED TO REMOVE SPIN  
FREQUENCY



SHAFT MOTION



SHAFT MOTIONS WITH WHIRL

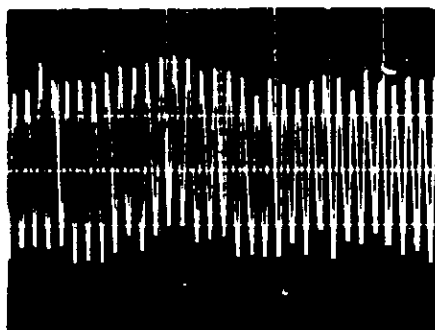


SHAFT MOTIONS WITH WHIRL  
FILTERED TO REMOVE SPIN FREQ.  
WHIRL FREQUENCY = 95 CPS

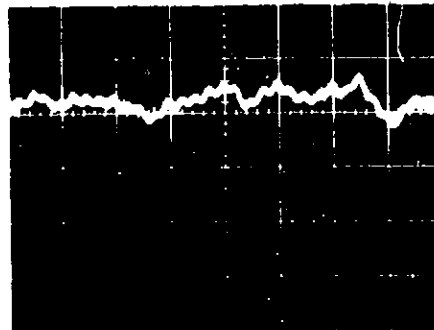


SHAFT MOTI

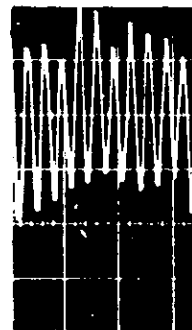
SHAFT SPEED = 38,500 RPM  
CRITICAL SPEED = 4.5 LBS



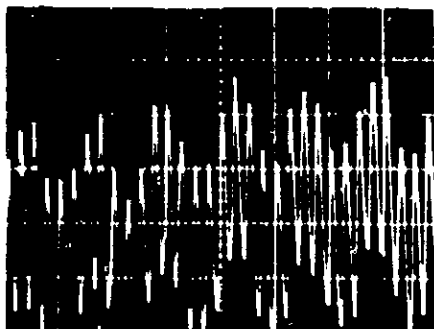
SHAFT MOTIONS WITHOUT WHIRL



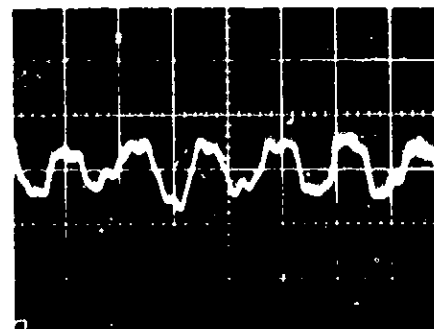
SHAFT MOTIONS WITHOUT WHIRL  
FILTERED TO REMOVE SPIN  
FREQUENCY



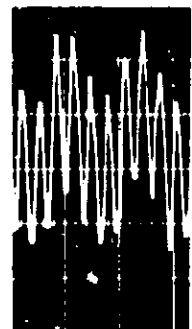
SHAFT MOTION



SHAFT MOTIONS WITH WHIRL

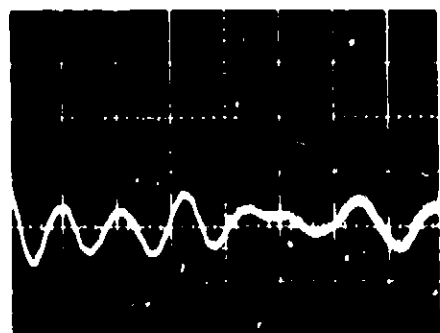
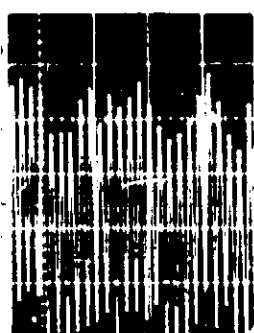


SHAFT MOTIONS WITH WHIRL  
FILTERED TO REMOVE SPIN FREQ.  
WHIRL FREQUENCY = 82 CPS



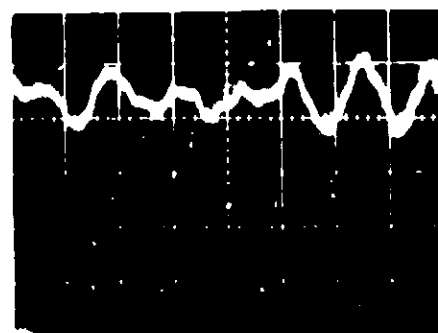
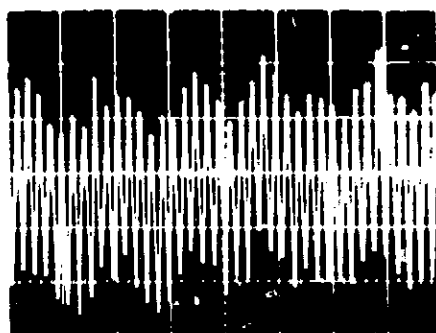
SHAFT MOTI

SHAFT SPEED 35,000 RPM  
CRITICAL LOAD = 3.05 LBS



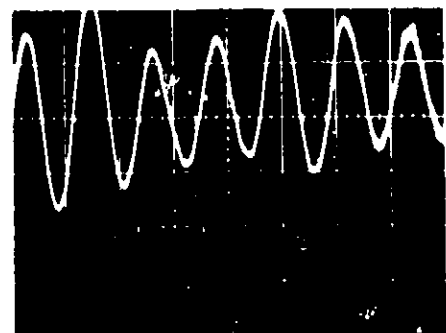
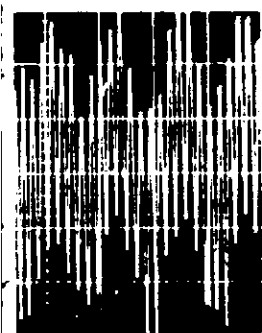
S WITHOUT WHIRL

SHAFT MOTIONS WITHOUT WHIRL  
FILTERED TO REMOVE SPIN  
FREQUENCY



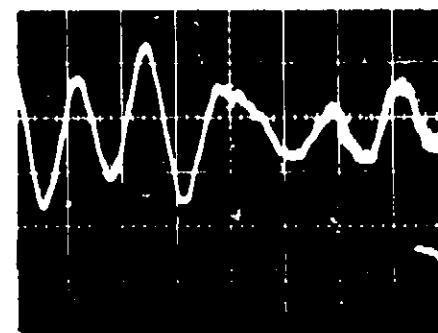
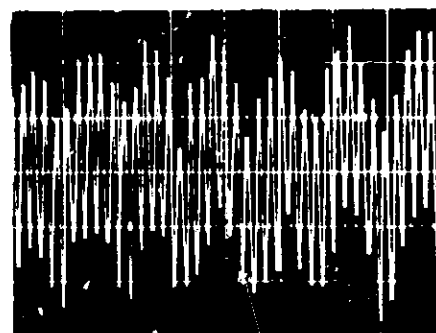
SHAFT MOTIONS WITHOUT WHIRL

SHAFT MOTIONS WITHOUT WHIRL  
FILTERED TO REMOVE SPIN  
FREQUENCY



ONS WITH WHIRL

SHAFT MOTIONS WITH WHIRL  
FILTERED TO REMOVE SPIN FREQ.  
WHIRL FREQUENCY = 92 CPS

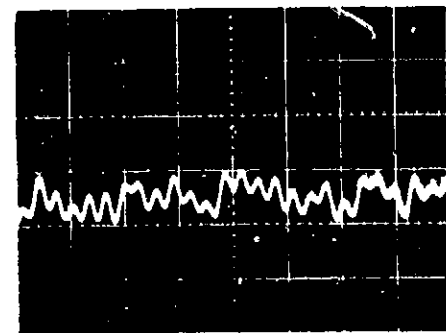
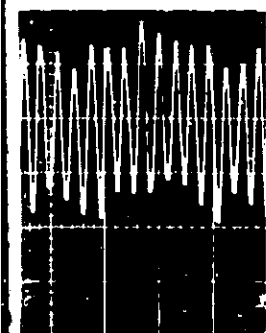


SHAFT MOTIONS WITH WHIRL

SHAFT MOTIONS WITH WHIRL  
FILTERED TO REMOVE SPIN FREQ.  
WHIRL FREQUENCY = 88 CPS

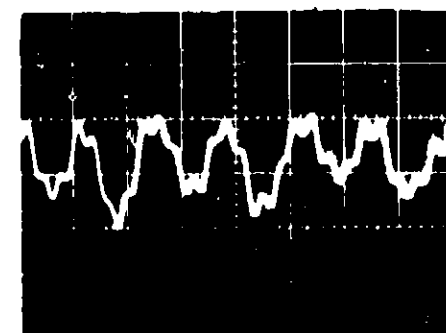
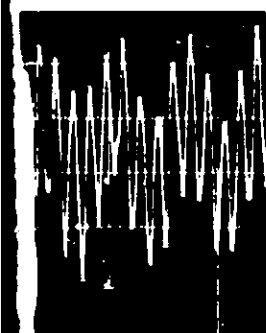
SHAFT SPEED = 35,000 RPM  
CRITICAL LOAD = 4.2 LBS

SHAFT SPEED = 30,000 RPM  
CRITICAL LOAD = 3.8 LBS



IS WITHOUT WHIRL

SHAFT MOTIONS WITHOUT WHIRL  
FILTERED TO REMOVE SPIN  
FREQUENCY



NS WITH WHIRL

SHAFT MOTIONS WITH WHIRL  
FILTERED TO REMOVE SPIN FREQ.  
WHIRL FREQUENCY = 79 CPS

SHAFT SPEED = 20,000 RPM  
CRITICAL LOAD = 2.6 LBS

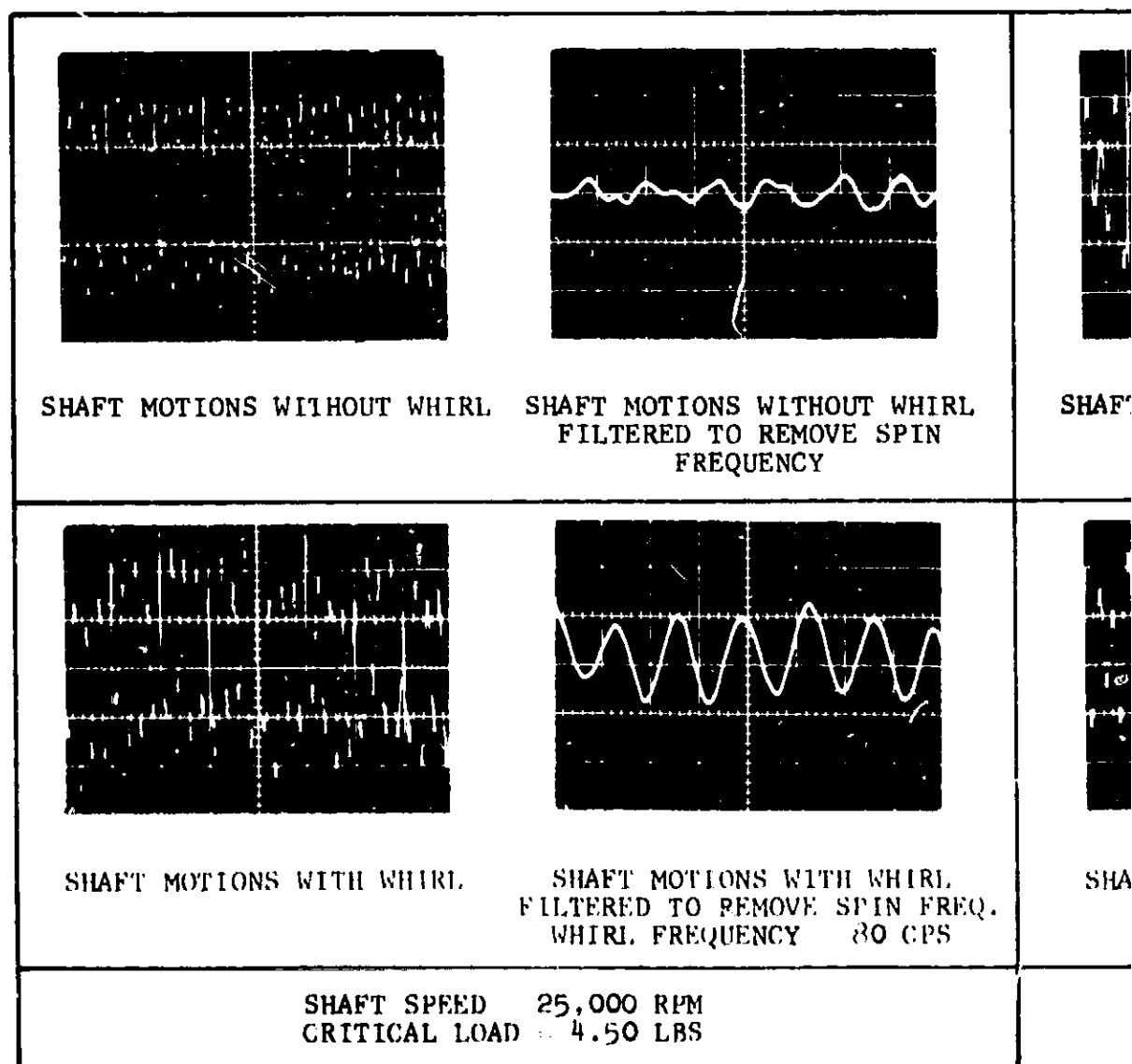
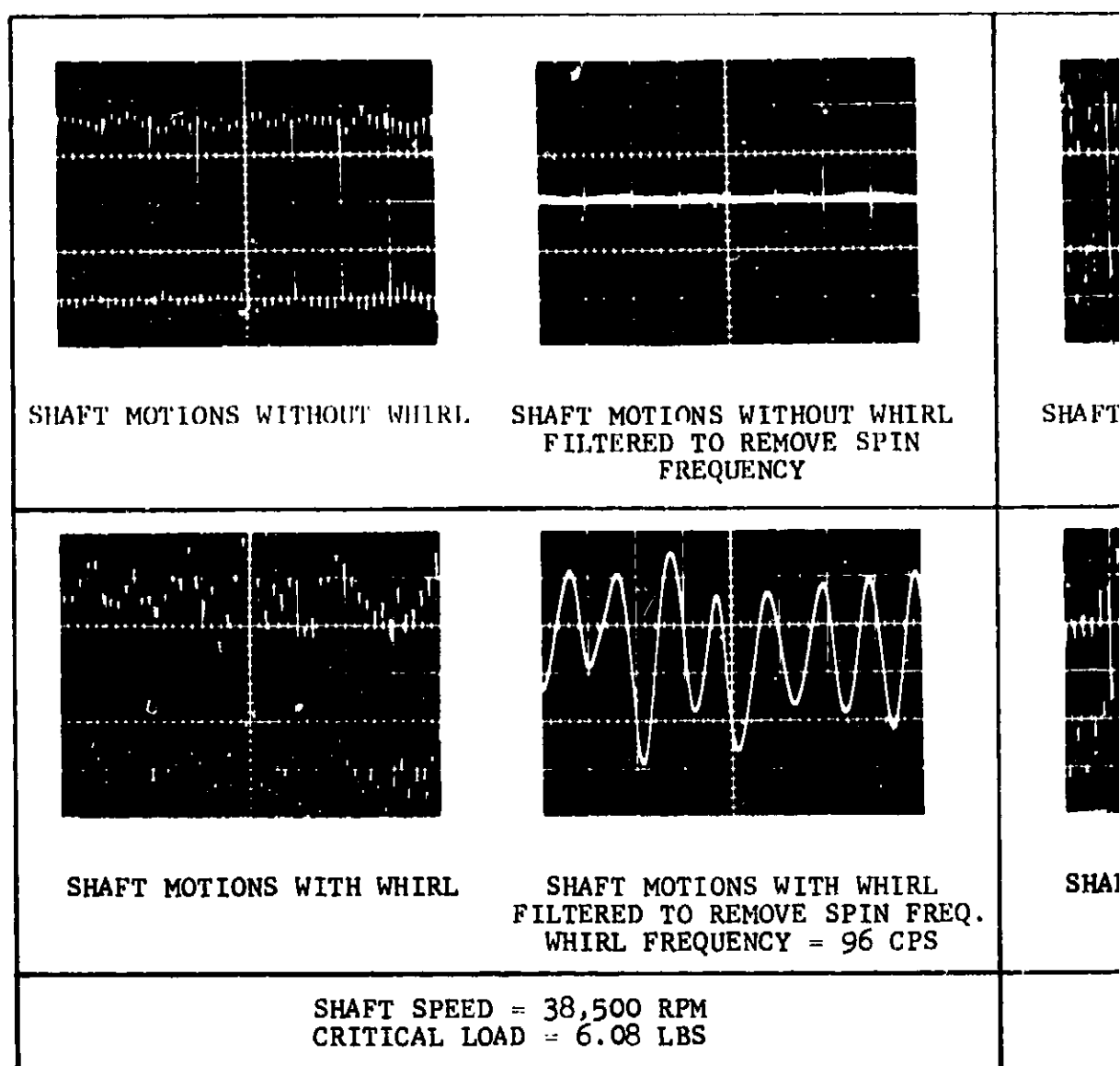
#### NOTES:

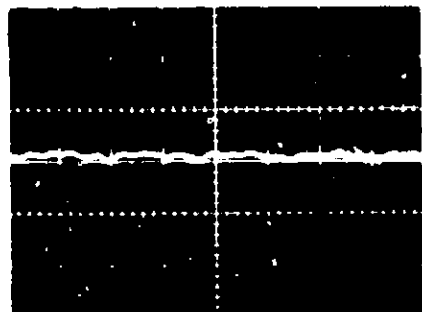
1. PAD RADIUS = 1.01105 IN.
2. JOURNAL RADIUS = 1.00980 IN.
3. PAD L/D = 0.75
4. SWEEP SCALE = 10 MS PER CM

NASA GAS BEARING STABILITY STUDY  
SHAFT MOTIONS AT 38,500 RPM, 35,000 RPM,  
30,000 RPM, 25,000 RPM, AND 20,000 RPM  
(ROTOR C)

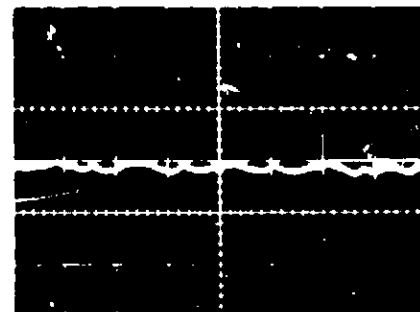
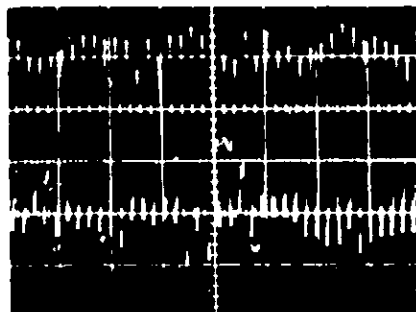
FIGURE 34

APS-5223 R  
Page 60-2

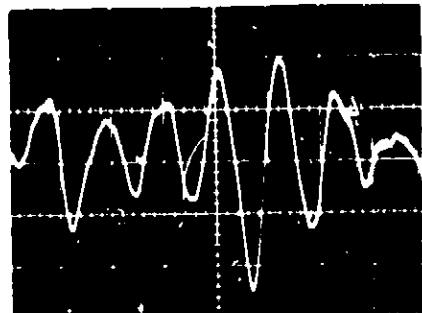




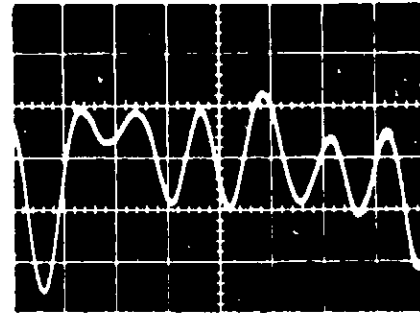
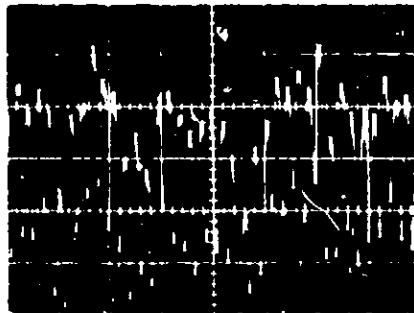
OUT WHIRL SHAFT MOTIONS WITHOUT WHIRL  
FILTERED TO REMOVE SPIN  
FREQUENCY



SHAFT MOTIONS WITHOUT WHIRL. SHAFT MOTIONS WITHOUT WHIRL.  
FILTERED TO REMOVE SPIN  
FREQUENCY



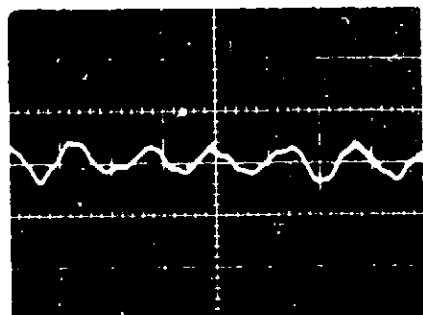
H WHIRL SHAFT MOTIONS WITH WHIRL  
FILTERED TO REMOVE SPIN FREQ.  
WHIRL FREQUENCY = 93 CPS



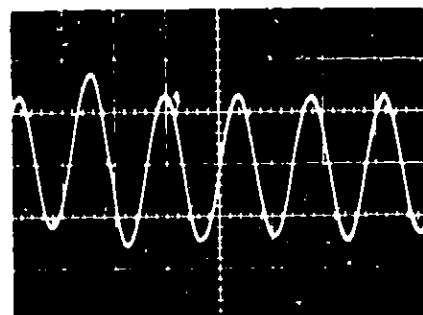
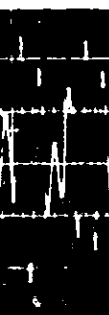
SHAFT MOTIONS WITH WHIRL. SHAFT MOTIONS WITH WHIRL.  
FILTERED TO REMOVE SPIN FREQ.  
WHIRL FREQUENCY 86 CPS

SHAFT SPEED = 35,000 RPM  
CRITICAL LOAD = 5.60 LBS

SHAFT SPEED = 30,000 RPM  
CRITICAL LOAD = 4.90 LBS



OUT WHIRL SHAFT MOTIONS WITHOUT WHIRL  
FILTERED TO REMOVE SPIN  
FREQUENCY



H WHIRL SHAFT MOTIONS WITH WHIRL  
FILTERED TO REMOVE SPIN FREQ.  
WHIRL FREQUENCY 76 CPS

SHAFT SPEED = 20,000 RPM  
CRITICAL LOAD = 3.55 LBS

NOTES:

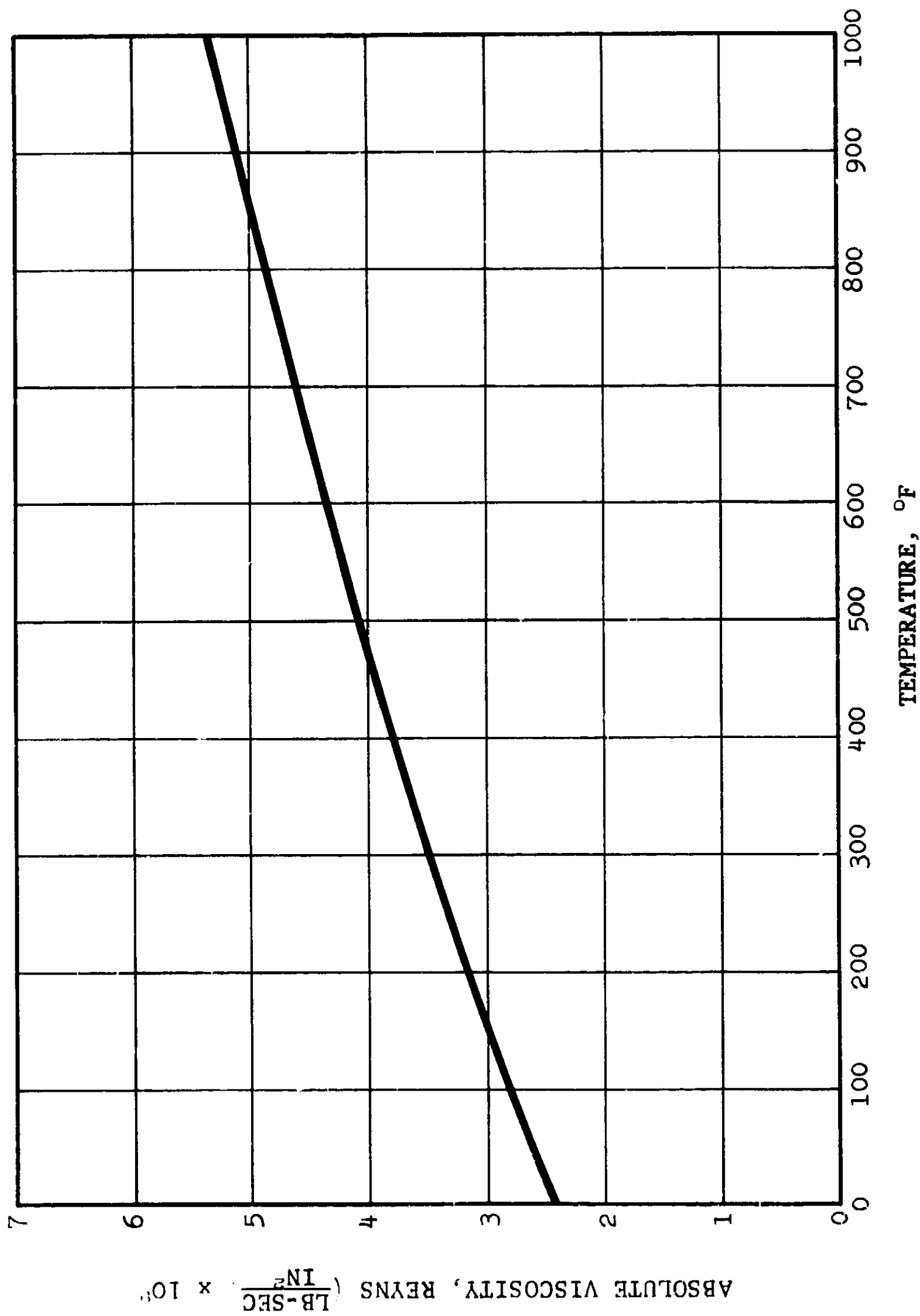
1. PAD RADIUS 1.01105 IN.
2. JOURNAL RADIUS 1.00300 IN.
3. PAD L/D 0.73
4. SWEEP SCALE 10 MS PER CM

NASA GAS BEARING STABILITY STUDY  
SHAFT MOTIONS AT 38,500 RPM, 25,000 RPM,  
30,000 RPM, 25,000 RPM, AND 20,000 RPM  
[ROTOR D]

FIGURE 35

APS 5223 R  
Page 61-2





ABSOLUTE VISCOSITY OF AIR  
AT ATMOSPHERIC PRESSURE

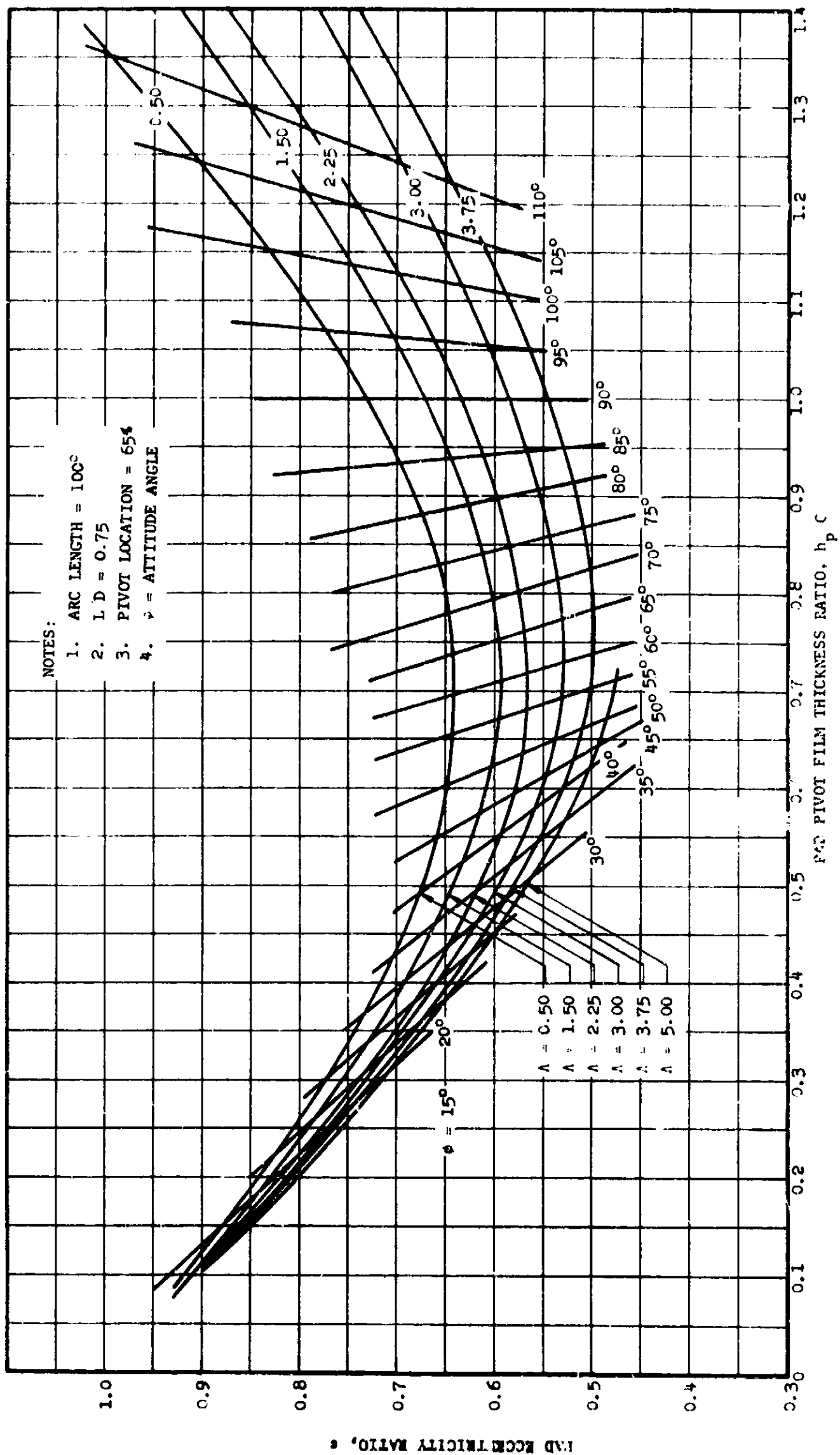
FIGURE 36

Figure 37 is a dimensionless plot of pad pivot film thickness, pad eccentricity ratio, and pad attitude angle for various constant values of  $\Lambda$ . Note that for a constant value of  $\Lambda$  there are two values of pivot film thickness for any value of eccentricity ratio. The reason for these double values is explained in Figure 38. The eccentricity ratio is determined by the position of the journal relative to a circle of which the pad is an arc. Therefore, the minimum film thickness can be off the pad. For the case of a 65-percent pivot location as shown in the above figure, the pad tilts as the journal moves away from it. As the journal continues to move away from the pad, a point is reached where further displacement from the pad results in an increase of eccentricity ratio.

Figures 39, 40, and 41 are dimensionless plots of bearing pad load versus pivot film thickness. As for the case of Figure 37, these curves apply only to pads with a 100-degree arc span, an  $L/D$  of 0.75, and a 65-percent pivot location.

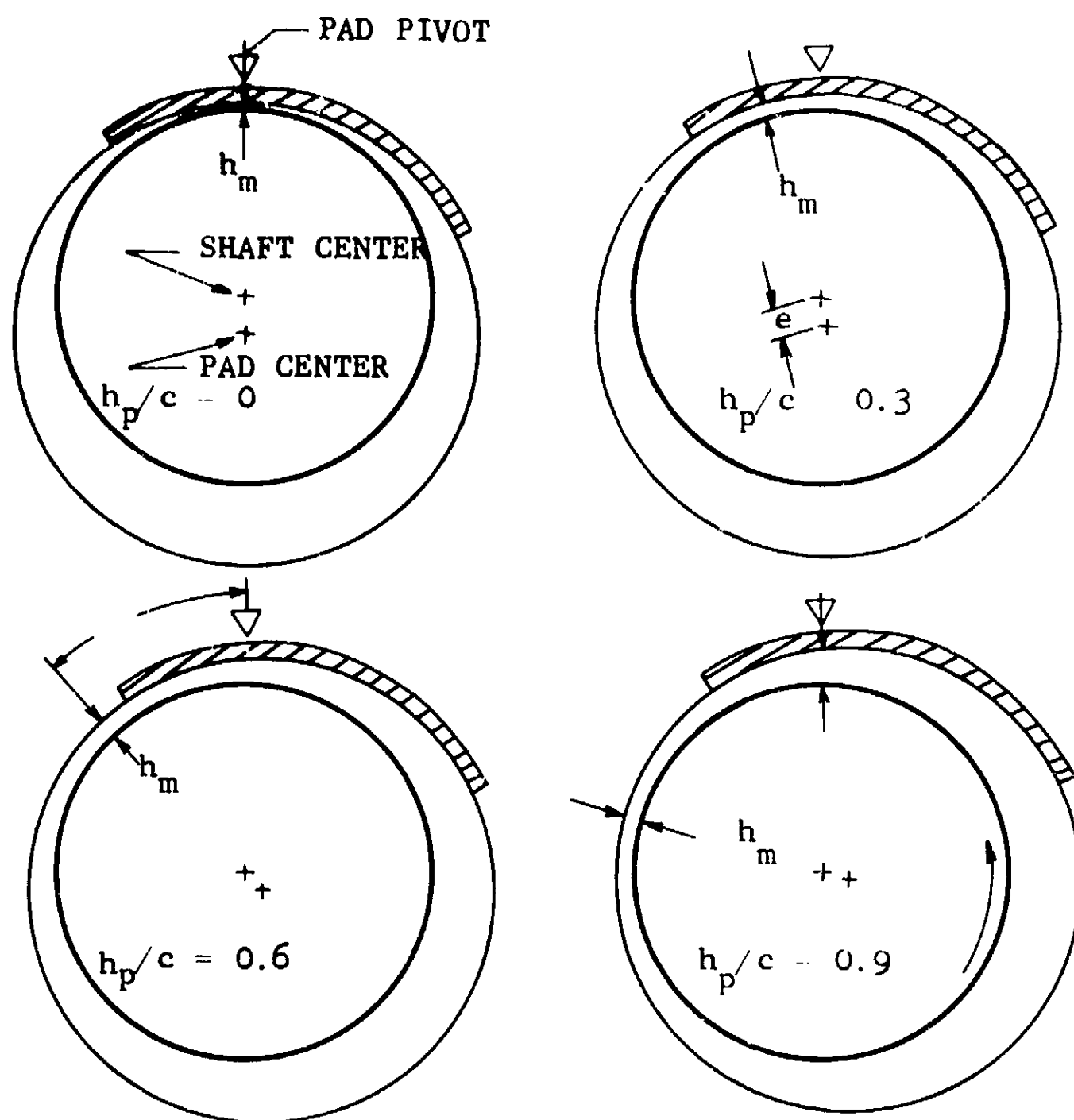
Changes in the journal and bearing pad geometry will result from thermal expansion and journal centrifugal growth. The good heat-transfer path between the journal and the bearing pad, provided by the thin gas film and the relatively poor heat transfer from the pad to the surrounding gas, results in pad temperatures nearly the same as journal temperatures. Therefore, even though the radius of both the journal and the pads increases with increasing temperature, it may be assumed that the change in the bearing pad clearance ( $c$ ) is small and may be neglected. The journal growth due to centrifugal stress has been calculated and is presented in Figure 42. This growth results in a decrease of operating bearing clearance and must be considered.

Figure 43 presents a dimensionless plot of bearing pad film spring rate versus pivot clearance for various values of  $\Lambda$ . This data was derived from the curves presented in Figures 39, 40, and 41.



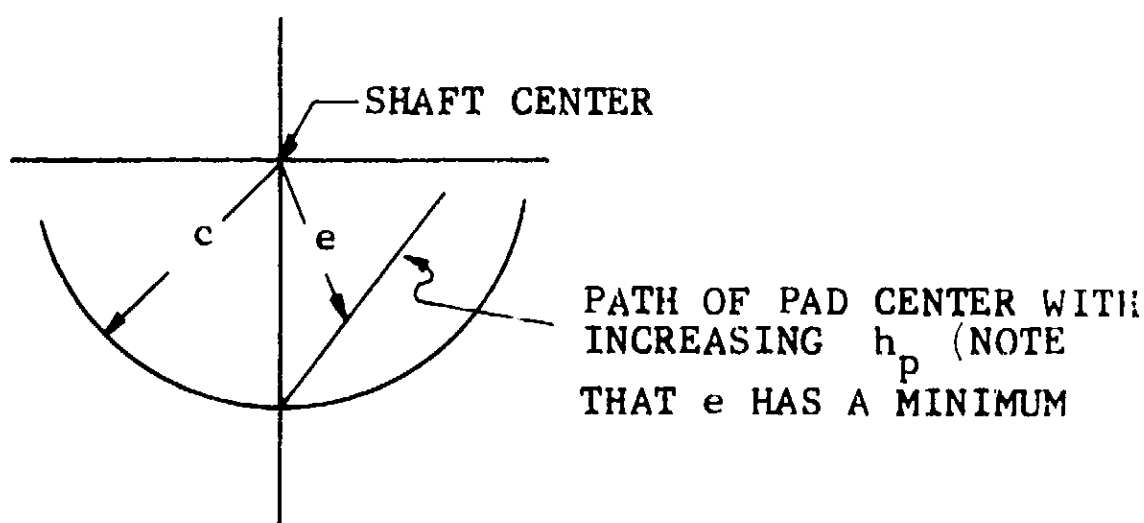
PREDICTED PERFORMANCE  
PAD ECCENTRICITY VS  
PIVOT FILM-THICKNESS RATIO

FIGURE 37



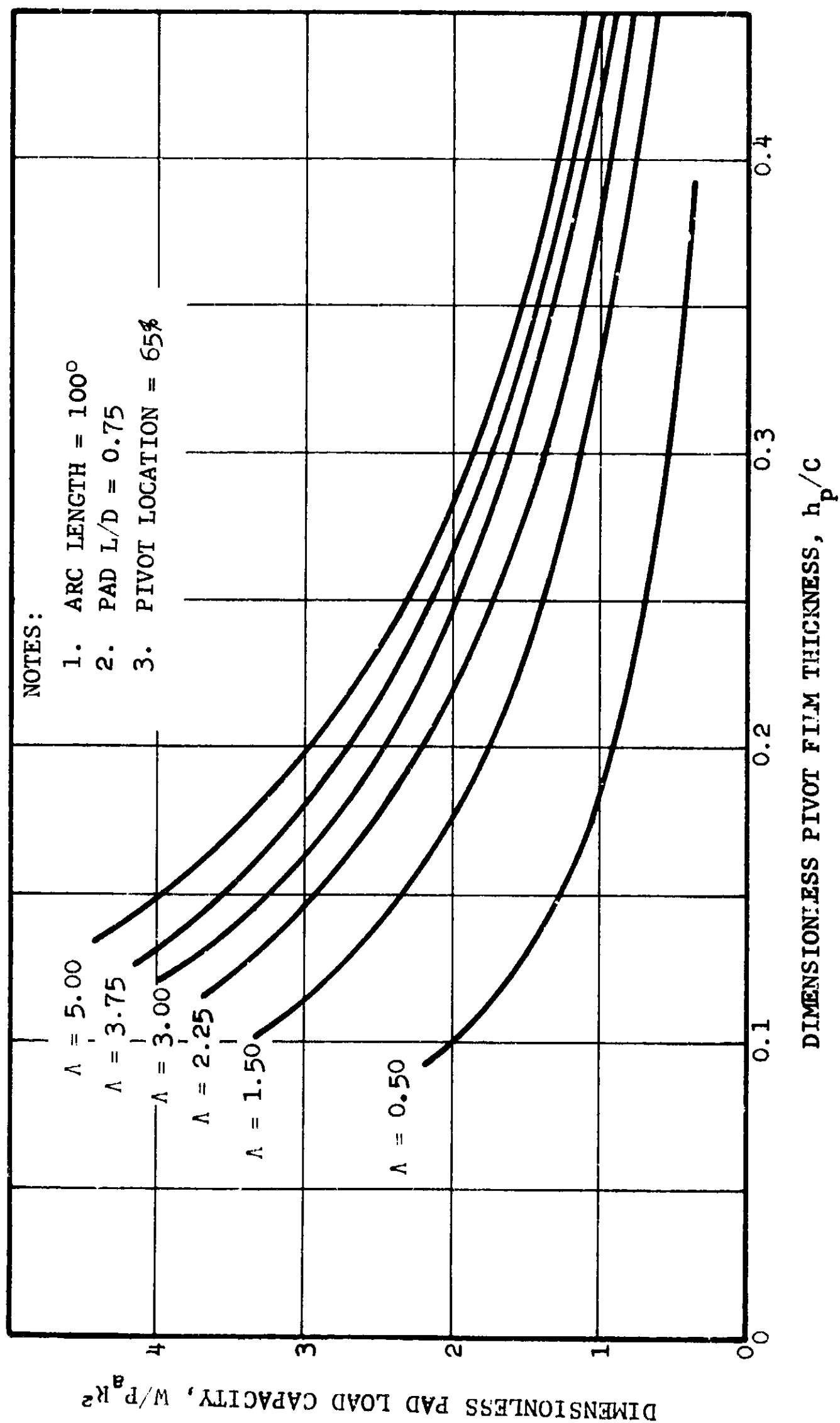
NOTES;

1.  $h_m$  = MINIMUM FILM
2.  $h_p$  = PIVOT FILM
3.  $\phi$  = ATTITUDE ANGLE
4.  $c$  = CLEARANCE
5.  $e = c - h_m$
6.  $\omega$  = SHAFT SPEED



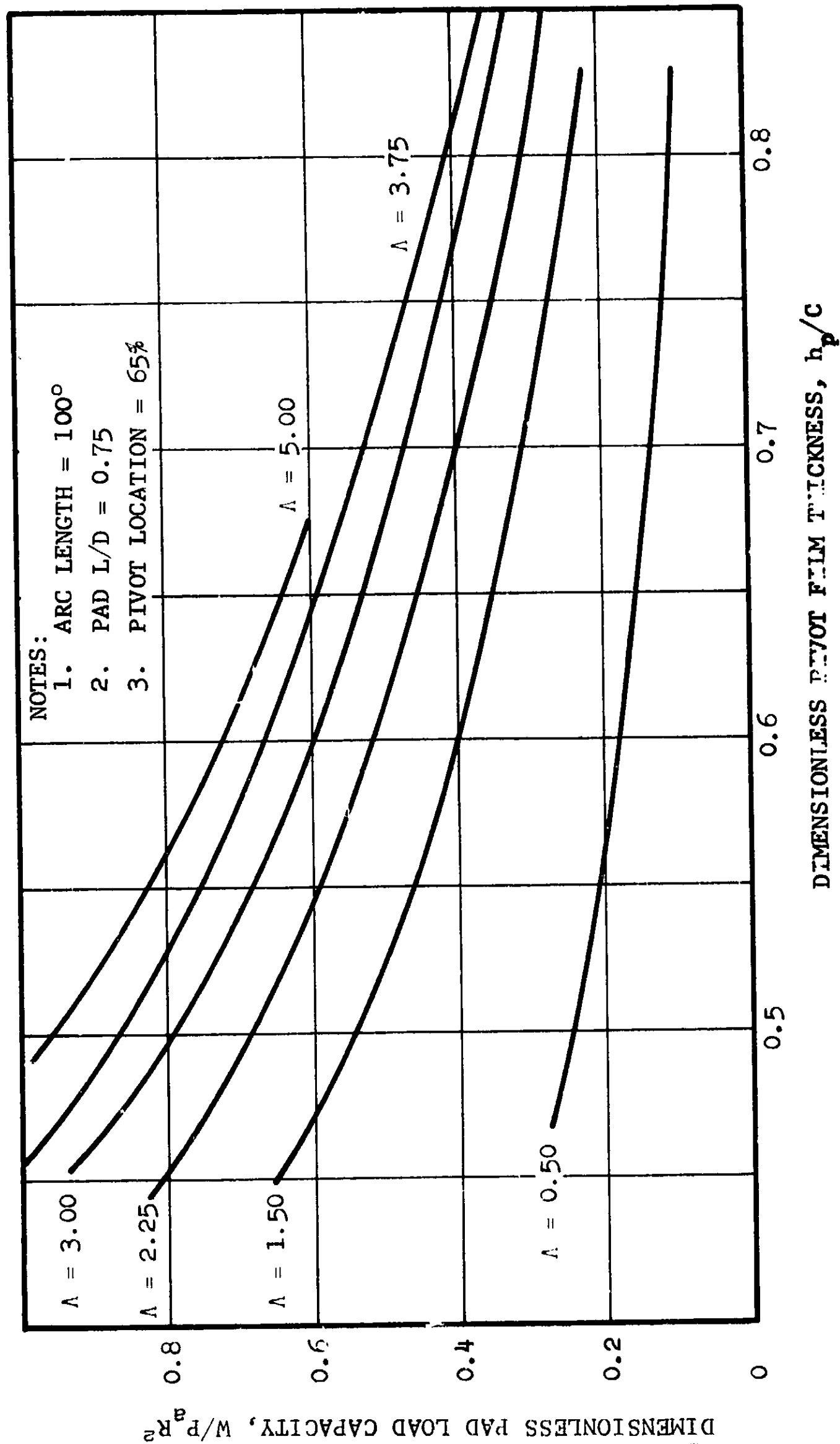
CHANGES IN PAD ORIENTATION WITH  
CHANGE IN PIVOT FILM THICKNESS  
( $\Lambda = 1.5$ )

FIGURE 38



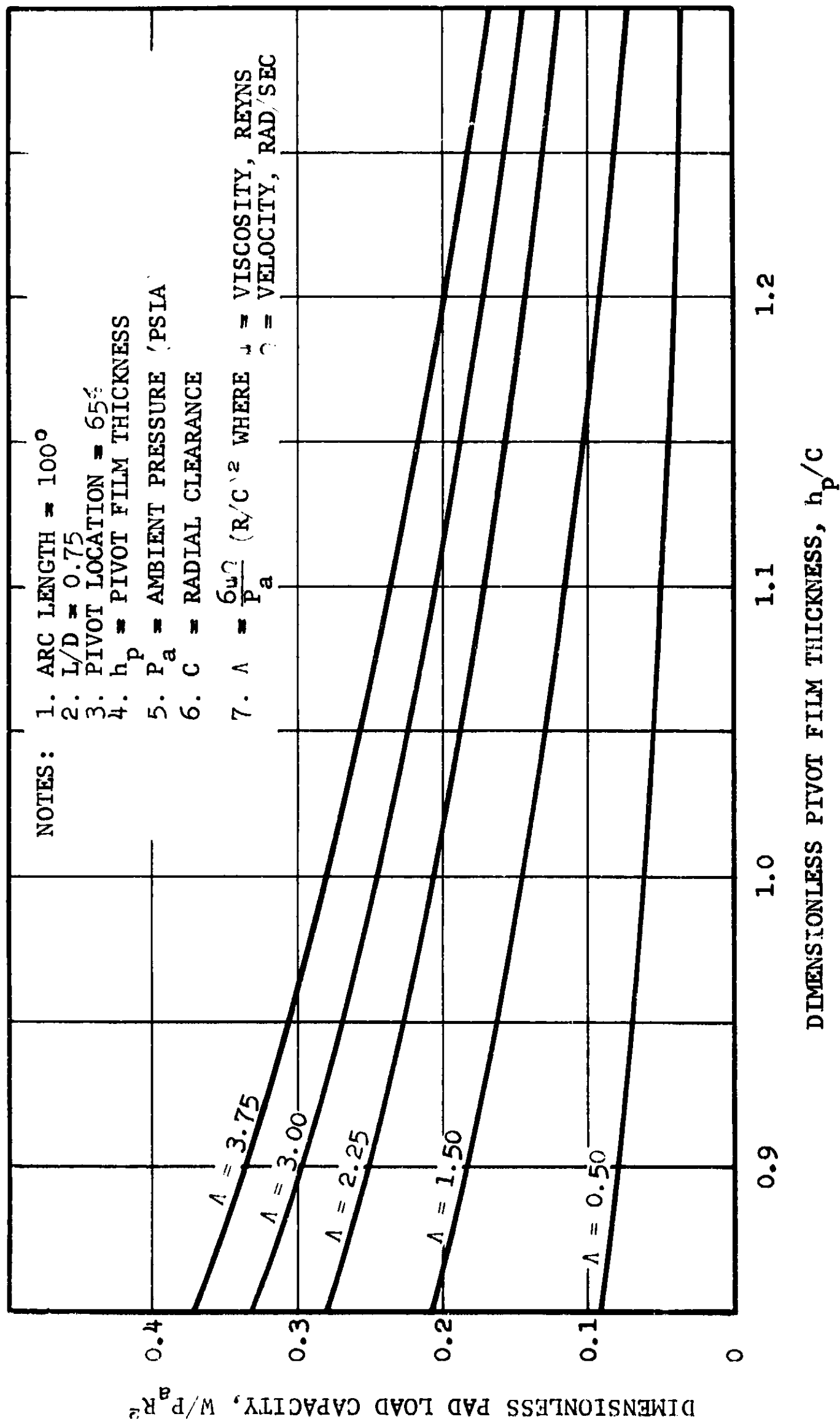
PREDICTED PERFORMANCE  
 PAD LOAD VS PIVOT FILM THICKNESS

FIGURE 39



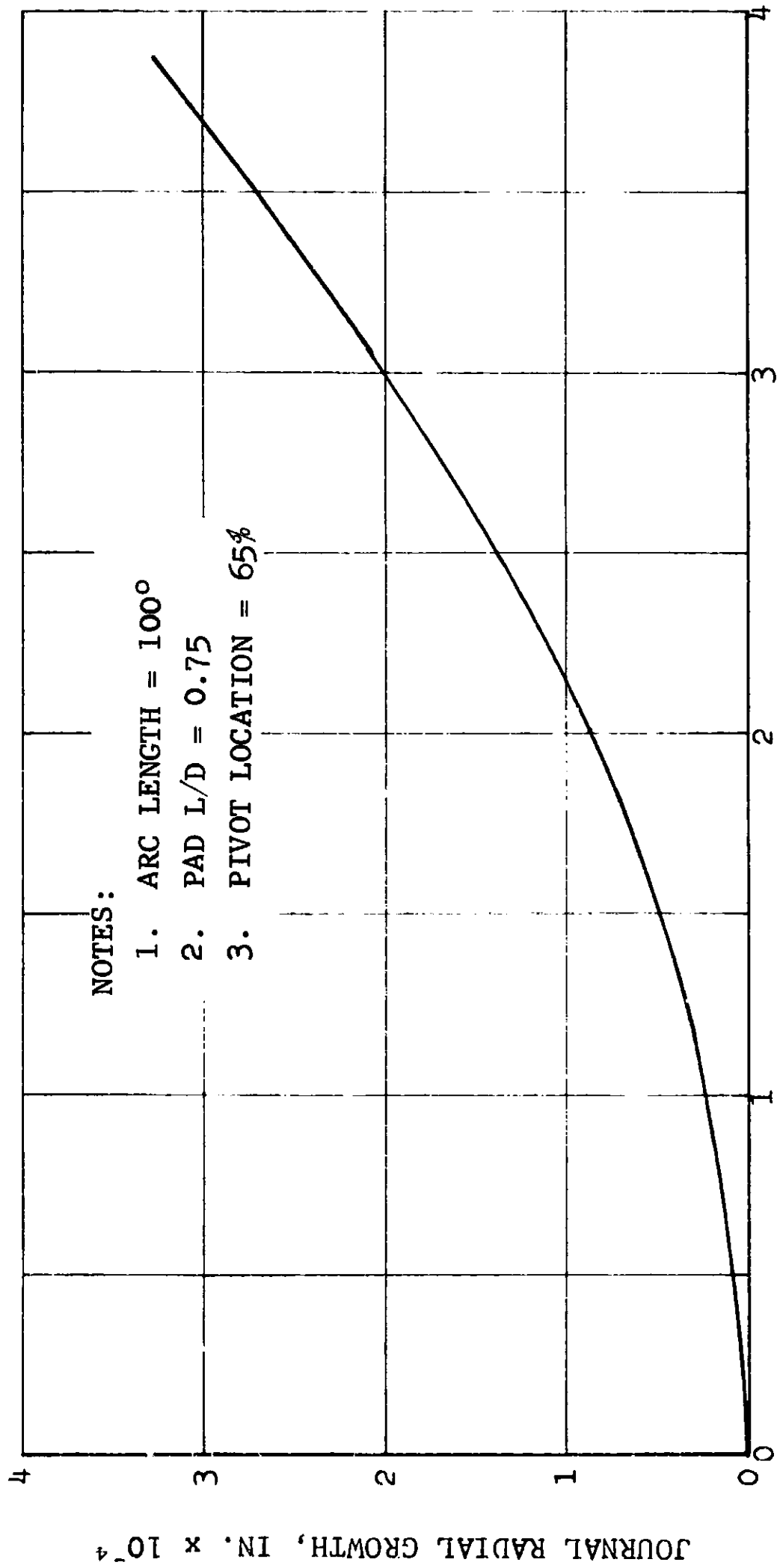
PREDICTED PERFORMANCE  
 PAD LOAD VS PIVOT FILM THICKNESS

FIGURE 40



PREDICTED PERFORMANCE  
 PAD LOAD VS PIVOT FILM THICKNESS

FIGURE 41

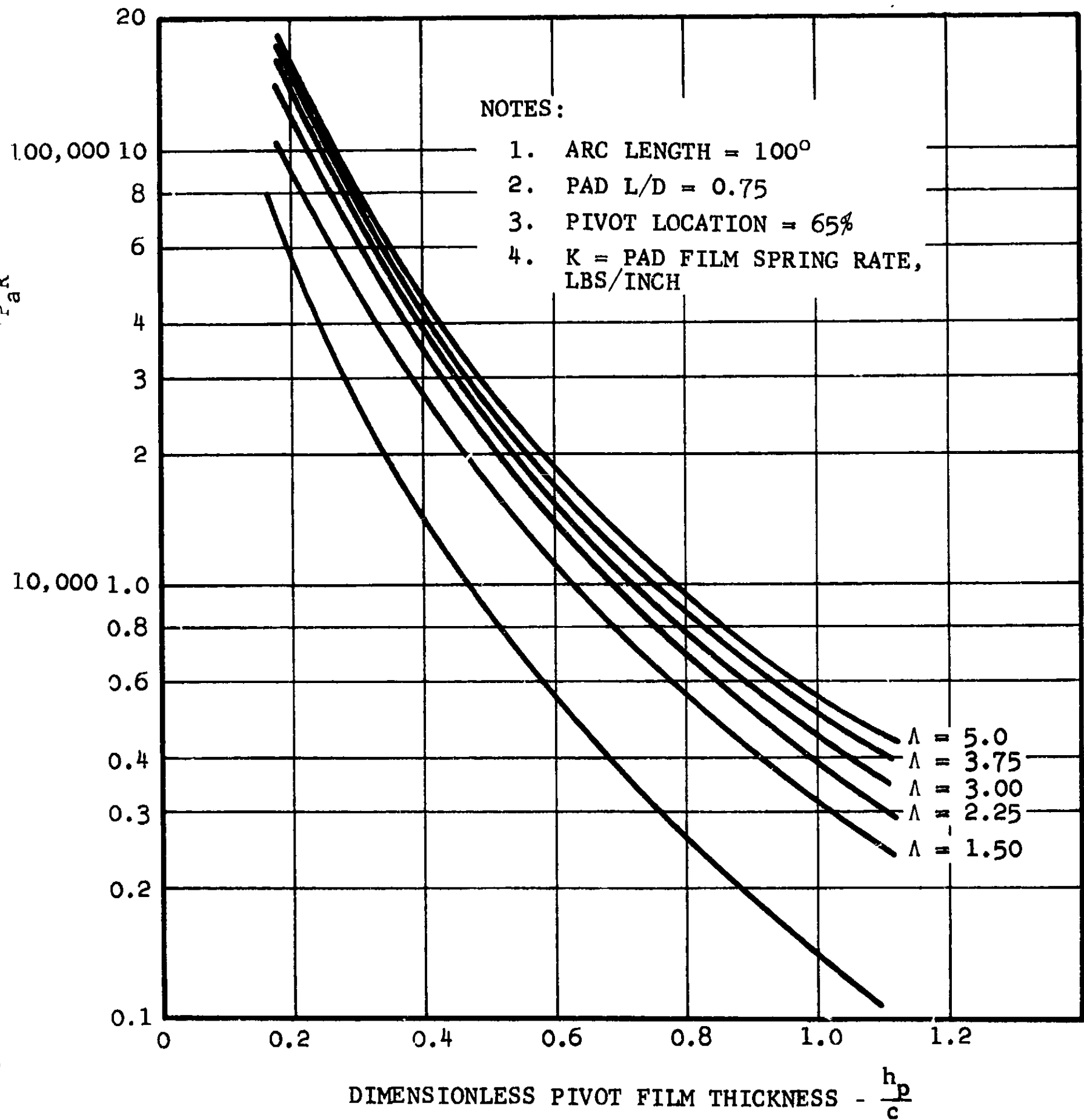


ROTOR SPEED, RPM  $\times 10^{-4}$

CENTRIFUGAL GROWTH AT JOURNALS  
OF TEST ROTORS

FIGURE 42





PREDICTED PERFORMANCE  
PAD FILM SPRING RATE VS  
PIVOT FILM THICKNESS

FIGURE 43

### 3.7.1 Sample Data-Reduction Calculation

To assist the reader in the use of the parametric curves as an aid in data reduction, a sample calculation will be reviewed. Consider the first data point logged for test rotor (a) as follows:

Rotor speed (rpm) - 38,500

Average bearing pad load at whirl (lbs) - 4.70

Average shoe temperature (°F) - 97

Rotor journal diameter (inches) - 2.0187

Pad curvature diameter (inches) - 2.0221

Ambient pressure (barometric, inches Hg) - 28.77 or 14.1 psia

#### (a) Determine Pad-to-Journal Clearance at 38,500 RPM

The clearance at 38,500 rpm is equal to the ground-in clearance (pad-to-journal) minus the increase in journal radius due to centrifugal growth (Figure 42).

$$C = \frac{(2.0221 - 2.0187)}{2} - 0.000325$$
$$= 0.00138 \text{ inch}$$

#### (b) Determine the Bearing Pad Compressibility Number $\Lambda$

$$\Lambda = \frac{6\mu\Omega}{P_a} \left(\frac{R}{C}\right)^2$$

where  $\mu$  = lubricant (air) viscosity, Reyns

$\Omega$  = rotor angular speed, radians per sec.

$P_a$  = ambient pressure, psia

$R$  = journal radius, inches

$C$  = pad-to-journal running clearance, inches

For the sample data point:

$$\mu = 2.77 \times 10^{-9} \text{ Reyns (air viscosity at pad temperature = } 97^{\circ}\text{F) from Figure 36}$$

$$P_a = 14.1 \text{ psia}$$

$$\Omega = 4.03 \times 10^3 \text{ radians per sec.}$$

$$R = 1.00935 + 0.000325 = 1.00967 \text{ inches}$$

$$C = 0.00138$$

$$\text{And } \Lambda = \frac{6 \times 2.77 \times 10^{-9} \times 4.03 \times 10^3}{14.1} \left[ \frac{1.00967}{0.00138} \right]^2$$

$$= 2.54$$

(c) Determine Bearing Pad Dimensionless Load Coefficient

$$\frac{W}{P_a R^2} = \frac{4.7}{14.1 \times (1.0097)^2} = 0.327$$

(d) Determine Pad Dimensionless Pivot Clearance

$$h_{p/C} = 0.81 \text{ (from Figure 40 for } \Lambda = 2.54$$

$$\text{and } \frac{W}{P_a R^2} = 0.327)$$

(e) Determine Pad Eccentricity Ratio and Attitude Angle

$$\epsilon = 0.56 \text{ (from Figure 37 for } \frac{W}{P_a R^2} = 0.327 \text{ and } h_p/c = 0.81)$$

$$\phi = 70 \text{ degrees (from Figure 37)}$$

(f) Determine Pad Film Spring Rate

$$K \left( \frac{c}{P_a R^2} \right) = 0.697 \text{ (from Figure 43 for } h_p/c = 0.81 \text{ and } \Lambda = 2.54)$$

$$K = \frac{14.1 \times (1.00967)^2}{.00138} \times 0.697 = 7,250 \text{ lb/in.}$$

### 3.7.2 Test Data Correlation and Discussion

The summarized theoretical calculations of the bearing pad parameters ( $\Lambda$ ,  $h_p/c$ ,  $\epsilon$ ,  $\phi$ , and  $K$ ) for the measured values of  $\frac{W}{P_a R^2}$ , obtained from the test program, are summarized in Table 4. The values of  $\frac{W}{P_a R^2}$  represent dimensionless pad loads at the threshold of whirl instability at zero bearing load (vertically oriented rotors).

For visual presentation, the data is plotted as  $\Lambda$  versus the following: (1) pad dimensionless load capacity, (2) pad pivot clearance ratio, and (3) pad attitude angle. These are found in Figures 44, 45, and 46, respectively. The fact that the data reduced to four curves (for the four rotors tested) instead of just one curve, for the parameters shown on these curves, implies that it makes a difference which combination of clearance and speed is used to obtain a given  $\Lambda$ . Moreover, since the test data in these figures displays a speed-clearance combination dependence, it is

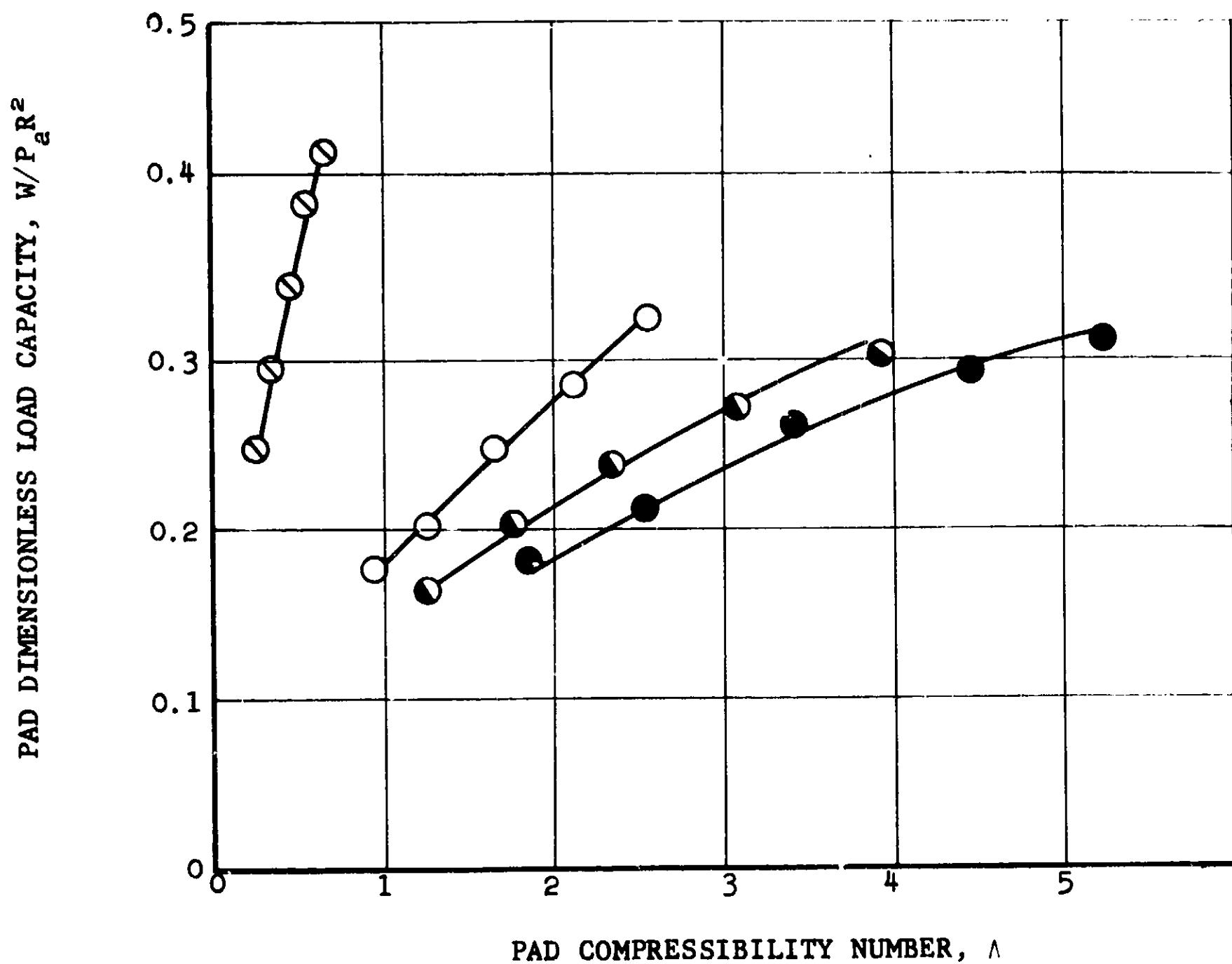
TABLE 4

SUMMARY OF THEORETICAL CALCULATIONS OF THE  
BEARING PAD PARAMETERS

<u>Rotor</u>	<u>Speed (rpm)</u>	<u><math>\Lambda</math></u>	<u><math>\frac{W}{P_a R^2}</math></u>	<u><math>\frac{h_p}{c}</math></u>	<u><math>\epsilon</math></u>	<u><math>\phi</math></u>	<u><math>\frac{K}{(lb/in.)}</math></u>
(a)	38500	2.54	.327	.81	.56	70	7250
	35000	2.13	.286	.82	.58	72	6270
	30000	1.66	.248	.81	.60	72	5420
	25000	1.27	.203	.81	.61	72	4220
	20000	.95	.178	.80	.63	71	3480
(b)	38500	3.96	.305	.93	.53	82	7300
	35000	3.09	.274	.92	.56	82	6600
	30000	2.35	.240	.91	.60	82	5780
	25000	1.78	.202	.90	.62	81	4670
	20000	1.29	.165	.90	.64	80	3880
(c)	38500	5.23	.313	.99	.45	90	8770
	35000	4.48	.292	.99	.52	90	7700
	30000	3.41	.264	.96	.56	86	5950
	25000	2.53	.212	.99	.62	90	5210
	20000	1.84	.181	.96	.64	87	4450
(d)	38500	.66	.426	.40	.71	32	8910
	35000	.58	.393	.40	.71	32	8240
	30000	.47	.344	.38	.72	31	7540
	25000	.37	.295	.37	.73	30	6890
	20000	.28	.249	.36	.74	29	6390

NOTES:

1. CONFIGURATION: THREE PIVOTED PADS, TWO RIGID MOUNTS AND ONE FLEXIBLE MOUNT AT 2075 LB/IN.
2. TEST ROTORS:
  - ROTOR (a)
  - ◐ ROTOR (b)
  - ROTOR (c)
  - ⊖ ROTOR (d)
3. LINES ARE BEST FIT CURVES THROUGH DATA POINTS



REDUCED TEST DATA  
GAS BEARING STABILITY STUDY

FIGURE 44

APS-5223-R  
Page 75

NOTES:

1 CONFIGURATION: THREE PIVOTED PADS, TWO RIGID MOUNTS AND ONE FLEXIBLE MOUNT AT 2075 LB IN.

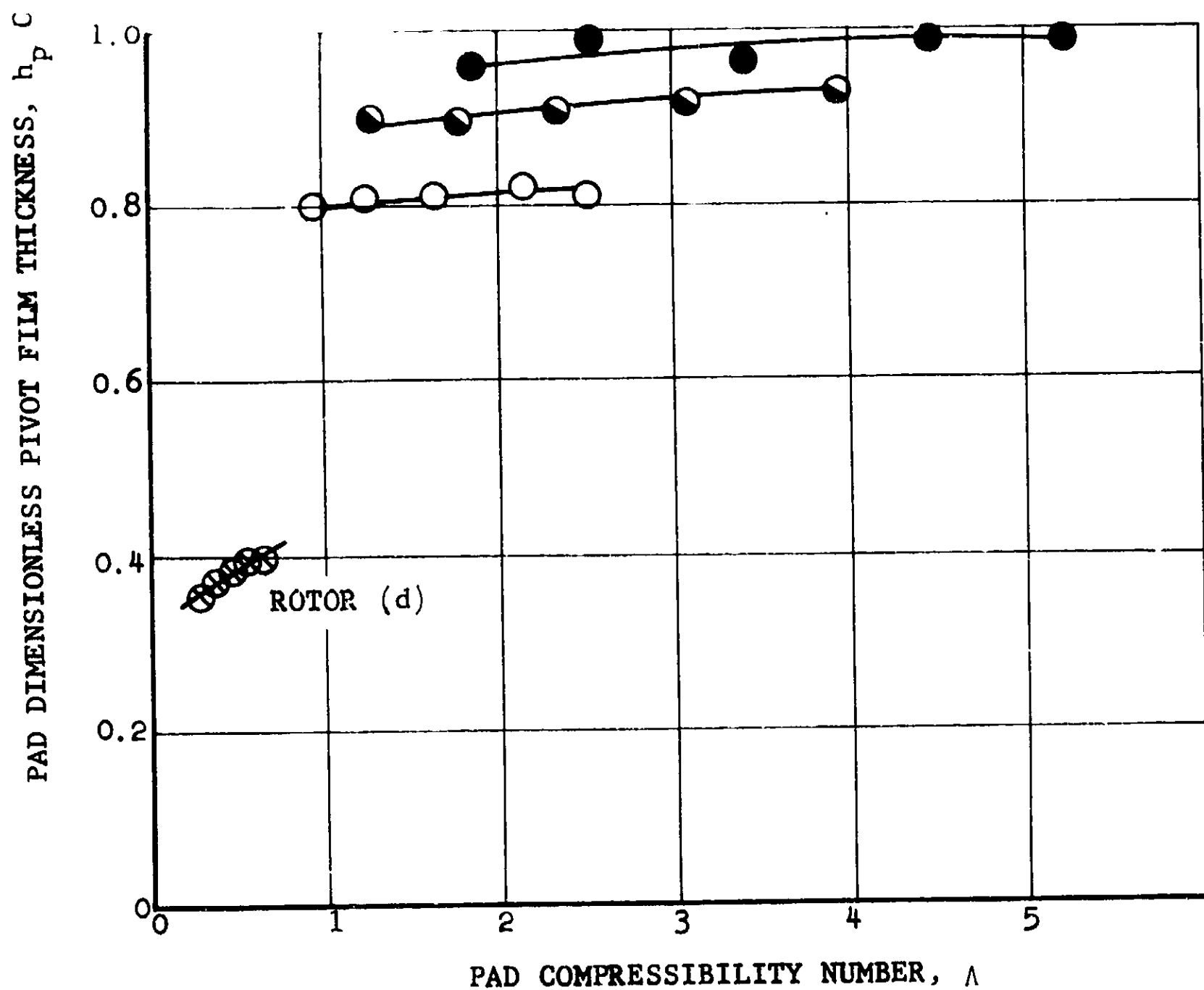
TEST ROTORS: ○ ROTOR (a)

● ROTOR (b)

● ROTOR (c)

○ ROTOR (d)

4 LINES ARE BEST-FIT CURVE THROUGH DATA POINTS

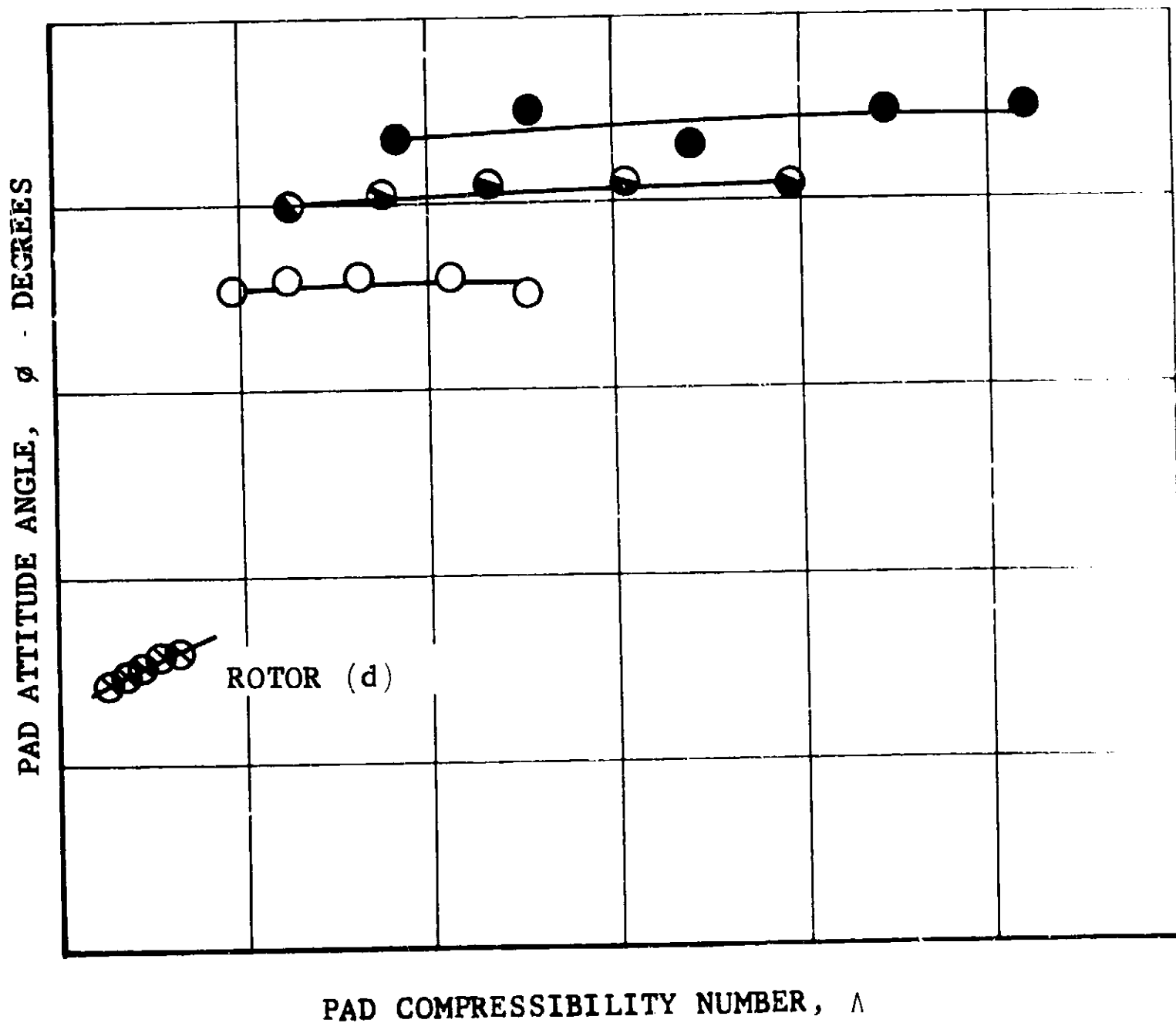


REDUCED TEST DATA  
GAS BEARING STABILITY STUDY

FIGURE 45

NOTES:

1. CONFIGURATION: THREE PIVOTED PADS,  
TWO RIGID MOUNTS AND ONE FLEXIBLE MOUNT AT 2075 LB/IN.
2. TEST ROTORS
  - ROTOR (a)
  - ◐ ROTOR (b)
  - ROTOR (c)
  - ◑ ROTOR (d)
3. LINES ARE BEST-FIT CURVES THROUGH DATA POINTS



PAD COMPRESSIBILITY NUMBER,  $\Lambda$

REDUCED TEST DATA  
GAS BEARING STABILITY STUDY

FIGURE 46

APS-5223-R  
Page 77



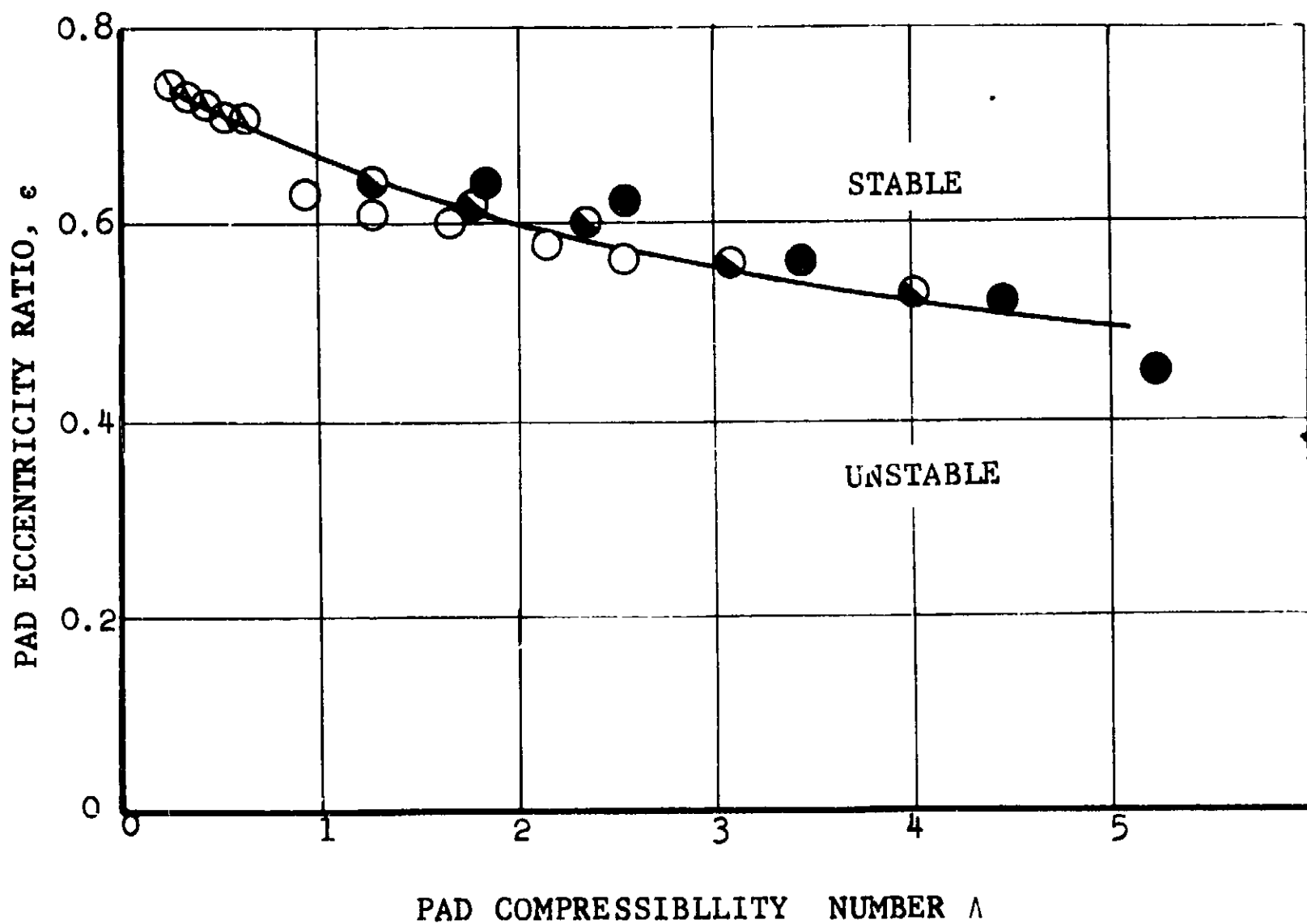
likely that a change in lubricant viscosity or ambient pressure (the other two parameters making up  $\Lambda$ ) would also display the same trend. To the extent that this is true, the plots shown in Figures 44, 45, and 46 are not satisfactory dimensionless parameters to use in determining bearing-rotor stability characteristics.

Figure 47 is a plot of the bearing eccentricity ratio ( $\epsilon$ ) versus  $\Lambda$  at the thresholds of whirl. The data for the four rotors, in this case, reduces to a single curve. This is a significant finding. The reader is invited to look once more at Figure 37. Note that at any particular value of pad eccentricity ratio ( $\epsilon$ ) and pad compressibility number  $\lambda$  ( $\Lambda$ ) there are two corresponding values of dimensionless pad pivot film thicknesses ( $h_p/C$ ). Then note that the values of pad  $h_p/C$  tested for Rotors a, b, and c are in the range of 0.80 to 0.99 (well to the right of the bend in the double-value curves). Historically, Rotors a, b, and c were tested first, and the program would have been declared to be completed (according to contractual requirements) except for the discovery of the above-mentioned double values of pad  $h_p/C$  shown in Figure 37. Rotor d was therefore created by further reducing the journal diameters of Rotor c to reduce the test values of pad  $h_p/C$  to approximately 0.40 (to the left of the bend of the double-value curves). The five test points of Rotor d, as plotted on Figure 47, form a smooth extension to those of Rotors a, b, and c.

The single curve indicates that the critical value of eccentricity ratio, for a given value of  $\Lambda$ , is independent of the values of the individual properties that combine to produce that particular  $\Lambda$ . Therefore, for the particular rotor-bearing-mounting system tested, this plot appears to be a satisfactory dimensionless correlation of the stability data. Since the bearing-rotor geometries of

NOTES:

1. CONFIGURATION: THREE PIVOTED PADS, TWO RIGID MOUNTS AND ONE FLEXIBLE MOUNT AT 2075 LB PER IN.
2. TEST ROTORS
  - ROTOR (a)
  - ◐ ROTOR (b)
  - ROTOR (c)
  - ◑ ROTOR (d)
3. LINES ARE BEST-FIT CURVES THROUGH DATA POINTS.



REDUCED TEST DATA  
GAS BEARING STABILITY STUDY

FIGURE 47

the referenced turbocompressor are quite similar to those tested in the rig, it is believed that this stability criteria is applicable, and can be used to check rotor stability at anticipated turbocompressor operating conditions. Once the steady-state bearing pad loads are established as a result of a thermal analysis (refer to par. 2.4 of Task I), a dimensionless pad pivot film clearance can be calculated. Entering this dimensionless pad pivot film clearance and appropriate pad compressibility number into Figure 37 will yield the operating bearing pad eccentricity ratio. This eccentricity ratio and the compressibility number can then be compared to the curve of Figure 47 to determine whether or not the system will be stable.

The above-mentioned use of Figure 47 to determine stability criteria is based purely on bearing pad properties and does not take into consideration rotor mass or inertial properties. During the analyses it became apparent that the developed data could be used to obtain a more general insight into stability criteria. In keeping with this, a study was conducted that made use of rotor properties in the correlation in an attempt to better understand the turbocompressor rotor-bearing system and to examine the possibility of determining a stability criterion that could be applied to other rotor-bearing systems. The following is a brief outline of the approach taken in this study.

The bearing system under consideration has two pads that are fixed radially and one pad that can move radially on a flexible support. The Contractor has observed in previous work that the critical speeds (resonant frequencies) of this type of system can be adequately predicted by including only the pad lubricant film spring rate in the calculation. The added mount flexibility introduced in one pad apparently does not influence the resonant frequency.

Since the critical speed is just a special case of the general rotor whirl phenomenon, an attempt was made to apply rigid rotor whirl equations to the resonant whirl problem by using the pad lubricant film spring rate as the rotor support.

To check the validity of this approach, the measured whirl frequencies (see Table 4) were used in the equation for the non-synchronous whirl of an asymmetric rigid rotor to determine the support spring rates required to sustain the rotor whirls. The equation is:\*

$$\frac{\lambda^2}{K(1+R)^2} = \frac{\beta_{11} m + \beta_{22} I_e \pm \sqrt{(\beta_{11} m + \beta_{22} I_e)^2 - 4(\beta_{11} \beta_{22} - \beta_{12}^2) m I_e}}{2(\beta_{11} \beta_{22} - \beta_{12}^2) m I_e}$$

where:

$\lambda$  = whirl velocity

$\omega$  = rotor angular velocity

$$I_e = I_d - \frac{\omega}{\lambda} I_p$$

$\beta$ ,  $m$ ,  $R$  = properties of the rotor system

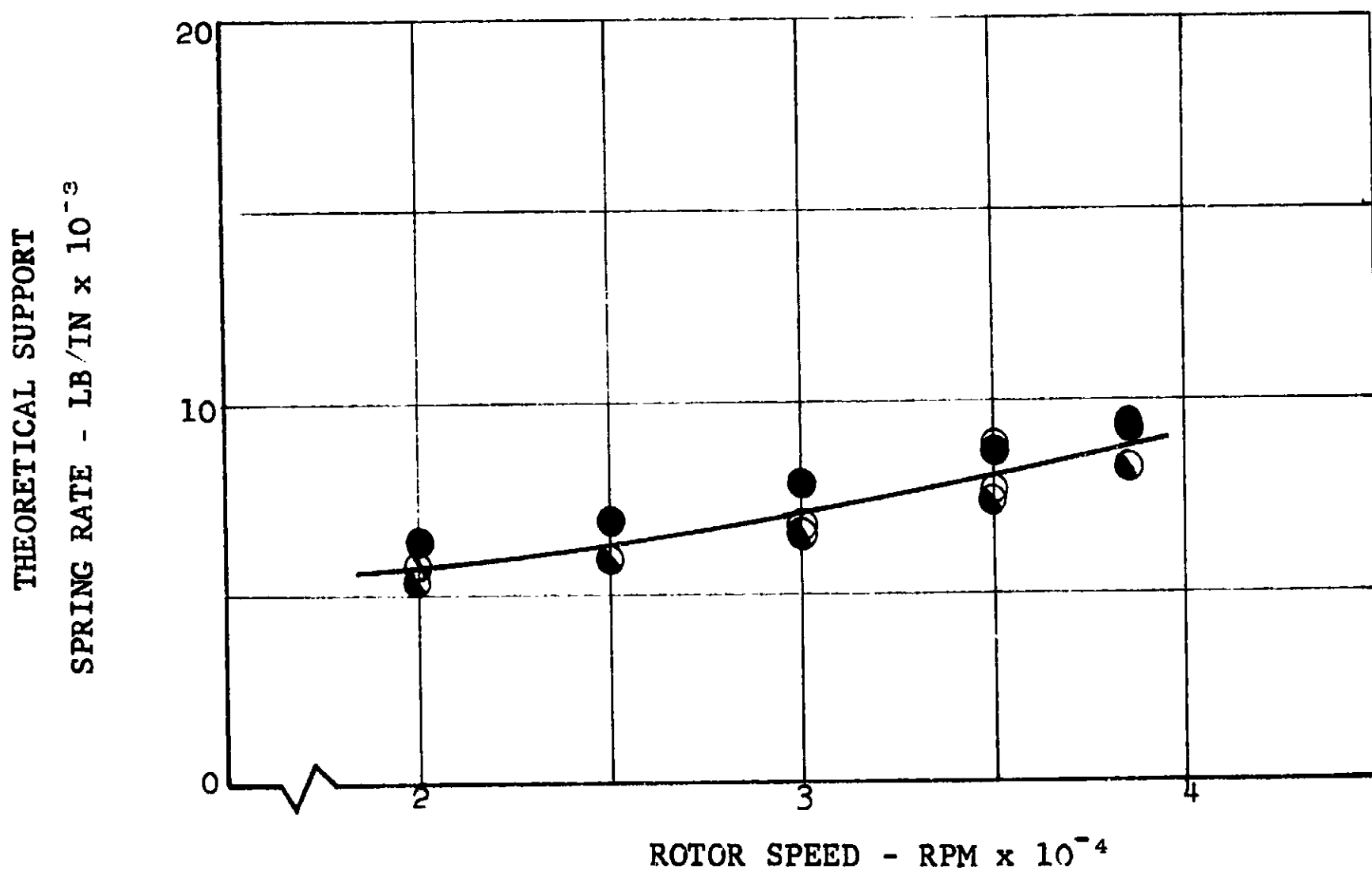
$K$  = spring constant

The mass and inertia of the test rotor were used in this calculation, and the resulting support spring rates are given in Figure 48.

\*Derivation of this equation can be found in Appendix I.

NOTES:

- ROTOR (a)
- ◐ ROTOR (b)
- ROTOR (c)
- ⊗ ROTOR (d)



THEORETICAL SUPPORT  
 SPRING RATE VERSUS SPEED  
 RIGID UNSYMMETRIC ROTOR EQUATIONS  
 USING EXPERIMENTAL WHIRL CPS

FIGURE 48

For comparison, the actual film spring rate for each data point at whirl threshold was determined from Figure 43 (tabulated in Table 2). These results are shown in Figure 49. Note the close agreement between the spring rate required by the rotor equations (Figure 48) and the film spring rates found by reducing the test data (Figure 49). Also note that the scatter in this data is a very small percent of the normal operating lubricant film spring rate of approximately 50,000 pounds per inch.

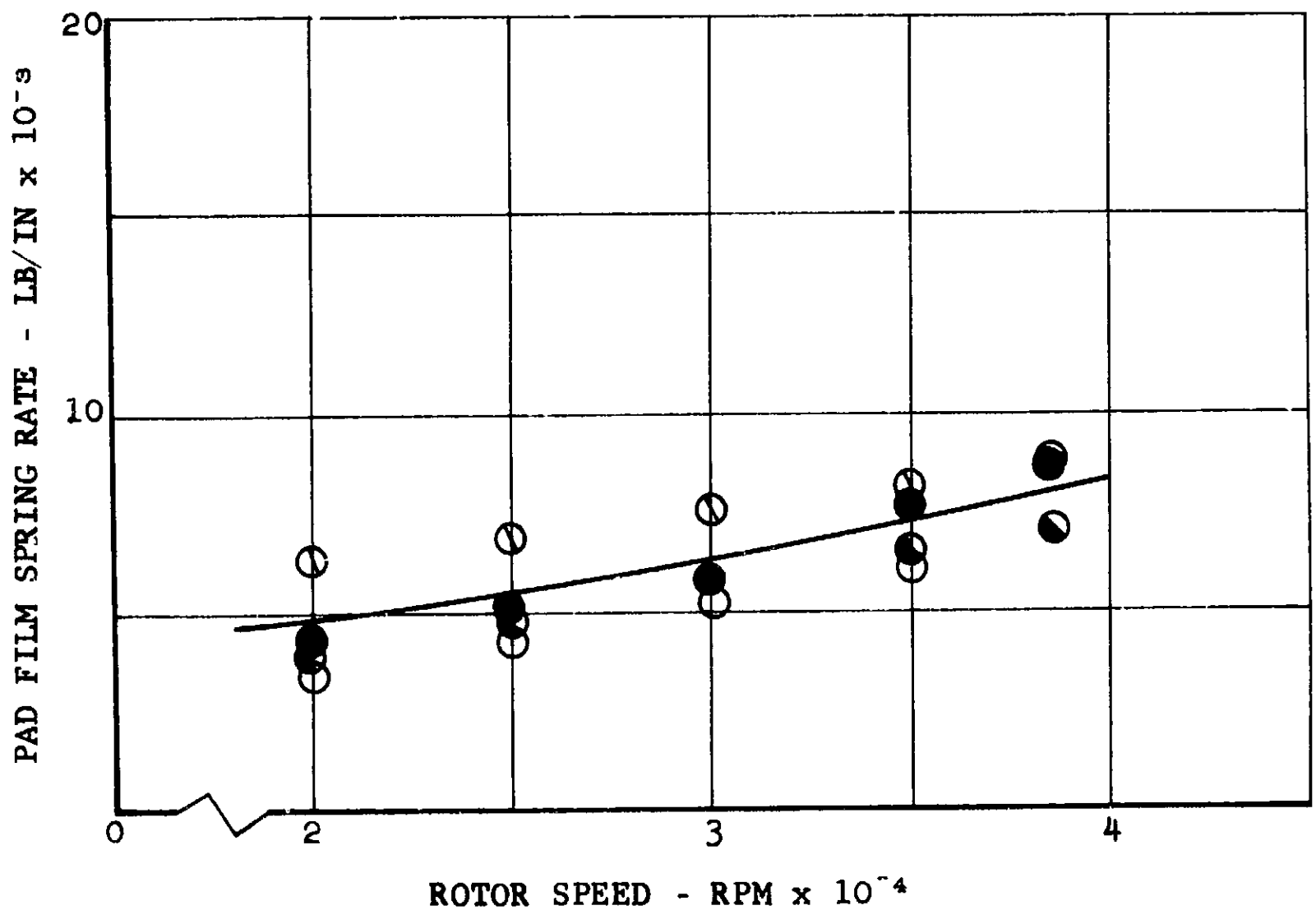
This agreement seems to verify that for the particular configuration tested, the rotor whirl frequency is controlled by the pad film spring rate, and that the spring rate of the flexible support does not have a strong influence on the whirl frequency. Applying this correlation to the gas generator provides an additional stability criterion. When an operating pad pivot film thickness has been determined, the pad film spring rate can be found from Figure 43. This spring rate can be compared to the curve of Figure 49 to determine whether the system will be stable.

This approach may also be useful for rotors with other mass and inertia properties. The rotor equations can be entered with any rotor geometry, and the spring rate for whirl at the frequency of the critical speed can be determined. Entering Figure 43 with this spring rate and compressibility number determines the pad pivot film thickness at the whirl threshold. Operation with smaller pivot film thicknesses (producing higher pad film spring rates) will result in stable operation. To explore this technique further would require testing with other rotor systems.

NOTES:

1. CONFIGURATION: THREE PIVOTED PADS,  
TWO-RIGID MOUNTS AND ONE FLEXIBLE  
MOUNT AT 2075 LB PER IN.
2. TEST ROTORS
 

○	ROTOR (a)
◐	ROTOR (b)
●	ROTOR (c)
◑	ROTOR (d)
3. LINE IS BEST FIT CURVE THROUGH  
DATA POINTS.



REDUCED TEST DATA  
PAD FILM SPRING RATE VS SPEED

FIGURE 49

### 3.8 Application of Stability Criteria to Delivered Turbocompressor

The stability criteria developed in this program may be used along with the thermal analysis of the turbocompressor to predict rotor stability at any required operating condition. The calculated temperature profile determines the thermal expansions of the parts of the machine. This information, along with the known bearing flexible mount spring rate and bearing pad film characteristics, permits the pad pivot film thickness to be determined. With this variable known, either the bearing pad eccentricity ratio may be found and compared with the appropriate stability curve, or the pad film spring rate may be found for use in the alternate stability correlation. With either approach the variable used (pad eccentricity ratio or pad film spring rate) should be well above the appropriate threshold curve if stability is to be assured.

Calculations of this type have been made for the gas generator by using the "as delivered" values of pad preload and the 4,000-pound-per-inch pad flexible mount spring rate. The thermal expansions were obtained by using the temperature profiles generated under Task I. The critical bearing was found to be the turbine end bearing due to the adverse thermal gradients. Results for the bearing pads are tabulated in Table 5. The cooling flows given are all percentages of the basic cycle mass flows.

TABLE 5

	$h_p/C$	$\epsilon$	$\Lambda$	$K, \text{ lb/in}$
12 psia 1/2 % Cooling	.728	.575	1.90	3,410
6 psia 1% Cooling	.597	.52	3.98	3,820
6 psia 2% Cooling	.531	.565	3.67	4,810
6 psia 4% Cooling	.377	.66	3.42	11,150



This data is presented along with both stability threshold curves in Figure 50. None of the points lie comfortably within the stable region; however, the machine could probably operate at the 6-psia, 4-percent cooling condition.

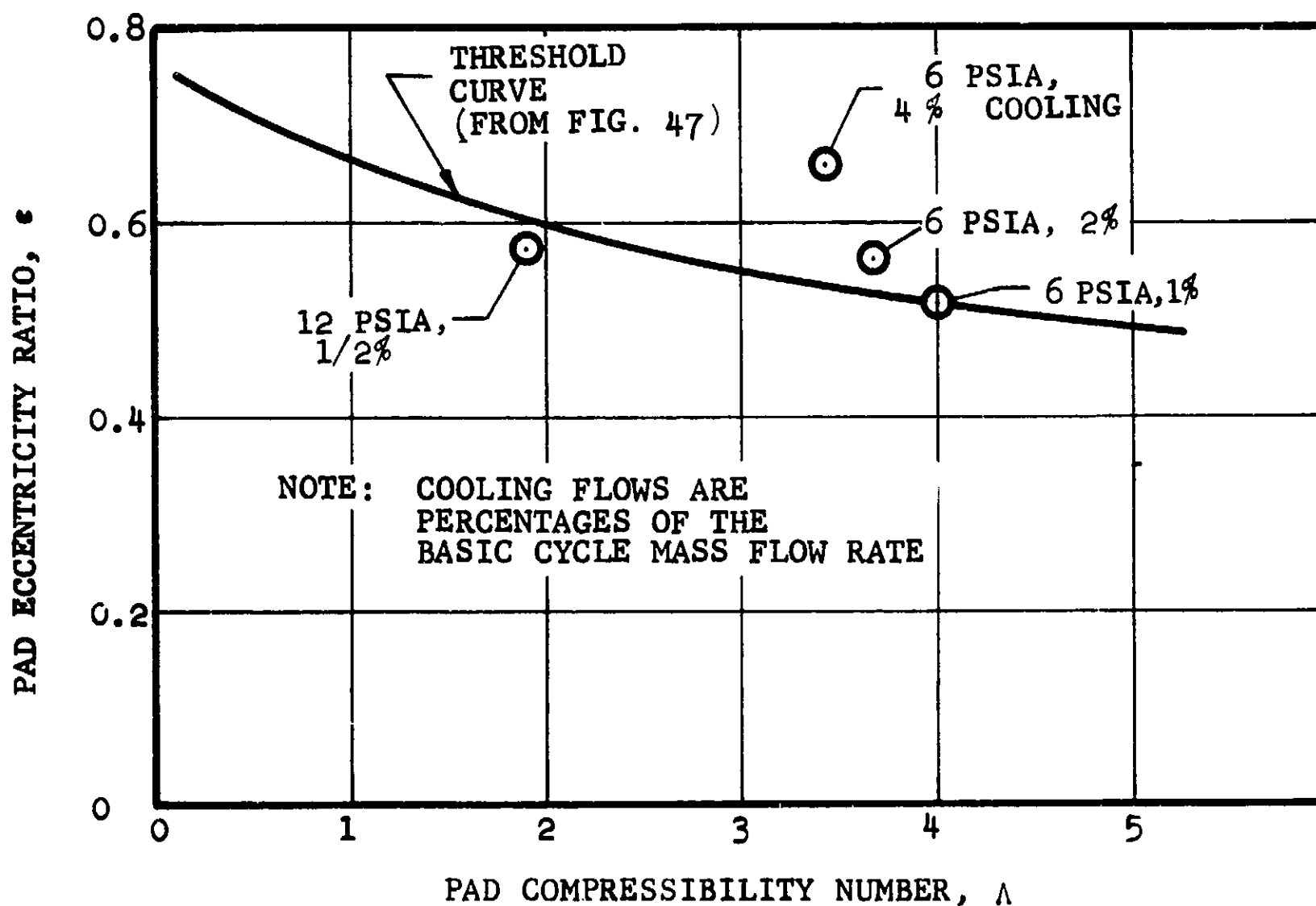
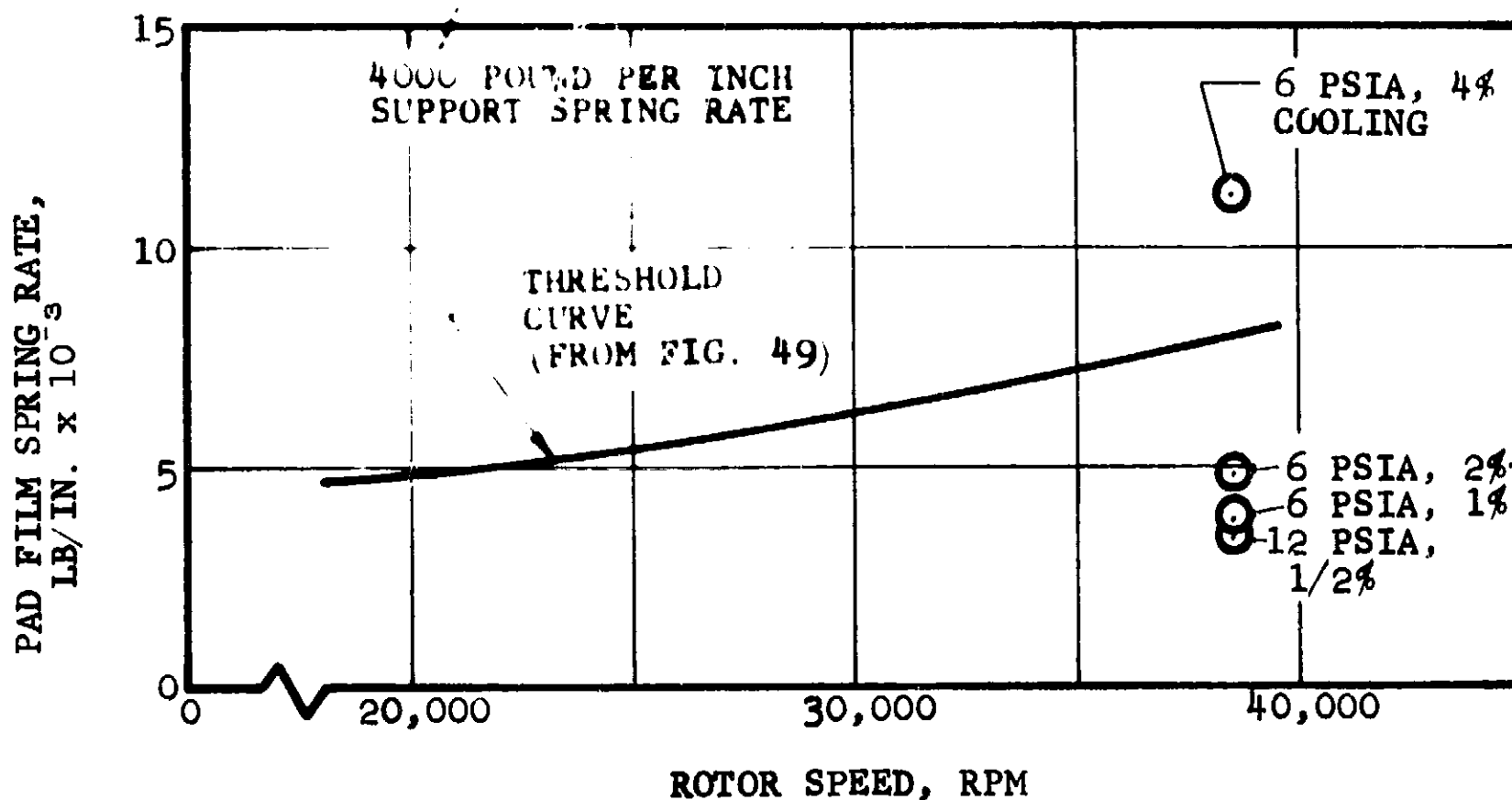
The low pad eccentricity ratios and pad film spring rates given above are the result of the thermal expansions which unload the pads. An attempt was made to analytically reduce the effect of the thermal expansions by reducing the spring rate of the pad flexible mount to 2,000 pounds per inch. Turbine end bearing properties resulting from this study are given in Table 6.

TABLE 6

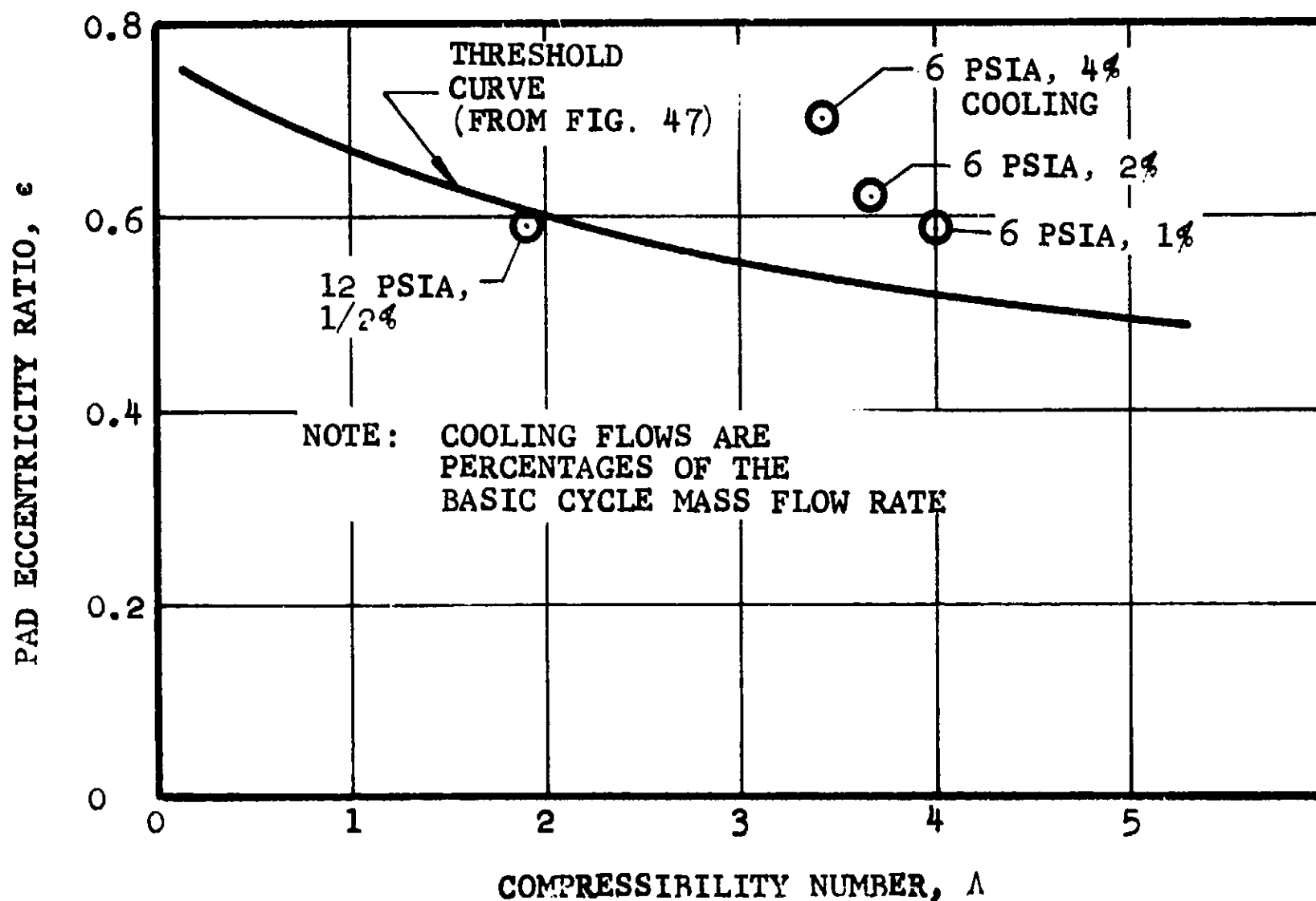
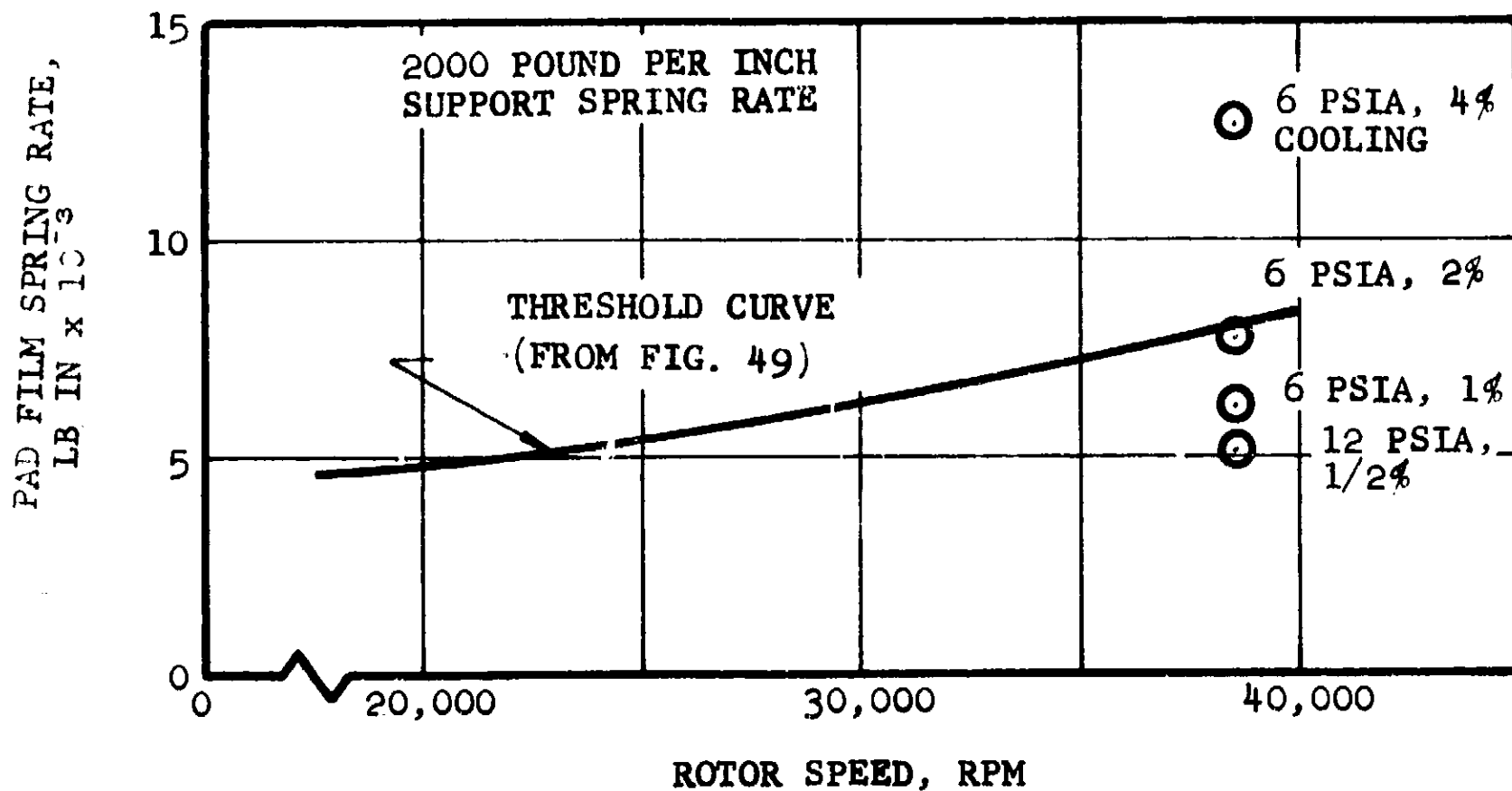
	<u><math>h_p/C</math></u>	<u><math>e</math></u>	<u><math>\Lambda</math></u>	<u><math>K, \text{ lb/in}</math></u>
12 psia 1/2 % cooling	.615	.59	1.90	5,030
6 psia 1% cooling	.485	.585	3.98	6,120
6 psia 2% cooling	.433	.62	3.67	7,650
6 psia 4% cooling	.34	.70	3.42	12,700

Figure 51 compares this data with the threshold of whirl curves. The lower pad flexible mount spring rate has moved the operating points only slightly toward the stable region. The basic thermal expansion problem is thus considered to still be present.

It is concluded that the most practical way to improve the stability of the referenced turbocompressor is to modify the hardware so that the temperature distribution and thermal expansion effects are more favorable.



PREDICTED GAS GENERATOR OPERATING  
POINTS COMPARED WITH THRESHOLD  
OF WHIRL CURVES



PREDICTED GAS GENERATOR OPERATING  
POINTS COMPARED WITH THRESHOLD  
OF WHIRL CURVES

FIGURE 51

APS-5223-R

Page 88

#### 4.0 TASK III, EXPERIMENTAL INVESTIGATIONS OF NONPIVOTED-TYPE, PARTIAL-ARC GAS BEARINGS

##### 4.1 General

The ball-and-socket pivot in the pivoted-pad bearing design delivered in the NASA gas generator under NASA Contract NAS3-2778 has the design goal of demonstrating an operational life of 10,000 hours. A potential problem in obtaining this long life is wear of the ball-and-socket pivot, which could cause pad lockup and/or serious loss of hydrodynamic back pressure at the lapped ball-and-socket interface. Nonpivoted bearings or, more specifically, elastically pivoted ("fixed-stem") partial-arc pad bearings had been successfully demonstrated by AiResearch during the development phase of NASA Contract NAS3-2778. These tests had been run with the following mount configurations:

- (a) Three flexibly mounted partial-arc pads per journal (mount radial flexibility 20,000 lbs per inch).
- (b) One flexibly mounted partial-arc pad (mount flexibility, 20,000 lbs per inch) and two "fixed" (constrained against radial motion) partial-arc pads per bearing. Note that although the two pads per bearing were constrained against radial motion, some degree of pivoting was afforded by the bending movement of the 20,000-lbs-per-inch mount diaphragms.

Even though successful operation was achieved with the aforementioned mount configurations, the system was not thought at that time to be a practical solution for a realistic machine. The difficult problems were the establishment of initial pad alignment and the inadequate thermal growth accommodation due to the high (20,000 lbs per inch) mount spring rates. Preliminary efforts to reduce the mount configuration to three flexibly mounted pads with a 10,000-lb-per-inch spring rate were not successful and, due to schedule limitations, this potential mounting system received no further evaluation under Contract NAS3-2778.

The objective of this program task was therefore to continue the work to determine whether or not dynamic stability may be obtained with greatly decreased resilient mount spring rates, which might provide improved alignment techniques and thus lead to a more practical design for incorporation in a turbocompressor package. Specific task requirements were to test two resilient mounting systems with different spring rates to determine the following:

- (a) Minimum preload required to obtain satisfactory rotor dynamic stability
- (b) Identification of the rigid-body critical speeds

#### 4.2 Test Rig

The two-bearing rotor dynamic test rig described in Section 3.2 was used for the testing. The variable loading device (pressurized diaphragms) described previously was not used for these nonpivoted

(fixed-stem) pad bearings because a change in diaphragm pressure (to effect a load change) introduces undesirable misalignment problems in the flexibly mounted partial-arc pads. For each test described hereafter, each change in pad preload was accomplished with the rotor at standstill and floating hydrostatically.

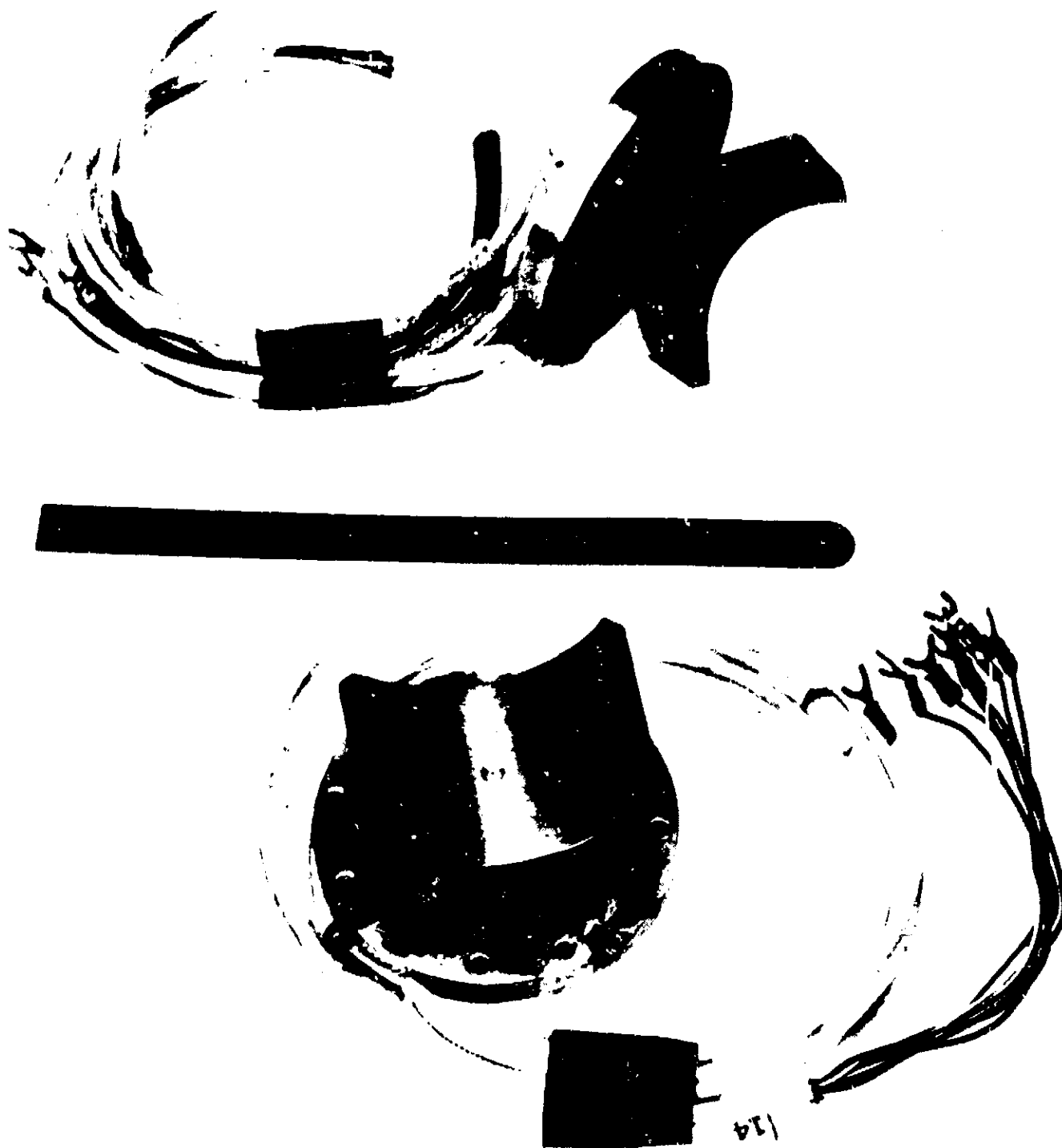
#### 4.3 Instrumentation

The instrumentation for these tests was essentially the same as reported in Section 3.3 except that no X-Y plotters were used, since the variable loading device was not employed.

#### 4.4 Test Hardware

The test components were as follows:

- (a) Rotor - 11-inch bearing span with 2.0187-inch-diameter journals (this was rotor "a" described in Section 3.4).
- (b) "Elastically pivoted partial-arc bearing pads with diametral curvature within the limits of 2.0223 - 2.0219 inches. These pads have an L/D ratio of 0.75, a pivot location of 65 percent back from the pad leading edge, and a hydrostatic lift-off supply system comprising one 0.0102 inch-diameter orifice and a 0.001/0.0005-inch deep by 0.160/0.150-inch-diameter recess (see Figure 52).



"ELASTICALLY" PIVOTED  
PARTIAL ARC BEARING PADS

FIGURE 52

The resilient mounting system used for the two test series was as follows:

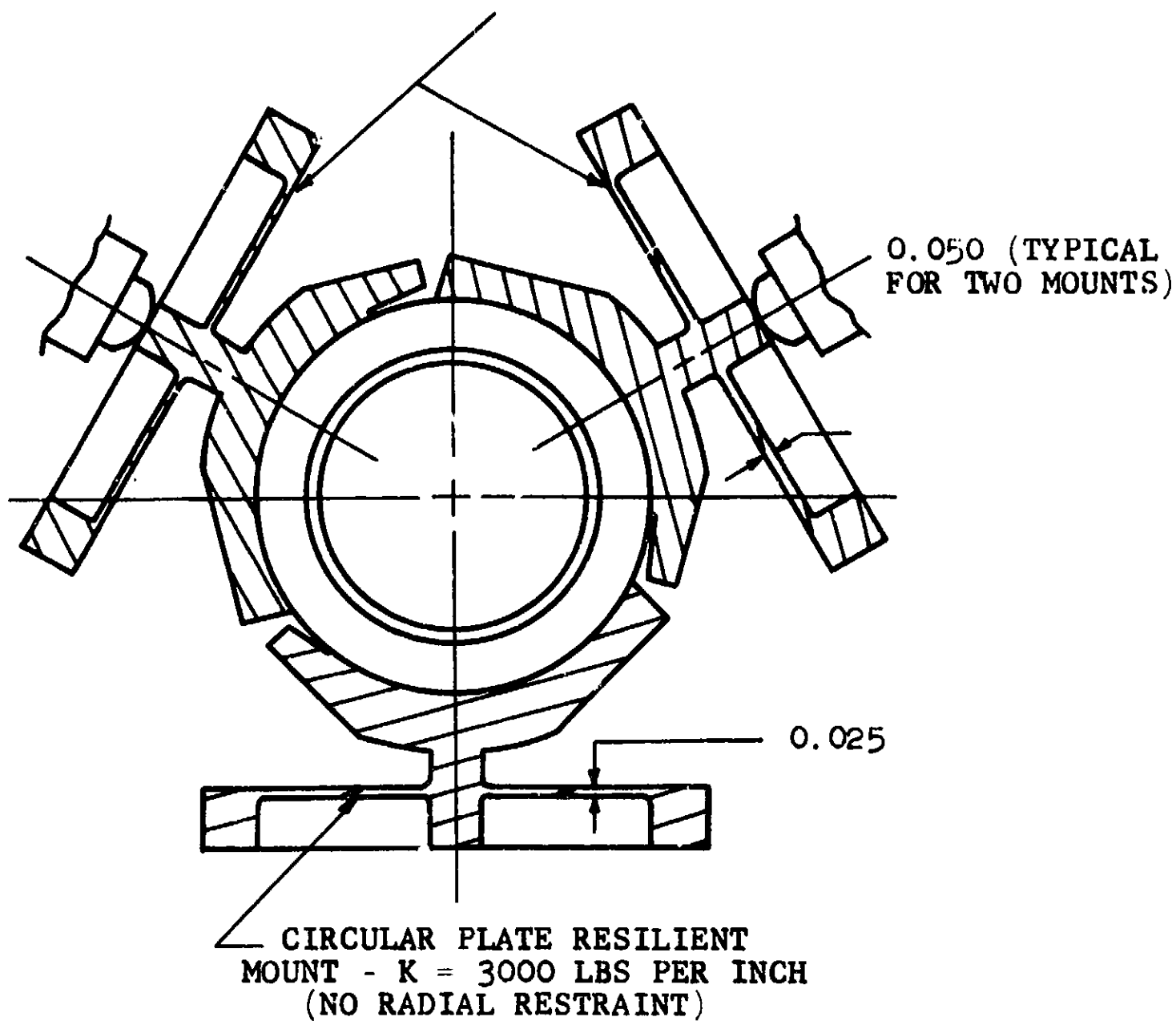
Test 1 - A resilient mount (Figure 53) consisting of one flexibly mounted pad per journal bearing (circular plate, "diaphragm," with an approximate spring rate of 3,000 lbs per inch), two "fixed" (constrained against radial motion) pads per bearing (bending movement or pad pitching afforded by 20,000-lb-per-inch spring rate of the circular plates).

Test 2 - A resilient mount (Figure 54) consisting of one flexibly mounted pad per journal bearing (circular plate, "diaphragm," with an approximate spring rate of 3,000 lbs per inch), two "fixed" (constrained against radial motion) pads per bearing (bending movement or pad pitching afforded by 3,000-lb-per-inch spring rate of the circular plates).

It should be noted that the same rotor and bearing pads were used for both test series. The only test variable introduced was the reduction of the "fixed mount spring rates (20,000 lbs per inch). This was accomplished by machining the circular plate thickness down from the original 0.050 inch to a nominal value of 0.025 inch.



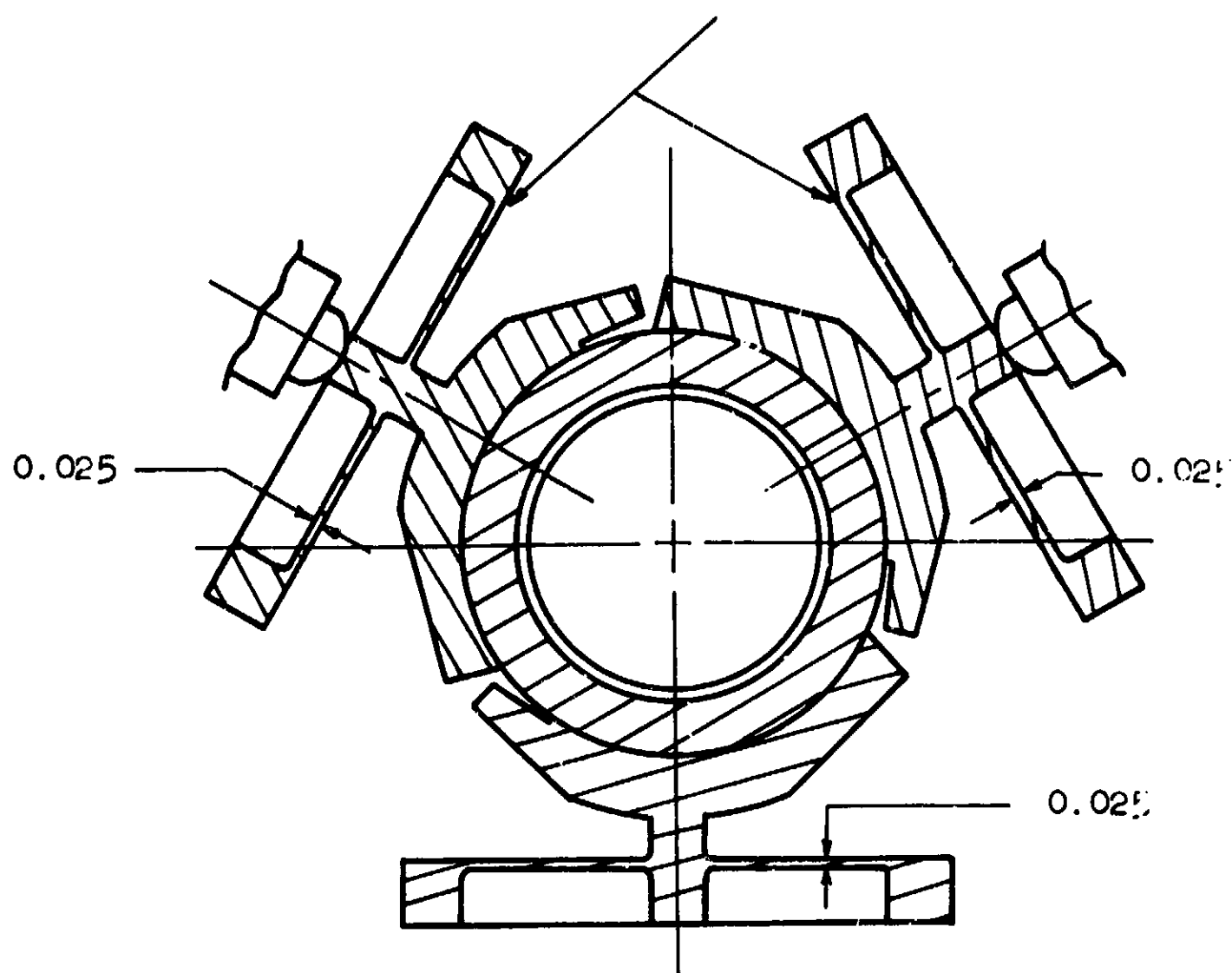
CIRCULAR PLATE RESILIENT  
MOUNT -  $K = 20,000$  LBS PER INCH  
(RESTRAINED RADIALLY)



TASK III  
NONPIVOTED TYPE, PARTIAL-ARC BEARING  
RESILIENT MOUNT CONFIGURATION - TEST 1

FIGURE 53

CIRCULAR PLATE RESILIENT  
MOUNT -  $K = 3,000$  LBS PER INCH  
(RESTRAINED RADIALLY)



CIRCULAR PLATE RESILIENT  
MOUNT -  $K = 3,000$  LBS PER INCH  
(NO RADIAL RESTRAINT)

### TASK III

NONPIVOTED TYPE, PARTIAL-ARC BEARING  
RESILIENT-MOUNT CONFIGURATION - TEST 2

FIGURE 54

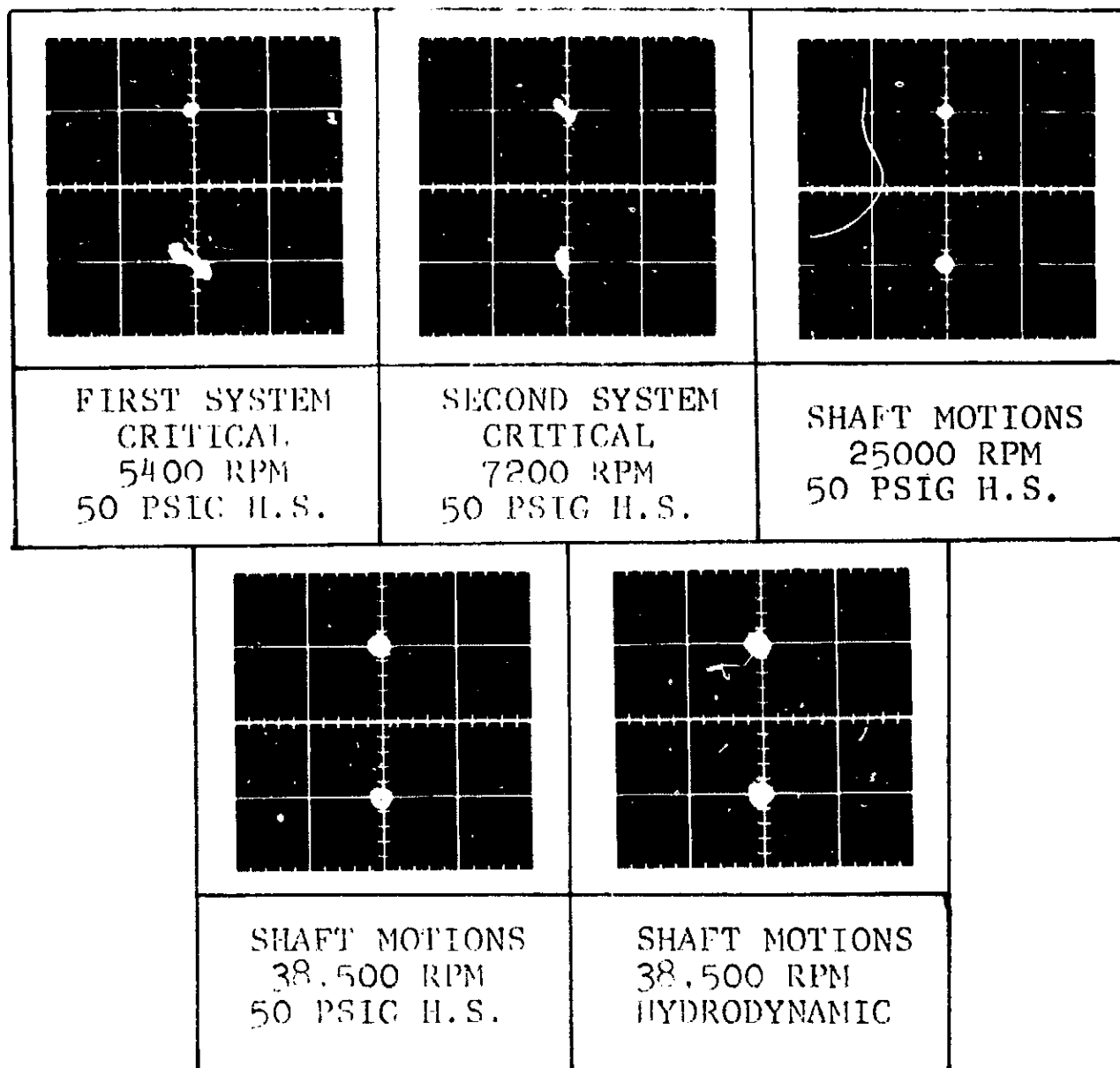
## 4.5 Test Procedure and Results

### 4.5.1 Test Series 1

The rotor was set up in a vertical position on the alignment pins. Each elastically pivoted pad was individually aligned with the journal diameter of the rotor by using the unique positioning supports of the two-bearing rotor dynamic test rig. The four strain-gauge outputs of each diaphragm were read out separately to detect slight movements in the diaphragm caused by uneven touching of the pad leading or trailing edges (upper and lower) as the pad was lightly loaded against the shaft by means of the radially directed track-mounted support assembly. Once a pad assembly was thought to be in proper alignment, a qualitative check was made by a feeler gauge of 0.001-inch shim stock (checking the clearance between the pad leading and trailing edge, top and bottom) with the pad in close proximity to its related journal. It should be emphasized that this procedure is qualitative only and does not give precise alignment. No precise alignment technique has yet been found to produce a perfect alignment. Satisfactory alignment at present can be obtained only through the skill and patience of a trained technician. Once the alignment of each pad was obtained, the two pads per bearing, with the 20,000-lb-per-inch spring rate diaphragm, were radially advanced to just touch the journal surface; and stops, with a micrometer adjustment, were advanced to just touch the back center of each diaphragm. The latter effectively prevent any radial motion of the "fixed" diaphragms. The flexibly mounted pads (one per journal with approximately 3,000-lb-per-inch spring-rate diaphragms) were then loaded against the rotor journals to produce a positive 5.0-pound bearing

preload. The fixture centers were then removed, and the bottom center was replaced with the hydrostatic thrust bearing. It was found that 50 psig pad hydrostatic supply pressure was required to float the rotor. The pad loads (at zero speed) with this supply pressure were determined to be approximately 9.8 pounds (5.0 pounds preload plus 4.8 pounds due to hydrostatic lift-off). The rotor was accelerated to 38,500 rpm. The average stabilized pad loads at this speed were found to be 17.05 pounds. As soon as these stabilized loads were obtained, the hydrostatic pressure was shut off, and the bearing became totally self-acting (hydrodynamic). The average stabilized pad loads at 38,500 rpm for hydrodynamic operation were observed to be 16.6 pounds. The hydrodynamic self-acting pressure (as measured at the supply orifice) was 8.0 psig. Operation through the entire speed range was completely stable and well behaved. Figure 55 shows the rotor Lissajous patterns of the rigid rotor criticals, the hydrostatic operation at 25,000 rpm and 38,500 rpm, and the hydrodynamic operation at 38,500 rpm. As soon as the stabilized self-acting pad loads were observed, the hydrostatic supply was readmitted and the rotor was allowed to coast to standstill.

The above procedure was repeated for pad preload values of 3.0 pounds, 1.0 pound, and a minus 1.0 pound (an actual diametral clearance of 0.00022 inch). In each case, stable dynamic operation was obtained throughout the speed range as illustrated in the Lissajous patterns in Figures 56, 57, and 58. The bearing pad loads at various conditions, as well as the developed pad hydrodynamic pressures, are presented in Table 7.



NOTES:

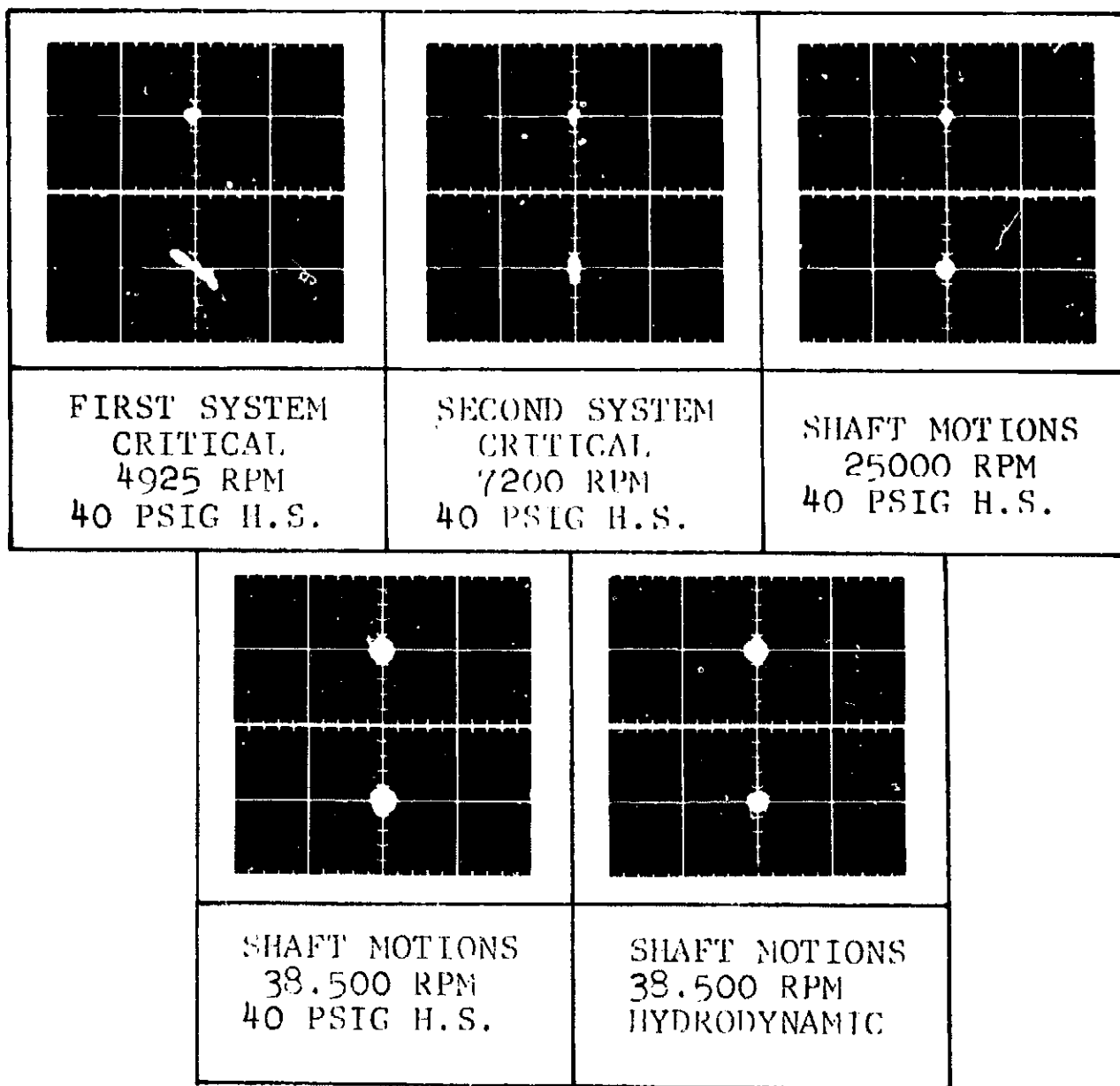
1. CALIBRATION OF LISSAJOUS FIGURES 0.001 INCH PER CM.
2. SUPPORT SYSTEM CONSISTS OF TWO "FIXED" RESILIENT MOUNTS (20,000 LB IN SPRING RATE) AND ONE FLEXIBLE MOUNT (3,000 LB IN)
3. INITIAL BEARING PAD RELOAD - 5.0 POUNDS
4. ACCELERATION HYDROSTATICALLY TO 38,500 RPM  
HYDRODYNAMIC OPERATION AT 38,500 RPM
5. AIR LUBRICANT AT 75°F

TEST SERIES 1  
NONPIVOTED PARTIAL ARC GAS BEARING TESTS  
5 POUND INITIAL PRELOAD

FIGURE 10

APS 6273 R

Page 97



NOTES:

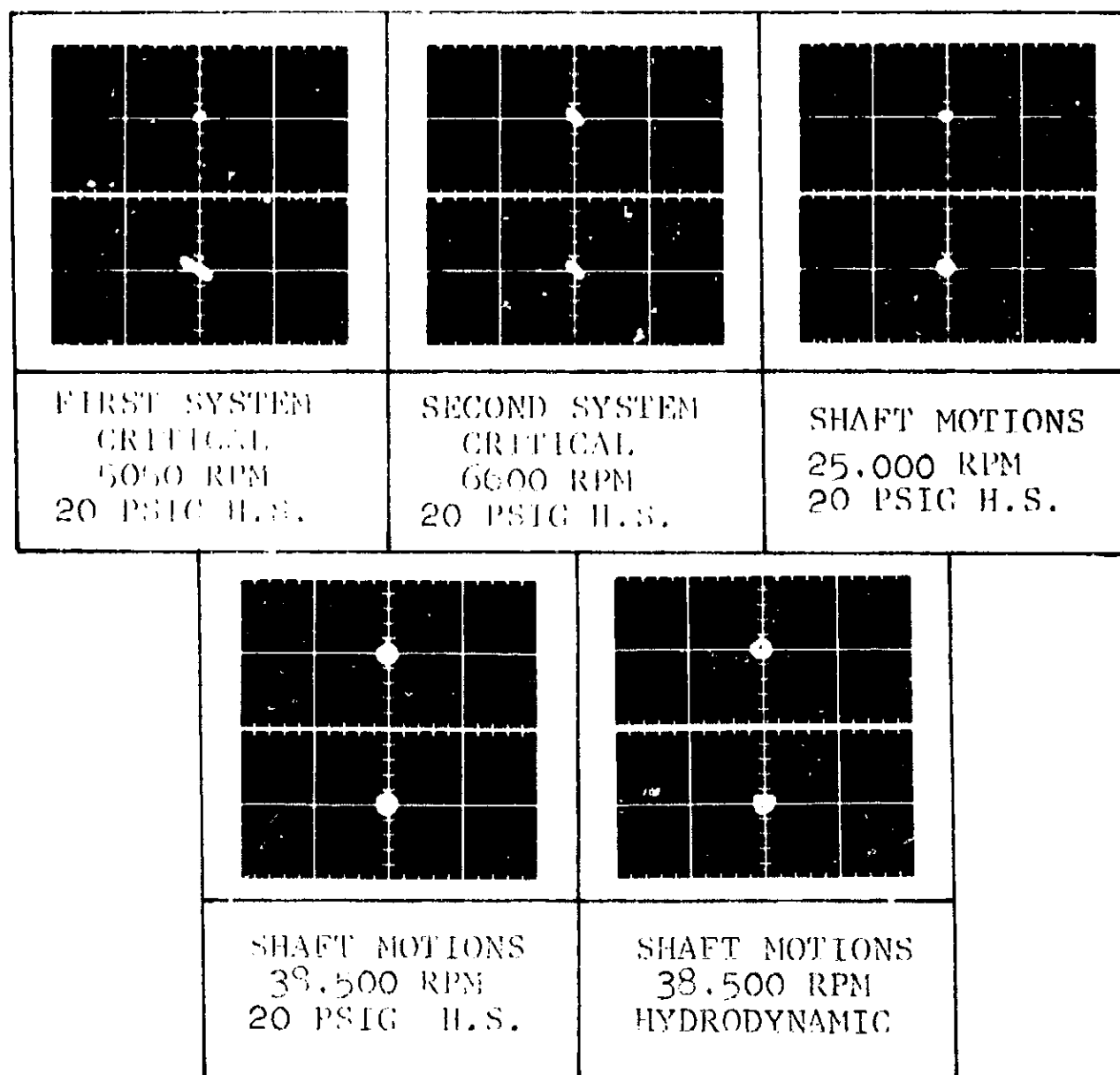
1. CALIBRATION OF LISSAJOUS FIGURES 0.001 INCH PER CM.
2. SUPPORT SYSTEM CONSISTS OF TWO "FIXED" RESILIENT MOUNTS (20,000 LB IN SPRING RATE AND ONE FLEXIBLE MOUNT (3,000 LB IN
3. INITIAL BEARING PAD PRELOAD - 3.0 POUNDS
4. ACCELERATION HYDROSTATICALLY TO 38,500 RPM  
HYDRODYNAMIC OPERATION AT 38,500 RPM
5. AIR LUBRICANT AT 75°F

TEST SERIES 1  
NONPIVOTED PARTIAL ARC GAS BEARING  
TEST, 3 POUND INITIAL PRELOAD

FIGURE 66

APR 1963 R

Page 10

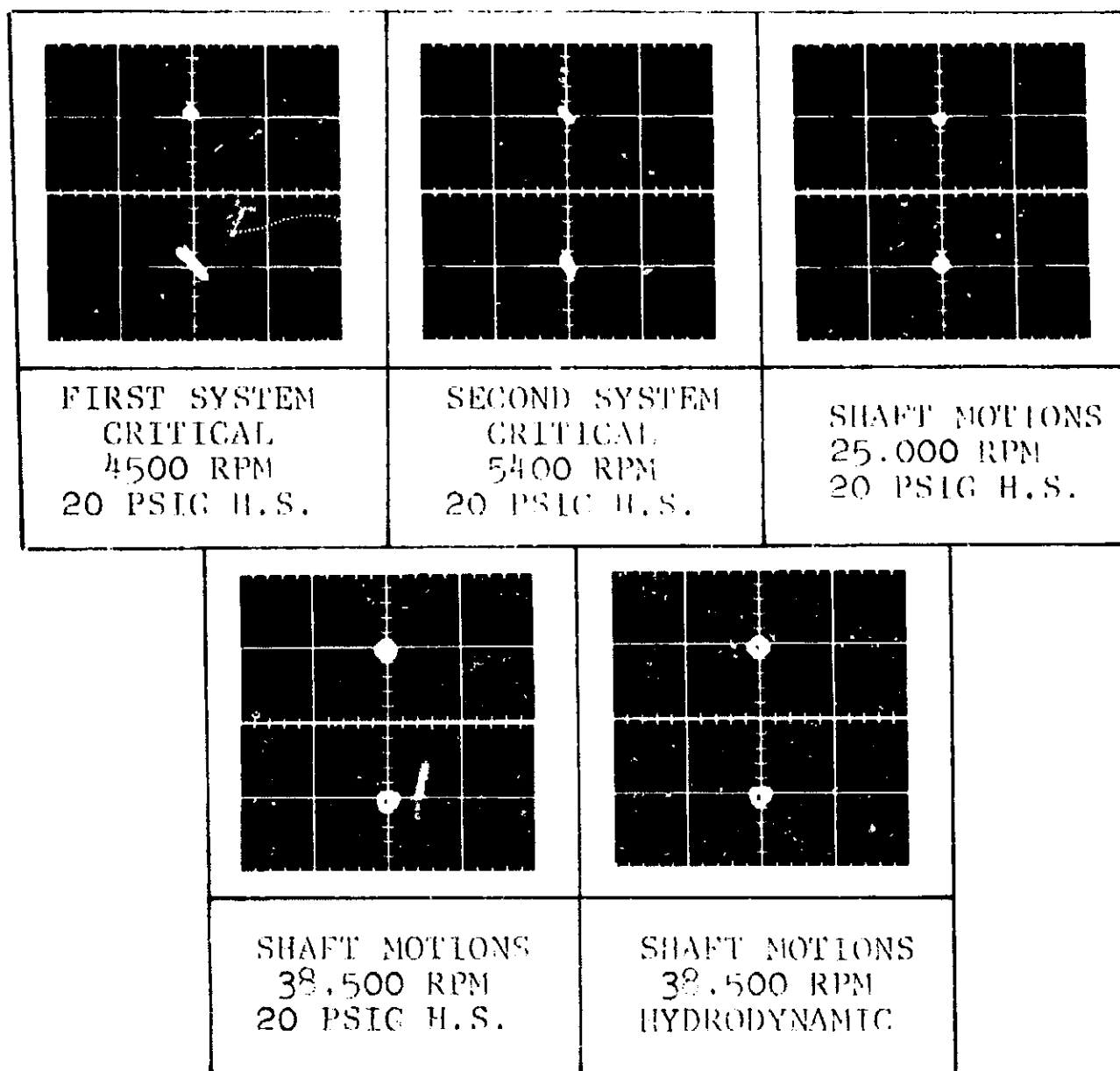


NOTES:

1. CALIBRATION OF LISSAJOUS FIGURES 0.001 INCH PER CM.
2. SUPPORT SYSTEM CONSISTS OF TWO "FIXED" RESILIENT MOUNTS 20,000 LB IN SPRING RATE AND ONE FLEXIBLE MOUNT 3,000 LB IN
3. INITIAL BEARING PAD PRELOAD - 1.0 POUND
4. ACCELERATION HYDROSTATICALLY TO 38,500 RPM  
HYDRODYNAMIC OPERATION AT 38,500 RPM
5. AIR LUBRICANT AT 75°F

TEST SERIES I  
NONPIVOTED PARTIAL ARC GAS BEARING  
TEST, 1 POUND INITIAL PRELOAD

FIGURE 7  
APR 1971 R  
PAGE 100



NOTES:

1. CALIBRATION OF LISSAJOUS FIGURES 0.001 INCH PER CM.
2. SUPPORT SYSTEM CONSISTS OF TWO "FIXED" RESILIENT MOUNTS (20,000 LB IN SPRING RATE AND ONE FLEXIBLE (3,000 LB IN
3. INITIAL BEARING PAD PRELOAD - NEGATIVE 1.0 POUND
4. ACCELERATION HYDROSTATICALLY TO 38,500 RPM  
HYDRODYNAMIC OPERATION AT 38,500 RPM
5. AIR LUBRICANT AT 75°F.

TEST SERIES I  
NONPIVOTED PARTIAL ARC GAS BEARING  
TEST NEGATIVE 1 POUND INITIAL PRELOAD

FIGURE 1

APR 1964

PAGE 101

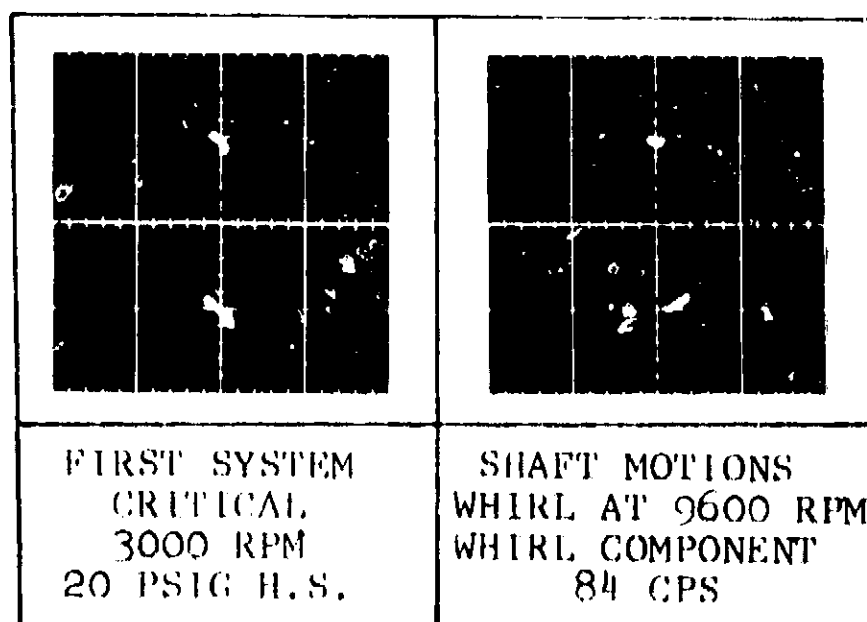


One final test was run on the same components. For this test a preload of minus 3.0 pounds was established (an actual diametral clearance of 0.00066 inch). This clearance produced a resonant whirl of 9,600 rpm, persisting to 12,000 rpm, which caused the test to be discontinued. No damage to either the rotor or the pads was experienced. The rotor first rigid body critical, as well as the observed whirl, is presented in Figure 59. The average measured bearing pad load at the whirl onset was of the order of 1.25 pounds, with a hydrostatic supply pressure of 20.0 psig.

TABLE 7  
TEST SERIES 1  
BEARING OPERATING PARAMETERS

<u>Pad Preload Lbs</u>	<u>Speed, rpm</u>	<u>Comp. Pad Load, Lbs</u>	<u>Turbine Pad Load, Lbs</u>	<u>Journal Bearing Pad Supply Pressure, psig</u>
5	0	9.7	9.9	50
	38,500	17.5	16.6	50
	38,500	17.0	16.25	8 H.D.
3	0	8.2	8.3	40
	38,500	15.6	14.7	40
	38,500	14.9	14.25	8 H.D.
1	0	6.0	6.0	20
	38,500	13.5	13.5	20
	38,500	13.25	13.5	7 H.D.
-1	0	2.75	3.25	20
	38,500	10.25	10.25	20
	38,500	9.9	10.1	5.5 H.D.
-3	0*	1.0	1.5	20

\*Encountered whirl at 160 cps  
H.D. - hydrodynamic operation



NOTES:

1. CALIBRATION OF LISSAJOUS FIGURES 0.001 INCH PER CM.
2. SUPPORT SYSTEM CONSISTS OF TWO "FIXED" RESILIENT MOUNTS (20,000 LB/IN SPRING RATE) AND ONE FLEXIBLE MOUNT (3,000 LB/IN)
3. INITIAL BEARING PAD PRELOAD - NEGATIVE (-) 3.0 POUNDS (ACTUAL DIAMETRAL CLEARANCE, 0.00066 INCH)
4. ACCELERATION HYDROSTATICALLY TO 38,500 RPM  
HYDRODYNAMIC OPERATION AT 38,500 RPM
5. AIR LUBRICANT AT 75°F

TEST SERIES 1  
NONPIVOTED PARTIAL-ARC GAS BEARING TEST  
NEGATIVE 3 POUNDS INITIAL PRELOAD

FIGURE 59

APS-5223-R  
Page 103

#### 4.5.2 Test Series 2

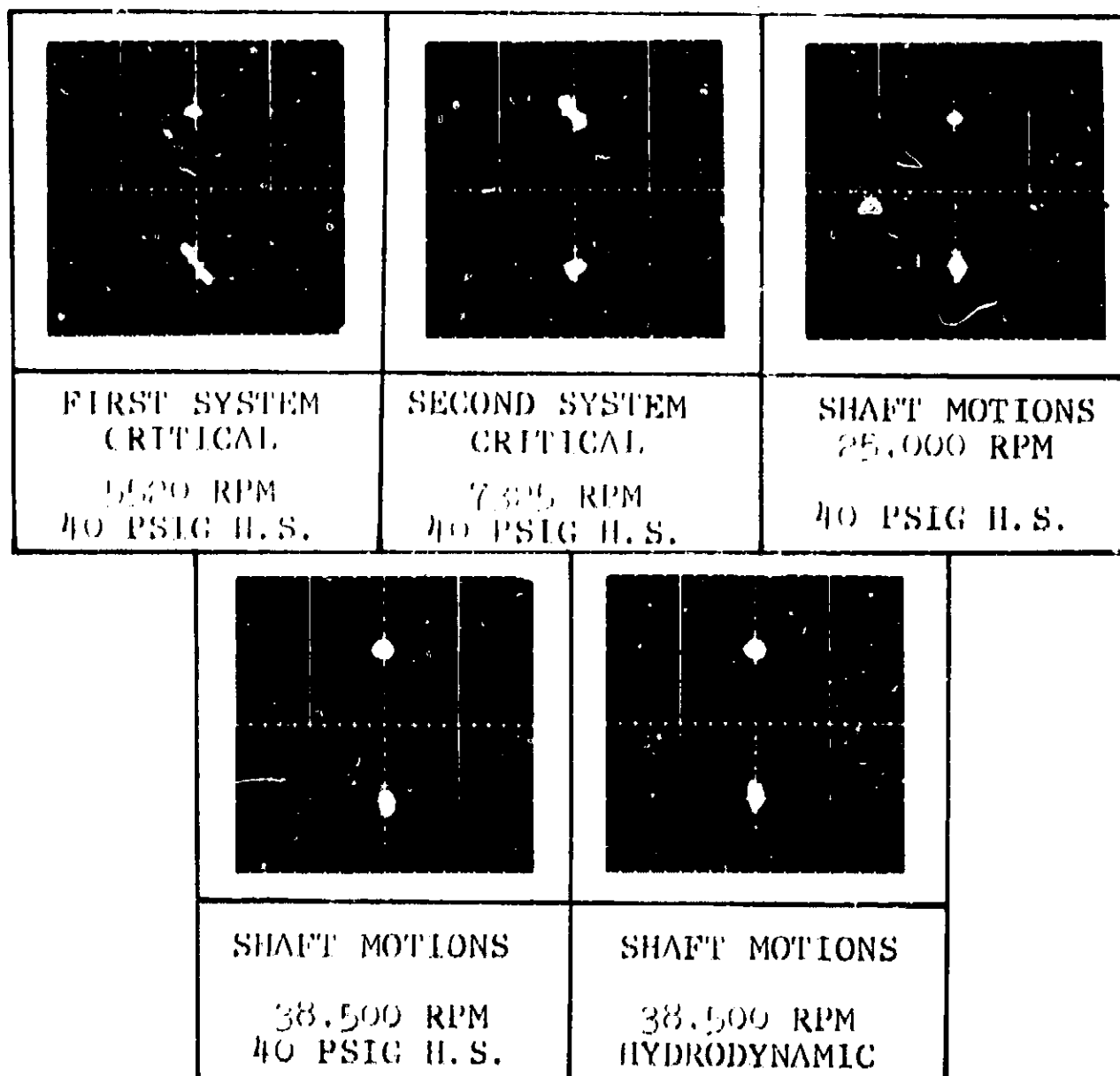
The test procedure for the second series of tests was identical with that mentioned previously. The bearing pad loads at various conditions, as well as the hydrodynamic pressure generated at the manifolded pad orifices, are presented in Table 8. Again, as reported for Test Series 1, stable rotor dynamic operation was obtained throughout the speed range (0 to 38,500 rpm) as illustrated in the Lissajous patterns presented in Figures 60, 61, 62, 63 and 64. Note that an actual diametral clearance in the bearing pad of 0.0033 inch was the limiting case run. Any attempts to increase this clearance nullified the capability of the hydrostatic supply system, and rotor flotation at zero speed could not be obtained.

#### 4.6 Discussion

The two test series described above were conducted at ambient conditions with almost isothermal conditions existing in the test rig. Under these ideal conditions, the tests demonstrated that the concept of elastically pivoted "fixed-stem" partial-arc bearings with greatly decreased resilient mount spring rates (in the order of 3,000 lbs per inch) is a workable system affording rotor dynamic stability over a wide range of bearing pad loads. Except for the rather formidable initial alignment difficulties inherent in this design, there appears to be little choice between this concept and true pivoted-pad bearings when operating under the defined condition.

TABLE 8  
TEST SERIES 2  
BEARING OPERATING PARAMETERS

<u>Pad Preload (lbs) or Diametral Clear- ance (inches)</u>	<u>Speed (rpm)</u>	<u>Compressor Bearing Pad Load (lbs)</u>	<u>Turbine Bearing Pad Load (lbs)</u>	<u>Journal Bearing Pad Supply Pressure (psig)</u>
5 lbs	0	10.4	10.0	40
	38,500	15.2	19.7	40
	38,500	15.2	19.0	9.0 H.D.
3 lbs	0	8.1	7.8	30
	38,500	15.2	16.5	30
	38,500	14.6	16.2	8.0 H.D.
1 lb	0	5.4	5.0	30
	38,500	11.9	13.2	30
	38,500	10.9	12.2	5.5 H.D.
0.0013 inch	0	2.3	2.0	20
	38,500	8.3	9.0	20
	38,500	7.6	8.4	4.0 H.D.
0.0033 inch	0	1.2	0.8	20
	38,500	6.4	6.4	20
	38,500	5.8	5.8	2.75 H.D.



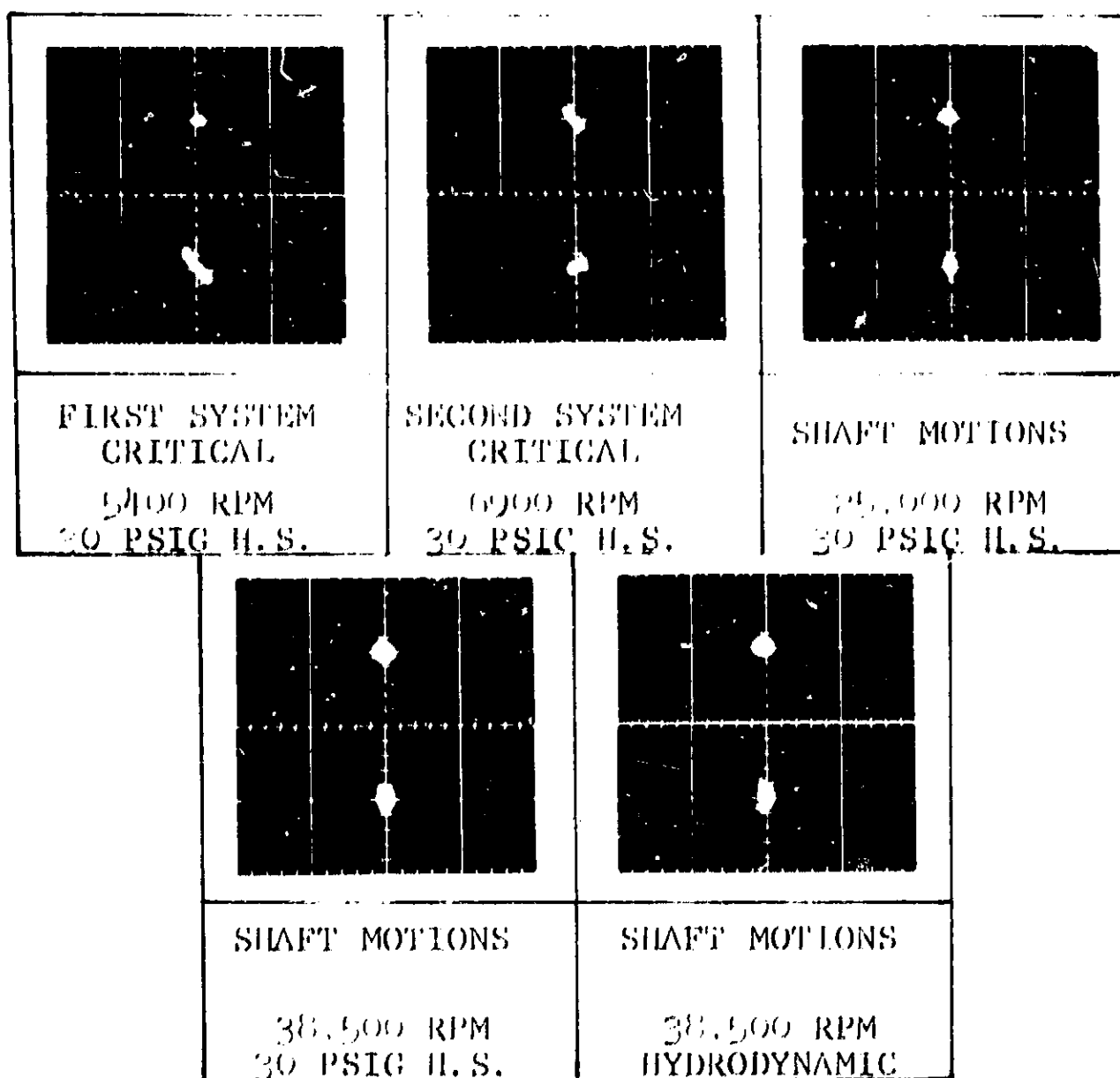
NOTES:

1. CALIBRATION OF LISSAJOUS FIGURES 0.001 INCH PER CM.
2. SUPPORT SYSTEM CONSISTS OF TWO "FIXED" RESILIENT MOUNTS (3,000 LB/IN SPRING RATE) AND ONE FLEXIBLE MOUNT (3,000 LB/IN).
3. INITIAL BEARING PAD PRELOAD - 5.0 POUNDS
4. ACCELERATION HYDROSTATICALLY TO 38,500 RPM  
HYDRODYNAMIC OPERATION AT 38,500 RPM
5. AIR LUBRICANT AT 75°F

TEST SERIES 2  
NONPIVOTED PARTIAL ARC GAS BEARING  
TESTS, 5 POUND INITIAL PRELOAD

FIGURE 60

APS 5223 R  
Page 106



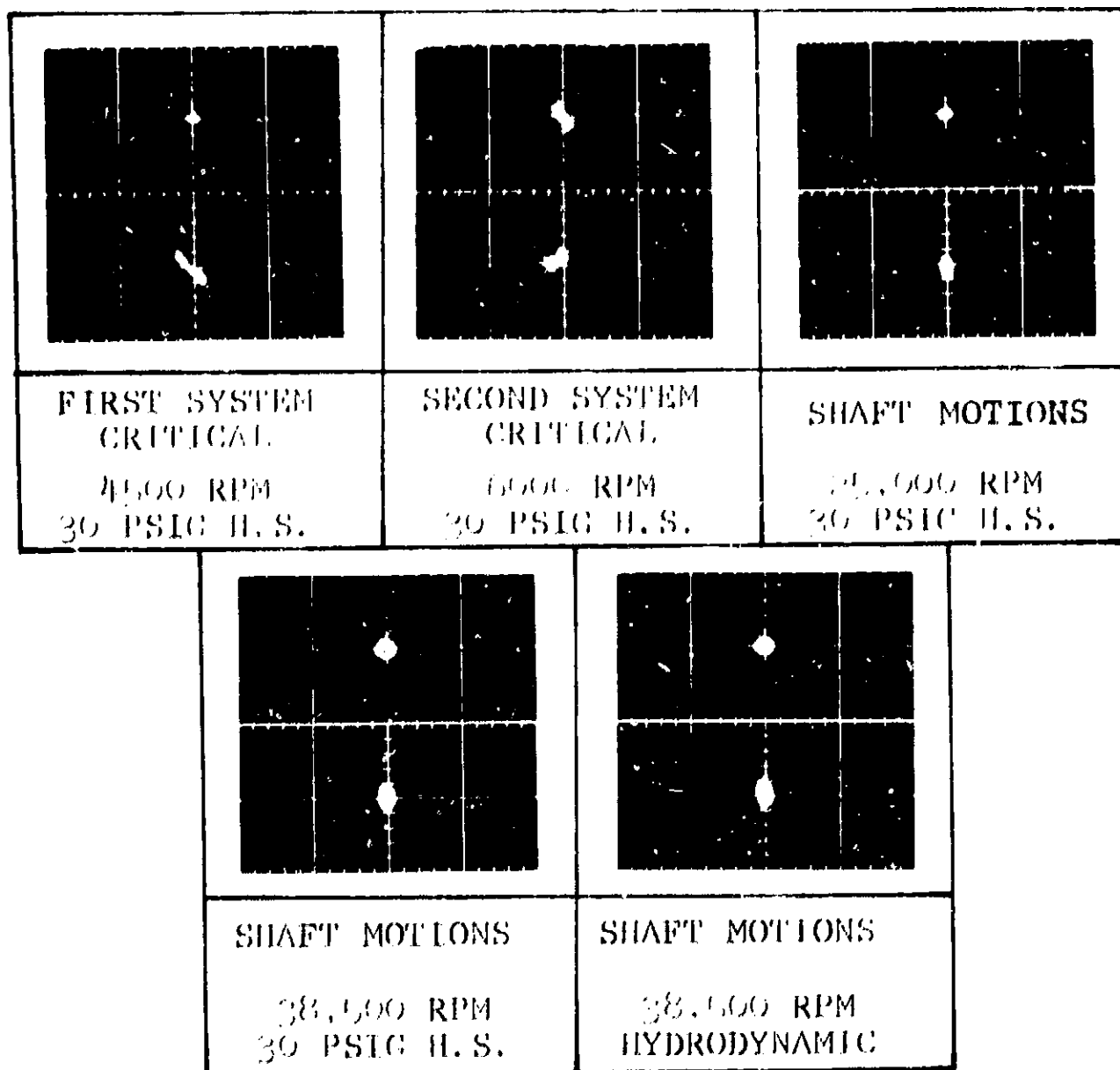
NOTES:

1. CALIBRATION OF LISSAJOUS FIGURES 0.001 INCH PER CM.
2. SUPPORT SYSTEM CONSISTS OF TWO "FIXED" RESILIENT MOUNTS (3,000 LB/IN SPRING RATE) AND ONE FLEXIBLE MOUNT (3,000 LB/IN.)
3. INITIAL BEARING PAD PRELOAD - 3.0 POUNDS
4. ACCELERATION HYDROSTATICALLY TO 38,500 RPM  
HYDRODYNAMIC OPERATION AT 38,500 RPM
5. AIR LUBRICANT AT 75°F

TEST SERIES 2  
NONPIVOTED PARTIAL ARC GAS BEARING  
TESTS, 3 POUND INITIAL PRELOAD

FIGURE 61

APS 1223 R  
Page 107



**NOTES:**

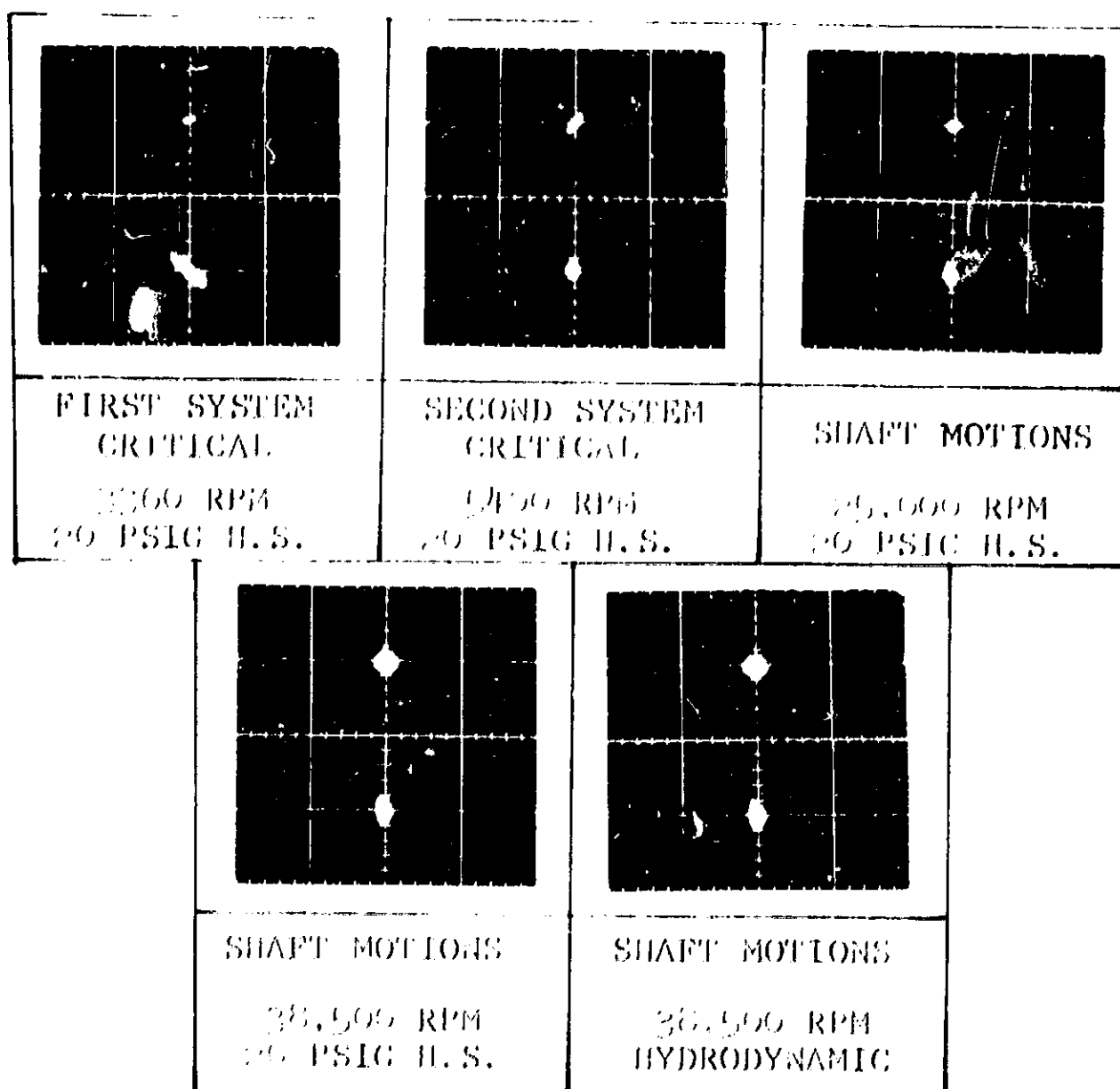
1. CALIBRATION OF LISSAJOUS FIGURES 0.001 INCH PER CM.
2. SUPPORT SYSTEM CONSISTS OF TWO "FIXED" RESILIENT MOUNTS (3,000 LB/IN SPRING RATE) AND ONE FLEXIBLE MOUNT (3,000 LB/IN).
3. INITIAL BEARING PAD PRELOAD - 1.0 POUND
4. ACCELERATION HYDROSTATICALLY TO 38,500 RPM  
HYDRODYNAMIC OPERATION AT 38,500 RPM
5. AIR LUBRICANT AT 75°F

TEST SERIES 2  
NONPIVOTED PARTIAL ARC GAS BEARING  
TESTS, 1 POUND INITIAL PRELOAD

FIGURE 62

APS 5223-R

Page 108



NOTES:

1. CALIBRATION OF LISSAJOUS FIGURES 0.001 INCH PER CM.
2. SUPPORT SYSTEM CONSISTS OF TWO "FIXED" RESILIENT MOUNTS (3,000 LB/IN SPRING RATE, AND ONE FLEXIBLE MOUNT (3,000 LB/IN).
3. NO INITIAL BEARING PAD PRELOAD - BEARING DIAMETRAL CLEARANCE 0.0013 INCH
4. ACCELERATION HYDROSTATICALLY TO 38,500 RPM  
HYDRODYNAMIC OPERATION AT 38,500 RPM
5. AIR LUBRICANT 75°F

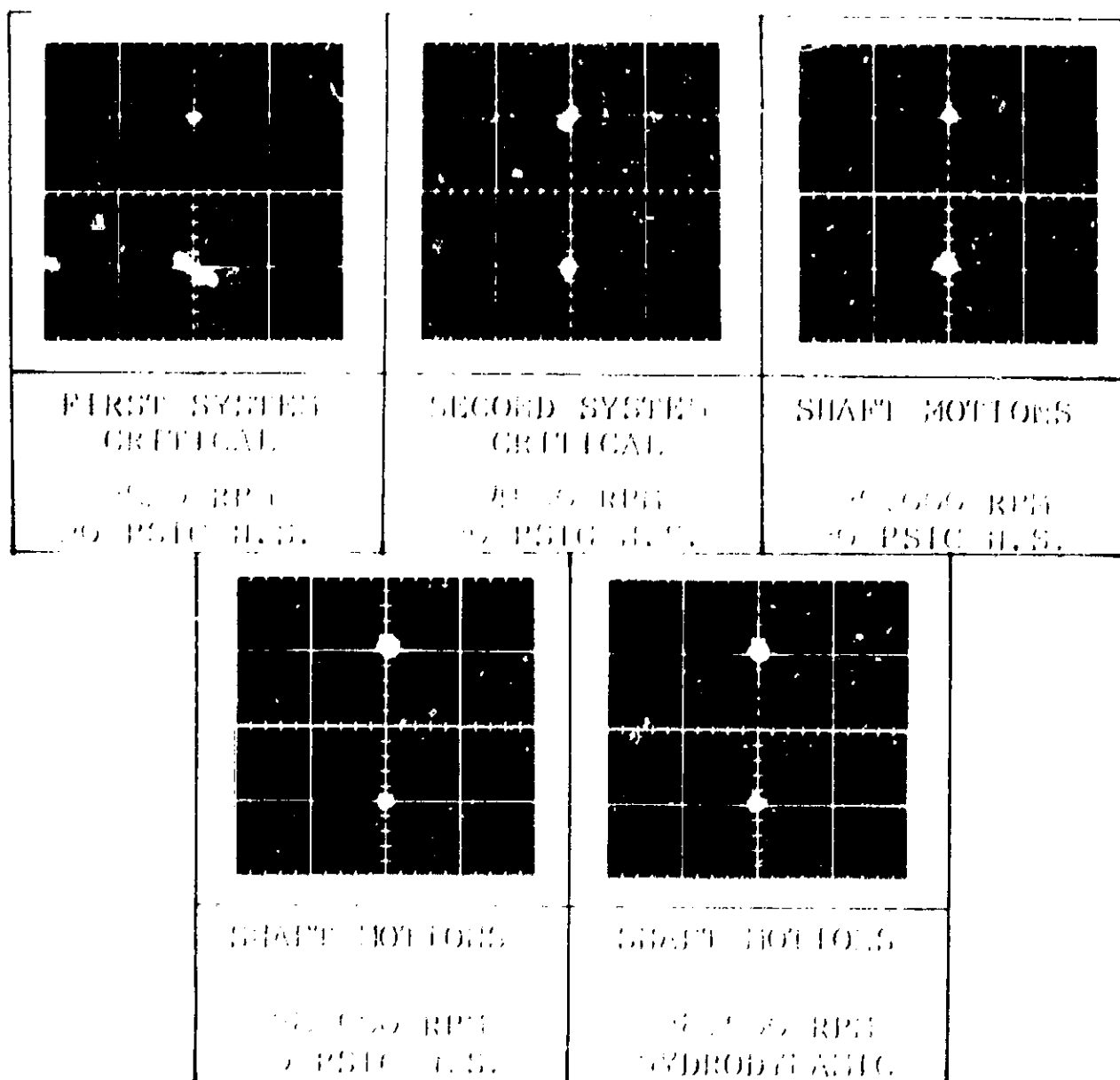
TEST SERIES 2  
NONPIVOTED PARTIAL ARC GAS BEARING  
TESTS, BEARING DIAMETRAL CLEARANCE  
0.0013 INCH

FIGURE 63

APS 5223-R

Page 109





NOTES:

1. CALIBRATION OF LISSAJOUS FIGURES 0.001 INCH PER CM.
2. SUPPORT SYSTEM CONSISTS OF TWO "FIXED" RESILIENT MOUNTS (3,000 LB IN. SPRING RATE) AND ONE FLEXIBLE MOUNT (3,000 LB IN.
3. NO INITIAL BEARING PAD PRELOAD BEARING DIAMETRAL CLEARANCE = 0.0033 INCH
4. ACCELERATION HYDROSTATICALLY TO 38,500 RPM HYDRODYNAMIC OPERATION AT 38,500 RPM
5. AIR LUBRICANT AT 75°F.

TEST SERIES 2  
NONPIVOTED PARTIAL ARC GAS BEARING  
TESTS, BEARING DIAMETRAL CLEARANCE  
0.0033 INCH

FIGURE 64

APS 5223 R

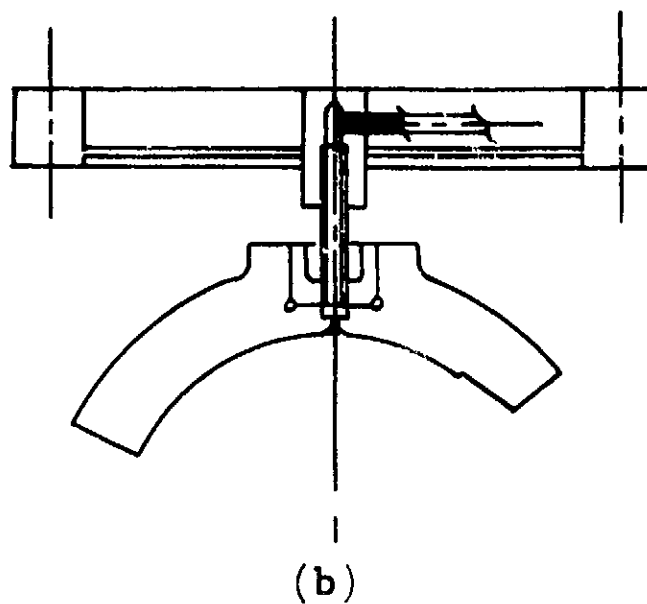
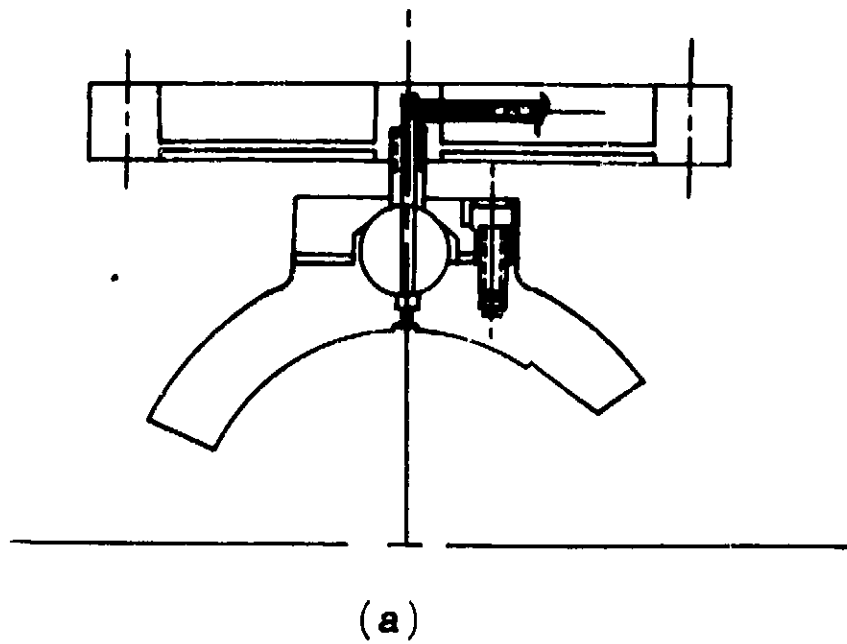
Page 110

The testing does indicate that decreasing the spring rate of the fixed mounts (constrained against radial deflection) provides improved pivotal flexibility. The above statement is substantiated by examining the maximum diametral clearance that produced stable rotor operation in the two test series. In the case of the first series of tests with pivotal freedom provided by the 20,000 lb-per-inch diaphragms, the maximum diametral clearance was found to be 0.00022 inch. This should be compared with the 0.0033-inch clearance in the second series of tests with the 3,000 lb-per inch diaphragms.

A note should be made as to initial rig alignment ease. As has been mentioned previously, satisfactory alignment can be obtained only through the skill and patience of a trained technician. Even at that, the accuracy of alignment cannot be ascertained. The same technician set up the test rig for both series of tests. In his judgment, the rig alignment problems were considerably eased by the use of the lower spring rate diaphragms. However, even with the improved alignment capability, this type of bearing cannot be considered to be applicable to the reference turbo compressor without substantial modifications.

Figure 65 depicts two possible methods for arriving at a fixed geometry mount between the journal bearing carrier and each journal bearing pad.

The scheme presented in Figure 65a utilizes a matched ball socket pivot similar in concept to that presently used in the AiResearch pivoted-pad gas bearings. A collar retains the ball within the socket such that pivoting action can occur at room



CONCEPTUAL DESIGN  
ELASTICALLY PIVOTED PADS  
WITH INITIAL ALIGNMENT CAPABILITY

FIGURE 65

temperature ambient. Materials having different coefficients of thermal expansion are selected for the ball and the collar. The collar-to-ball clearance is adjusted so that lock-up of the pivot will occur when some predetermined range of pivot temperature is reached during the transient start-up cycle. It is readily apparent that this configuration provides for initial alignment during setup, establishment of the proper pad altitude during the hydrostatic and into the hydrodynamic modes of bearing operation, and accommodation of most of the thermal distortion of the unit structure during the thermal transient cycle.

The configuration shown in Figure 65b utilizes a high-slenderness-ratio column having a low moment spring rate and a high resistance to buckling. Bearing pad pitch and roll is accommodated by column bending and yaw by the rotation of a matched sleeve joint at the bearing pad. Materials having different coefficients of thermal expansion, chosen for the matched sleeve joint, provide the required lock-up feature when some predetermined range of joint temperature is reached during the transient start-up cycle.

## 5.0 TASK IV. GAS BEARING PARTS AND SPECIAL HARDWARE

### 5.1 General

During the conduct of the program under NASA Contract NAS-3-2778, for the gas bearing radial-flow turbocompressor, several requirements were generated and were thus incorporated into the tasks required by the subject contract. These requirements were:

- (a) The availability of certain essential spares in support of the turbocompressors during their development by the NASA at the Lewis Research Laboratories.
- (b) The utilization of a bearing surface coating that would be possibly more tolerant to any intermittent contact rubs that might occur during the development tests.
- (c) The provisions of hardware to allow the future incorporation of proximity probes in certain bearing pads to determine operating lubricant film thickness (shaft-to-shoe) at the bearing pivot location.

### 5.2 Essential Spares

The spares considered necessary for future development support comprised one turbocompressor shaft assembly, one set of pad bearing shoes, and one set of pad bearing matched mounts. Four of

the mounts were of the fixed configuration, and two incorporated the flexible feature necessary for the resilient mounting system employed in the turbocompressors. All parts were required to be fully interchangeable with those in the delivered units. The delivered hardware is shown in Figure 66.

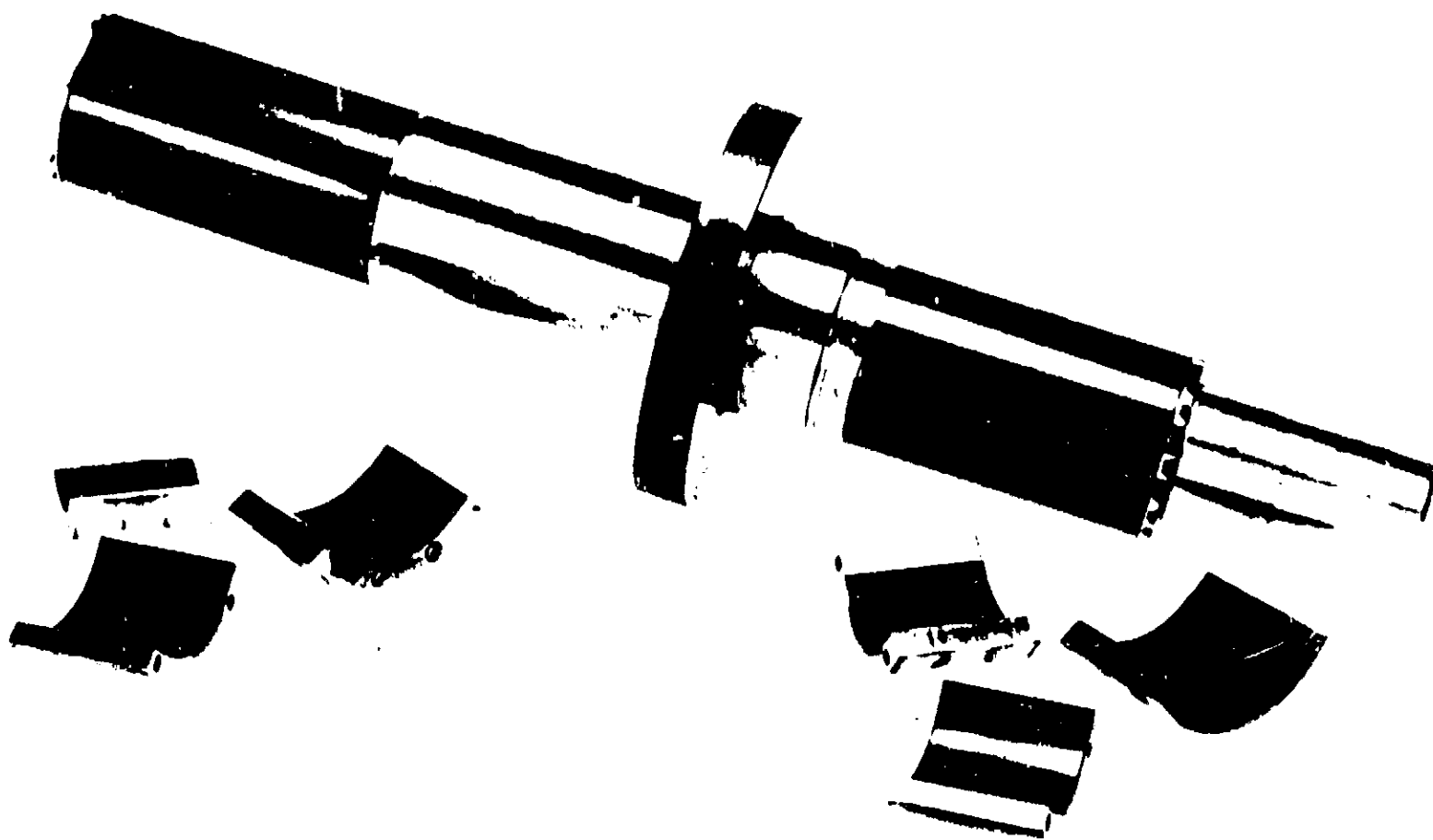
### 5.3 Surface Coatings of Bearings

Prior to initiation of the program, the NASA had been able to determine, from other contractual efforts, that the most promising surface coating material would be chrome-oxide operating against chrome-oxide. This was based upon the evaluation of several candidate materials, which were subjected to controlled and repetitive tests under conditions representative of gas bearing operation in general. A proprietary process, Linde LC-4, was considered initially for the chrome-oxide coating. This had a defined porosity no greater than 4 percent. As the program progressed, but before coating of the bearing surfaces on the shaft and pad-bearing shoes was undertaken, the NASA obtained further data, which revealed that increased porosity in the chrome-oxide had beneficial effects on wear tests. Upon the recommendation of the NASA, the bearing surfaces were coated with a process provided by the Avco Corporation, designated MTI-38-U, and controlled by Contractor Specification SC-5670. Porosity generated by this process was reported to be greater than 8 percent but less than 18 percent.

Evaluation of test samples of the chrome-oxide coatings, furnished with the coated parts, provided the following results:

#### (a) Porosity of the Deposited Coating

This varied between 5 and 20 percent, but the general average was in the range of 10 to 15 percent.



DELIVERED GAS BEARING  
PADS AND SHAFT

FIGURE 66

(b) Material Hardness

Base material, A-286	36 Rc
Nickel-chrome substrate	Less than Rb 92
Chrome oxide coating	
High	62.5 Rc
Nominal	54 Rc
Low	34 Rc

(c) Thickness of Coatings

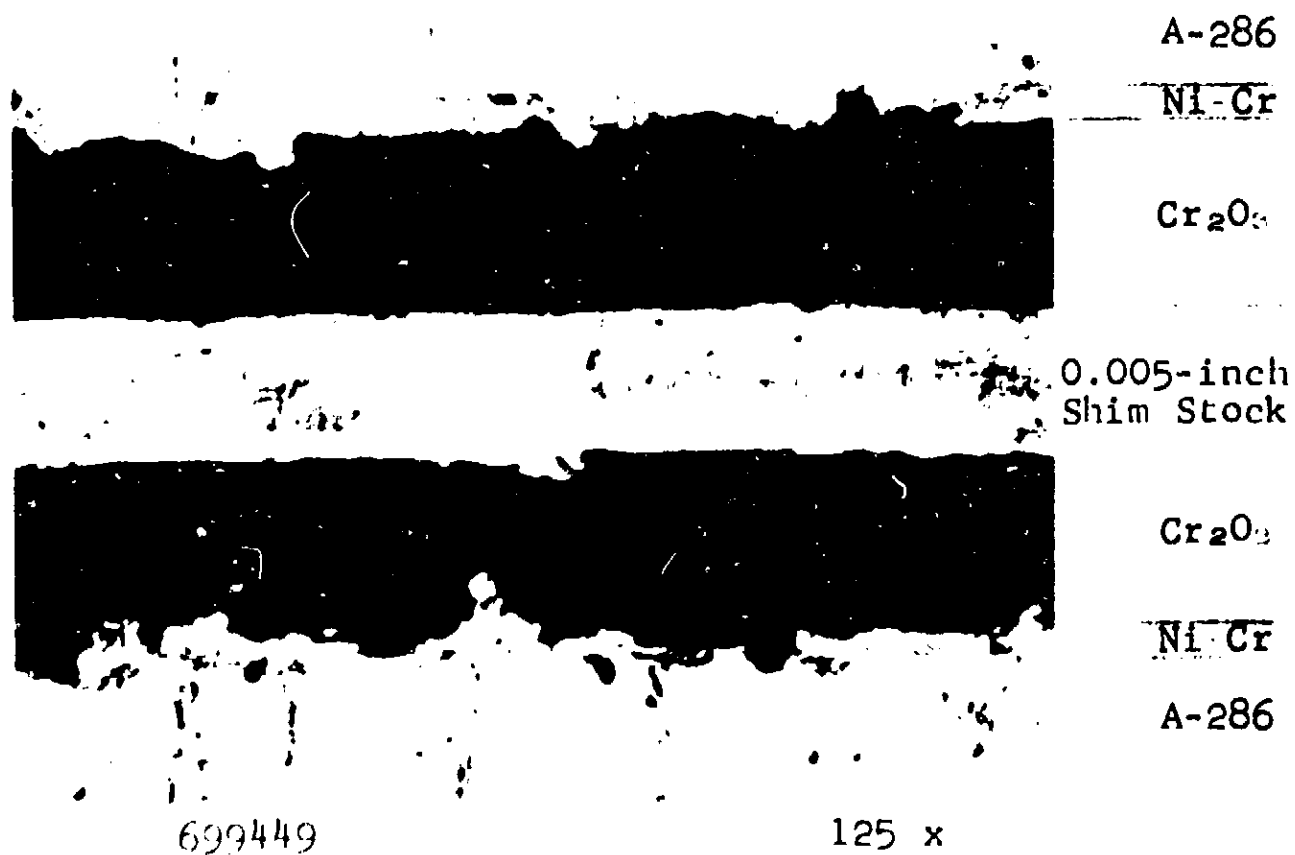
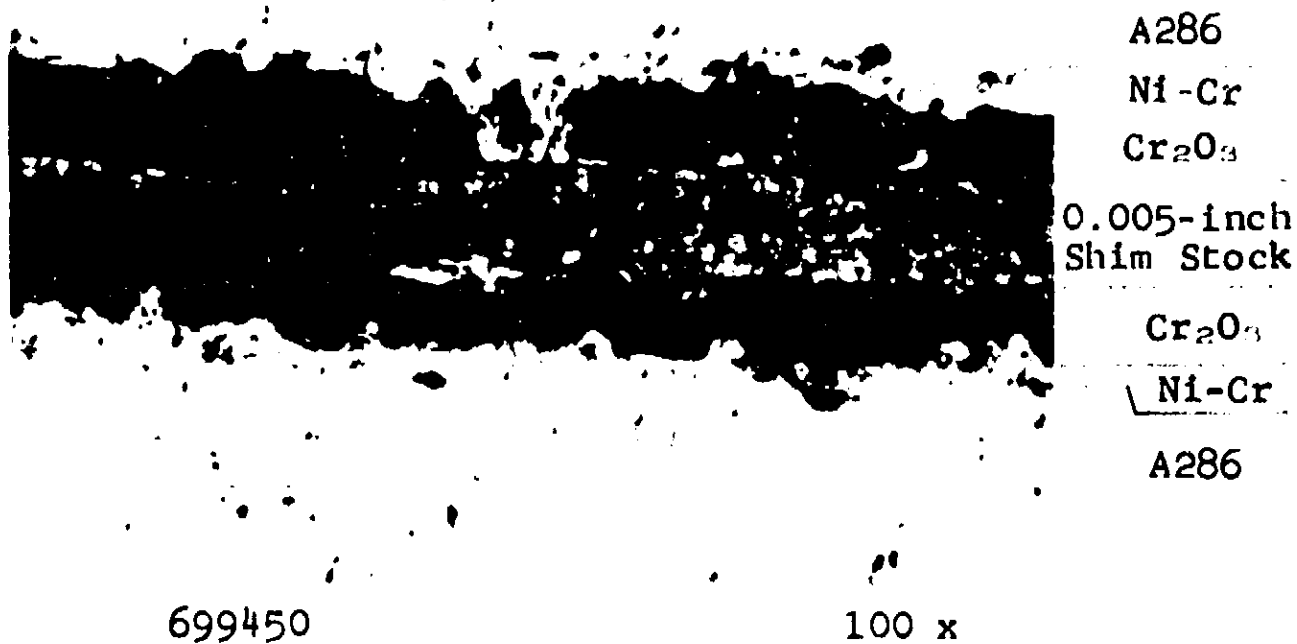
Nickel-chrome substrate	0-0.0034 inch
Chrome oxide coating	0-0.0053 inch

Particles of material, presumed to be nickel-chrome, were found to be randomly mixed throughout the chrome oxide.

These results are the averages of two samples analyzed. To determine this data, a 1/4-inch strip was cut from each sample and mounted in Bakelite, separated by a 0.0050-inch-thick shim stock to separate the ground chrome-oxide platings and for ease of measurement. Due to the irregularity of the coatings, thicknesses are estimated. Figure 67 shows magnified cross sections of the samples.

The bearing shoes were completed by final grinding to the required surface contour and by machining of the hydrostatic lift-off pads and supply ports. Prior to final grinding of the shaft bearing surfaces, an evaluation was conducted into the fabrication processes involved with the bearing shoes. The results of the evaluation were as follows:





CROSS SECTION OF CHROME-OXIDE PLATINGS  
FIGURE 67

- (a) The chrome-oxide surfaces were susceptible to chipping and flaking, particularly at the shoe edges and in the area of the hydrostatic lift-off pads.
- (b) Due to the greatly increased surface porosity, previously established methods to determine shoe curvature to close tolerances could not be employed. Indications were, however, that the shoes were within the total tolerance allowable.
- (c) No guarantee of performance with this coating could be given by the vendor for operation above 600°F, and it was stated that the coating was also subject to damage by thermal shock.

Discussions with the NASA established that other vendors were having difficulty with this plating process; and after evaluation of the potential effects of the coating on the future operation of the turbocompressor, it was decided that Linde LC-4 should be used.

The Linde LC-4 coating was successfully applied to the shaft and shoe bearing surfaces, finished and delivered in accordance with contract requirements. Certification of compliance with the plating requirements is shown in affidavits, Figures 68 and 69, provided by Union Carbide. The Linde LC-4 coating is guaranteed to have not more than 4 percent porosity. The chrome-oxide coatings were deposited on the shaft and shoe bearing surfaces in the locations shown in Figures 70 and 71.

"REPRODUCIBILITY OF THE ORIGINAL PAGE IS POOR."

UNION CARBIDE CORPORATION

LINDE DIVISION

1245 MAIN STREET, INDIANAPOLIS, INDIANA 46224

AIResearch Mfg. Co. of Arizona  
402 S. 36th St.  
Phoenix, Arizona

Shipping Date: 7-1-66

We hereby certify that in plating your part name and number noted below, we have complied in all respects with blueprints and specifications furnished by you.

<u>Part Name</u>	<u>Part Number</u>	<u>Quantity</u>	<u>Purchase Order</u>	<u>S.O. No.</u>
SHOE ASSY	#699449	7	3044	08774

  
Authorized Signature

J.A. REDMAN

ADV. PROJ. GEN. PROJ.

AUG 15 1966

DEPT. #93-12

FIGURE 68

APS-5223-R  
Page 120

"REPRODUCIBILITY OF THE ORIGINAL PAGE IS POOR."

UNION CARBIDE CORPORATION

LINDE DIVISION

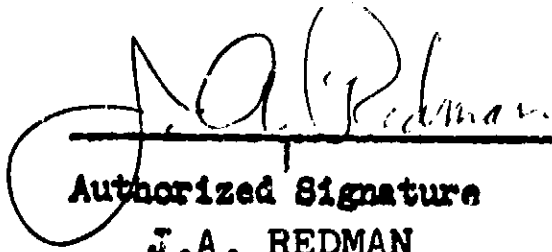
1215 MAIN STREET, INDIANAPOLIS, INDIANA 46224

AiResearch Mfg. Co. of Arizona  
402 S. 36th St.  
Phoenix, Arizona

Shipping Date: 5-20-66

We hereby certify that in plating your part name and number noted below, we have complied in all respects with blueprints and specifications furnished by you.

<u>Part Name</u>	<u>Part Number</u>	<u>Quantity</u>	<u>Purchase Order</u>	<u>S.O. No.</u>
ROTOR SHAFT	#699450-1	<del>EXXEX</del> 1	F-324	08816

  
Authorized Signature  
J.A. REDMAN

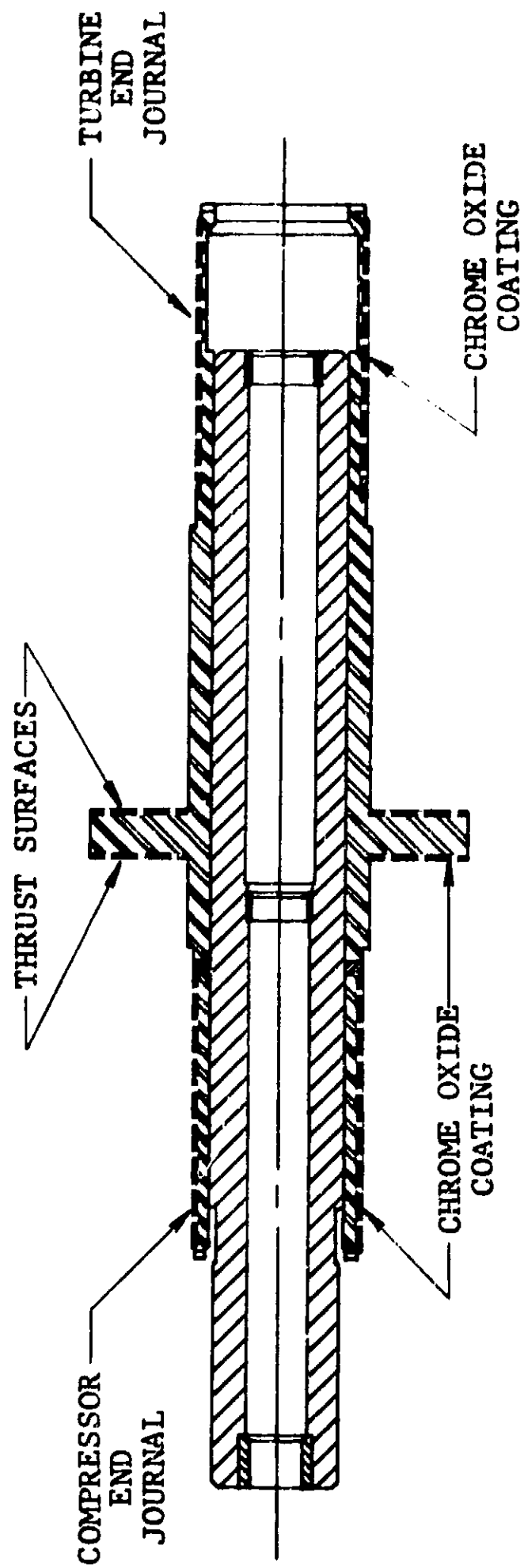
ADV. POW. GEN. PROJ.

AUG 15 1966

FIGURE 69

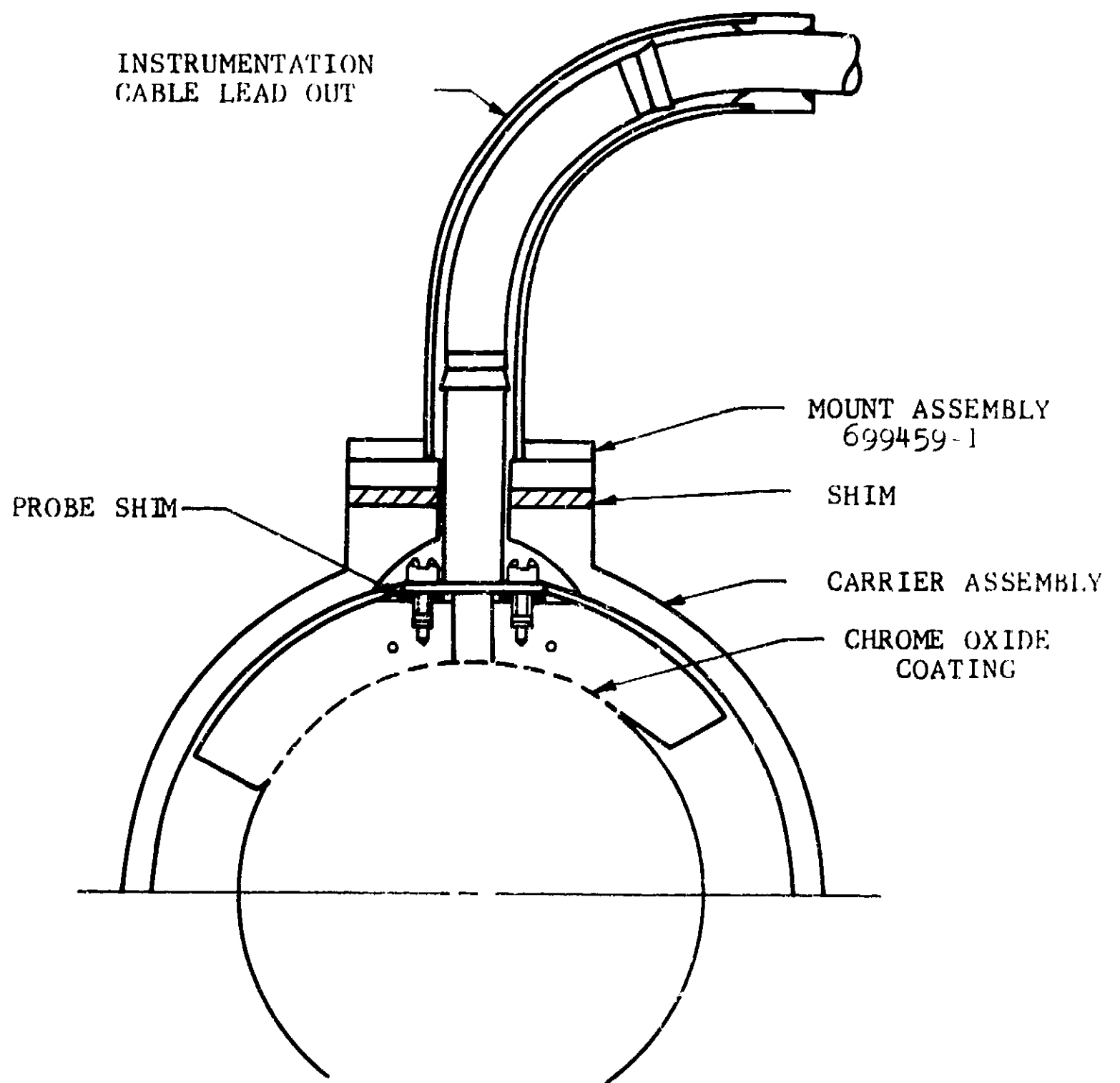
APS-5223-R  
Page 121

DEPT. #93-12



LOCATION OF CHROME-OXIDE PLATING  
ON P/N 699450-1 SHAFT ASSEMBLY

FIGURE 70



INSTALLATION OF PROXIMITY PROBE IN  
INSTRUMENTED SHOES PART 699453-1 AND PART 699454-1

FIGURE 71

#### 5.4 Proximity Probe Installation

In order to assist the development evaluation of the journal gas bearings, the capability of measurement of the lubricant film thickness between the bearing pad and the shaft surface was required. It was thus required that a proximity probe be mounted in the bearing shoe trailing that shoe which is flexibly mounted in the turbocompressor. Both turbocompressors had been modified prior to delivery in order to assist this proposed installation, without rework of the delivered hardware. The probe was mounted in the bearing shoe on the shoe pitch axis of the pivot point, and as close to the pivot as possible. This installation, including the shoe mount modification for the instrument cable lead-out, is shown in Figure 71. Since operating proximity probes were not required by the contract, dummy probes were fabricated to represent, as closely as possible, the operating probe mass. Thus, the shoe can be made operational in a turbocompressor without the installation of operating probes. Shims are provided such that the probes may be adjusted for the desired operating distances. The instrumentation cable feed tubes have been delivered in a sealed configuration to assist initial operation without operating probes.

#### 5.5 Hardware Identification

The following part numbering describes the hardware delivered by the contract, together with additional hardware transferred from Contract NAS3-9652. This latter material was supplied in order that it might be matched to its referenced bearing shoes. The part numbering describes those parts in the delivered turbocompressors that may be replaced by this hardware.

	<u>Contract Deliveries</u>	<u>Part No. of Turbocompressor Components</u>
(a)	699364-4 Bearing set, flexible mount, matched	699364-1
	<u>699449-1</u> Shoe assembly	699330-1
	<u>699588-1</u> Mount assembly, diaphragm, bearing	699317-1
(b)	699363-2 Bearing set, fixed mount, matched	699363-1
	<u>699449-1</u> Shoe assembly	699330-1
	<u>699315-1</u> Mount assembly, bearing	699315-1
(c)	699460-1 Bearing set, fixed mount, matched	699363-1
	<u>699453-1</u> Shoe assembly, compressor journal, instrumented bearing	699330-1
	<u>699459-1</u> Mount assembly, bearing	699315-1
	<u>699457-1</u> Probe, blank	-
	<u>699458-1</u> Shim, probe	-
(d)	699460-2 Bearing set, fixed mount, matched	699363-1
	<u>699454-1</u> Shoe assembly, turbine journal, instrumented bearing	699330-1
	<u>699459-1</u> Mount assembly, bearing	699315-1
	<u>699457-1</u> Probe, blank	-
	<u>699458-1</u> Shim, probe	-
(e)	<u>699450-1</u> Shaft assembly, gas generator	699310-1
(f)	<u>699317-1</u> Mount assembly, diaphragm, bearing	699317-1

699449-1 Denotes hardware components (typical)

\*Denotes material transferred from Contract NAS3-9652.

Two sets of Items (a) and (b), one set of each of Items (c), (d), and (e), and two components of Item (f) were delivered.



## 5.6 Hardware Calibration

The strain-gauge assemblies attached to the two Part 699317-1 and two Part 699588-1 Diaphragm Mount Assemblies were calibrated in accordance with procedures established previously during the turbocompressor contract task. These calibrations are shown in Tables 9 through 12.

Critical dimensions of the shaft assembly, immediately after completion of fabrication, with respect to its installation and use with the gas bearings were observed as follows:

Compressor-end bearing journal diameter	1.75003 inches
Turbine-end bearing journal diameter	1.75002 inches
Bearing journal roundness	Better than 0.000040 inch
Bearing journal concentricity	0.00005 inch T.I.R. (using master curvics)
Distance between thrust faces	0.5004 inch
Thrust face flatness	Better than 0.0001 inch

During October 1966, while awaiting shipment, damage to the LC-4 plate on the compressor-end journal bearing surface was observed. This appeared to be in the form of a two-turn helix, 3/8-inch pitch, where the plating surface was raised and was darker in color than the remainder of the journal. Investigation by Union Carbide of their process, a material composition evaluation of the damaged area, and a review of the grinding and finishing processes resulted in the findings that in preparation for silver-plate of the compressor stub-end heat shunt, a cleaning process

was used on the heat shunt copper. Plater's protective tape had been wound spirally around the journal surface for protection while cleaning the copper with a muriatic acid solution. This acid leaked under the tape and attacked the chrome-oxide plating, which resulted in the characteristic spiral pattern. This phenomenon was also observed on another shaft fabricated for a similar purpose, but not part of this contract. Union Carbide confirmed that the specified acid was one of the few that would attack chrome-oxide platings. The two other known fluids are potassium permanganate and ammonium citrate. This data has resulted in a modification of the process operations for manufacture of all future shafts utilizing this plating material.

In view of the cost of salvage of the shaft and the fact that additional back-up shafts were already in fabrication on a later contract, the shaft was shipped to the NASA in the "as-damaged" condition.

TABLE 9  
BEARING FLEXIBLE DIAPHRAGM CALIBRATION  
DIAPHRAGM NO. 45  
PART NO. 699317-1  
CALIBRATION AT 75°F

LOAD (lbs)	DEFLECTION (inches)	STRAIN (microinches/inch)
0	0.00000	0
2	0.00051	70
4	0.00106	143
6	0.00166	216
8	0.00226	290
10	0.00286	367
12	0.00356	436
14	0.00421	522
16	0.00484	610

Gauge Factor 1.54

Bridge Connections:

Excitation leads 1 and 4  
Signal leads 2 and 3

With calibration resistor of  $56K \pm 1/10$  percent across leads  
1 and 3 strain reading = 690 microinches/inch (17.5 lbs load)

Spring rate between 5 and 10 lbs load  $\approx 3330$  lbs/inch.

TEMPERATURE (degrees F)	STRAIN (microinches/inch at zero load)
100	0
200	25
300	65
400	87
500	125
600	165

TABLE 10  
BEARING FLEXIBLE DIAPHRAGM CALIBRATION  
DIAPHRAGM NO. 46  
PART NO. 699317-1  
CALIBRATION AT 75°F

LOAD (lbs)	DEFLECTION (inches)	STRAIN (microinches/inch)
0	0.00000	0
1.1	0.00040	30
3.1	0.00105	90
6.1	0.00200	180
8.1	0.00265	240
11.1	0.00355	325
13.1	0.00420	380
16.1	0.00515	455
18.1	0.00560	505

Gauge Factor 1.75 (minimum)

Bridge Connections:

Excitation leads 1 and 4  
Signal leads 2 and 3

With calibration resistor of 56K  $\pm 1/10$  percent across leads  
1 and 3 strain reading = 560 microinches/inch (20.1 lbs load)

Spring rate between 5 and 10 lbs load  $\approx$  3100 lbs/inch

TEMPERATURE (degrees F)	STRAIN (microinches/inch at zero load)
80	0
100	30
200	150
290	260
405	375
500	465
610	570

TABLE 11  
BEARING FLEXIBLE DIAPHRAGM CALIBRATION  
SERIAL NO. 45  
PART 699588-1  
CALIBRATED AT 80°F

Load (lbs)	Deflection (inches)	Strain (microinches/inch)
0	0.0000	0
2	0.00088	95
5	0.0020	240
7	0.00285	335
10	0.00400	470
12	0.00475	555
15	0.00580	675
17	0.00640	760

Gauge factor = 1.75

Bridge connection:

Excitation leads 1 and 4

Signal leads 2 and 3

56K Resistor across leads 1 and 3 = 380 microinches/inch

Spring rate between 5 and 10 lbs load  $\approx$  2,500 lbs/inch

Temperature (degrees F)	Strain (microinches/inch) at zero load)
80	0
200	+50
300	+135
400	+85
500	+110
550	+125

TABLE 12  
BEARING FLEXIBLE DIAPHRAGM CALIBRATION  
SERIAL NO. 46  
PART 699588-1  
CALIBRATED AT 80°F

Load (lbs)	Deflection (inches)	Strain (microinches/inch)
0	0.0000	0
2	0.0008	75
5	0.0020	190
7	0.0028	265
10	0.0040	380
12	0.0047	450
15	0.0059	560
17	0.00655	625

Gauge factor = 1.75

Bridge connection:

Excitation leads 1 and 4

Signal leads 2 and 3

56K Resistor across leads 1 and 3 = 365 microinch/inch

Spring rate between 5 and 10 lbs load  $\approx$  2,500 lbs/inch

Temperature (degrees F)	Strain (microinches/inch) at zero load)
80	0
200	40
300	-95
400	-185
500	-225
550	-215

## 6.0 CONCLUSIONS

The effort required under this program has resulted in the generation of significant data applicable to the turbocompressor already delivered to the NASA. Conclusions may be drawn as follows:

Task I      The bearings in the turbocompressor will have adequate capability for operation at the off-design condition, and a cooling flow value can be obtained to limit the bearing temperature to safe values.

Task II     Application of the generated stability criteria to the configuration of the turbocompressor as delivered indicates, analytically, that the rotor system would be unstable under full-power conditions. There exists a possibility that the turbocompressor rotor system may be stable at the half-power conditions with a 4-percent cycle bleed cooling flow rate.

Task III    Alignment of the elastically pivoted journal bearings during initial setup, or during transient thermal operation, is still considered to require a complex bearing installation which necessitates extensive development.

Task IV    (a)    Bearing surface coatings of chrome oxide require that very close control of the component processes be established for each item in fabrication.

              (b)    Two of the bearing pads and their matching mounts have been so constructed as to allow the future installation of proximity probes for measurement of shoe pivotal running clearances.

## 7.0 RECOMMENDATIONS

Based upon the results of the experimental and analytical work undertaken during the program, the following recommendations are worthy of further consideration:

- (a) Journal bearing carrier components should be reworked in the delivered turbocompressors in order to provide better control over the local thermal gradients and to prevent adverse differential growths. These differential growths are predicted to create unstable rotor behavior at design operating conditions.
- (b) Experimental verification of the applicability of the relationship between whirl frequency and journal bearing lubricant film spring rate, as a stability criterion, should be obtained for rotors of various mass and inertia properties.
- (c) Development of the installation of elastically pivoted journal bearings should be considered only if evidence is available that high wear factors may be present within the existing ball-and-socket pivoted journal bearings.



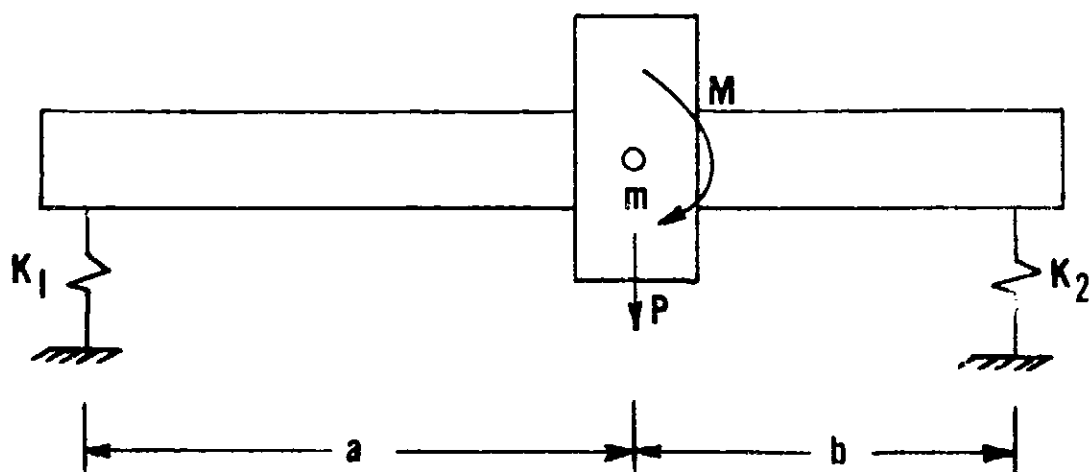
**BLANK PAGE**

## APPENDIX I

### DERIVATION OF RIGID ROTOR RESONANT FREQUENCY EQUATIONS

Consider a rigid rotor of mass ( $m$ ) supported on linear elastic supports of rates  $K_1$  and  $K_2$ .

FIGURE 1



The distance between the elastic supports is  $(a+b)$  and the mass center is located at a distance  $(a)$  from the left support as shown.

The elastic properties of the system may be defined in terms of actions applied at the rotor mass center as follows:

$$\delta = \alpha_{11}P + \alpha_{12}M \quad (1)$$

$$\varphi = \alpha_{21}P + \alpha_{22}M \quad (2)$$

where

$\delta$  = radial deflection, inches

$\varphi$  = angular deflection, radians

$P$  = radial force, lbs

$M$  = moment about an axis normal to the rotor axis, in. lb

The influence coefficients are defined as follows:

$\alpha_{11}$  = deflection at rotor c.g. due to a unit load applied at rotor c.g., ( $\text{in. lb}^{-1}$ )

$\alpha_{12}$  = deflection at rotor c.g. due to a unit moment applied about an axis normal to the rotor axis ( $\text{lb}^{-1}$ )

$\alpha_{21}$  = angular deflection of rotor due to a unit radial load applied at rotor c.g. ( $\text{lb}^{-1}$ )

$\alpha_{22}$  = angular deflection of rotor due to a unit moment applied about an axis normal to rotor axis ( $\text{in. lb}^{-1}$ )

By the reciprocity theorem of Maxwell,

$$\alpha_{21} = \alpha_{12}. \quad (3)$$

Letting  $R = a/b$  and  $K = K_2/K_1$ , the influence coefficients for the rigid rotor system of Figure 1 are defined as follows:

$$\begin{aligned} \alpha_{11} &= \frac{\beta_{11}}{K_1(1+R)^2}, \quad \beta_{11} = \left[\frac{R^2}{K} + 1\right] \\ \alpha_{12} &= \frac{\beta_{12}}{K_1(1+R)^2}, \quad \beta_{12} = \frac{1}{b}\left[\frac{R}{K} - 1\right] \\ \alpha_{22} &= \frac{\beta_{22}}{K_1(1+R)^2}, \quad \beta_{22} = \frac{1}{b^2}\left[\frac{1}{K} + 1\right] \end{aligned}$$

Consider now that the rotor is in perfect static balance and is whirling in a circular orbit of angular velocity  $\lambda$  and that the eccentricity of the rotor mass center from the whirl center is  $\delta$ . The following centrifugal force is thus experienced by the rotor:

$$P = m\lambda^2\delta \quad (4)$$

By virtue of the rotor whirl, a gyroscopic moment will also be experienced by the rotor as follows:

$$M = -\lambda[I_p\Omega\sin\phi - I_d\lambda\sin\phi\cos\phi] \quad (5)$$

where  $\Omega$  = motor spin velocity, rad/sec.

$I_p$  = rotor polar moment of inertia (in. lb. sec<sup>2</sup>)

$I_d$  = rotor diametral (transverse) moment of inertia  
with respect to the mass center (in. lb. sec<sup>2</sup>)

and  $\lambda$  = rotor whirl (precession) velocity, rad/sec.

By virtue of the small angle approximation for  $\psi$ , the gyroscopic moment may be expressed in the following simplified form:

$$\begin{aligned} M &= \lambda^2 \phi \left( I_d - \frac{\Omega}{\lambda} I_p \right) \\ &= I_e \lambda^2 \psi \end{aligned} \quad (6)$$

The rotor deflection equations (1) and (2) may thus be expressed in terms of the dynamic loads given by (5) and (6) as follows:

$$[\beta_{11} m \lambda^2 - K_1 (1+R)^2] \delta + [\beta_{12} I_e \lambda^2] \phi = 0 \quad (7)$$

$$[\beta_{12} m \lambda^2] \delta + [\beta_{22} I_e \lambda^2 - K_1 (1+R)^2] \psi = 0 \quad (8)$$

Resonant frequencies of the system are computed based upon the indeterminacy of either  $(\delta)$  or  $(\phi)$  in (7) and (8). Thus

$$\frac{\lambda_{1,2}^2}{K_1 (1+R)^2} = \frac{\beta_{11} m + \beta_{22} I_e \pm \sqrt{(\beta_{11} m + \beta_{22} I_e)^2 - 4(\beta_{11} \beta_{22} - \beta_{12}^2) m I_e}}{2(\beta_{11} \beta_{22} - \beta_{12}^2) m I_e} \quad (9)$$

Values  $\lambda_1$  and  $\lambda_2$  from equation (9) are the rigid rotor whirl natural frequencies. Advanced specification of the spin-to-whirl ratio,  $\Omega/\lambda$ , is required for their computation.